TISSUE-ENGINEERED ISLET GRAFT DESIGN AND ASSESSMENT

A DISSERTATION
SUBMITTED TO THE FACULTY OF THE GRADUATE SCHOOL
OF THE UNIVERSITY OF MINNESOTA

BY

Thomas Mark Suszynski

IN PARTIAL FULFILLMENT OF THE REQUIREMENTS
FOR THE DEGREE OF
DOCTOR OF PHILOSOPHY
IN BIOMEDICAL ENGINEERING

Advisor: Klearchos K. Papas, Ph.D.

September 2012

Acknowledgements

I express my deepest gratitude to my wife, Megan, who has been a constant in my life, exhibiting patience, support, love, and a continued understanding that my professional training is just at its infancy. I thank my mother, father, both brothers and all of my friends for their support. I particularly appreciate their understanding for the intractability of my schedule.

I thank my advisor, Prof. Klearchos K. Papas, who has taught me a significant amount about science, engineering, human decency and ethics. I thank him for showing me how to think large and small about a problem, how to critically review, how to write, how to present, how to collaborate, and maybe most importantly how to balance professional and personal responsibilities. I thank him for providing me opportunities to initiate or to contribute to nearly any basic or clinical work that interested me. I also thank him for sending me on many trips to collaborators, and to many domestic and international conferences or meetings – all which would be the envy of any graduate student.

I thank Prof. Efstathios S. Avgoustiniatos, a savant of thoroughness. You may wonder what that characterization even means. To explain, he once jokingly told me: “regardless of how much work you put into it, even if you think it is perfect, I will find something wrong with it!” [7/11/2011; 16:18]. I thank him not only for this lesson, but I also thank him for endless scientific discussion, for his hunger to uncover the truth, for guidance on experimental design, and for his knowledge of and passion for oxygen transport limitations and basketball.

I express gratitude to my committee members, Profs. Bruce E. Hammer, Paul A. Iaizzo, and David E.R. Sutherland for their insightful comments and discussion. I thank Profs. Meri Firpo and Michael Garwood for their mentorship over the last year.

I thank my clinical mentors, in particular Drs. Blanche M. Chavers, Peter M. Eckman, Erik B. Finger, Raja Kandaswamy, Ranjit John, Arthur J. Matas, Timothy P. Pruett, and, of course, Dr. Sutherland.

I thank some of the current or former members of the Transplant Division team, including Barbara Bailey, Stephanie Daily, Dr. Kristen J. Gillingham, Hang McLaughlin, Ann Marie Papas, Dr. Jay Stone, Dr. Gerardo Tamayo, Jerry Vincent, and Dr. Elliot Zahtz.

I thank some of the members of the human anatomy education program, including Prof. Mark S. Cook, Dr. James V. Harmon, Prof. Stephen A. Katz, Dr. Peter J. Kernahan, Dr. Steven J. Waisbren, Dr. Michael J. Walker, Prof. Anthony J. Weinhaus and Prof. Martin Wessendorf.

I thank my colleagues and labmates over the last 6 years, including Janine Abouaish, Dr. Tanaka Anazawa, Dr. Appakalai N. Balamurugan, Dr. Ryan Chamberlain, Christopher S. Chapman, Eric J. Falde, Dr. Joana Ferrer-Fabrega, Dr. Brian Flanagan, Thomas Gilmore, Dr. Melanie L. Graham, Rebecca Hooper, Dr. Lou S. Kidder, Jenna P. Kitzmann, Dr. Shuichiro Matsumoto, Dr. Kristen S. Maynard, Kathryn R. Mueller, Dr. Timothy D. O'Brien, Brian Perrault, Philip R. Rozak, William E. Scott III, Dr. Henk-Jan Schuurman, Sajjad M. Soltani, Samuel A. Stein, Dr. C. Julia Vance, Brad P. Weegman,

Gina M. Wildey, and Josh J. Wilhelm (and anyone else that I may have forgotten to mention).

I thank Keith Williams for helping *ad hoc* fabricate a number of parts needed for various experiments over the years.

I thank some of our many collaborators, especially Dr. Warren Breidenbach III (University of Arizona [UAZ]), Dr. Nic Chronos (St. Joseph's Translational Research Institute [SJTRI]), Dr. Gary W. Cline (Yale), Dr. Clark K. Colton (MIT), Mickey Dunning (Experimental Surgical Services [ESS]), Dr. James D. Fonger (SJTRI/Emory), Diana Freeman (Research Animal Resources [RAR]), Dr. Evan Goldberg (SJTRI), David J. Kennedy (IKOTECH, LLC), Austin Lam (SJTRI), Dr. Jinsheng Li (SJTRI), Dr. Thomas Minor (University Hospital of Cologne), Simon Stone (Giner, Inc), Dr. Michael J. Taylor (Cell & Tissue Systems, Inc), Dr. Linda A. Tempelman (Giner, Inc), Dr. Paul W. Todd (Techshot, Inc), Dr. Tolga Türker (UAZ), Dr. William A. Walker (Cardiovascular and Thoracic Surgery Group, Johnson City, TN), and John R. Wilson (Wilson-Wolf Manufacturing).

Chapter 2

This review was supported by grants from the National Center for Research Resources, National Institutes of Health (#U42 RR 016598-01 and #RO1-DK063108-01A1), the Juvenile Diabetes Research Foundation (#4-1999-841), the Iacocca Foundation, the Schott Foundation, and the Carol Olson Memorial Diabetes Research Fund. The authors would like to thank Drs Stathis Avgoustiniatos and Lou Kidder for critically reviewing the manuscript.

Chapter 3

The authors thank Innovara Inc. for sponsoring Ms. Ko in her Women in High Places internship, and Dr. Efstathios Avgoustiniatos and Bradley Weegman from our Diabetes Institute for Immunology and Transplantation for reviewing the manuscript. This work was supported by the National Institutes of Health, National Center for Research Resources, (U42 RR016598), the Iacocca Foundation, the Schott Foundation, and the Carol Olson Memorial Diabetes Research Fund.

Chapter 4

This work was supported by funding from the Iacocca Foundation, the Schott Foundation, and the Minnesota Lions Diabetes Foundation. The authors would like to thank Josh Wilhelm of the Schulze Diabetes Institute for providing size distribution data and for thoughtful discussions on the topics presented herein.

Chapter 5

This work was supported by funding from the Iacocca Foundation, the Schott Foundation, and the Minnesota Lions Diabetes Foundation.

Chapter 6

This work was supported in part by funding from the Iacocca Foundation, the Schott Foundation, the Minnesota Lion Diabetes Foundation, and the National Institute of Diabetes and Digestive and Kidney Diseases SBIR Phase II (R44 DK069865). The authors would like to thank the University of Pennsylvania and the Integrated Islet Distribution Program for supplying the islets used in this study. Additional thanks to all members of the Schulze Diabetes Institute for their thoughtful discussions, especially Dr.

Louis Kidder, Dr. Michael Rizzari, Rebecca Hooper, Jennifer Kitzmann, Kathryn Mueller, William Scott III, Garrett Swindlehurst, Jikku Thomas, and Bradley Weegman.

Chapter 7

This work (Suszynski *et al*. Cryobiology [2012]) was supported in part by Health Resources and Services Administration contract 231-00-0115 and by the National Institutes of Health, National Institute of Diabetes and Digestive and Kidney Diseases grant number: R44 DK07040. The content is the responsibility of the authors alone and does not necessarily reflect the views or policies of the Department of Health and Human Services, nor does mention of trade names, commercial products, or organizations imply endorsement by the U.S. Government.

Research funding (for Suszynski *et al*. Xenotransplant [2011]) provided by the National Institute of Diabetes and Digestive and Kidney Diseases (NIDDK) (2R44DK072647-02A1), the Schott Foundation, the Carol Olson Memorial Diabetes Research Fund, and the Iacocca Foundation.

Pracę tą dedykuję
moim rodzicom,
Elżbiecie i Wiesławowi Suszyńskim,
którzy wyjechali z Polski,
aby zapewnić swoim dzieciom
lepszą przyszłość,
dla mojej żony
i dla wszystkich diabetyków.

I am dedicating this work
to my parents,
Elizabeth and Wiesław Suszyński,
who left Poland
to secure a better future
for their children,
to my wife,
and to all diabetics.

Abstract

Diabetes mellitus is a metabolic disease characterized by an inability to maintain normoglycemia and is usually associated with an insufficient β-cell mass. Islet transplantation (IT, a β-cell replacement therapy) has exhibited promise in reversing the diabetic state, yet it remains an experimental therapy only among a small subset of patients and widespread availability remains elusive. A main reason for its limited use is the large islet dose required to produce insulin independence, often requiring tissue from multiple donor pancreata. Abundant evidence exists suggesting that acute and chronic islet loss and dysfunction occur in the post-IT period. The minimum islet dose could be reduced if the quality (potency, viability) of the islet product is improved. Since islets do not possess the cellular machinery to produce energy effectively in the absence of oxygen, strategies that improve oxygenation during the ischemic period (donor cardiac death to complete revascularization) are important to develop. Due to the many steps involved in the process (pancreas preservation, and islet isolation, purification, culture, assessment, transplant and engraftment), the quality of an islet preparation can change. Thus, it is critical to develop improved islet quality assessment tools that enable accurate and quantitative characterization of islet viability and potency, which can be performed prospectively, and which do not require much tissue for assessment or which rely on non-invasive methods. Furthermore, intrahepatic IT may not be the optimal approach, and tissue-engineered strategies for extrahepatic IT may be better. The work presented herein focuses on improving islet quality assessment, examining the oxygenation status of the intraportally transplanted islet, and developing a tissue-engineered strategy for the design and non-invasive assessment of islet graft viability – all with the hope that someday IT could be used to successfully treat many more diabetics.

Table of Contents

List of Tables

Chapter 1

None

Chapter 2

Chapter 3

None

Chapter 4

List of Figures

Chapter 1

None

Chapter 2

None

Chapter 3

Chapter 4

Chapter 5

List of Abbreviations

2D	two-dimensional
3D	three-dimensional
7-AAD	7-aminoactinomycin D
^{19}F-MRI	fluorine-19 magnetic resonance imaging
^{19}F-MRS	fluorine-19 magnetic resonance spectroscopy
ADP	adenosine diphosphate
AMP	adenine monophosphate
AO	acridine orange
A-PSF	anterograde persufflation
ATP	adenosine triphosphate
AUC	area-under-the-curve
AVF	anoxic volume fraction
B_0	external magnetic field
C	calcein AM
CD3	cluster of differentiation 3
CL	calibration line
COV	coefficient of variation
CPB	cardiopulmonary bypass
CPS	cold preservation solution
CT	celiac trunk
ΔOCR_{glc}	difference between oxygen consumption rates at high and low glucose levels
δ_t	thickness of thrombus
DCD	donation after cardiac death

DCCT	Diabetes Control and Complications Trial
DNA	deoxyribonucleic acid
DR	diabetes reversal
DTZ	diphenylthiocarbazone
EB	ethidium bromide
EDIC	Epidemiology of Diabetes Interventions and Complications
EH	ethidium homodimer
ELISA	enzyme-linked immunosorbent assay
EM	electron microscopy
EP	Edmonton protocol
EU	endotoxin unit
FACS	fluorescence-activated cell sorting
FDA	Food and Drug Administration
FM	fluorescence microscopy
GSIS	glucose-stimulated insulin secretion
HE	hematoxylin and eosin
HIF-1α	hypoxia inducible factor-1 alpha
HMP	hypothermic machine perfusion
HPLC	high-performance liquid chromatography
HT	heat-treated
IBMIR	instant blood-mediated inflammatory reaction
IE	islet equivalent
IL-2	interleukin-2
INS-1	insulinoma-1
IT	islet transplantation

kgBW	kilogram of body weight
LC/MS/MS	electrospray tandem mass spectroscopy
mAb	monoclonal antibody
MMP	mitochondrial membrane potential
MP	microparticle
MS	magnetic separation
mTOR	mammalian target of rapamycin
MTT	3-(4,5-dimethylthiazol-2-yl)-2,5-diphenyl tetrazolium bromide
NFVF	non-functional volume fraction
NMB	nude mouse bioassay
OBS	oxygen biosensor system
OCR	oxygen consumption rate
OCR/DNA	oxygen consumption rate normalized to DNA content
OCR_{GS}	glucose-stimulated oxygen consumption rate
OCR_{hglc}	oxygen consumption rate at high glucose level
OCR_{lglc}	oxygen consumption rate at low glucose level
OCR_{TX}	transplanted oxygen consumption rate
PETG	glycol-mediated polyethylene terephthalate
PFC	perfluorocarbon
PFD	perfluorodecalin
PI	propidium iodide
POD	post-operative day
PP	pancreatic polypeptide
PS	phosphatidylserine
PSF	persufflation

pO_2	oxygen partial pressure
QMS	quadrupole magnetic sorting
$R1$	longitudinal relaxation rate
R_i	islet radius
RFU	relative fluorescence unit
RLU	relative luminescence units
R-PSF	retrograde PSF
SCS	static cold storage
SD	standard deviation
SE	standard error
SIR	sirolimus
SLM	standard light microscopy
SMA	superior mesenteric artery
SOD	superoxide dismutase
SYTO	commercially-available green membrane-permeable fluorescent dye
$T1$	spin-lattice relaxation time
T1D	type 1 diabetes
$T2$	spin-spin relaxation time
T2D	type 2 diabetes
TAC	tacrolimus
TE	tissue-engineered
TF	tissue factor
TLM	two-layer method
TNF	tumor necrosis factor
UNOS	United Network for Organ Sharing

UV	ultraviolet
UW	University of Wisconsin solution
VADFMK	membrane-permeable caspase ligand (inhibitor)
VEGF	vascular endothelial growth factor
WIT	warm ischemia time

CHAPTER 1: Background, Objectives and Summary

Background

Diabetes mellitus describes a class of disease characterized by a defect of carbohydrate metabolism and an inability to control blood glucose levels within the normal range. The term ‘diabetes’ is derived of the Greek word *διαβήτης* meaning ‘siphon’ and ‘mellitus’ is a Latin word meaning ‘honeyed or sweetened’ – both referring to cardinal features of the disease (polyuria, glycosuria). There are two main types of diabetes mellitus, type 1 diabetes (T1D) and type 2 diabetes (T2D), and each has distinct pathophysiology and onset; T1D is caused by near-total or total autoimmune destruction of the insulin-secreting β-cells in the native pancreas and is characterized by relatively rapid onset, whereas T2D is caused by the development of glucose intolerance resulting from a number of non-immune phenomena (peripheral insulin resistance, metabolic stress, amyloidosis) and is characterized by relatively gradual onset. T1D and T2D exhibit different environmental [1; 2; 3; 4; 5; 6; 7] and genetic associations [5; 8; 9; 10]. However, it can be argued that both diseases manifest due to a single reason – the β-cell mass is insufficient for tight glycemic regulation. Before insulin therapy became available, most patients with T1D became severely fatigued, would lose significant amounts of weight due to both dehydration and starvation, and would need to be maintained on strict diets in order to survive [11]. Since the discovery of insulin in 1921-1922 by Dr. Frederick G. Banting and Charles H. Best at the University of Toronto [12; 13; 14], the acute effects of uncontrolled hyperglycemia (ketoacidosis, dehydration, confusion, coma and death) became preventable.

Exogenous insulin administration has enabled patients to live with diabetes. However, this therapeutic approach is not perfect. Patients that require daily insulin injections find it cumbersome to manage their disease. These patients are more susceptible to dangerous hypoglycemic excursions caused by inaccurate insulin dosing. Furthermore, though the acute, life-threatening effects of diabetes are avoided, the chronic effects are not. Most patients with diabetes eventually develop micro- and macro-vascular complications affecting all organs and in particular the eyes (retinopathy), kidneys (nephropathy), autonomic and peripheral nerves (neuropathy) [15], of which the timing and severity depends on the degree of blood glucose control [16; 17; 18; 19; 20; 21; 22; 23; 24]. From 1983-1993, ~1400 patients with T1D at 21 different U.S. and Canadian centers were enrolled in a randomized clinical trial (the Diabetes Control and Complications Trial [DCCT]) in which about half of patients were assigned to undergo intensive insulin therapy (≥3 daily injections or pump) and half were assigned to undergo standard insulin therapy (1-2 daily injections) [16]. The results of the DCCT at a mean of 6.5 years of follow-up indicated that intensive insulin therapy delayed the onset and slowed the progression of major diabetic complications [18]. Similar findings were observed in the Stockholm Diabetes Intervention study conducted with fewer patients (~100) but similar follow-up (7.5 years) [19]. After the DCCT was terminated by an independent data monitoring committee, most of the enrolled patients were re-enrolled in the Epidemiology of Diabetes Interventions and Complications (EDIC) study, aimed to continue following these patients [20; 21; 22; 24]. The results of this ongoing study have been reported over the last decade and have indicated that the intensive insulin therapy early in the disease course exhibited sustained reduction in the risk of progressive diabetic complications [20; 21; 24; 25] and cardiovascular disease [22] despite worsening glycemic control. Even though the DCCT and EDIC involved patients with

T1D, the same lower risk of microvascular complications have been shown in patients with T2D receiving intensive insulin therapy [23; 26]. Collectively, these studies illustrate that tight glycemic regulation with exogenous insulin can prevent many of the long-term effects of diabetes. However, the primary adverse event associated with intensive insulin administration is severe hypoglycemia, which in some cases has been shown to occur 2-3 times more frequently with such therapy [17; 18], and which suggests that daily insulin injections cannot mimic the feedback-controlled secretory function of pancreatic β-cells.

In December of 1966, Drs. William D. Kelly and Richard C. Lillehei at the University of Minnesota performed the first (segmental) pancreas transplant [27]. This graft failed due to technical reasons and rejection, however this experience initiated a series of an additional 13 pancreaticoduodenal transplants performed from 1966-1973 [28; 29]. Of these grafts, only 1 survived with function for >1 year, but these efforts indicated that glycemic normalization was possible with pancreas transplantation. Most of the first 14 pancreas transplants (8/14) were characterized by technical complications, which initiated the first clinical series of islet transplants in 1974-1978 [29; 30; 31; 32] – a much less technical and invasive procedure. Whether pancreas or islet transplantation, the β-cell mass is replaced in order to reverse (allo-) or prevent (auto-) overt diabetes and its complications. Numerous studies have shown that islet [33; 34; 35; 36; 37] or pancreas transplants [38; 39; 40; 41] can either prevent the progression or encourage regression of microvascular diabetic complications like retinopathy [33; 35; 36; 37; 41], glomerular nephropathy [33; 34; 36; 37; 38; 39], and polyneuropathy [36; 37; 40; 42]. Several studies have directly compared outcomes with standard [40; 42] or intensive medical (insulin) therapy [35; 36; 37], all showing improved complication profile following β-cell replacement therapy with either pancreas or islet transplantation.

Both allogeneic pancreas and islet transplant remain potential therapeutic options for the treatment of diabetes. Data have indicated that long-term allo-islet outcomes have improved in the last decade [43; 44; 45; 46; 47; 48; 49; 50; 51; 52], and are comparable to outcomes following pancreas transplant (~50% insulin independence at 5-years) [51]. Islet transplant remains intriguing because it is less invasive and technically-demanding than pancreas transplant, retains the potential of treating multiple diabetic recipients with a single donor pancreas, may require less immunosuppression and may reduce overall health care costs (decreased hospital stay) [53]. Islet transplant is currently being undertaken in a phase III multicenter clinical trial for these reasons. However, widespread applicability for islet transplant currently remains unattainable in part due to limitations in the accurate characterization of the quality and potency of islet preparations, the possibility that the intraportal transplant site may not be optimal and that tissue-engineered approaches may enable improved islet engraftment. The work presented in this thesis aims to improve our understanding in these areas in hope that islet transplantation can be used to successfully treat many more diabetics.

Objectives and Summary

The objectives and summary of work presented in each of the remaining chapters is briefly presented herein.

Chapter 2 is a reproduction of our published review article (Papas *et al*. [54]) which details the current status of clinical islet product assessment prior to transplant. This article critically reviews the approaches used to characterize islet safety, quantity, and quality (including viability and potency), with an emphasis on the most promising assays

that are based on the assessment of mitochondrial function (detection of high-energy phosphates, mitochondrial membrane potential, oxygen consumption rate).

Chapter 3 is a reproduction of our published study (Suszynski *et al*. [55]) which describes an islet quality assessment assay based on measuring the ATP/DNA ratio, and compares its efficacy in predicting islet viability with a commonly used assay based on the ADP/ATP ratio. Results of the study indicate that the ATP/DNA ratio better predicts islet viability as compared to the ADP/ATP ratio because it can account for non-viable cells.

Chapter 4 is a copy of a manuscript in preparation that describes a theoretical diffusion-reaction model which can predict the formation of an anoxic, non-viable core or hypoxic, non-functional core within an intraportally transplanted islet. The model examines the impact of four variables that affect the islet oxygenation (islet size and viability, available oxygen supply, thrombus formation). Results of the study indicate that islet size exhibits the greatest relative impact on anoxic or non-functional islet volume fractions, but that all model variables contribute synergistically to the degree of islet oxygenation. Extrapolation of model results to an entire islet preparation suggests that a significant fraction of the total islet volume may be non-viable or non-functional following intraportal transplantation.

Chapter 5 is a copy of a review in preparation that describes tissue-engineered graft or device design taking into account the provision for oxygen supply that is available. The review discusses the importance of accounting for oxygen transport limitations when designing a tissue-engineered graft or device. In addition, the review summarizes the

design parameters that are critical to consider from the standpoint of oxygenation, and specifically discusses the impact of improved oxygen supply and permeability on graft or device size and cell or tissue seeding densities.

Chapter 6 a reproduction of our published study (Suszynski *et al*. [56]) which describes the use of fluorine magnetic resonance spectroscopy (^{19}F-MRS) in the assessment of tissue-engineered islet graft viability. ^{19}F-MRS measurements in combination with diffusion-reaction theory can be used to estimate the fractional viability (OCR/DNA) of the islets seeded within the graft. The techniques described in the publication and newer data are presented in this chapter. ^{19}F-MRS and the associated theory could be used for the non-invasive pre- and possibly post-transplant assessment of tissue-engineered islet graft viability by estimating the OCR/DNA.

Chapter 7 is a reproduction of several publications illustrating other related work aimed at improving islet product quality through improvements in pancreas preservation (Suszynski *et al*. [57]) and islet isolation (Suszynski *et al*. [58]; Rizzari *et al*. [59]). Given the complexity of islet transplantation, it is important to improve each step involved in process (islet isolation, purification, culture, shipping, assessment and engraftment). These publications are meant to illustrate some of the work done in a few of these other related areas. Additional work done is not presented [60; 61; 62; 63; 64; 65; 66; 67].

Future work will include developing non-invasive methods for the accurate measurement of the oxygen partial pressure at the level of the intraportally transplanted islet, to determine the validity of conclusions drawn in *Chapter 4*. Other future work will include developing corollary methods for the characterization of tissue-engineered islet graft

viability, and may include development of a bioreactor system that incorporates flow-through oxygen sensors that would directly measure the overall oxygen consumption rate based on a species mass balance. Translation of the ^{19}F-MRS technique described in *Chapter 6* for non-invasive estimation of the *in vivo* oxygenation status may enable characterization of the transplant milieu, and any events occurring near or around a transplanted graft that would otherwise impact the oxygen supply (such as inflammation, vascularization).

CHAPTER 2: **Islet Assessment for Transplantation**

Papas K.K., Suszynski T.M., Colton C.K. Islet assessment for transplantation. *Curr Opin Org Transplant*. 14(6): 674-682 (2009)

Summary

There is a critical need for meaningful viability and potency assays that characterize islet preparations for release prior to clinical islet cell transplantation. Development, testing, and validation of such assays have been the subject of intense investigation for the last decade. These efforts are reviewed, highlighting the most recent results while focusing on the most promising assays. Assays based on membrane integrity do not reflect true viability when applied to either intact islets or dispersed islet cells. Assays requiring disaggregation of intact islets into individual cells for assessment introduce additional problems of cell damage and loss. Assays evaluating mitochondrial function, specifically mitochondrial membrane potential, bioenergetic status, and cellular oxygen consumption rate, especially when conducted with intact islets, appear, appear most promising in evaluating their quality prior to islet cell transplantation. Prospective, quantitative assays based on measurements of oxygen consumption rate with intact islets have been developed, validated, and their results correlated with transplant outcomes in the diabetic nude mouse bioassay. More sensitive and reliable islet viability and potency tests have been recently developed and tested. Those evaluating mitochondrial function are most promising, correlate with transplant outcomes in mice, and are currently being evaluated in the clinical setting.

Abbreviations

2D	two-dimensional
3D	three-dimensional
7-AAD	7-aminoactinomycin D
ADP	adenosine diphosphate
AO	acridine orange
ATP	adenosine triphosphate
C	calcein AM
ΔOCR_{glc}	difference between oxygen consumption rates at high and low glucose levels
DNA	deoxyribonucleic acid
DTZ	dithizone
EB	ethidium bromide
EH	ethidium homodimer
ELISA	enzyme-linked immunosorbent assay
EU	endotoxin unit
FACS	fluorescence-activated cell sorting
FDA	Food and Drug Administration
FM	fluorescence microscopy
GSIS	glucose-stimulated insulin secretion
IE	islet equivalent
IT	islet cell transplantation
kgBW	kilogram of body weight
MMP	mitochondrial membrane potential
MTT	3-(4,5-dimethylthiazol-2-yl)-2,5-diphenyl tetrazolium bromide

NMB	nude mouse bioassay
OBS	oxygen biosensor system
OCR	oxygen consumption rate
OCR_{GS}	glucose-stimulated oxygen consumption rate
OCR_{hglc}	oxygen consumption rate at high glucose level
OCR_{lglc}	oxygen consumption rate at low glucose level
OCR_{TX}	transplanted oxygen consumption rate
PI	propidium iodide
PS	phosphatidylserine
pO_2	oxygen partial pressure
SLM	standard light microscopy
SYTO	commercially-available green membrane-permeable fluorescent dye
VADFMK	membrane-permeable caspase ligand (inhibitor)

Introduction

Islet transplantation (IT) is emerging as a promising approach for the treatment of selected patients with type 1 diabetes mellitus [52; 68; 69; 70; 71; 72; 73; 74]. IT is currently in a phase III multicenter clinical trial to determine whether it will become the standard of care. There is an urgent need for reliable assays that characterize the islet product for release prior to transplantation. Development of such assays is mandated by the US Food and Drug Administration (FDA) and has been the subject of investigation for the last decade. To provide a framework for understanding the current state of the art, this article first reviews the numerous approaches that have been proposed and tested, then focuses on the most recent results and promising assays for clinical IT.

Current specifications for lot release prior to clinical islet transplantation

The FDA mandates that for any cellular and tissue-based product, the manufacturer must be able to demonstrate that it can be safely and reproducibly manufactured [75]. This assessment is generally done by characterizing the product and establishing specifications for release. Lot release specifications for islet products include demonstration of safety (i.e., sterility, mycoplasma, pyrogenicity/endotoxin, and freedom from adventitious agents) and assessments of several key product characteristics that include, but are not limited to, identity, purity, viability, and potency. The current specifications for release of islet products within the United States are summarized in **Table 2-1**. These specifications function to exclude preparations that are contaminated, highly impure, grossly damaged, or do not contain significant numbers of islets. It is currently accepted that these specifications provide reasonable estimates of islet safety, identity, and purity, but do not provide meaningful measures of viability or potency of the preparation [76; 77; 78; 79]. Therefore, the establishment and validation of useful islet

viability and potency tests is urgently needed. The sections that follow focus on existing and emerging islet viability and potency tests, including those that are based on measurements of oxygen consumption rate (OCR), which appear to be the most promising.

Limitations of the tests currently used for islet lot release prior to clinical transplantation

Many of the methods currently used to assess islet preparations were developed nearly 20 years ago [80]. The advantages and limitations of tests currently used for islet product release, which were recently discussed in detail [81], are summarized in **Table 2-2**.

Sampling from an islet suspension

An important issue in characterizing islet preparations, relevant to all assays, is sampling. Obtaining a sample that is representative of the whole preparation is critical [80; 81]. Nevertheless, maintaining a homogeneous islet suspension while sampling is challenging, as islets settle rapidly. Differences in the size and the density of aggregates can lead to significant differences in settling velocity and exacerbate this problem. The extent of the systematic error introduced during this type of sampling is unknown. To minimize random error during sampling, multiple replicates should be collected. However, the additional

time and analysis required for collection of multiple samples and the concern about introducing contamination and removing islets that otherwise could be transplanted to benefit the recipient all pose limitations. Currently, only duplicate samples of 100-ml

(derived from a 100-ml islet suspension) are collected and counted, an amount that may or may not represent the entirety of the preparation.

Measurements of the amount of islet tissue

Quantification of the total amount of islets in an islet preparation is critical because it ultimately determines the islet dose that is transplanted. The method most widely used currently is manual, visual counting of islet equivalents (IEs) under a light microscope following dithizone (DTZ) staining to determine the total volume of islet tissue and its purity. This method has advantages and limitations (see *Table 2-2*) that are described in detail elsewhere [80; 81]. Methods for estimating the total number of cells or volume of tissue in a preparation include measurements of intracellular DNA, cellular nuclei counts, large particle flow cytometry [82], and packed tissue volume. These methods do not provide islet or β-cell-specific information, so they require an independent estimate of the purity (fractional volume of islets tissue or β-cells). Such estimates can be obtained using a variety of methods [81], including morphological analysis with electron and light microscopy [83], immunohistochemistry with either laser scanning confocal microscopy or laser scanning cytometry [84]. Recent studies indicate that conventional DTZ staining overestimates purity by 20–30% as compared with measurements using electron and light microscopy [85] and total number of IEs by as much as 90% [83] as compared with recently developed, more accurate methods that combine nuclei counting with light microscopy.

Measurements of viability

The current viability assay used for clinical islet product release is based on assessing membrane integrity with fluorescein diacetate/propidium iodide (FDA/PI) (see *Table 2-1*).

Strengths and limitations of this assay are outlined in Table 2 and detailed elsewhere [80; 81]. A major limitation of this assay is that it does not reflect true viability because it may not account for cells undergoing early apoptosis or dying by other modes of cell death, during which cells have not yet developed damage to their cell membrane. Furthermore, it does not correlate with the diabetic nude mouse bioassay (NMB) or clinical IT outcomes.

Measurements of islet function (potency)

The β-cells within the islets have a specific, dedicated function, that is, the dynamic release of insulin in response to a glucose stimulus. Therefore, one would expect that assessment of islet function should be straightforward, particularly if the insulin secretion rate of a preparation can be easily measured. Measurements of basal and glucose-stimulated insulin secretion (GSIS) could theoretically be used to provide a meaningful measure of the amount of viable and functional IEs (or β-cells) in a preparation if one assumes that insulin secretion from an islet population is relatively constant when normalized on a per viable IE or per viable b-cell basis. Unfortunately, GSIS does not correlate with clinical transplant outcomes [78; 79; 86]. There are several probable reasons for this persistent finding. Stresses associated with pancreas preservation, islet isolation, and islet purification may lead to extensive degranulation, insulin leakage (from dead or dying islet cells), or both. Conceivably, islets that do not secrete insulin at expected rates, but are nonetheless viable,may recover when transplanted into the recipient. In other words, low GSIS may not necessarily imply irreversibly impaired secretory function and, thus, GSIS does not correlate with clinical outcomes. Furthermore, insulin leakage from dead or damaged cells may be difficult to account for (because this contribution to the total insulin cannot be reliably estimated), may interfere

with proper calculation of insulin secretion rate and stimulation index, and may complicate the interpretation of the results of the GSIS assay. Insulin secretion is also particularly sensitive to the local oxygen partial pressure (pO_2), and assay procedures usually do not account for that [87].

The mouse bioassay as an in-vivo islet potency test and a surrogate islet potency validation tool

According to the FDA [75], a suitable potency assay is the one that demonstrates that the clinical product possesses the specific ability to provide the desired clinical effect. The diabetes reversal resulting from islets engrafted under the kidney capsule of immunodeficient nude mice correlates with clinical transplant outcomes and is currently accepted as the gold standard for testing islet potency [78; 79; 88; 89]. However, the time (days to weeks) required for this assay to produce interpretable results renders it retrospective. Nonetheless, correlation of real-time, *in vitro* tests with transplant outcomes in the NMB can establish other such tests as acceptable surrogate potency tests. Several recently proposed islet potency tests are, therefore, being judged on the basis of their ability to predict diabetes reversal in the NMB [84; 90; 91; 92; 93; 94; 95; 96; 97; 98; 99; 100; 101]. Even though the NMB is the premiere method available to researchers for the assessment of islet potency, it suffers from numerous limitations (see **Table 2-3**). These limitations include the length of time required to obtain a meaningful outcome, the complexity of the surgical procedure, the difficulties in maintaining diabetic mice healthy and timing diabetes induction with the unpredictable availability of human islets, the negative impact of impurities on outcome [79; 102; 103; 104], the transplant site (the kidney capsule), which may be more prone to the presence of impurities and/or dead tissue than the clinical transplant site (the liver), and the inability to account for

immune rejection or the effects of immunosuppressive drugs that are present in the clinical setting. There have been recent attempts [105; 106] to provide other in-vivo islet potency tests that are alternatives to the diabetic NMB. These alternatives can potentially overcome some, but not all, of the limitations of the NMB.

Desired characteristics of islet potency tests

The assays under consideration for use as potency tests for islet characterization prior to clinical transplantation should be reliable, cost-effective, operator-independent, reproducible and transferable to other laboratories, work with relatively small (yet representative) islet numbers (100–500 IEs), not require islet handpicking (which may bias the results), and should be able to provide real-time results (i.e., completed within hours). Given the heterogeneity of islet preparations and the intrinsic difficulties in characterizing them, assays that possess all of the desired characteristics may be very difficult to develop. This difficulty is reflected in the fact that, despite the intense effort dedicated to develop, implement, and validate a number of assays over the last decade, consensus behind any single assay has not yet been reached. Key viability and potency assays under consideration for the assessment of clinical islet preparations are described next.

Islet viability and potency tests under consideration

Table 2-4 [55; 76; 79; 81; 84; 90; 92; 93; 94; 95; 96; 98] summarizes some of the more recently explored assays used in islet quality assessment, highlighting their key strengths and identified weaknesses. Despite the landscape of flavors available to researchers, many of these assays are most valuable when used in the study of individual cells rather than cell aggregates. Islets are three-dimensional, multicellular

aggregates composed of several different cell types, including the β-, α-, δ-, and pancreatic polypeptide cells. Most assays used to assess cellular viability, apoptosis, or mitochondrial health have been designed for suspensions or cultures of individual cells, not aggregates. Consequently, the development of techniques to study the quality of an islet preparation provides unique challenges. Because the diameter of an IE is 150 mm, it is necessary to consider mass transport limitations, particularly if an assay relies on the availability of molecular oxygen. The relatively large size of the islet makes fluorescence microscopy difficult, subjecting any such analysis to background signal and operator bias that is simply unique to the study of intact multicellular clusters. To circumvent some of the islet shape and size limitations, techniques have been developed to break apart the islets. Digestion with serine proteases and mechanical agitation may be used to dissociate islets into suspensions of their constituent cells, but these techniques result in significant damage to the cells and possibly death by anoikis [107; 108], leading to the loss of as much as 50% of the original cell populations [109; 110; 111]. To minimize the problems associated with islet disaggregation, gentler formulations have been created and used [84]. Yet, it is unclear whether the negative effects of dissociating individual islet cells from one another can be fully minimized. Furthermore, islet preparations have varying amounts of impurities, which complicate the use of any technique designed with the expectation that the studied tissue is comprised entirely of islets. Differentiating the nonendocrine tissue from the islets poses additional difficulties.

Cell membrane integrity tests

These assays interrogate the integrity of the cellular plasma membrane and rely on differential staining using newer combinations of both cell membrane-permeable and

impermeable dyes [76; 81], but have been unable to fully obviate the problems encountered with the current viability stains used prior to product release (i.e., FDA/PI). In fact, some of these proposed stains introduce new issues such as islet toxicity [81]. 7-Aminoactinomycin D (7-AAD, a membrane-impermeable dye) has been used on disaggregated cells in combination with flow cytometry (fluorescence-activated cell sorting or FACS) to enable quantification of the fraction of cells that are viable by membrane integrity, but the method nonetheless requires the undesirable dissociation of the intact islets [81]. An alternative approach relies on sequential staining of membrane-compromised cells within intact islets using 7-AAD. After initially staining with 7-AAD, the nuclei of the entire preparation are released from intact islets using a detergent and subsequently counted by hemocytometer or FACS [112; 113]. The initial count (of nonviable cells) is divided by the second count (of total nuclei) to present a ratio equivalent to fractional viability. This technique bypasses the limitations associated with disaggregation of multicellular spheroids such as islets; however, as a membrane integrity test, it only accounts for dead cells with compromised cell membranes [81; 113].

Other cell death and mitochondrial assays

Several assays attempt to characterize the degree of apoptosis within islet preparations [94; 96]. These assays may depend on the timing of the measurement as it relates to the onset of apoptosis. The magnitude and timing of the responses may also vary between cell types and the unique nature, intensity, and duration of encountered stresses [81]. Importantly, these cell death markers may not be reliable indicators of irreversible damage. Even though mechanistic information regarding the cell death process can be obtained, individual assays may not capture all dying cells and still suffer from limitations that are related to islet size and its three-dimensional structure. A recent study [94]

describes a method to study several apoptosis and cell death-related markers (including VADFMK, Annexin V, and Fura Red) simultaneously using FACS and shows that this sort of multiparametric analysis may more reliably characterize the quality of an islet sample. Another study [96] describes an elegant approach to combine fluorescence imaging of mitochondrial membrane potential (MMP) and Ca^{2+} leakage with measurements of insulin secretion, determined by ELISA. The system involved perfusing a microfluidic chip containing intact islets. The future of islet quality assessment may continue to leverage these types of multimodal techniques in the attempt to map a quality 'fingerprint' of islet preparations prior to their consideration for transplantation. Assays have also been developed to probe the state of mitochondrial health, which span a range of relevant indicators, through assessing the ability of a cell to reduce tetrazolium salts [81; 98], to replenish ATP [55; 92; 93; 95], or to maintain MMP [81; 84; 96]. Tetrazolium salt assays such as MTT have fallen slightly out of favor because many variables, not limited to mitochondrial activity, can affect the ability of a preparation to reduce tetrazolium salts [81]. In contrast, tests that measure the relative abundance of high-energy phosphates (or the ADP/ATP ratio) have reportedly shown promise in predicting IT outcome in mice [92; 93]. However, the ADP/ATP ratio must be interpreted with caution because the concentrations of these metabolites fluctuate rapidly with changing conditions. Furthermore, as recently pointed out [55], the ADP/ATP ratio does not reflect the true viability of an islet preparation, and unlike the ATP/DNA ratio, fails to account for nonviable cells containing no ADP or ATP. Additionally, even though ATP and ADP measurements are simple, inexpensive, and quick to obtain, islet ADP measurements based on luminescence may be unreliable as they frequently provide negative concentration estimates [55]. MMP dyes are used as surrogate measures of mitochondrial health in that they preferentially accumulate in healthy and polarized

mitochondria. Both laser scanning cytometry [84] and the microfluidic system described earlier [96] have been used to correlate MMP with the quality of preparations composed of dissociated and intact islets, respectively.

Oxygen consumption rate

Measurements based on OCR, which is related to mitochondrial function, have been extensively used to assess the viability and health of cells in a variety of fields [114; 115; 116; 117; 118; 119], including islets [91; 97; 98; 99; 120; 121; 122] and β-cell lines in tissue-engineered constructs [123; 124; 125]. Several groups [91; 97; 99; 121] have recently focused their efforts on characterizing islet viability and potency using OCR measurements, and in some cases, correlating these measurements with outcomes in the NMB. Reports [91; 97; 98; 99; 120; 121; 122] on islet respiratory activity include measurements based on scanning electrochemical microscopy [92] and oxygen-sensitive phosphorescence lifetime or fluorescence intensity in a variety of configurations. The instrumentation and methodologies employed along with the strengths and limitations of each approach are outlined in **Table 2-5**. The approach for indirectly measuring OCR using fluorescence intensity in a multiwell plate oxygen biosensor system (OBS) has the distinct advantage of being high throughput and convenient, but in its current form, suffers from several major limitations that prohibit its reliable use [81; 91]. Recent efforts to bypass some of the inherent limitations of the OBS [126] may enable more reliable and effective use of this method in islet potency assessment. Recently published data obtained with the most basic approach, using optical pO_2 sensors in stirred microchambers [98], demonstrate that transplanted OCR (OCR_{TX}, a measure of the amount of viable transplanted tissue) and OCR/DNA (a measure of viability) are sufficient when used in combination to predict outcomes in

diabetic mice transplanted with rat [120; 121], porcine [98], and human [81; 97; 99; 122] islets. These studies suggest that information on the functional capacity of the islets or β-cells is not necessary for predicting transplantation outcomes in mice. In fact, the most recently reported study [121] with rat islets transplanted in immunosuppressed diabetic mice clearly demonstrated this relationship between OCR_{TX} and OCR/DNA of the transplanted islets and diabetes reversal in mice. When the results of these transplantations were plotted such that the ordinate was OCR_{TX} and the abscissa was OCR/DNA of the transplanted islet sample, the data segregated into three regions: an upper and right-most portion in which diabetes was reversed in all animals, a lower left portion in which diabetes was not reversed in any animals, and a narrow band in the middle in which both outcomes were represented. In this study [121], sensitivity and specificity analyses on OCR_{TX} and OCR/DNA exhibited values of 93 and 94%, respectively, in predicting diabetes reversal. Importantly, the marginal mass for diabetes reversal was not fixed [121] but rather depended on OCR/DNA and increased from 2800 to over 100,000 IEs per kilogram recipient body weight (kgBW) as OCR/DNA decreased. These findings are consistent with reports that neither OCR_{TX} nor OCR/DNA, when used individually, correlated with transplant outcomes in mice [79; 127].

Correlation of transplantation outcomes with rat islets was substantially better than that obtained with human islet preparations [97]. There are several likely explanations for this finding, which include the absence of nonislet tissue in rat preparations, the large fraction of nonviable tissue at low OCR/DNA, and the large number of human islets, in contrast with the small number of rat islets, required to reverse diabetes in mice. The predicted probabilities of diabetes reversal with rat islet transplants were sharply defined with a large domain at 100% cure, whereas the analogous plot for human islet

transplants [97] had angled contours of roughly constant slope with virtually no domain of 100% cure, although such a domain might have been attainable if there had been preparations of higher OCR/DNA. The absence of data in the high OCR/DNA range was a limitation of the study with human islets [97]. Data obtained with a porcine-to-nonhuman primate (xenogeneic) model suggest that sustained insulin independence is dependent on both OCR_{TX} per kgBW and OCR/DNA (unpublished observations). Interestingly, initial data obtained with pure and impure clinical autologous and single-donor, allogeneic islet transplants suggest that in these cases (especially islet autotransplants), the OCR dose normalized per kgBW alone may sufficiently correlate with clinical outcomes (unpublished observations). Of particular interest are attempts to extract information on islet potency based on glucose-stimulated OCR, which may be more representative of β-cells and their functional capacity [91; 92; 99; 120; 122]. This index has been represented either as a ratio of the measured OCR in the presence of high glucose divided by the OCR in low glucose (OCR_{hglc}/OCR_{lglc}) or simply the difference in measured OCR in the presence of high and low glucose (ΔOCR_{glc}) [99; 120; 122]. Studies detailing these procedures report reasonable correlations with the NMB and suggest that there may be an advantage in using these indices for clinical islet potency assessment. It remains to be seen whether the challenges associated with widespread implementation and inherent limitations of these complicated methodologies [81] can be overcome and whether the promising results attained with research models will translate into the clinical setting. Work currently under way with clinical autotransplant and allotransplant and preclinical xenotransplant models is expected to provide further insight into these issues and helps identify and establish islet potency tests that are truly predictive of transplant outcomes.

Conclusion

The islet product release criteria that screen preparations before clinical allogeneic IT are currently unable to predict posttransplant success from failure. More sensitive and reliable islet viability and potency tests have been recently developed and tested. Those tests that assess mitochondrial function, particularly those ones that measure the OCR of an islet preparation, appear to be the most promising and correlate with transplant outcomes in the NMB. These tests are currently being evaluated in the clinical setting, and preliminary results are encouraging. Assays that characterize cell composition and molecular profiles may be useful to further define the islet product and may provide useful information on islet immunogenicity and proinflammatory potential. The recent clinical success in reversing diabetes with single-donor, allogeneic ITs will further enhance our ability to define potency tests and islet characteristics that are predictive of transplant outcome.

Table 2-1: Product release criteria for clinical islet preparation

Type of test	Product test	Specification	Type of sample
Safety	Endotoxin	<5 EU/kg	Supernatant of islet suspension in transplant media
	Gram stain	No organisms detected within limits of assay	
Identity	Islet count (IEs/kgBW)	5000-20,000 (1st transplant) 3000-20,000 (Re-transplants)	Islets in transplant media
	Purity	≥30%	
Viability	Dye exclusion (FDA/PI)	≥70%	Islets after overnight culture and in transplant media
Potency	Glucose stimulated insulin release (ELISA)	Stimulation Index >1	Islets after overnight culture

An islet equivalent is defined as a volume of islet tissue equal to that of a sphere having a 150-μm diameter (as given in [80; 81]).
Abbreviations: DTZ, dithizone; ELISA, enzyme-linked immunosorbent assay; EU, endotoxin unit; FDA/PI, fluorescein diacetate/propidium iodide; IE, islet equivalent; kgBW, kilogram recipient body weight.

Table 2-2: Strengths and weaknesses of assays currently used prior to islet product release for clinical transplantation

Assay	Strengths	Weaknesses
Islet count (IE)	Relatively easy to perform counts	Visual assessment of 3D islet in 2D planes contributes to error
	Experienced islet isolation centers have standardized procedures	Sample may not be representative of whole preparation
		Presence of contaminant tissue (e.g., exocrine cells, ganglia, etc) may complicate counts
Purity (DTZ)	Stain differentiates between exocrine and islet tissue	Visual assessment of 3D islet in 2D planes contributes to error
	Relative ease of use	Provides no information regarding viability of preparation
	Rapid assessment	
Cell membrane integrity (FDA/PI)	Relative ease of use	Visual assessment of 3D islet in 2D planes contributes to error
	Can be performed prospectively	Impossible to identify irreversibly damaged cells whose plasma membranes have not yet been permeabilized
	Fractional viability can be estimated by dye exclusion	FDA may be additionally cleaved by lipases or esterases from non-endocrine tissue, over-estimating the true islet viability
		Visual counting is operator-dependent
		Background fluorescence (with certain combinations or high concentrations of dyes) can obscure approximations
		Counterstain may not provide enough contrast
		Dyes rely on diffusion to penetrate into islet core
		Lack of correlation with mitochondrial function assays, NMB and clinical outcomes
		Does not discriminate endocrine (islet) from exocrine (contaminant) tissue
Glucose-stimulated insulin secretion (GSIS)	May provide information regarding potency of islet preparation	Unable to predict true islet potency or transplant outcome
		Islets may not be as responsive to glucose stimulus *in vitro* but may still reverse diabetes *in vivo*
		Difficult to account for degranulation of β cells following glucose stimulus or “leaky” cells with damaged plasma membranes

An islet equivalent is defined as a volume of islet tissue equal to that of a sphere having a 150-μm diameter (as given in [80; 81]).
Abbreviations: 2D, two-dimensional; 3D, three-dimensional; DTZ, dithizone; FDA/PI, fluorescein diacetate/propidium iodide; IE, islet equivalent; NMB, nude mouse bioassay).

Table 2-3: Strengths and weaknesses of the nude mouse bioassay

Assay	Strengths	Weaknesses
Nude mouse bioassay	Most reliable *in vivo* assessment of islet potency	Assay can only be used retrospectively (days to weeks for outcomes)
	Results correlate with clinical outcome	Impure preparations may yield false negative transplant outcomes
		The severity and duration of the diabetic state in the mouse recipient affects the predictive outcome of the assay
		Islets are transplanted under the kidney capsule, not into the hepatic portal vascular tree (and does not represent the current clinical protocol)
		Mice are susceptible to developing other conditions (e.g., infection) that can also affect outcome
		Does not account for immunologic rejection, autoimmune recurrence or islet toxicity associated with immunosuppressive agents
		The assay has several practical challenges (e.g., induction of diabetes needs to be times with islet isolation)

Table 2-4: Advantages and disadvantages of assays being under consideration for clinical islet quality assessment

Assay	Ref.	Advantages	Disadvantages
Membrane integrity tests			
SLM/FM C/EH SYTO/EB AO/PI		Similar advantages as FDA/PI (*Table 2-1*); some stains may exhibit greater sensitivity in detecting islet cell membrane damage	Similar disadvantages as FDA/PI (*Table 2-1*); some dyes are chemically unstable or form crystals which result in visual artifacts; some dyes (like C) can exhibit islet toxicity
FACS 7-AAD[a] Topro3[a]		Minimizes diffusion limitations; semi-quantitative; minimizes operator-dependence; may be β-cell specific; accurate DNA quantification using 7-AAD sequential staining procedure	Requires dissociation of islet aggregates (except with 7-AAD sequential staining), which can cause irreversible cell damage and loss; gating cellular subpopulations in FACS is subjective; requires expensive equipment and training
Other cell death and mitochondrial assays			
Caspase activation (VADFMK[a])		Detects early apoptosis; rapid measurement	Provides only 'snapshot' of early apoptotic events, but may not detect late apoptotic events or necrosis; may require islet dissociation
PS externalization (Annexin V[a]) *DNA fragmentation* (TUNEL[a]) *Ca^{2+} leakage* (Fura Red[a])		May detect both apoptosis and necrosis	Difficult to use prospectively because assay may require histological staining (Annexin V); may require islet dissociation
Reduction potential (Tetrazolium salts)		Detects reducing capacity; easy to use; inexpensive; useful in comparing single variables; can be used with intact islets	Salt reduction involves complex reactions that can be affected by other factors (pO_2, composition of culture medium); accumulation of insoluble byproduct (of MTT) is toxic
Bioenergetic status ADP/ATP ATP/DNA ATP/protein ATP/IE		Easy to use; inexpensive; low islet requirement (~100 IEs); ATP and ADP are important for insulin secretion; can be used with intact islets	ATP concentrations fluctuate rapidly (half-life = ~7 seconds) and are sensitive to transient condition changes (glucose levels, pO_2, pH); islet may have spatial gradients in ATP and ADP; ADP/ATP does not account for nonviable cells; ADP measurements by luminescence assay may be unreliable
Mitochondrial membrane potential JC-1 TMRE[a] Rh123		Detects loss of mitochondrial polarization (early event of apoptosis or necrosis)	Difficult to quantify absolute changes in MMP; may require islet dissociation

DNA can be measured using commercial fluorimetric assay.

[a]Assay has been used on islets in conjunction with FACS, which requires islet dissociation into single cells. Dissociation involves enzymatic digestion and serine proteases which results in disruption of cell-matrix connections, cellular damage, and death (anoikis). FACS analysis is associated with notable limitations, including: subjectivity in gating cell subpopulations, large sample required (~1000 IEs), high cost of equipment, extensive training, and complex methodology which is subject to error.

Abbreviations: 7-AAD, 7-aminoactinomycin D (membrane-impermeable fluorescent dye); AO, acridine orange (membrane-permeable fluorescent dye); C, calcein AM (membrane-permeable fluorescent dye); EH/EB, ethidium homodimer or ethidium bromide (membrane impermeable fluorescent dye); FACS, fluorescent-activated cell sorting (or flow cytometry); FDA, fluorescein diacetate (membrane-permeable that fluoresces green after being cleaved by nonspecific esterases); FM, fluorescence microscopy; IE, islet equivalent (defined as a spherical aggregate of pancreatic endocrine cells or 150-μm diameter); MMP, mitochondrial membrane potential; MTT, tetrazolium salt, 3-(4,5-dimethylthiazol-2-yl)-2,5-diphenyl tetrazolium bromide; PI, propidium iodide (membrane-impermeable fluorescent dye); PS, phosphatidylserine; SLM, standard light microscopy; SYTO, commercially-available membrane-permeable fluorescent dye; VADFMK, membrane-permeable caspase ligand (inhibitor).

Table 2-5: Current methodologies used in the measurement of oxygen consumption rate

System	Method	Ref.	Measured quantities	Assayed tissue	Advantages	Disadvantages
Perifusion bioreactor	Phosphorescence lifetime	[120]	ΔOCR_{glc}	Rat islets	Real-time of transient events (glucose responsiveness, Ca2+ blockade, protein synthesis inhibition); may provide β-cell specific information	Complex system with use currently limited to research
		[99]	ΔOCR_{glc}, OCR_{TX}	Human islets		
Stirred microchamber	Fluorescence quenching	[98]	OCR/DNA, OCR/cell	βTC3 cells; rat islets; porcine islets	Quantitative, rapid and prospective assessment of an islet preparation; operator-independent	May not differentiate between OCR attributed to islets and other cells in a preparation (like acinar)
		[97]	OCR_{TX}, OCR/DNA			
		[121]	OCR_{TX}, OCR/DNA			
Static culture	Fluorescence microplate reader	[122]	OCR_{GS}, OCR_{hglc}/OCR_{lglc}	Non-human primate islets; human islets	Simple, inexpensive and rapid assessment	May not provide accurate estimates of OCR; limited experience with its use in this application; complex theoretical estimation of pO_2
		[91]	OCR, ΔOCR_{glc}/DNA	Human islets		

Abbreviations: ΔOCR_{glc}, the measured increment in OCR when stimulated by glucose (3-20 mmol/L); ΔOCR_{glc}/DNA, the OCR index, a ratio of the estimated ΔOCR_{glc} normalized to DNA; OCR, oxygen consumption rate; OCR/DNA, measure of OCR normalized to DNA, represents the fractional viability of a cellular/islet preparation; OCR_{GS}, glucose-stimulated OCR; OCR_{hglc}/OCR_{lglc}, the stimulation index, a ratio of OCR measured at high glucose concentrations (16.7 or 33.3 mmol/L) to OCR measured at basal concentrations (2.8 or 5.6 mmol/L); OCR_{TX}, transplanted OCR, which represents the islet dose.
DNA can be measured using a commercial fluorimetric assay.

CHAPTER 3: **The ATP/DNA ratio is a better indicator of islet cell viability than the ADP/ATP ratio**

Suszynski T.M., Wildey G.M., Falde E.J., Cline G.W., Maynard K.S., Ko N., Sotiris J., Naji A., Hering B.J., Papas K.K. The ATP/DNA ratio is a better indicator of islet cell viability than the ADP/ATP ratio. Transplant Proc. 40(2): 346-350 (2008)

Permission to reproduce the above publication was given by *Elsevier*, and the agreement (license number: 2924361380000) is found in Appendix 3-1.

Summary

Real-time, accurate assessment of islet viability is critical for avoiding transplantation of non-therapeutic preparations. Measurements of the intracellular ADP/ATP ratio have been recently proposed as useful prospective estimates of islet cell viability and potency. However, non-viable cells may be rapidly depleted of both ATP and ADP, which would render the ratio incapable of accounting for non-viable cells. Since the DNA of non-viable cells is expected to remain stable over prolonged periods of time (days), we hypothesized that use of the ATP/DNA ratio would take into account non-viable cells and may be a better indicator of islet cell viability than the ADP/ATP ratio. We tested this hypothesis using mixtures of healthy and lethally heat-treated (HT) rat insulinoma cells and human islets. Measurements of ATP/DNA and ADP/ATP from the known mixtures of healthy and HT cells and islets were used to evaluate how well these parameters correlated with viability. The results indicated that ATP and ADP were rapidly depleted (within 1 hour) in HT cells. The fraction of HT cells in a mixture correlated linearly with the ATP/DNA ratio, whereas the ADP/ATP ratio was highly scattered, remaining effectively unchanged. Despite similar limitations in both ADP/ATP and ATP/DNA ratios, in that ATP levels may fluctuate significantly and reversibly with metabolic stress, the results indicated that ATP/DNA was a better measure of islet viability than the ADP/ATP ratio.

Abbreviations

ADP	adenosine diphosphate
ATP	adenosine triphosphate
DNA	deoxyribonucleic acid
HPLC	high-performance liquid chromatography
HT	heat-treated
IE(s)	islet equivalent(s)
INS-1	insulinoma-1
LC/MS/MS	electrospray tandem mass spectroscopy
RLU	relative luminescence units
UV	ultraviolet

Introduction

Islet cell transplantation is emerging as a promising therapy for the treatment of type 1 diabetes [49; 50; 68; 128; 129]. Despite recent advances, the transplantation of islets poses a unique challenge with respect to achieving a consistent clinical outcome. Part of this challenge is in being able to reliably and rapidly assess clinical islet quality through the quantification of viability and function before transplantation. Current viability assays are limited in their ability to accurately predict transplantation outcomes *in vivo* [93]. Consequently, to improve the clinical islet transplantation outcomes, it is imperative to develop more accurate viability assays. A proposed method to assess islet viability and potency before transplantation is quantification of the ADP/ATP ratio [90; 93; 130; 131; 132]. This ratio has been specifically applied in discriminating islet preparations that are suitable for clinical transplantation from those that are not [93]. However, this application may be problematic under certain conditions. Intracellular ADP and ATP levels fluctuate rapidly because these high-energy phosphate molecules are rapidly produced and consumed in many intracellular biochemical reactions. It is widely known that viable cells turn over entire ATP stores on the order of minutes, and that dead cells are incapable of replenishing their ATP stores when depleted [81; 133]. Furthermore, dead cells are rapidly depleted of their ADP and ATP [93; 130; 131; 134]. If dead cells are rapidly depleted of their ADP and ATP content, then the ADP/ATP ratio would be incapable of accounting for any dead cells found within an islet preparation and would be effectively overestimating the viability of the preparation.

To better account for dead cells and to more accurately assess the viability of an islet preparation, we suggest the use of an ATP/DNA ratio. DNA does not degrade as rapidly as ADP or ATP in a dead cell. Therefore, using direct measurements of DNA, dead cells

in an islet preparation can be accounted for. Herein, we have described how the ATP/DNA ratio correlates more accurately with viability than the ADP/ATP ratio in mixtures of varying, known proportions of healthy/dead insulinoma-1 (INS-1) cells and human islets.

Methods

INS-1 Cell Culture and Human Islet Isolation and Culture

Clonal INS-1 832/13 cells expressing the human insulin gene (a gift from Dr. Christopher Newgard, Duke University) [135], were grown in culture at 37°C, 5% CO_2 in 75-cm^2 cell culture T-flasks (Corning Inc., Corning, NY). Standard RPMI-1640 culture medium (Sigma-Aldrich, St. Louis, MO) was supplemented with 10% fetal calf serum (Mediatech, Herndon, VA), 10 mmol/L HEPES (Mediatech, Herndon, VA), 2 mmol/L L-glutamine (Sigma-Aldrich, St. Louis, MO), 1 mmol/L sodium pyruvate (Sigma-Aldrich, St. Louis, MO), and 50 µmol/L 2-mercaptoethanol (Sigma-Aldrich, St. Louis, MO). Cells were grown to 60-80% confluence. Human islets were isolated and cultured as described previously [50].

Heat Treatment of INS-1 Cells and Human Islets

Media was aspirated from each flask and cells were treated with 3 mL of 0.05% trypsin/EDTA (Invitrogen, Eugene, OR). After 2 minutes of incubation, trypsin was neutralized with 6 mL of standard serum-supplemented culture media [135]. The cell suspension was transferred into a 15-mL conical tube which was placed into a 60°C water bath for 60 minutes. For time course experiments, aliquots of INS-1 cells were removed from the 15-mL conical tube at specified timepoints (1, 3, 5, 25, and 47 hours). Heat treatment of human islets was performed by transferring 3000 islet equivalents (IEs)

in CMRL 1066 media to a conical tube, which was placed in a 60°C water bath for 5 hours. In the case of the human islet time course experiments, aliquots of 200 IEs in CMRL 1066 media added to 1.5-mL microcentrifuge tubes were placed in a 60°C water bath for 5 hours. Aliquots were removed from the water bath and placed on ice at the specified timepoints (15 minutes, 30 minutes, and 1, 3, 5, and 30 hours). The time 0 samples were placed on ice immediately after preparation. Samples were prepared in triplicate. Prior to deciding on using heat treatment as the method of damaging the cells or islets, other methods were examined (chemical treatment with sodium dithionate or sodium azide, pelleting), and some of this testing is summarized in **Appendix 3-2**.

Preparation of Cellular Mixtures of Known Viability

Heat-treated (HT) cells were considered 100% non-viable (dead), whereas healthy, untreated, surface-attached cells were considered 100% viable. Mixtures containing 0%, 20%, 50%, 80%, and 100% HT cells were prepared from proportioned HT and untreated INS-1 cells or human islets based on DNA measurements. DNA content in healthy and HT cells was determined using the Quant-iT PicoGreen dsDNA assay kit (Invitrogen, Eugene, OR) per manufacturer's instructions. Samples were analyzed using a SpectraMax M5 plate reader system (Molecular Devices, Sunnyvale, CA).

ADP and ATP Measurement with Luminescence-Based Assays

The CellTiter-Glo Luminescent Cell Viability Assay (Promega Corp, Madison, WI) was used per manufacturer instructions to measure ATP. The ApoGlow BioAssay (Adenylate Nucleotide Ratio Assay) kit (Cambrex Bio Science Rockland, Inc., Rockland, ME) was used for ADP/ATP determination per manufacturer instructions as described previously [93]. Sample preparation for analysis using the CellTiter-Glo and ApoGlow assays kit

was performed in the same manner: three 100-µL cell suspension samples were taken from each mixture immediately after preparation. Each sample was diluted 10-fold in Dulbecco's phosphate buffered saline (DPBS, Mediatech, Herndon, VA) and sonicated at an amplitude of 11% for 15 seconds (Sonic Dismemberator Model 500, Fisher Scientific, Hampton, NH). Samples prepared per kit instructions were plated in 96-white-well plates (Corning 3912, Corning Inc., Corning, NY) for luminescence readings on a SpectraMax M5 (Molecular Devices, Sunnyvale, CA) plate reader. Serially diluted ATP (Sigma-Aldrich, St. Louis, MO) was used as a standard in both the CellTiter-Glo and ApoGlow assays. To measure DNA content, the same samples, which had been analyzed using the CellTiter-Glo and ApoGlow kits for ATP and ADP/ATP measurement were diluted an additional 10-fold in an aqueous solution of 1 mol/L ammonium hydroxide (Mallinckrodt, St. Louis, MO) and 3.4 mmol/L Triton X-100 (Sigma-Aldrich, St. Louis, MO). DNA content was then determined using the Quant-iT PicoGreen dsDNA assay kit per manufacturer instructions.

Electrospray Tandem Mass Spectroscopy (LC/MS/MS) Analysis of Nucleotides

LC/MS/MS was used to measure the concentrations of purine nucleotides in cell samples [136]. Tandem mass spectroscopy provides an advantage over high-performance liquid chromatography (HPLC) with ultraviolet (UV) detection in that each purine nucleotide is monitored by unique ion pairs, thereby minimizing artifactual signals from co-eluting metabolites. Viability mixtures and time course samples were centrifuged at 175 x *g* for 4 minutes at 4°C and the supernatant was aspirated. Cells were resuspended in a 50:50 mixture of water and acetonitrile containing 2 mmol/L ammonium acetate and subsequently sonicated at an amplitude of 11% for 15 seconds with a Sonic Dismemberator (Model 500, Fisher Scientific, Hampton, NH). Samples were

stored at -80°C until shipped to Yale University on dry ice for assay. ATP and ADP concentrations in samples of INS-1 and islet cell extracts were measured with an API 4000 Qtrap LC/MS/MS (PE Sciex, Foster City, CA) equipped with a turbo ion spray as described previously [136; 137]. D4-Taurine was used as an internal standard for quantification of MS/MS ion intensities.

Results

A typical set of ATP and ADP measurements obtained for untreated, healthy INS-1 cells using the ApoGlow BioAssay kit following manufacturer instructions as well as published protocols [93] is presented in **Figure 3-1**. Based on the published protocol, the ADP/ATP ratio is calculated by dividing the difference in relative luminescence units (RLU) between points *C* and *B* as indicated in the curve (a measure of the amount of ADP in the sample) by the RLU measured at point *A* (a measure of the amount of ATP in the sample). According to the protocol ADP/ATP = (*C* – *B*)/*A.* The expectation is that the value for *C* will be higher than *B,* resulting in a positive (*C* – *B*) value and thus positive ADP value and ADP/ATP ratio. Although ATP measurements yielded positive and reasonable values (see point *A* on *Figure 3-1*), negative ADP values were commonly observed (point *C* in experimental data was lower than point *B*). ADP values obtained from INS-1 cell and human islet samples, and ADP standards with this method yielded negative values in the vast majority of cases. Human islets as well as mixtures of ATP and ADP standards sent to a collaborating lab at the University of Pennsylvania, where they examined the samples with the same ApoGlow kit and concluded that negative ADP values were very common, confirming our observations. The negative values obtained for ADP do not have a physical meaning, were deemed unreliable, and limited the utility of the ADP/ATP ratio generated by this method. Consequently, LC/MS/MS was

utilized as an alternative method for the measurement of high-energy phosphates. It was used to successfully measure ADP and ATP, as well as to calculate ADP/ATP ratios in INS-1 cells and human islets of varying viability. ATP and ADP measurements on HT INS-1 cells and human islets conducted with LC/MS/MS analysis confirmed that intracellular ATP as well as ADP content was effectively zero within 30 minutes of HT in a 60°C water bath. On the contrary, the DNA content in the same samples as determined using the Quant-iT PicoGreen DNA assay remained constant, even two days after initiation of heat treatment. These findings confirm that DNA, as measured with these assays was significantly more stable under conditions of cellular stress or death than ATP and ADP. The differences between the kinetics of degradation for ATP, ADP, and DNA in cells undergoing heat treatment are demonstrated In **Figure 3-2**. Using the LC/MS/MS measurements of ATP and ADP of 100% HT and 100% healthy INS-1 cells and human islets, we estimated the expected ATP/DNA and ADP/ATP ratios in mixtures of healthy and HT INS-1 cells and human islets. Based on the data presented in *Figure 3-2*, we assumed that ATP and ADP in dead cells was equal to zero and that the DNA in healthy and HT cells was constant (for HT cells this is true for at least two days as indicated in *Figure 3-2*). **Equation 3-1** was used to estimate the ADP to ATP ratio of the mixtures,

(3-1) $$\left(\frac{ADP}{ATP}\right)_{mix} = \frac{x \cdot ADP_{HC} + (1-x) \cdot ADP_{HTC}}{x \cdot ATP_{HC} + (1-x) \cdot ATP_{HTC}}$$

and **Equation 3-2** was used to estimate the ATP/DNA of the mixtures,

(3-2) $$\left(\frac{ADP}{ATP}\right)_{mix} = \frac{x \cdot ATP_{HC} + (1-x) \cdot ATP_{HTC}}{x \cdot DNA_{HC} + (1-x) \cdot DNA_{HTC}}$$

where *x* is the fraction of healthy cells, (1 – *x*) is the fraction of HT cells in the mixtures, HC denotes healthy cells and HTC denotes HT cells. Using *Equations 3-1* and *3-2*, and the assumptions listed, we generated values for ATP/DNA and ADP/ATP ratios for mixtures with varying proportions of HT and healthy INS-1 cells or islets. The values were normalized and expressed as a percentage of those measured in 100% healthy cells. These values were plotted versus the fraction of HT cells in mixtures of HT and healthy cells (**Figure 3-3**). These results illustrated that ATP/DNA correlated linearly with the viability expected in mixtures of healthy and HT (non-viable) cells, whereas ADP/ATP did not.

Normalized ATP/DNA ratios measured in INS-1 cell preparations with three methods (CellTiter-Glo, ApoGlow, and LC/MS/MS) exhibited linear correlations with the fraction of HT cells in the preparation (**Figure 3-4**). The slopes (mean values ± standard deviation) and R^2 of the linear correlations shown in *Figure 3-4* are estimated using linear regression analysis of the data obtained with the three methods: -1.03 ± 0.03, R^2 = 0.997 for CellTiter-Glo; -1.00 ± 0.06, R^2 = 0.956 for ApoGlow; and -1.01 ± 0.04, R^2 = 0.976 for LC/MS/MS. Similar results were obtained with human islets (data not shown, see **Appendix 3-3**). On the contrary, ADP/ATP ratios measured from the same INS-1 and human islet cell samples using either the ApoGlow bioassay or LC/MS/MS exhibited significant scatter and did not correlate with viability in mixtures of healthy and HT INS-1 cells or human islets (data not shown, see **Appendix 3-4**).

Discussion

It seems rather safe to assert that intracellular DNA levels remain relatively stable during heat treatment, whereas ATP and ADP levels drop rapidly to zero (or near-zero) after application of heat stress. Both ATP and ADP levels fall so rapidly after death that any contribution of dead cells to an overall viability estimate becomes negligible. The commercially-available assays themselves may pose limitations that make this measurement practically difficult, in that they may lack adequate sensitivity to measure low ATP and ADP levels. Another issue with the ADP/ATP ratio is how this quantity is interpreted. In one study, an ADP/ATP ratio of a certain magnitude was interpreted to indicate high islet viability [93], whereas in a separate study, a similar ADP/ATP ratio was interpreted to suggest a cellular preparation exhibited a significant level of apoptosis [138]. Additionally, a different study asserted that an elevation in cytosolic ATP, and thus a decline in the ADP/ATP ratio even below levels detected in healthy cells, was necessary for propagation of apoptosis [139]. Therefore, there is even significant disagreement in the literature concerning the meaning of the ADP/ATP ratio as it relates to the quality of a cellular preparation; both high and low ADP/ATP ratios have been associated with increased cell death. It has been hypothesized that the increase in cytosolic ATP in cells undergoing apoptosis will not be sustained and that ATP as well as ADP will be depleted shortly after the execution phase of apoptosis. In this sense, the ADP/ATP ratio is strictly dependent on the timing of the measurement as it relates to the onset of apoptosis. This ambiguity in interpretation by different groups and the dependence of the ratio on the kinetics of the cell death process suggest that there is limited potential for use of the ADP/ATP ratio as a predictive tool to assess the viability of a cellular preparation before transplantation. Despite these facts, the ADP/ATP ratio, when measured properly, provides a snapshot into the bio-energetic status of a cell or

tissue. It has been successfully used to assess the metabolic state of a variety of tissues under various conditions [140; 141; 142]. The ATP/DNA ratio suffers similar limitations, but DNA does not degrade as quickly in dead cells as either ATP or ADP. Because of this profound difference in the kinetics of degradation of DNA under conditions of stress, the ATP/DNA ratio permits the inclusion of dead cells into a viability estimate once the apoptotic process is fully executed. Consequently, the ATP/DNA ratio may provide a more accurate assessment of islet cell viability compared to with the ADP/ATP ratio. This was clearly demonstrated in the current study with HT INS-1 cells and islets. Additional studies are necessary to establish whether the mode of cell death or the type of lethal stress has an impact on the kinetics of nucleotide and DNA degradation and how that affects viability estimates based on either the ATP/DNA or the ADP/ATP ratio under actual islet manufacturing and culture conditions.

Figure Captions

Figure 3-1: Trace of recordings for an ATP and ADP/ATP ratio measurement in an individual sample using the ApoGlow kit according to the included protocol. Data illustrates the mean of five wells from a sample of healthy, untreated INS-1 cells. The dotted line illustrates the expected kinetics of the assay. ADP/ATP ratio is calculated by dividing the difference in RLU between points *C* and *B* (a measure of the ADP content in the sample) by the RLU measured at point *A* (a measure of the ATP content in the sample). Accordingly ADP/ATP = (*C* – *B*)/*A*. *Abbreviations*: ADP, adenosine diphosphate; ATP, adenosine triphosphate; RLU, relative luminescence unit.

Figure 3-2: ATP and DNA content measured in INS-1 cells and ATP and ADP content measured in human islets plotted versus the time from the onset of heat treatment in 60°C water bath. Measurements were conducted with the method indicated in the legend for *Figure 3-1*. ATP, ADP, and DNA content are expressed as percent of time zero measurements (before the onset of heat treatment). Data illustrates the mean of three separate experiments (n = 3), with triplicates taken for each sample. Note the staggered x-axis scale. *Abbreviations*: ADP, adenosine diphosphate; ATP, adenosine triphosphate; DNA, deoxyribonucleic acid.

Figure 3-3: Predicted ADP/ATP and ATP/DNA ratios in mixtures of healthy and HT cells. Ratios were calculated assuming zero ATP or ADP present in the HT cells. HT cells were regarded as possessing measurable levels of only DNA, which was supported by our measurements shown in *Figure 3-2* as well as LC/MS/MS measurements from samples of HT cells. Predictions for ADP/ATP and ATP/DNA are projected to mixtures containing close to but not equal to 100% HT cells or islets. In samples containing 100%

HT cells or islets the ADP/ATP that is undetermined (0/0), and the ATP/DNA ratio is zero. *Abbreviations*: ADP, adenosine diphosphate; ATP, adenosine triphosphate; DNA, deoxyribonucleic acid; HT, heat-treated.

Figure 3-4: ATP/DNA ratio presented as a function of the fraction of dead cells in mixtures of HT and healthy INS-1 cells. ATP/DNA values for mixtures of healthy and HT INS-1 cells were normalized to the ATP/DNA value measured in healthy cells and are reported as percentages of that value. Data illustrate three methods of measuring ATP from the same original samples. Samples were measured in triplicate with each method. *Abbreviations*: ATP, adenosine triphosphate; DNA, deoxyribonucleic acid; HT, heat-treated; INS, insulinoma.

Figure 3-1

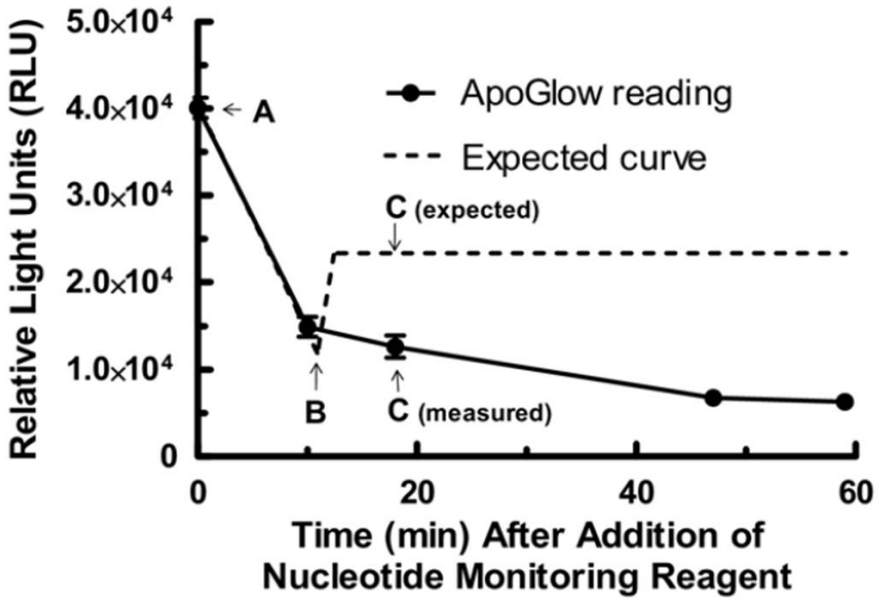
Relative Light Units (RLU)
5.0×10⁴
4.0×10⁴
3.0×10⁴
2.0×10⁴
1.0×10⁴
0
A
B
C (measured)
C (expected)
ApoGlow reading
Expected curve
0
20
40
60
Time (min) After Addition of
Nucleotide Monitoring Reagent

Figure 3-2

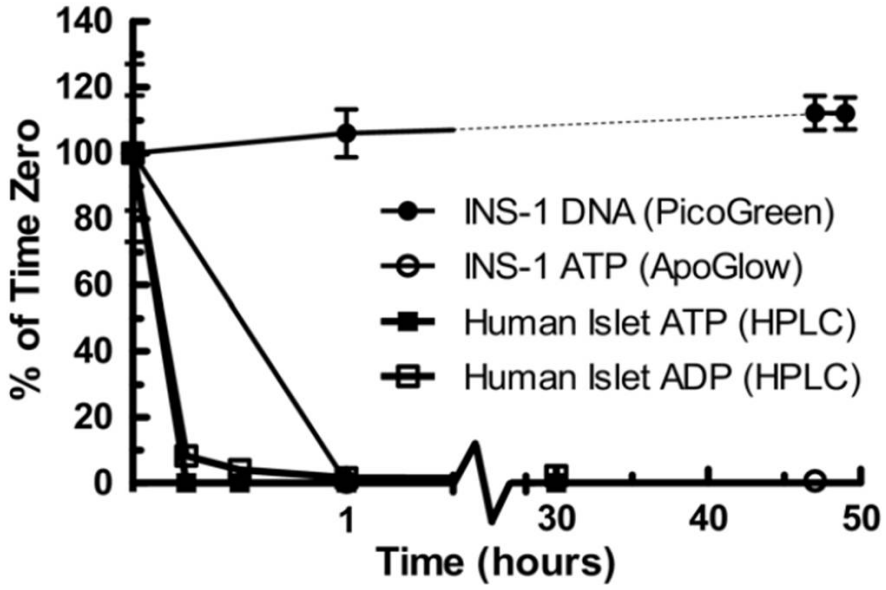
140
120
100
80
60
40
20
0
% of Time Zero
1
30
40
50
Time (hours)
INS-1 DNA (PicoGreen)
INS-1 ATP (ApoGlow)
Human Islet ATP (HPLC)
Human Islet ADP (HPLC)

Figure 3-3

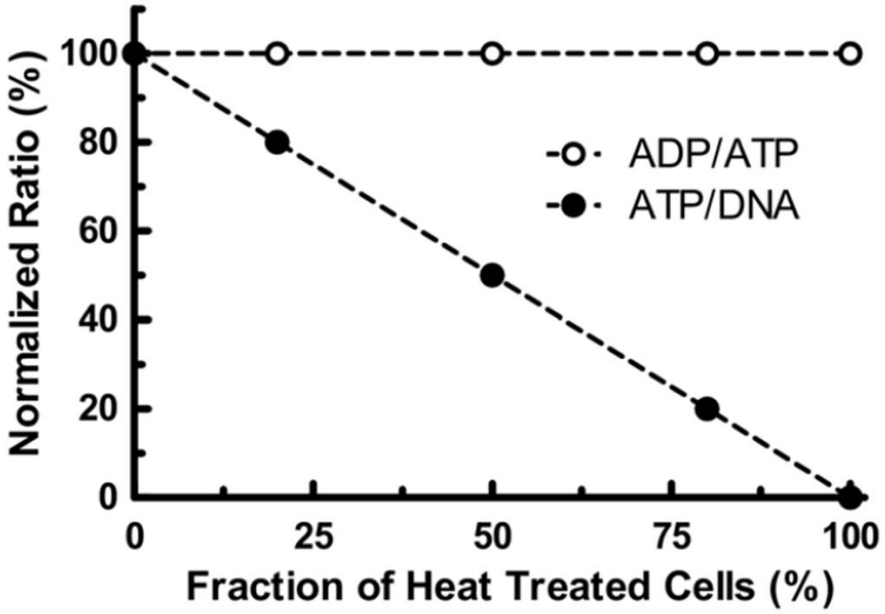
Normalized Ratio (%)
100
80
60
40
20
0
0
25
50
75
100
Fraction of Heat Treated Cells (%)
ADP/ATP
ATP/DNA

Figure 3-4

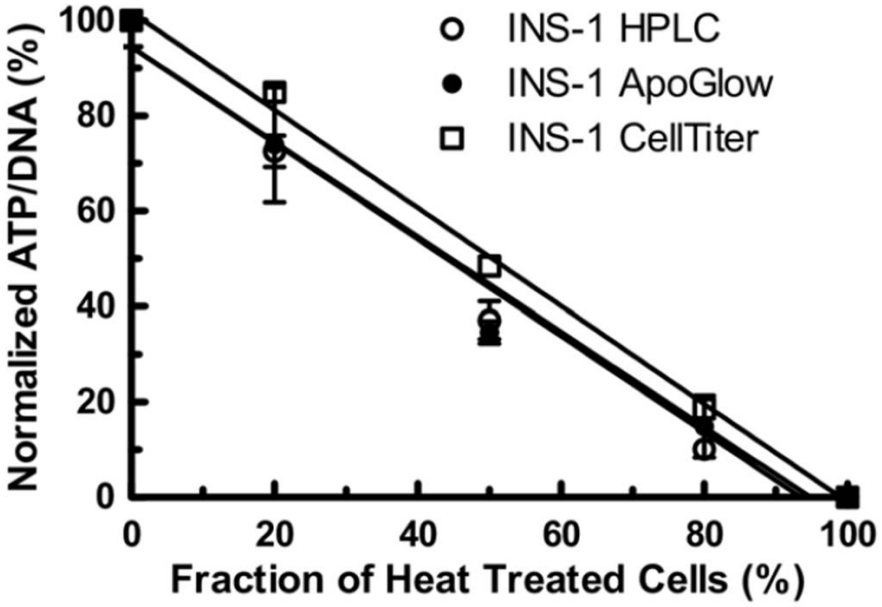
INS-1 HPLC
INS-1 ApoGlow
INS-1 CellTiter
Normalized ATP/DNA (%)
Fraction of Heat Treated Cells (%)
0
20
40
60
80
100

CHAPTER 4: Oxygenation of the Intraportally Transplanted Islet

Summary

Islet transplantation (IT) is not widely utilized as a treatment for type 1 diabetes in part because of the large numbers of islets needed to achieve durable insulin independence. Many islets are lost in the early post-IT period, suggesting that the liver may not be the optimal site. Oxygenation at the individual islet level has not been studied extensively in this setting. We present a diffusion-reaction model that predicts the formation of an *anoxic*, *non-viable* core and a *hypoxic*, *non-functional* core within an intraportally transplanted islet. Four variables are studied: islet diameter and fractional viability, external pO_2 (in the surrounding portal blood), and presence or absence of a 100-μm thick thrombus on the surface of the islet. The anoxic volume fraction (AVF) was defined as the region of the islet below a critical anoxic pO_2 (P_a) of 0.1 mm Hg, and the non-functional volume fraction (NFVF) below a critical non-functional pO_2 (P^*) of 5, 10 and 15 mm Hg. Results indicate that for an islet with average size (150-μm diameter) and viability, the AVF approached 14% but the NFVF ($P^* \leq 15$ mm Hg) was up to 91%, at an external pO_2 of 5 mm Hg. Thrombus formation increased AVF by up to 17% and NFVF by up to 35%, suggesting that the effect of thrombosis on oxygen delivery may be substantial. Larger and more viable islets exhibit greater AVF and NFVF for all cases examined, with islet diameter exhibiting the greater overall impact. At our institution, high-purity, post-culture human islets with an average diameter <200-μm account for ~80% of total islet number, but only ~28% of total islet volume, indicating that a significant fraction of total islet volume is accounted for by islets of large diameter (>200-μm) and may be non-viable or non-functional after islet infusion. The liver may not be the best site for IT and that may be in part due to poor oxygenation.

Abbreviations (Text)

ATP	adenosine triphosphate
AVF	anoxic volume fraction
CD3	cluster of differentiation 3
δ	thickness of thrombus
DNA	deoxyribonucleic acid
DR	diabetes reversal
EP	Edmonton protocol
GSIS	glucose-stimulated insulin secretion
HIF-1α	hypoxia inducible factor-1 alpha
IBMIR	instant blood-mediated inflammatory reaction
IE	islet equivalent
IL-2	interleukin-2
IT	islet transplantation
kgBW	kilogram body weight
mAb	monoclonal antibody
mTOR	mammalian target of rapamycin
NFVF	non-functional volume fraction
OCR	oxygen consumption rate
pO_2	oxygen partial pressure
PP	pancreatic polypeptide
R	islet radius
SE	standard error
SIR	sirolimus

TAC	tacrolimus
TF	tissue factor
TNF	tumor necrosis factor
VEGF	vascular endothelial growth factor

Abbreviations (Formulaic)

$(\alpha D)_i$	oxygen permeability in constituent *i* [mol/cm/mm Hg/sec)]
K_m	Michaelis-Menten constant [mm Hg]
OCR	maximum oxygen consumption rate per unit islet volume [mol/cm^3/sec]
OCR/DNA	maximum oxygen consumption rate per islet DNA content [nmol/min/mg DNA]
P^*	critical pO_2 for insulin secretion (function) [mm Hg]
P_a	critical pO_2 for oxygen consumption (viability) [mm Hg]
P_{ext}	external blood oxygen partial pressure [mm Hg]
P	local oxygen partial pressure [mm Hg]
S	local insulin secretion rate [amount/time]
S_{max}	maximum insulin secretion rate (non-oxygen-limited) [amount/time]
V_{O_2}	local rate of oxygen consumption per unit islet volume [mol/cm^3/sec)]

Introduction

Islet transplantation (IT) remains a promising therapy for diabetes mellitus, but current results have justified its clinical use only with a small subset of type 1 diabetics with low body mass index and metabolic instability (hypoglycemic unawareness, advanced secondary complications despite insulin therapy). In 2000, the Edmonton Protocol (EP), which recommended the transplantation of a large number of islets (>10,000 islet equivalents [IEs] per kilogram body weight [kgBW]) with a specialized steroid-free immunosuppressive protocol (low-dose tacrolimus, sirolimus and IL-2 receptor antibody induction), enabled consistent diabetes reversal (DR) and short-term (<1 year) insulin independence [43; 44; 45]. These results were replicated at other institutions [68; 143], but long-term (>5 years) outcomes on the EP remained elusive [46]. Despite being a major breakthrough, the EP required donor islets isolated from 2-4 pancreata, The requirement of multiple pancreas donors is a major limitation that prohibits widespread availability of IT due to increased costs and clinical risk (of multiple procedures), and the additional strain on an already limited donor pancreas supply. In the mid-2000s, new trials were undertaken to establish protocols that enable successful IT using islets from a single donor pancreas [47; 50]. Newer induction immunosuppressive agent combinations (T-cell depleting antibody [anti-CD3 antibody, alemtuzumab, or antithymocyte globulin] and a TNF-α inhibitor [etanercept or infliximab]) have in part improved long-term DR rates (~50% at 5 years at the most experienced centers) [51], presumably by preserving transplanted β-cell mass, but allo-IT cannot yet be offered to all type 1 diabetics. It remains unclear whether immunologic or nonimmunologic causes are primarily responsible for the gradual attrition of durable insulin independence with respect to time.

Many investigators believe that the liver may not be the optimal IT site and there are numerous reasons, including but not limited to: (1) intraportal thrombus formation, complement-mediated cell lysis, and local inflammation [144], sometimes collectively referred to as the 'instant blood-mediated inflammatory reaction', are believed to contribute to alloimmune rejection and early islet loss [145]; (2) the possible immediate exposure to islet cell-directed T memory cells and recurrence of autoimmune rejection [146]; (3) the higher local concentrations of orally-administered immunosuppressants [147], which can impair insulin secretion or islet revascularization [148; 149]; (4) slow reestablishment of surrounding extracellular matrix, which can adversely affect islet survival [107; 150]; (5) inability to easily track, image or retrieve the graft [151; 152]; and (6) poor oxygenation due to the mixed portal circulation, significant oxygen gradients within the hepatic tissue [153], and slow and possibly incomplete revascularization [154; 155; 156; 157], which is of particular importance since insulin-secreting β-cells are not designed to function during hypoxia [158]. The last reason, poor oxygenation, is not well-appreciated and has not been well-studied by the field. The assumption may be that oxygen levels are adequate for islet survival and function simply because islets are in direct contact with the blood stream. However, there are major differences in the route and mechanism for oxygen delivery when comparing a native islet in a healthy pancreas and an intraportally transplanted islet (**Figure 4-1**). First, a native islet is highly perfused with oxygen-saturated arterial blood (receiving 15-20% of total blood flow to the pancreas [159] despite accounting for 1-2% of the total pancreatic volume [160] or mass [161]), but the intraportal islet has no blood perfusion starting at the time of organ procurement and from that point relies on oxygen diffusion from its surface until it can be revascularized. Second, most native islet cells are within the distance of a single cell from the nearest oxygen source [162], whereas cells in the core can be >200 μm away

from the intraportal islet surface and even further away from the oxygen source if there is thrombus formation.

To illustrate the effect of oxygenation, we present a model that predicts the formation of an anoxic, non-viable core and a hypoxic, non-functional core within an intraportally transplanted islet, in the presence or absence of thrombus formation. We also discuss its potential implications for clinical IT.

Methods

Modeling of steady-state oxygen delivery into islets was performed using COMSOL Multiphysics (Burlington, MA). An islet was assumed to be a spherical body of uniformly-viable, oxygen-consuming tissue that is lodged near a bifurcation of a distal hepatic sinusoid, and only has access to blood oxygen from its proximal half surface. Oxygen transport is by diffusion alone, either directly from the bloodstream or through a thrombus which surrounds the islet, and which obeys the mass conservation relation, which for a perfect sphere and in its general form accounts for steady-state diffusion and oxygen consumption (reaction) within the islet (**Equation 4-1**).

(4-1) $$(\alpha D)_i \nabla^2 P = V_{O_2}$$

where $(\alpha D)_i$ is the oxygen permeability (which is the product of oxygen solubility and diffusion coefficients) within each constituent *i* – either the islet or thrombus, ∇^2 is the Laplacian operator (which represents the second-derivative with respect to all three spatial directions), *P* is the spatially-dependent local pO_2, and V_{O_2} is the rate of oxygen

consumption per unit islet volume. We solve this equation as a two-dimensional axisymmetric problem because we assume there is no azimuthal variation.

A no-flux boundary condition ($\partial P/\partial r = 0$) is applied at a 100-μm semi-circle behind the lodged islet. We obtained most model constants from literature, including oxygen permeabilities for both an islet [163; 164] and thrombus [165]. There are four independent variables that are adjusted in this model:

(a) Islet fractional viability [*OCR/DNA*];

(b) Islet diameter [$2 \cdot R$];

(3) External oxygen partial pressure [pO_2, or P_{ext}]; and

(4) Presence or absence of thrombus [with specified thickness, δ], which is only located on the proximal half-surface of the islet.

The thrombus is assumed to contain no oxygen-consuming tissue and thus solely represents an additional oxygen transfer resistance. All independent variables are studied within ranges that are reasonable based on prior experimental evidence. All values for model constants and variables used in this study are presented in **Table 4-1**.

The oxygen consumption rate (*OCR*) of the islet is modeled using Michaelis-Menten kinetics (**Equation 4-2**):

(4-2) $$V_{O_2} = \left(V_{O_2}\right)_{max} \cdot \frac{P}{K_m + P}$$

where $\left(V_{O_2}\right)_{max}$ is the maximum volumetric islet oxygen consumption rate, which can be directly measured by conventional methods, and K_m is the Michaelis-Menten constant for islet oxygen consumption, which is estimated to be ~0.5 mm Hg [166]. We used a representative range of values for $\left(V_{O_2}\right)_{max}$ [units of mol/sec/cm^3] which were obtained by converting from actual values of *OCR/DNA* [units of nmol/min/mg DNA] obtained via characterization of β-cells [98], porcine islets [58], and human auto- and allo-islets using the stirred microchamber system [97; 167]. The unit conversion between *OCR/DNA* and $\left(V_{O_2}\right)_{max}$ was done by assuming that a spherical islet of 150-μm diameter contains 10.4 ng of DNA [81], and the conversion factor is shown in **Equation 4-3**.

(4-3) $$\left(V_{O_2}\right)_{max} = (OCR/DNA) \cdot (9.8 \cdot 10^{-11})$$

To model an anoxic core within the islet, a critical pO_2 (P_a) at which the islet is anoxic and becomes non-viable (at P_a < 0.1 mm Hg) was defined, and which has been shown experimentally [168]. At calculated pO_2 values below or equal to P_a ($P \leq P_a$), V_{O_2} was assumed to be zero. Using this model, the anoxic volume fraction (AVF) could be calculated using **Equation 4-4**.

(4-4) $$AVF = \frac{V|_{P \leq P_a}}{\left(\frac{4\pi}{3}\right)R^3}$$

where V is calculated volume and R is the islet radius.

To model a non-functional core within the islet, another critical pO_2 (P^*) at which the islet becomes non-functional (at P^* < 5, 10 or 15 mm Hg) was defined and which was distinct

from the P_a at which the islet becomes non-viable (at P_a < 0.1 mm Hg). The values selected for non-functional P^* were determined from past studies of impaired insulin secretion rate with hypoxia [87; 164; 169; 170], and where it has been shown in freshly isolated rat islets that second-phase insulin secretory capacity decreases by ~50% at 25 mm Hg and by ≥98% at 5 mm Hg [87; 164]. There were three regimes defined by distinct rates of insulin secretion capacity relative to normal under specified conditions. Above P^*, the local insulin secretion rate (S) was assumed to remain constant at a healthy level, which we define as a maximum insulin secretion rate (S_{max}). Between P^* and P_a, S was assumed to decrease in proportion with P. Below P_a, S was assumed to be zero.

We applied a 2-step *ad hoc* model for local insulin secretion that has been previously described [166], where the first step is a first-order reaction in terms of P and the second step is a zero-order reaction with a modification that insulin-secreting β-cells are located homogeneously throughout the volume of the islet. Using this model, the non-functional volume fraction (NFVF) could be calculated (**Equation 4-5**).

$$NFVF = 1 - \frac{\int_V \min\left(\frac{P}{P^*},1\right)\Big|_{P>P_a} dV}{\left(\frac{4\pi}{3}\right)R^3} \tag{4-5}$$

where V is the volume of a spherical islet. **Figure 4-2** depicts a schematic that illustrates the generalized model geometry, key variables and boundary conditions.

Results

We calculated the anoxic volume fraction (AVF) and the non-functional volume fraction (NFVF) for intraportally transplanted islets of different nature (size, viability) and in different local environments (external pO_2, thrombosis). The AVF was calculated assuming a P_a of 0.1 mm Hg (the minimum pO_2 for islet cell survival), and the NFVF was calculated assuming a P^* of 5, 10 or 15 mm Hg (the range of pO_2 studied for impaired islet cell insulin secretion). These data are summarized for all cases without thrombosis (**Table 4-2**) and with thrombosis (**Table 4-3**). The percent change in AVF and NFVF that is attributable to thrombus formation has also been summarized (**Table 4-4**). Additionally, the minimum and maximum calculated intraislet pO_2 values have been noted for all cases without thrombosis (**Table 4-5**) and with thrombosis (**Table 4-6**), including the magnitude change in intraislet pO_2 with the addition of a thrombus (**Table 4-7**).

For illustration, consider a *Baseline Case*: an intraportal islet with average size [$2 \cdot R$ = 150 μm] and viability [*OCR/DNA* = 200 nmol/min/mg DNA], exposed to a reasonable but low external pO_2 [P_{ext} = 15 mm Hg] and with no thrombus formation at its proximal half-surface (**Figure 4-3**). In this case, the calculated AVF is 0%. However, depending on the critical pO_2 required for normal insulin secretion in that particular islet, the NFVF can be 13% (P^* = 5 mm Hg) and up to 51% (P^* = 15 mm Hg). The relative impact of thrombus formation, islet size and viability, and external pO_2 can be examined by adjusting single model variables (**Figure 4-4**). If the same intraportal islet described by the *Baseline Case* has a 100-μm thick thrombus form on its proximal half-surface, then a small anoxic core (AVF = 3%) and a much larger non-functional core (NFVF = 42-78%) will form (*Case A*). If the same islet is highly viable and has a greater OCR/DNA (300 instead of 200), then it will develop a small anoxic core (AVF = 3%) and a significant non-functional

core (NFVF = 29-62%). Of note, the relative impact on oxygenation appears to be similar to thrombus formation (*Case B*). If the same islet is exposed to much lower external pO_2 (P_{ext} = 5 mm Hg), then it will develop a larger anoxic core (AVF = 14%) and non-functional core (NFVF = 72-91%) (*Case C*). Finally, if the same islet is larger in size ($2 \cdot R$ = 300 μm), then it develops the largest anoxic core (AVF = 31%) and non-functional core (NFVF = 63-81%) for any single variable adjustment within a reasonable range of values (*Case D*). If the single variable adjustments (of *Cases A-D*) are combined so that the islet proposed in the *Baseline Case* is now with a thrombus on its proximal half-surface, of higher viability [*OCR/DNA* = 300 nmol/min/mg DNA] and size [$2 \cdot R$ = 300 μm], and exposed to a very low external pO_2 [P_{ext} = 5 mm Hg], then the anoxic core is most of the islet (AVF = 77%) and the islet is effectively not secreting insulin (NFVF = 98-100%); this represents the worst case scenario from the standpoint of oxygenation (**Figure 4-5**, *Worst Case*).

The relative impact of islet viability and size is further examined by plotting the AVF (**Figure 4-6**) and NFVF (for P^* = 5 mm Hg, **Figure 4-7**) with variable external pO_2 (P_{ext} = 5-40 mm Hg) and with or without thrombus formation. Within the range of islet OCR/DNA values and diameters examined, it appears that islet size more strongly affects the magnitude of both AVF and NFVF. Additionally, the formation of a thrombus appears to markedly affect islet cell death and non-function.

These data suggest that oxygenation is important at the individual islet level, but the results can be also applied to an entire islet preparation. For example, actual size distribution data from 23 clinical human islet preparations (high-purity, cultured prior to transplant) prepared at the University of Minnesota (5/19/2009-1/8/2012) show that the

vast majority of islets are <200 μm in diameter (~80%) (**Figure 4-8**). If these islets are assumed to be spherical, then the number fractions can be converted to volume fractions. These calculations indicate that despite accounting for most of the islets by number, islets with <200 μm diameter account for only ~28% of the total volume of an islet preparation, which may have significant practical implications regarding intraportal islet viability and function. The AVF and NFVF calculated for an individual islet can be extrapolated for an entire islet preparation based on the actual number and estimated volume fraction data (**Tables 4-8** and **4-9**). Assuming that no thrombosis occurs, the AVF for an entire islet preparation of average viability may be >30% at low external pO_2 (P_{ext} = 5 mm Hg) and ~4% at higher external pO_2 (P_{ext} = 40 mm Hg), and the NFVF may be >10% (for P_{ext} = 40 mm Hg, P^* = 5 mm Hg) and in some cases >90% (for P_{ext} = 5 mm Hg, P^* = 15 mm Hg). When thrombus formation is assumed to occur, the AVF for an entire islet preparation of average viability may be >40% at low external pO_2 (P_{ext} = 5 mm Hg) and ~10% at higher external pO_2 (P_{ext} = 40 mm Hg), and the NFVF may be ~24% (for P_{ext} = 40 mm Hg, P^* = 5 mm Hg) and in some cases >97% (for P_{ext} = 5 mm Hg, P^* = 15 mm Hg). These theoretical estimates indicate that a large proportion of the therapeutic β-cell mass in a representative human islet preparation may be adversely affected by poor oxygenation post-IT.

Discussion

Our model results indicate the relative effect of four important variables (islet size and OCR, local pO_2 and thrombosis) on the oxygenation of the intraportally transplanted islet. Islet size appears to have the greatest single effect on islet viability (i.e., AVF) and function (i.e., NFVF) in any individual islet, but all of these variables are found to contribute synergistically. Thrombosis can also have a significant effect on islet

oxygenation, regardless of the specific conditions. As discussed earlier, allo-IT has not been expanded into widespread clinical use because durable insulin independence remains elusive. However, it is unclear what is responsible for the gradual attrition of islets over time, and likely involves some combination of immunologic (inflammation, autoimmune or alloimmune rejection, cytokine-mediated injury, immunosuppressant toxicity) and nonimmunologic causes (stress-mediated apoptosis, amyloidosis, oxygen/nutrient deprivation). Our historical experiences in IT have helped define the important factors that influence therapeutic success, are the basis for the design of our current (intraportal) approach and serve to frame the trajectory of future advances in the field.

Pancreatic islets were first isolated from guinea pigs in 1965 [171], from rats in 1967 [172], and from pigs [173] and humans [173; 174] in 1974-1975. The first successful ITs resulting in sustained reduction of blood glucose levels in diabetic animals were performed in 1972, and were done by transplanting rat islets into the peritoneum or muscle of isogeneic rats [175]. Ballinger and Lacy indicated that the outcome of IT was correlated with the transplanted islet mass, a concept undisputed even today. During the same period, Kemp *et al*. compared the efficacy of IT at three different sites (subcutaneous, intraperitoneal, intraportal) and found that intraportal IT was the only approach that reversed diabetes in isogeneic rats with chemically-induced diabetes [176; 177] and did so with the fewest number of islets when comparing the three transplant sites. The earliest animal experiments indicated that transplanted islet mass and transplant site were among the most important determinants of success following IT.

In 1974-1978, allo-IT was translated into the clinical setting, and two series were performed at the University of Minnesota, involving 18 ITs and 13 recipients [29]. The first series involved intramuscular, intraperitoneal, and intraportal IT, and the most consistent reduction in exogenous insulin requirements were shown following intraportal IT. However, permanent reversal of hyperglycemia was not achieved in any of seven recipients [30; 31]. The second series involved only intraportal IT, and results indicated that IT produced transient insulin independence in two recipients for no longer than a few days [32]. These two series established that intraportal IT could potentially reverse diabetes and did so better than any other transplant site, but it was unclear whether the primary reason for islet loss was immunologic or nonimmunologic in nature.

In 1977-1980, Najarian *et al*. developed a protocol for surgical pancreatectomy followed by intraportal auto-IT for patients suffering from intractable pain from chronic pancreatitis [178; 179]. The primary objective of the therapy was to eliminate the source of the unrelenting pain, while the secondary objective was to prevent the diabetes that would occur with removal of most (>95%) of the pancreas. Since auto-IT cannot involve rejection, this would be the first time that the relative impact of nonimmunologic islet injury and loss could be studied. Their initial series revealed that auto-IT can produce sustained insulin independence in some (30%) and reduce the severity of diabetes in others (40%) [178]. Islet function exhibited by C-peptide positivity was established in all recipients who were not overtly diabetic following auto-IT, despite near-total or total pancreatectomy. These early experiences with auto-IT suggested that rejection is likely to play an enormous role in islet loss following allo-IT, and that future success will be determined in large part by advances in both islet isolation (to improve islet yields) and immunosuppression (to prevent rejection).

Following the efforts of the 1970s, the next two decades were characterized by inconsistent outcomes and the field of allo-IT experienced stagnation. In 1988-1989, Ricordi *et al*. developed an automated method for islet isolation which enabled more consistent islet isolation and improved islet yields retrieved from human donor pancreata [180; 181]. In 2000, Shapiro *et al*. made a breakthrough by developing the Edmonton Protocol (EP) which helped standardize islet isolation, established a requirement of a large minimum dose of islets (≥9000 IEs per kgBW), and featured a newer immunosuppressive regimen which eliminated (steroids) or minimized (calcineurin-inhibitors) the use of diabetogenic agents [43; 45]. The availability of daclizumab in 1997 and sirolimus in 1999 made the discontinuation of steroids and minimization of tacrolimus possible. Their initial trial of the EP showed that intraportal allo-IT can reverse diabetes and maintain 100% insulin independence for a median duration of 12 (4-15, range) months in seven consecutively transplanted recipients [43]. However, as recipients reached longer follow-up, rates of insulin independence dropped (80% at 1-year, 10% at 5-years) [44; 45; 46]. Furthermore, no recipients became insulin independent following transplantation of islets from a single donor, and islets from 2-4 donor pancreata were usually needed. Despite the reinvigoration of interest in the field, many new challenges were identified. First, in order to make allo-IT more widely available, the number of islet infusions, and thus required donor organs, would need to be limited to one. A need for multiple infusions would increase the associated heathcare costs and clinical risks to the recipient, and a need for multiple pancreata would stretch the already limited donor organ availability. It is important to note that one of the major advantages of IT (as compared to pancreas transplant) is that there remains the possibility that multiple recipients could be treated using islets from a single donor.

Second, long-term (>5 years) insulin independence was low (~10%), but islet function (C-peptide positivity) remained high (~80%) – suggesting that alloimmune rejection and/or autoimmune recurrence may not fully explain the islet attrition over time and nonimmunologic factors may be involved.

An international trial was done to test the EP at 9 centers worldwide, and found that some success was achievable (~60% achieved insulin independence for all recipients at some point during the trial follow-up), but that the outcomes were highly-dependent on the experience of the transplant center and ~80% of recipients required insulin by 2 years post-IT [68]. Around this time, several centers made adjustments to the EP and conducted independent studies, one showing that IT using islets from a single donor pancreas is possible [47], while another showing that a much higher islet dose (>13,000 IEs per kgBW) is necessary to consistently achieve insulin independence [48]. In 2004-2005, Hering *et al*. conducted two trials in which islets retrieved from a single donor pancreas were sufficient to achieve insulin independence under the cover of more potent induction immunosuppression with a T-cell-depleting antibody only [182] or with a T-cell-depleting antibody, an anti-TNF-α antibody (etanercept) and an anti-IL2 receptor antibody (daclizumab) [50]. In both trials, all recipients were transplanted with islets from a single donor. In the second trial, the islet dose was considered marginal relative to the EP (~7000 IEs per kgBW vs. >9000 IEs per kgBW), but all recipients (n = 8) became insulin independent [50]. However, even with the most potent induction immunotherapy, the most recent data indicates that the 5-year insulin independence rates following allo-IT are ~50%, which is similar to the rates following whole pancreas allo-transplant [51].

Improvements in induction immunosuppression seem to be the origin for improved outcomes with allo-IT over the last decade at the most experienced centers (~10% insulin independence in 2005, ~50% in 2012). However, despite the progress, islet attrition still occurs over time and not much attention has been given to nonimmunologic causes for islet loss and dysfunction. Sutherland *et al*. recently revisited the comparison between auto-IT and allo-IT [183]. As the authors have indicated, allo-IT imposes additional stresses on the islets that do not occur with auto-IT, including brain death (associated with an increase in systemic inflammatory cytokine levels), increased cold ischemia time, alloimmune rejection, autoimmune recurrence, and immunosuppressant toxicity. When comparing auto-ITs done from 1977-2007 at the University of Minnesota and allo-ITs reported to the Collaborative Islet Transplant Registry from 1999-2006, the data indicate that rates of insulin independence (74% versus 45% at 2 years) and islet function (85% versus 66% at 2 years) are better following auto-IT. Also, insulin independence can be achieved using islet doses lower than 5000 IEs per kgBW (7% with <2500 IEs per kgBW, 27% with 2501-5000 IEs per kgBW at 1 year) following auto-IT, whereas the same outcome is rarely achieved at such doses following allo-IT. A more recent study has indicated that the same glycemic control can be achieved with about half of the islet mass following auto-IT (~4600 IEs per kgBW) versus allo-IT (~9900 IE per kgBW) [184]. Collectively, these data confirm that stresses unique to allo-IT contribute to islet attrition. However, in both auto-IT and allo-IT, loss of islet viability and function still occurs at relatively high rates and may be in part explained by causes of nonimmunologic nature.

Recent basic and clinical findings have suggested that gradual islet loss and dysfunction post-IT exhibits features of non-insulin-dependent (type 2) diabetes. Like insulin-

dependent (type 1) diabetes, type 2 diabetes is a disease characterized by an insufficient β-cell secretory capacity. However, the pathophysiological causes of reduced insulin reserve are very different; Type 1 diabetes results from the rapid, near-total or total destruction of islets by the native immune system, whereas type 2 diabetes results from a gradual development of insulin resistance, a defect of insulin secretion due to chronic hyperglycemia [185; 186; 187], metabolic stress [188] and amyloid-mediated apoptosis [189]. Type 2 diabetes is believed to cause a systematic loss of islets [190] that compounds the stress on the remaining islet mass, resulting in further islet dysfunction. A recent study has shown that islets isolated from type 2 diabetic pancreata indeed do not function normally [191]. Unless acutely lost due to new alloimmune rejection or recurrent autoimmunity, data indicate that an islet allograft typically follows a time course comparable to disease progression in type 2 diabetes. The preserved C-peptide positivity that accompanies outcomes of major trials over the last decade suggests that most islet allografts are not overtly rejected when recipients are adequately immunosuppressed. A recent report summarized an analysis of a 52 year-old female who died of a hypertensive stroke two years after undergoing the last of two ITs on the EP, and who experienced gradual loss of insulin independence with sustained C-peptide secretion throughout her follow-up [192]. In the analysis, Smith *et al*. indicated that there was no support for an immunological explanation for the loss of both islet grafts, citing no evidence of intraislet or periislet inflammation on histopathologic examination of her liver and no reactivation of an islet-directed autoantibody response. Another recent report summarized histologic findings following an autopsy of a 55 year-old male who died of a myocardial infarction six months after undergoing the last of three ITs on the EP, who died nearly five years after the first IT, and who also experienced gradual decline of islet allograft function [193] – similar to the recipient in the previously

mentioned report [192]. This second report noted both extracellular and intracellular amyloid deposits in >40% of the engrafted islets. Westermark *et al*. recently published a more extensive report showing similar findings from four deceased islet allograft recipients [194]. In addition to these reports, studies have shown that chronic hyperglycemia impairs islet allograft insulin secretion [195; 196], and that this defect is exacerbated when the β-cell mass is reduced [185]. Other recent evidence has suggested that islet allografts exhibit indicators of elevated stress-mediated apoptosis, which is enhanced with hyperglycemia [197]. These studies support a nonimmunologic basis for loss and dysfunction of the transplanted islet mass.

If late islet loss occurs in part due to nonimmunologic causes, it must be assumed that the transplanted islet mass decreases and becomes insufficient over time, which contributes to more islet loss. However, the islet doses that are currently transplanted should be adequate to reverse diabetes, at least in theory. Experience with surgical pancreatectomy has indicated that the native pancreas exhibits considerable reserve, requiring in some cases the removal of >90% of the pancreas to cause overt diabetes [198]. If the native normal adult pancreas contains 1-1.5 million islets [199; 200], roughly 100-150 thousand islets may be considered sufficient to prevent diabetes. It is understood that there is likely no universal minimum threshold for islet mass given the number of individual factors that impact blood glucose control (insulin sensitivity and requirements, β-cell regenerative capacity, etc.). However, our experience with clinical IT has shown that the transplanted islet mass far exceeds what appears to be necessary to achieve permanent normoglycemia. Consider a 70-kilogram patient and assume their native pancreas contained one million islets (which amounts to 14,286 IEs per kgBW). To prevent diabetes in this patient, >10% of the islet mass (~100 thousand islets, or

1429 IEs per kgBW) would need to remain following partial islet destruction or pancreatectomy. However, if this patient were a type 1 diabetic and a candidate for islet allo-IT, empirical clinical evidence would indicate that the minimum islet dose required to achieve insulin independence would be >60% of their original islet mass (~630 thousand islets, or ~9000 IEs per kgBW) [43; 44; 45; 46; 47] and on average is probably higher at >70-90% (~700-910 thousand islets, or ~10,000-13,000 IEs per kgBW) [43; 44; 45; 46; 48; 68; 182], even with the most potent induction immunosuppression currently-available [51]. If this patient was a candidate for near-total or total pancreatectomy followed by auto-IT, then >35% of their original islet mass (~350 thousand islets, or ~5000 IEs per kgBW) may be required to prevent overt diabetes [183; 184; 201], and the rate of insulin independence may only be ~50-70% at 3-5 years post-IT [183; 201]. Whether considering allo- or auto-IT, in both cases many more islets seem to be required than appear to be necessary. The differences between the islet dose requirements for allo- versus auto-IT do indeed suggest that immunologic (alloimmune rejection, autoimmune recurrence, immunosuppressant toxicity) and nonimmunologic (brain death, prolonged cold ischemia time) factors unique to allo-IT are probably responsible for a significant proportion of total islet loss following allo-IT. However, experiences with auto-IT indicate that perhaps >25% of the original islet mass (~250 thousand, or ~3500 IEs per kgBW in a 70-kilogram recipient) may be lost due to nonimmunologic factors unique to the transplant site (the liver) and that are present in both auto-IT and allo-IT.

There is evidence suggesting that the transplanted islet mass, which should be sufficient at the time of transplant, is reduced to levels that are inadequate due to islet loss early in the post-IT period [145]. One of the possible causes for early islet loss may be inadequate oxygenation. Of all causes of islet loss following intraportal IT, islet

oxygenation is overlooked due to the assumption that direct access to the blood stream should be enough to provide the necessary oxygen supply. However, there have been few attempts to confirm that this assumption is true. Studies have begun to indicate that the hepatic environment may be poor from the standpoint of oxygenation [154; 155; 156; 157; 202; 203]. There have been two studies that have attempted to directly [202] or indirectly [157] measure the pO_2 near or within intraportally transplanted islets, and both indicate that the pO_2 may be very low. Carlsson *et al*. presented data of pO_2 measurements of <5 mm Hg via microelectrode probes in both islet (rat, syngeneic) and hepatic tissue and in both nondiabetic and diabetic animals [202]. Olsson *et al*. used pimonidazole, an oxygen-sensitive intracellular dye that accumulates under conditions of <10 mm Hg, to illustrate that ~70%, ~60% and ~30% of intraportally transplanted islets (mouse, syngeneic) stained positive for reduced oxygenation at 1-day, 1-month and 3 months post-IT, respectively [157]. The measurements by Carlsson *et al*. and Olsson *et al*. need to be considered with caution because they do not reveal much information about significant oxygen gradients that may exist in either the islet [204] or hepatic tissue [153]. These measurements also do not provide any information regarding the longitudinal gradients that may exist along intraportal arterioles in the direction of the blood flow [205], which may vary and which would affect the oxygen availability near the intraportal islet. The model presented herein considered the data presented in Carlsson *et al*., Olsson *et al*. and actual measurements of portal venous and hepatic arterial pO_2 [206], but future studies of islet oxygenation would benefit greatly from direct measurements of pO_2 at the level of the intraportal islet. It is important to note that measurements of available intraportal oxygen supply may not only be relevant during the early post-IT period (10-14 days), when it is expected that islets rely on passive diffusion from their surfaces alone, but also at an advanced post-IT period. There is evidence

suggesting that the islets revascularize poorly (15-20% vascular density of the native islet) [154; 156] or that revascularization takes longer (>1 month) [157].

Islet oxygenation may have significant implications for the outcomes of auto-, allo- and possibly xeno-IT. Our model results indicated that islet size (diameter) has the greatest impact on the calculated AVF and NFVF. This makes sense when considering that a 300-μm diameter spherical islet has 27 times the volume of a 100-μm diameter spherical islet. Even though the vast majority of islets in an islet preparation are <200-μm in diameter, the larger islets contribute more to the overall transplantable tissue volume and thus the insulin-secreting volume. When extrapolating to an entire human islet preparation as based on actual size distribution data, and without thrombus formation, it was determined that up to 31% of the total transplanted islet volume may be anoxic and up to 92% may be non- or poorly functioning. With thrombus formation, the result is worse; up to 45% of the total transplanted islet volume may be anoxic and up to 98% may be non- or poorly functioning. The range in results is primarily attributable to the uncertainty in the actual values for available external pO_2. However, the calculated values are reasonable (at P_{ext} of 15 mm Hg, the AVF is ~25% and an average NFVF [at P^* = 10 mm Hg] is ~70%). It should be noted that extrapolation of AVF and NFVF values for an entire islet preparation carries an important *caveat*: each islet experiences very different local conditions (thrombosis versus no thrombosis, low versus high pO_2, etc.). These extrapolations are only meant to illustrate the potential impact of oxygenation on the scale of the entire transplantable islet volume, may help explain some early islet loss and dysfunction, and should be studied further.

Conclusion

Oxygenation of the intraportally transplanted islet has not been studied extensively and may be an important contributor to islet loss and dysfunction, primarily in the early post-IT period. Future studies need to be conducted to accurately measure the intraportal pO_2 at the level of the engrafted islet. The liver may not be the optimal IT site, and it may be in part due to poor oxygenation.

Table 4-1: Summary of model constants and independent variables.

Description	Formulaic Abbreviation	Prescribed Value(s)	Units	Reference(s)
Oxygen permeability				
Islet	$(\alpha D)_1$	$1.31 \cdot 10^{-14}$	mol/cm/mm Hg/sec	[163; 207]
Thrombus	$(\alpha D)_2$	$2.7 \cdot 10^{-14}$	mol/cm/mm Hg/sec	[165]
Oxygen supply				
External pO_2	P_{ext}	5-40	mm Hg	[206]
Oxygen threshold				
Critical pO_2 (viability)	P_a	0.1	mm Hg	[168; 207]
Critical pO_2 (function)	P^*	5-15	mm Hg	[87; 164]
Fractional Viability				
Islet	*OCR/DNA*	100-300	nmol/min/mg DNA	[97; 98; 121]
Size/Thickness				
Islet diameter	$2 \cdot R$	100-300	μm	-
Thrombus thickness	δ	100	μm	[208; 209; 210; 211]

Table 4-2: AVF and NFVF with no thrombosis

	AVF [%] (P_a = 0.1 mm Hg)			NFVF [%] (P^* = 5 mm Hg)			NFVF [%] (P^* = 10 mm Hg)			NFVF [%] (P^* = 15 mm Hg)		
P_{ext} [mm Hg]	5	15	40	5	15	40	5	15	40	5	15	40
$2 \cdot R$ [µm]	*OCR/DNA* [nmol/min/mg DNA]											
	100											
150	0.36	0	0	57.7	0	0	78.8	5.1	0	85.9	27.3	0
	200											
100	0	0	0	53.6	0	0	76.8	2.5	0	84.5	23.7	0
150	13.6	0	0	72.1	12.7	0	86.0	32.5	0	90.6	50.7	0
300	53.0	30.8	7.7	87.8	62.6	24.1	93.9	73.1	33.1	95.9	80.5	40.7
	300											
150	24.9	3.0	0	78.0	29.3	0	89.0	48.1	0	92.7	62.3	0.1

Abbreviations: AVF, anoxic volume fraction; NFVF, non-functional volume fraction; OCR, oxygen consumption rate; *OCR/DNA*, islet OCR normalized to DNA content, an indicator of fractional viability; P^*, non-functional critical pO_2; P_a, non-viable (or anoxic) critical pO_2; P_{ext}, external pO_2; R, islet radius.

Table 4-3: AVF and NFVF with thrombosis

	AVF [%] (P_a = 0.1 mm Hg)			NFVF [%] (P^* = 5 mm Hg)			NFVF [%] (P^* = 10 mm Hg)			NFVF [%] (P^* = 15 mm Hg)		
P_{ext} [mm Hg]	5	15	40	5	15	40	5	15	40	5	15	40
$2 \cdot R$ [µm]	*OCR/DNA* [nmol/min/mg DNA]											
	100											
150	6.88	0	0	81.9	1.8	0	91.0	26.3	0	94.0	50.6	0
	200											
100	4.2	0	0	80.5	0.2	0	90.2	20.0	0	93.5	46.3	0
150	30.2	2.8	0	91.5	41.8	0	95.8	67.4	0	97.2	78.2	0
300	69.2	47.4	19.8	97.6	84.4	46.3	98.8	92.1	57.9	99.2	94.7	77.2
	300											
150	44.1	14.5	0	94.6	62.0	0.2	97.3	80.2	4.2	98.2	86.8	12.1

Abbreviations: AVF, anoxic volume fraction; NFVF, non-functional volume fraction; OCR, oxygen consumption rate; *OCR/DNA*, islet OCR normalized to DNA content, an indicator of fractional viability; P^*, non-functional critical pO_2; P_a, non-viable (or anoxic) critical pO_2; P_{ext}, external pO_2; R, islet radius.

Table 4-4: Change in AVF and NFVF with thrombosis

	AVF [%] (P_a = 0.1 mm Hg)			NFVF [%] (P^* = 5 mm Hg)			NFVF [%] (P^* = 10 mm Hg)			NFVF [%] (P^* = 15 mm Hg)		
P_{ext} [mm Hg]	5	15	40	5	15	40	5	15	40	5	**15**	**40**
$2 \cdot R$ [µm]	*OCR/DNA* [nmol/min/mg DNA]											
	100											
150	-6.5	0	0	-24.3	-1.8	0	-12.1	-21.2	0	-8.1	-23.2	0
	200											
100	-4.2	0	0	-26.9	-0.2	0	-13.4	-17.6	0	-9.0	-22.6	0
150	-16.6	-2.8	0	-19.5	-29.1	0	-9.7	-34.9	0	-6.5	-27.6	0
300	-16.2	-16.7	-12.1	-9.8	-21.8	-22.2	-4.9	-19.0	-24.8	-3.3	-14.3	-25.5
	300											
150	-19.2	-11.5	0	-16.6	-32.7	-0.2	-8.3	-32.1	-4.2	-5.5	-24.5	-12.0

Abbreviations: AVF, anoxic volume fraction; NFVF, non-functional volume fraction; OCR, oxygen consumption rate; *OCR/DNA*, islet OCR normalized to DNA content, an indicator of fractional viability; P^*, non-functional critical pO_2; P_a, non-viable (or anoxic) critical pO_2; P_{ext}, external pO_2; R, islet radius.

Table 4-5: Minimum intraislet pO_2 with no thrombosis

	P_{min} [mm Hg]		
P_{ext} [mm Hg]	5	15	40
$2 \cdot R$ [µm]	*OCR/DNA* [nmol/min/mg DNA]		
		100	
150	0.1	6.5	31.2
		200	
100	0.1	7.5	32.3
150	0.1	0.3	22.4
300	0.1	0.1	0.1
		300	
150	0.1	0.1	13.7

P_{max} for islets with no thrombosis is equal to the specified P_{ext}.

Abbreviations: OCR, oxygen consumption rate; *OCR/DNA*, islet OCR normalized to DNA content, an indicator of fractional viability; P_{ext}, external oxygen partial pressure; P_{max}, maximum intraislet pO_2; P_{min}, minimum intraislet pO_2; R, islet radius.

Table 4-6: Minimum and maximum intraislet pO_2 with thrombosis

	P_{min} [mm Hg]			P_{max} [mm Hg]		
P_{ext} [mm Hg]	5	15	40	5	15	40
$2 \cdot R$ [µm]	*OCR/DNA* [nmol/min/mg DNA]					
	100					
150	0.1	3.3	27.6	2.7	11.3	36.1
	200					
100	0.1	4.4	28.8	2.5	11.2	36.0
150	0.1	0.1	15.3	2.0	8.8	32.3
300	0.1	0.1	0.1	1.4	6.3	24.2
	300					
150	0.1	0.1	3.8	1.6	7.4	28.6

Abbreviations: OCR, oxygen consumption rate; *OCR/DNA*, islet OCR normalized to DNA content, an indicator of fractional viability; P_{ext}, external oxygen partial pressure; P_{max}, maximum intraislet pO_2; P_{min}, minimum intraislet pO_2; R, islet radius.

Table 4-7: Change in minimum and maximum intraislet pO_2 with thrombosis

	P_{min} [mm Hg]			P_{max} [mm Hg]		
P_{ext} [mm Hg]	5	15	40	5	15	40
$2 \cdot R$ [µm]	*OCR/DNA* [nmol/min/mg DNA]					
	100					
150	0	-3.2	-3.6	-2.3	-3.7	-3.9
	200					
100	-0.02	-3.2	-3.5	-2.5	-3.8	-4.0
150	0	-0.2	-7.1	-3.0	-6.3	-7.7
300	0	0	0	-3.6	-8.7	-15.8
	300					
150	0	0	-8.9	-3.4	-7.6	-11.4

Abbreviations: OCR, oxygen consumption rate; *OCR/DNA*, islet OCR normalized to DNA content, an indicator of fractional viability; P_{ext}, external oxygen partial pressure; P_{max}, maximum intraislet pO_2; P_{min}, minimum intraislet pO_2; *R*, islet radius.

Table 4-8: Representative extrapolation of AVF and NFVF for a islet preparation (no thrombosis)

		AVF [%] (P_a = 0.1 mm Hg)			NFVF [%] (P^* = 5 mm Hg)			NFVF [%] (P^* = 10 mm Hg)			NFVF [%] (P^* = 15 mm Hg)		
P_{ext} [mm Hg]		5	15	40	5	15	40	5	15	40	5	15	40
$2 \cdot R$ [µm]	VF[a] [%]	*OCR/DNA* [nmol/min/mg DNA]											
							200						
100	7.4	0	0	0	4.0	0	0	5.7	0.3	0	6.3	1.8	0
150	12.0	1.6	0	0	8.7	1.7	0	10.3	1.9	0	10.9	6.1	0
300	20.2	10.7	6.2	1.6	17.8	12.6	4.9	19.0	14.8	6.7	19.4	16.3	8.2
Subtotal[b]	39.6	12.3	6.2	1.6	30.5	14.3	4.9	35.0	17.0	6.7	36.6	24.2	8.2
Total[c]	100.0	31.1	15.7	4.0	77.0	36.1	12.4	88.4	42.9	16.9	92.4	61.1	20.7

[a]VF indicates the proportion of the total preparation volume accounted for by islets of a particular size. These values are estimated from the size distribution data illustrated in Figure 4-8 for high-purity, cultured, allogeneic islet preparation. For example, we calculated the mean VF for islets of 100 µm diameter, the VF data for islets ranging in diameter from 50-100 and 100-150 µm were averaged.

[b]Subtotal is the sum of VFs from $2 \cdot R$ = 100, 150 and 300 µm only.

[c]Total is the sum of VFs from the entire islet preparation and are estimated by dividing each subtotal AVF or NFVF by 0.396 (the subtotal VF).

Abbreviations: AVF, anoxic volume fraction; NFVF, non-functional volume fraction; OCR, oxygen consumption rate; *OCR/DNA*, islet OCR normalized to DNA content, an indicator of fractional viability; P^*, non-functional critical pO_2; P_a, non-viable (or anoxic) critical pO_2; P_{ext}, external oxygen partial pressure; R, islet radius; VF, volume fraction.

Table 4-9: Representative extrapolation of AVF and NFVF for a islet preparation (with thrombosis)

		AVF [%] (P_a = 0.1 mm Hg)			NFVF [%] (P^* = 5 mm Hg)			NFVF [%] (P^* = 10 mm Hg)			NFVF [%] (P^* = 15 mm Hg)		
P_{ext} [mm Hg]		5	15	40	5	15	40	5	15	40	5	15	40
$2 \cdot R$ [µm]	VF[a] [%]	*OCR/DNA* [nmol/min/mg DNA]											
							200						
100	7.4	0.3	0	0	6.0	0.01	0	6.7	1.5	0	6.9	3.4	0
150	12.0	3.6	0.3	0	11.0	5.0	0	11.5	8.1	0	11.7	9.4	0
300	20.2	14.0	9.6	4.0	19.7	17.0	9.4	20.0	18.6	11.7	20.0	19.1	15.6
Subtotal[b]	39.6	17.9	9.9	4.0	36.7	22.0	9.4	38.2	28.2	11.7	38.6	31.9	15.6
Total[c]	100.0	45.2	25.0	10.1	92.7	55.6	23.7	96.5	71.2	29.5	97.5	80.6	39.4

[a]VF indicates the proportion of the total preparation volume accounted for by islets of a particular size. These values are estimated from the size distribution data illustrated in Figure 4-8 for high-purity, cultured, allogeneic islet preparation. For example, we calculated the mean VF for islets of 100 µm diameter, the VF data for islets ranging in diameter from 50-100 and 100-150 µm were averaged.

[b]Subtotal is the sum of VFs from $2 \cdot R$ = 100, 150 and 300 µm only.

[c]Total is the sum of VFs from the entire islet preparation and are estimated by dividing each subtotal AVF or NFVF by 0.396 (the subtotal VF).

Abbreviations: AVF, anoxic volume fraction; NFVF, non-functional volume fraction; OCR, oxygen consumption rate; *OCR/DNA*, islet OCR normalized to DNA content, an indicator of fractional viability; P^*, non-functional critical pO_2; P_a, non-viable (or anoxic) critical pO_2; P_{ext}, external oxygen partial pressure; R, islet radius; VF, volume fraction.

Figure Captions

Figure 4-1: Sketch illustrating an islet in the native pancreas (left) and an islet which has been intraportally transplanted (right). The native islet is well-perfused with oxygen-saturated arterial blood, whereas the transplanted islet obtains oxygen from the deoxygenated intraportal blood and relies solely on oxygen diffusion from its surface.

Figure 4-2: Schematic depicting the intraportal islet which is modeled as a spherical body containing viable oxygen-consuming cells. The transplanted islet is lodged at a bifurcation in a distal hepatic sinusoid and has access to portal blood at its proximal half-surface. The distal half of the islet equilibrates with the surrounding environment and is modeled by the presence of a no-flux boundary condition at a specified distance away from its back surface [$\partial P/\partial r = 0$]. There are four independent variables that are adjusted in this model, including: (1) fractional viability, or oxygen consumption rate normalized to DNA content [*OCR/DNA*]; (2) islet diameter [$2 \cdot R$]; (3) external pO_2 [P_{ext}]; and (4) presence or absence of thrombus with a specified thickness [δ], located only on the proximal half-surface.

Figure 4-3: Surface plot illustrating model results for a 'baseline case', which involves an islet with average diameter [$2 \cdot R$ = 150 μm] and fractional viability [*OCR/DNA* = 200 nmol/min/mg DNA], exposed to a reasonable oxygen supply [P_{ext} = 15 mm Hg], and no thrombus formation at its proximal half-surface [δ = 100 μm]. The colors within and behind the islet depict the calculated spatial pO_2 gradients, as indicated by the legend (left). *Abbreviations*: δ, thickness of the thrombus; OCR, oxygen consumption rate; P_{ext}, external oxygen partial pressure; R, islet radius.

Figure 4-4: Surface plots illustrating model results for four different cases in which the baseline case [no thrombus, *OCR/DNA* = 200 nmol/min/mg DNA, P_{ext} = 15 mm Hg, and $2 \cdot R$ = 150-μm) is perturbed by adjusting only 1 of the 4 independent variables with each case. Case A depicts the baseline case with the addition of a 100-μm thrombus on the proximal half-surface of the islet. Case B depicts the baseline case with an increase in the OCR/DNA from 200 to 300 nmol/min/mg DNA. Case C depicts the baseline case with a decrease in the external pO_2 from 15 to 5 mm Hg. Case D depicts the baseline case with an increase in the islet diameter from 150 to 300 μm. The anoxic volume fraction (AVF) is depicted by the achromatic core, and note the magnitude of the AVF associated with each perturbation. *Abbreviations*: AVF, anoxic volume fraction; OCR, oxygen consumption rate; P_{ext}, external oxygen partial pressure; R, islet radius.

Figure 4-5: Surface plot illustrating model results for the worst-case scenario analyzed in this study, which combines the baseline case and the 4 individual perturbations of 4 independent variables [addition of thrombus, increase in fractional viability, decrease external pO_2, and an increase in islet diameter] that were shown separately in *Figure 4*. Note the very large anoxic volume fraction (AVF). *Abbreviation*: AVF, anoxic volume fraction.

Figure 4-6: Graphs depicting a summary of model results for calculation of anoxic volume fraction [AVF (%)] with respect to external pO_2 [P_{ext}], islet diameter [$2 \cdot R$] and fractional viability [*OCR/DNA*], and with or without thrombus formation [δ = 100 μm]. The graph on the left (A) illustrates the change in AVF for an islet of average diameter (150 μm) with increasing OCR/DNA. The graph on the right (B) illustrates the change in AVF in an islet with average OCR/DNA (200 nmol/min/mg DNA) with increasing islet diameter.

AVF is defined as the region of the islet that is non-viable, occurring below a critical pO_2 (P_a) of 0.1 mm Hg. *Abbreviations*: AVF, anoxic volume fraction; δ, thickness of the thrombus; OCR, oxygen consumption rate; P^*, non-functional critical pO_2; P_a, non-viable (or anoxic) critical pO_2; P_{ext}, external pO_2; R, islet radius.

Figure 4-7: Graphs depicting a summary of model results for calculation of non-functional volume fraction [NFVF (%)] with respect to external pO_2 [P_{ext}], islet diameter [$2 \cdot R$] and fractional viability [*OCR/DNA*], and with or without thrombus formation [δ = 100 μm]. The graph on the left (A) illustrates the change in NFVF for an islet of average diameter (150 μm) with increasing OCR/DNA. The graph on the right (B) illustrates the change in NFVF for an islet with average OCR/DNA (200 nmol/min/mg DNA) with increasing islet diameter. In this case, NFVF is defined as the region of the islet with impaired insulin secretion, occurring below a critical pO_2 (P^*) of 5 mm Hg. *Abbreviations*: NFVF, non-functional volume fraction; δ, thickness of the thrombus; OCR, oxygen consumption rate; P^*, non-functional critical pO_2; P_{ext}, external pO_2; R, islet radius.

Figure 4-8: Islet size distribution as stratified by ranges of islet diameter. Mean (± standard error, SE) number fractions are actual data from our institution (University of Minnesota) from 23 human islet preparations (high-purity, cultured fractions) prior to clinical transplantation. Mean (± SE) volume fractions are estimated from number fraction data by calculating the mean islet volumes under the assumption that the islets are spherical with a median radius for that size range. *Abbreviations*: SE, standard error.

Figure 4-1

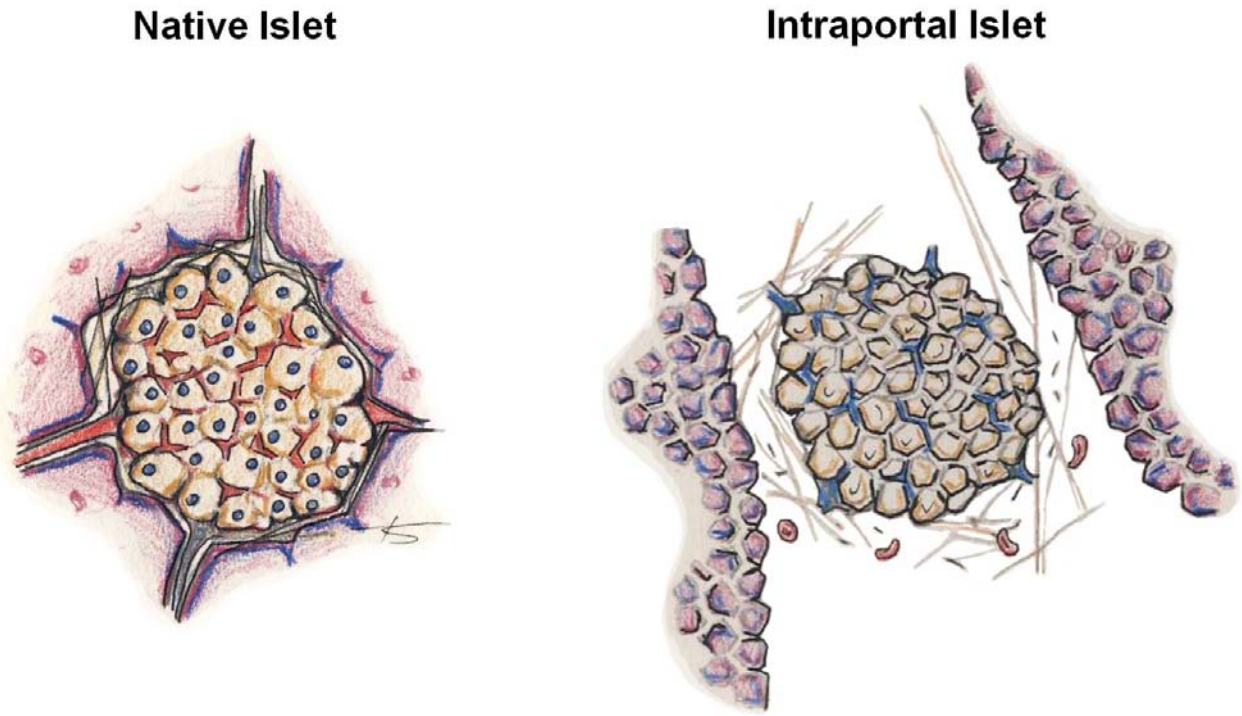

Figure 4-2

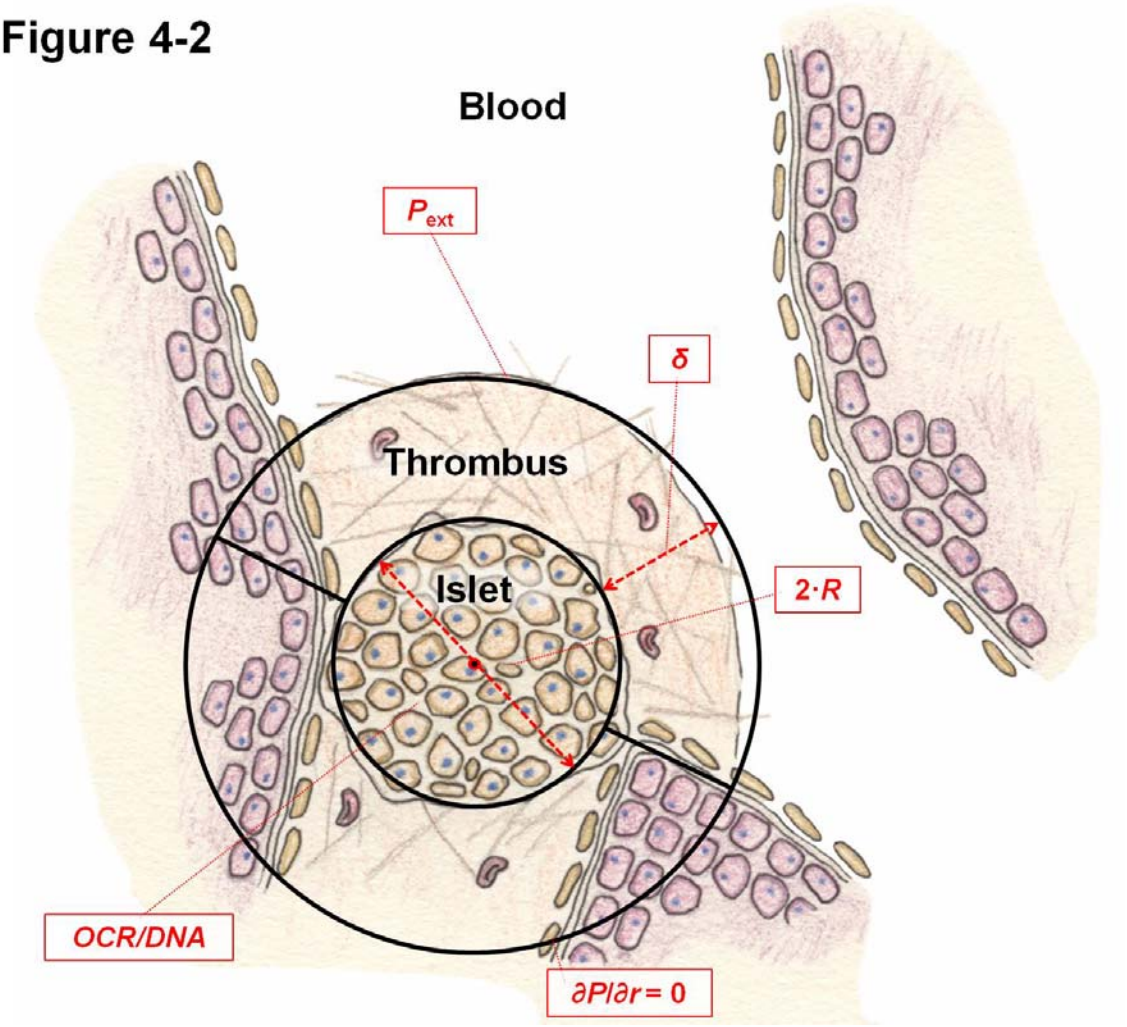

Figure 4-3: Baseline Case

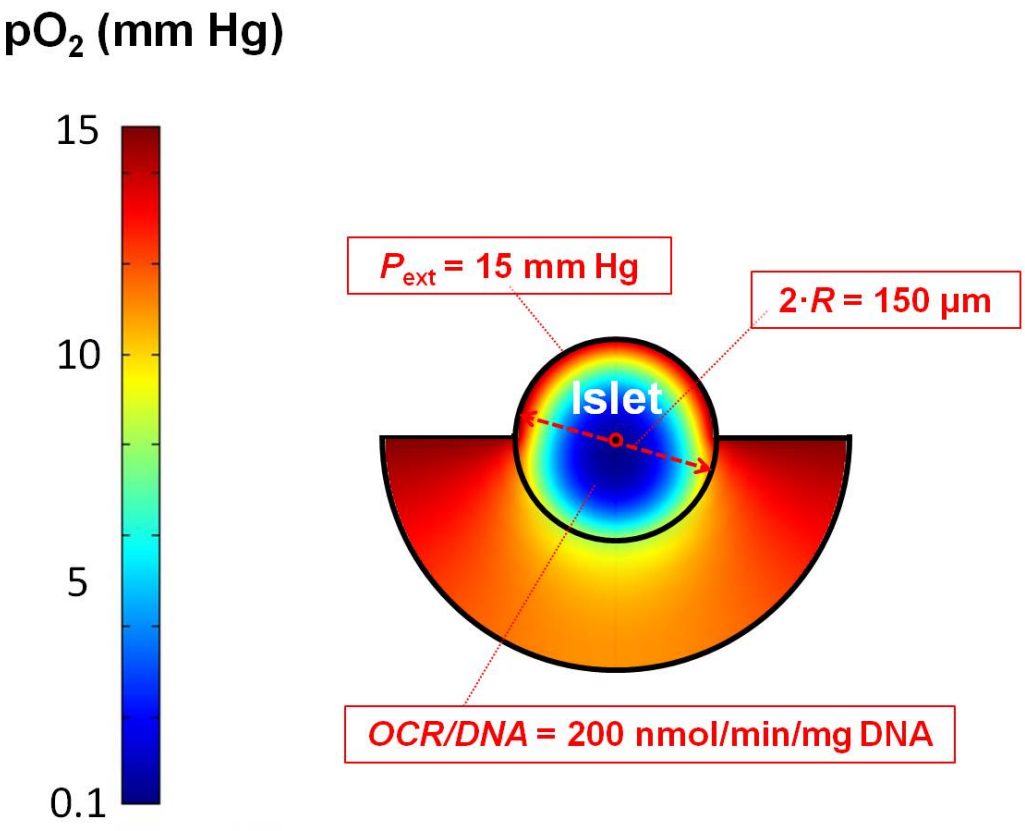

Figure 4-4

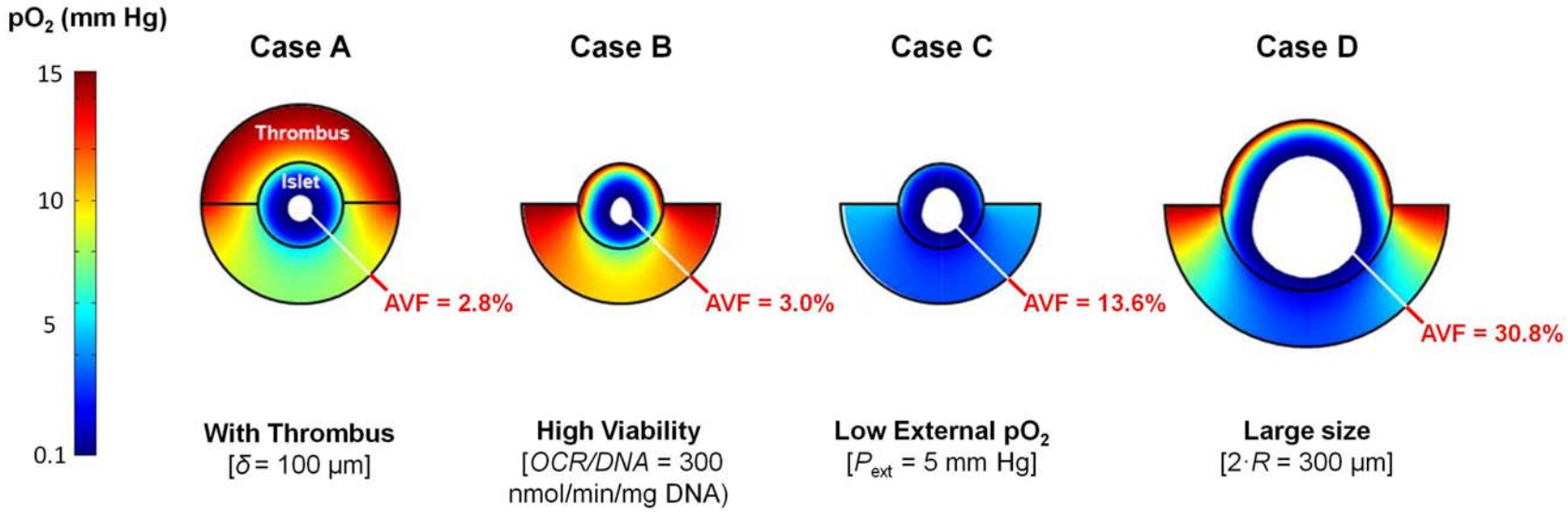
pO2 (mm Hg)
15
10
5
0.1
Case A
Case B
Case C
Case D
Thrombus
Islet
AVF = 2.8%
AVF = 3.0%
AVF = 13.6%
AVF = 30.8%
With Thrombus
[δ = 100 μm]
High Viability
[OCR/DNA = 300
nmol/min/mg DNA)
Low External pO2
[Pext = 5 mm Hg]
Large size
[2·R = 300 μm]

Figure 4-5: Worst Case

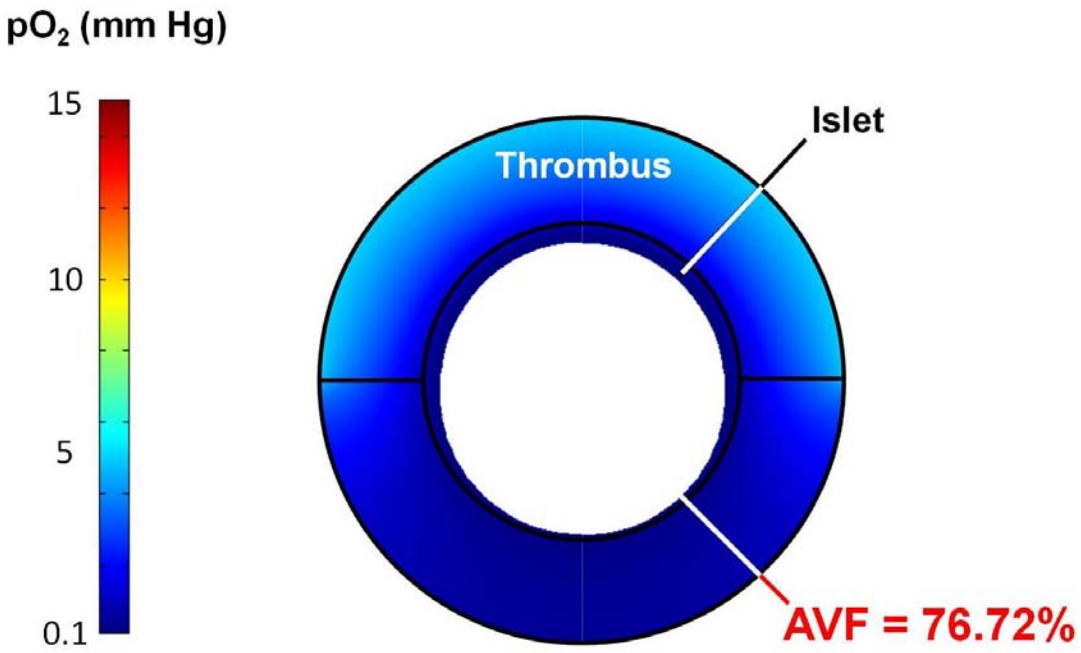

Figure 4-6: Anoxic Volume Fraction (P_a = 0.1 mm Hg)

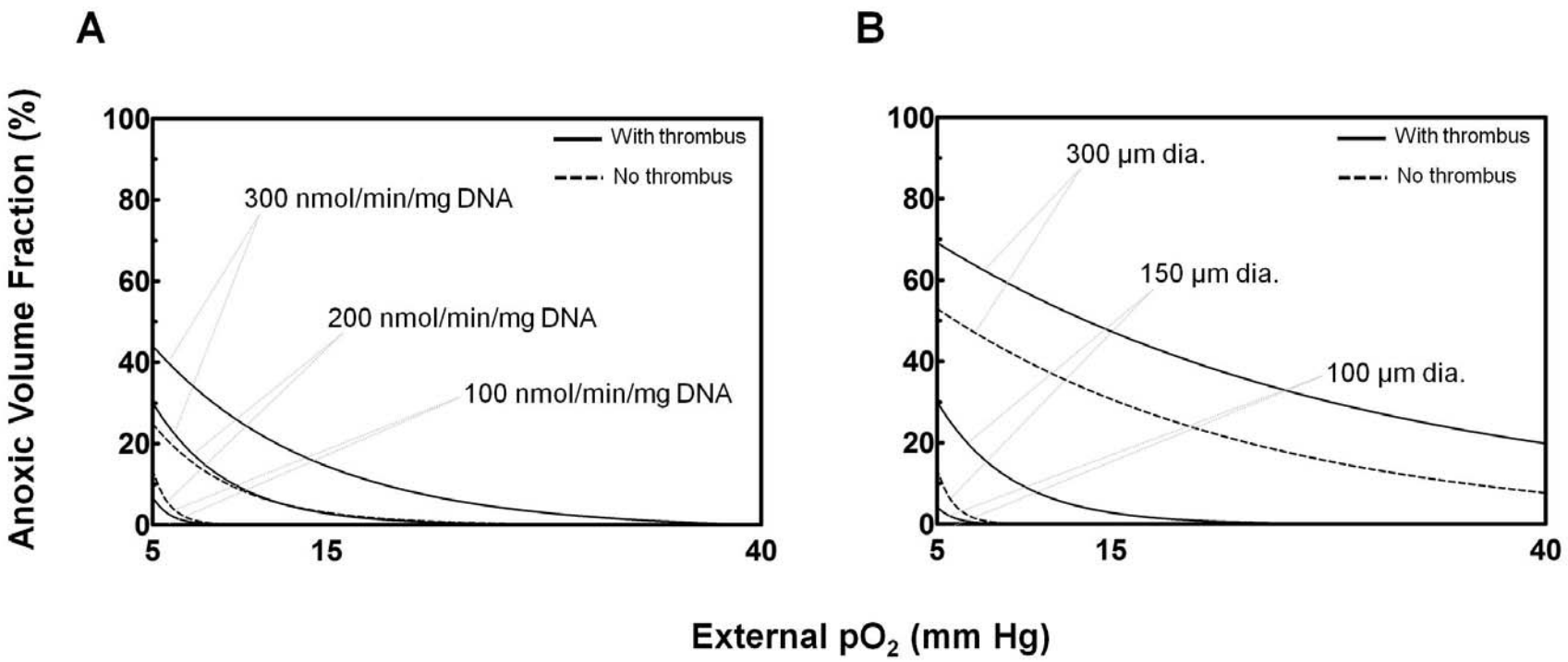

Figure 4-7: Non-functional Volume Fraction (P^* = 5 mm Hg)

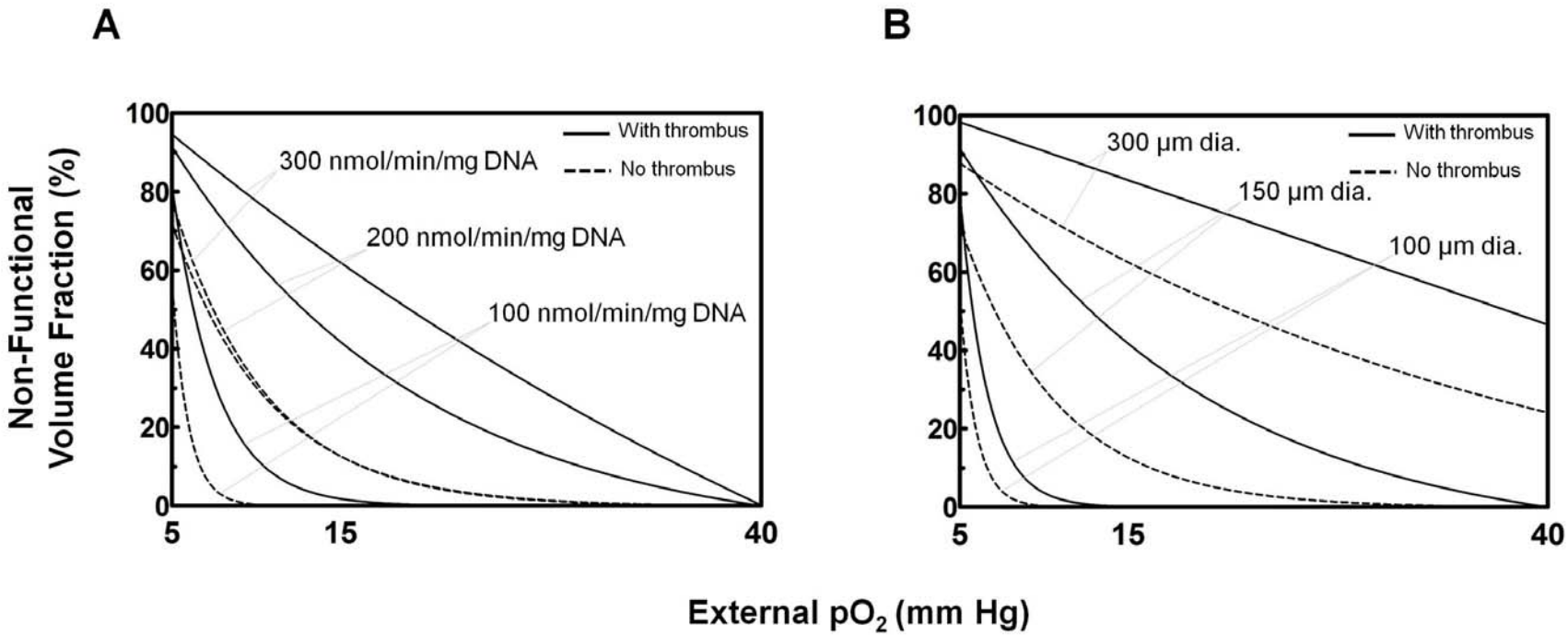

Figure 4-8: Human Islet Size Distribution

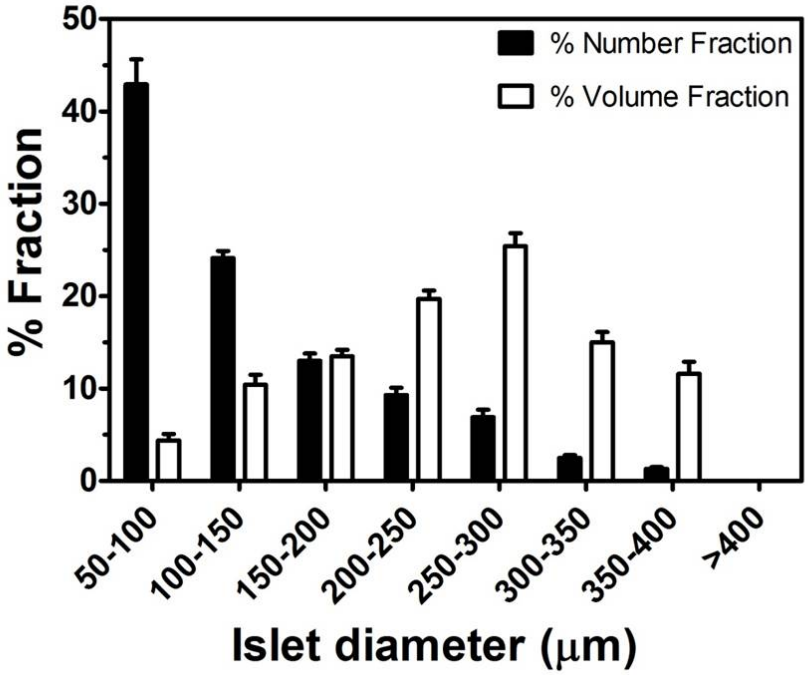

Supplementary Discussion

Importance of Oxygen on Islet Survival and Function

One of the most significant reasons why islets are thought to either function poorly and/or struggle to survive following intraportal IT is the lack of adequate delivery of oxygen during the early engraftment period. The oxygenation status of islets engrafted in the liver remains a perplexing problem. Hepatic blood flow is a mixture of arterial blood from the hepatic artery and venous blood from the portal vein. Roughly 75% of the total blood flow entering the mixed portal circulation is deoxygenated and derived of venous drainage from the abdomen. The portal venous pO_2 is variable but has been measured to be approximately 30-70 mm Hg [206; 212], while the hepatic arterial pO_2 is approximately 100 mm Hg [206] – meaning that the pO_2 of the mixed portal blood should be around 48-78 mm Hg. Carlsson *et al.* showed that the liver is amongst the most poorly oxygenated organs used or explored as a site for IT, uncovering mean pO_2 values of 5-10 mm Hg within the hepatic parenchyma [202]. It is important to note that these data should be interpreted with caution because point measurements of pO_2 in tissue does not reveal anything about the significant gradients that may exist [153]. Islets in the pancreas are typically perfused by a disproportionately large percentage (nearly 15-20%) of the total arterial blood flow supplying the pancreas, while only accounting for a small percentage (about 1-2%) of the total mass of the organ [213]. Native islets exhibit rich blood supplies which have evolved directly from their unique and demanding metabolic requirements, as they fuel the energy-consuming reactions of peptide hormone synthesis and secretion. Consequently, islets are less equipped to handle the lower pO_2 found in the portal circulation. It has been shown that pancreatic β-cells exhibit a limited capacity to generate adenosine triphosphate (ATP) through anaerobic glycolysis [158]. Ahn *et al*. has shown that islets up-regulate lactate dehydrogenase-A mRNA production

following transplantation [214], suggesting that islets (1) encounter low oxygenation during this time and; (2) exhibit some capacity for non-oxidative energy production. The question remains whether islets can fully adapt to the relative hypoxic conditions of the liver.

Dionne *et al.* have published data showing that the magnitude of the second phase glucose-stimulated insulin secretion (GSIS) is decreased in dispersed islet cells at a pO_2 of about 12 mm Hg [169]. Similarly, Papas *et al.* presented data on βTC3 cells (an immortalized insulin-secreting cell line) showing that insulin secretory function is adversely affected below a pO_2 of 7 mm Hg [170]. These results suggest that if the pO_2 is and remains low, cell function is severely diminished. The Uppsala group has suggested that there may be a sub-set of islets, possibly comprising 25-30% of the total islet population of the pancreas, that are operating at a lower metabolic rate and would be otherwise considered dormant in the native setting [215; 216]. It may be that dormant islets are more adept at surviving in the liver and, as a direct result, may constitute a significant proportion of the islets that survive transplantation over the longer term. It is known that the native pancreas has a very large β-cell reserve and normal regulation of blood sugars only requires a small fraction of the total islet population [217]. Microelectrode measurements of pO_2 within transplanted islets corroborate with expectations that the oxygen delivered to freshly transplanted islets may be insufficient for survival [202; 218]. Studies by the Uppsala group have shown that intraportally transplanted islets may not only be subjected to significantly lower pO_2 as compared with their native state [202; 218], but may also be poorly vascularized as a direct function of their transplant site [216]. In addition to the lower pO_2 of the mixed portal blood entering the liver, the exact location of a transplanted islet within the portal vascular tree will

impact the pO_2 available to the islet tissue [153]. There may be significant oxygen gradients between the proximal mixed portal blood and the terminal sinusoids, where many of the islets lodge, especially since the hepatic tissue is highly metabolically active and consumes significant amounts of oxygen [217]. Regions of lower pO_2 may not be able to support the metabolic requirements of transplanted islets. Carlsson *et al*. reported that the measured average pO_2 within islets transplanted into the rat liver, spleen and kidney was approximately 5 mm Hg at 9-12 weeks post-transplant, while the average pO_2 measured in native, healthy islets was 40 mm Hg [202]. Since it is generally postulated that islet re-vascularization is completed by 10-14 days [219; 220; 221; 222], these data suggest that even with ample time for new blood vessel formation the islets may not be fully vascularized or may never be.

Currently, it is still unclear how similar or different the newly-formed vascular bed is when compared with the native microvascular architecture. The unique microvasculature of the native islet has been implicated to be of importance to overall islet function, in that the direction of blood flow may determine the sorts of paracrine signals individual α-, β-, δ- and PP-cells experience [223; 224]. Whether β-cells are upstream or downstream of δ-cells may be important to both of their functions [223; 224]. Menger *et al.* investigated the capillary network of hamster islets engrafted into a dorsal skin fold chamber to find that the direction of blood flow varied, but that the majority of islets (88%) exhibited some semblance of the traditional core-to-mantle arrangement [225]. Despite evidence suggesting that there is a re-establishment of blood flow from the center of the islet to the periphery, the origin of the new vascular endothelium and the robustness of these newer vessels are actively being studied. Following 2-4 days in culture, the microvessels within the pancreatic islet lose their endothelium [226]. It is largely unknown whether the

presence of an intact native endothelium, lining the intravascular spaces of the islet, is critical for proper and rapid re-vascularization or to prevent post-transplant intraislet thrombosis. Gaber *et al.* implicates longer culture periods following isolation in the improvement of islet function post-transplant [227]. However, Olsson *et al.* suggest that prolonged culture delays the capacity transplanted islets have to re-vascularize quickly [228]. Lukinius *et al.* showed that re-endothelialization may take longer than six weeks in some transplanted islets [226]. It was also suggested that microvessels lacking endothelium may promote the formation of thrombi that would be deleterious to the re-establishment of patent intravascular blood flow [226]. A lack of intra-islet endothelium likely contributes to the diminished ability for transplanted islets to re-establish a full-bodied capillary network. Evidence supports that both the donor and recipient endothelial cells contribute to the formation of new capillaries within the islet [229]. Also, it has been shown that the islet vascular endothelium is lost [226; 230] and its re-growth may be largely dependent on host endothelial cells [231].

Hypoxia has been found to adversely affect islet insulin secretion until normoxia is restored [87; 232], as discussed already. Many studies have shown that under hypoxic conditions, islets upregulate hypoxia-induced factor-1α (HIF-1α), a key regulator of vascular endothelial growth factor (VEGF) synthesis and release [233; 234; 235; 236; 237; 238; 239; 240]. Studies have also suggested that higher concentrations of VEGF stimulate the formation of new blood vessels [233; 234] and even promote cellular survival [241; 242; 243]. It may not be as simple as increasing the amount of circulating VEGF, however. For instance, VEGF increases the permeability of capillary blood vessels in a dose-dependent manner [234]. Consequently, if the blood vessels supplying the transplanted islet are leaky, than islet perfusion is diminished. VEGF has been

shown to be produced and released at greater rates in isolated islets [244]. It has also been shown that cultured and transplanted islets upregulate the expression of VEGF receptors [237]. Following devascularization of the pancreatic islets (during isolation), the cells rely on diffusive transport to obtain oxygen which had been previously delivered via the microvasculature. Hence, many of the islet cells, particularly those found near the core of the larger islets, are hypoxic or even anoxic throughout the culture period and during early engraftment. Prior to complete revascularization, which may or may not fully occur, the transplanted islet continues to rely on diffusive transport from the surroundings to obtain oxygen and nutrients, which may still be insufficient. Hypoxia during the early engraftment period can result in diminished functional capacity or a necrotic central core and significant β-cell loss.

Current limitations with the intraportal IT protocol

Despite the significant progress of the last decade, there is still considerable variability in clinical outcomes for patients receiving an IT. As suggested earlier, one of the many reasons for this variability resides in the loss of islet mass during the engraftment process. Little is known about what exactly happens to the islets at this time. Currently, clinical IT is performed through intraportal injection of a suspension of purified islets either percutaneously under the guidance of fluoroscopy [245] or via mini-laparatomy. The islets embolize throughout the hepatic parenchyma and, depending on their size, may lodge into terminal sinusoids [246]. There are many reasons why the liver may not allow for optimal islet function and survival and are the subject of the next sections of discussion.

Poor oxygenation in the liver may adversely affect islet engraftment

As discussed earlier, the islets enter the portal venous circulation and are carried by the bloodstream. Even though the islets are as close to a blood supply as possible (by being within the lumen of vessels), this may not afford sufficient oxygenation. The blood draining the abdomen is already deoxygenated and the portal venous pO_2 has been measured to be somewhere between 33-72 mm Hg [206]. Furthermore, there is evidence suggesting the presence of regional oxygen gradients throughout the hepatic parenchyma [153], which could certainly have an impact on transplanted islet oxygenation. In the ideal case, most (if not all) islets would obtain sufficient oxygen by passive transport from surfaces alone.

Instant blood-mediated inflammatory reaction may make intraportal environment unfavorable

Significant islet cell loss has been reported by a mechanism described as an inflammatory and thrombotic reaction occurring when islets contact ABO-compatible plasma, as they do when infused into the portal vein. This reaction is termed 'instant blood-mediated inflammatory reaction' (IBMIR) and it has been partly implicated in explaining early graft failure [144; 208; 247; 248; 249; 250]. Investigators have been able to re-create IBMIR *in vitro* using closed loop perfusion systems [247; 248]. IBMIR is likely elicited by numerous plasma proteins, from complement to clotting factors to chemokines [251], but it has been shown that the content of tissue factor (TF) produced by the islets' endocrine cells correlates with the extent of this reaction. It appears that TF is sequestered in the secretory granules of α- and β- cells, but not in the acinar cells or endothelium [144]. In an *in vitro* setting, it has been shown that IBMIR can be tempered by treating with anti-TF monoclonal antibody (anti-TF mAb) [144], site-inactivated factor

VIIa [144], or a small molecule inhibitor of TF [249]. Systemic administration of recombinant tissue factor pathway inhibitor, though considered an emerging approach, has not been tried in this application [252]. Blocking TF with anti-TF mAb administered in co-culture and intravenously appears to minimize IBMIR in the non-human primate model and results in prolonged graft function [253]. Additionally, treating islets with nicotinamide has shown to decrease TF expression *in vitro* [251], suggesting an alternative approach (as the administration of anti-oxidant therapy) for limiting thrombosis after intraportal infusion of islets [254]. Even though some success has been attained using singular pharmacotherapeutics, IBMIR is probably more generalized than believed and involves numerous mediators of both inflammation and clotting. Islets have been found to be locally entrapped by activated platelets, which can stimulate phagocytes to release chemokines that have been shown to be deleterious to islets [255]. Also, activated phagocytes can release free radicals, against which islets do not have robust defenses [255; 256]. This local inflammation around the islets may contribute to their diminishing acceptance by the host immune system, in that, it attracts (and even entraps) leukocytes, decreasing the chance that the graft is tolerated [257].

IBMIR exacts detrimental effects on the islets via the initiation of thrombosis and stimulation of an early inflammatory response near the transplanted islets [144; 208; 247; 248; 249; 250; 258]. Active inflammation around the newly transplanted graft hinders successful engraftment due to an assault by hostile innate effector cells [259; 260], bombardment with caustic cytokines known to harm islets [255; 260; 261; 262; 263; 264] and by stimulating a greater immunologic response which may lead to rejection. It is well established that inflammation and clotting are tightly linked processes [265; 266; 267; 268] and that abrogation of thrombosis stunts IBMIR and improves islet cell survival [209;

253; 269; 270; 271; 272]. Nevertheless, even though islets are located in direct contact with oxygen-carrying blood, it may be that intravascular delivery of islets is not optimal for some of these reasons.

Portal blood contains higher concentrations of caustic immunosuppressive agents

In addition to IBMIR, the intrahepatic portal blood may be deleterious to islet function and survival because of the higher concentrations of immunosuppressive agents [147; 273]. There is abundant literature on the topic of the known toxic effects of immunosuppressants used in IT. Studies provide evidence that tacrolimus (TAC) impairs insulin transcription and secretion *in vitro* [274; 275; 276; 277]. Sirolimus (SIR) has been shown to impair insulin [148; 278] and VEGF [149; 279] release and the combination of TAC and SIR may increase islet cell apoptosis [280]. Another study showed that *in vivo* administration of TAC can negatively impact graft survival [281]. One study illustrated that mammalian target of rapamycin (mTOR) blockade may contribute to β-cell loss by increasing autophagy [282]. The installment of corticosteroid-free immune suppressive therapy was motivated partly to prevent post-transplant hyperglycemia, though there is evidence that two mainstay replacements, TAC and SIR, may promote insulin resistance [280]. The mTOR is ubiquitously found in many cells other than lymphocytes. Therefore, immune suppression with SIR not only limits proliferation and activation of an adaptive immune response, but subverts proliferation and migration of intraislet vascular endothelium in a dose-dependent manner [219]. Dampening the rate at which these processes occur compromises the rapid reconstitution of the blood supply to the transplanted islets. So, while suppressing cellular rejection, the trade-off lies with exposing the transplanted islets to a longer duration of hypoxia in the early engraftment

period, when the islets already have a difficult time adapting to the foreign environment. Sufficient dose of anti-rejection drugs are necessary, but it may be more favorable to seek alternative strategies for IT in which local (but still therapeutic) immunosuppression could be used.

Diminished interactions with extracellular matrix contributes to islet loss and diminished capacity for insulin secretion

It is clearly understood that the isolation process, which involves aggressive enzymatic digestion, temperature fluctuations and mechanical shear, bears significant stress on the islets. Tearing these fragile clusters of cells away from their surrounding extracellular framework can only harm them and there is evidence to support this claim. Cell anchorage to a matrix is critical in preventing apoptosis by a unique mechanism termed anoikis [283; 284]. A loss of connections between islet cell and basement membrane has been shown to result in significant cell loss following isolation. Establishment of new cell-matrix interactions have been shown to contribute to increased islet cell survival [285; 286]. In one study, for instance, culturing disaggregated (from isolated islets) adult β-cells on an extracellular matrix (derived from a rat bladder carcinoma cell line) protects these cells from apoptosis when encountered with serum deprivation and exposure to the pro-inflammatory interleukin-1β [287]. Some groups have shown that interactions with collagen, the components of matrigel, and fibrin help maintain insulin secretion and gene expression in fetal porcine islet-like cell clusters [288] and isolated human islets [289; 290] during culture. In fact, one group has shown that isolated rat β-cells exhibit enhanced insulin secretion when cultured on tumor-derived basement membrane [291; 292]. Another study showed that insulin secretion of fetal β-cells in response to a basal glucose stimulus can be increased by four or five times that of controls by culturing on

collagen type IV [293]. Yet another group has showed that culture of adult rat islets on extracellular matrix can potentiate insulin secretion by a factor of five to eight following an acute glucose stimulus [294]. Several more articles have been published that support the concept that re-establishing extracellular matrix interactions preserves β-cell insulin secretory capacity [295]. Interestingly, insulin secretion has been shown to remain relatively constant when comparing β-cells attached on glass or a poly-L-lysine coated surface, but increased significantly when β-cells were cultured on 804G, and extracellular matrix [291]. These data emphasize the importance of specific cell-matrix interactions and not just attachment to islet function, even though cell spreading on a surface has been shown to trigger influx of free Ca^{2+} ions [296]. On the other hand, different groups have shown that long-term exposure to purified or complexed constituents of extracellular matrix negatively impact insulin secretory capacity [295; 297; 298; 299]. More recent work has shown that encapsulation of murine β-cells [300] and islets [301] using hydrogels functionalized with laminin-recognition peptide sequences improve their viability and function. From what has thus far been published, albeit many studies have been performed on β-cells and not islet cell clusters, it is apparent that interactions with the extracellular matrix may play a critical role in achieving and possibly maintaining glucose homeostasis. Thus, quickly re-establishing these connections between islets and extracellular matrix may only be achieved at an alternative transplant site using tissue-engineered approaches.

Monitoring transplanted islet survival and function is challenging in the liver

The liver (~1 liter of tissue) as an engraftment site for an islet preparation (few milliliters of tissue) creates a challenging size discordance which complicates imaging. As mentioned previously when discussing the difficulties experienced with islet graft

retrieval, groups have devised hepatic models to limit the embolization of islets into smaller segments of the liver, just so that the engraftment can be more easily studied [221]. These models have made it slightly easier to obtain adequate numbers of islets per biopsy, but this sort of manipulation does little for minimally-invasive imaging. The main problem is that the liver can be conservatively estimated to have a volume of approximately one liter, whereas the volume of islets being infused through the portal vein is a few milliliters. This difference of nearly three orders of magnitude makes detecting islets very difficult. The depth of human liver into makes imaging strategies involving optical detection of luminescence challenging and almost entirely restricted to applications in small animals [151; 302; 303; 304]. Even spotting islets using conventional magnetic resonance imaging [305; 306; 307] poses problems, yielding limited information about the location of individual islets and even less information on their viability or function. Other limitations of the liver as a site for IT are lipotoxicity [308] and glucotoxicity [217], but will not be discussed in this supplementary discussion.

CHAPTER 5: Design of a Tissue-Engineered Graft or Device for Transplantation

Summary

Tissue engineering strategies have provided an opportunity to regenerate or replace diseased cells and tissues through the design and fabrication of grafts or devices in the laboratory. Unlike solid organ or many composite tissue transplants, tissue-engineered (TE) grafts or devices can be transplanted extravascularly and as such are not revascularized immediately. As a direct consequence, oxygen diffusion limitations become more apparent. These limitations require certain design provisions to enable healthy engraftment, particularly in the early posttransplant period before new blood vessels grow into or near a device (<14 days). Design of a TE construct containing either cells or tissue should be performed to adequately account for oxygen transport limitations. This can be done by diffusion-reaction modeling with which the governing equations depend on the TE graft or device geometry (planar, cylindrical, and spherical).

Prior to designing a TE construct, a number of parameters need to be defined, some which can be defined from values found in literature, and others which depend on characterization of the materials, and cells or tissue that are used in the construction of the graft or device. These design parameters include (but are not limited to): (1) the number and volume of the cells or tissue equivalents to be seeded; (2) the composition (including purity) of the cells or tissue equivalents to be seeded; (3) the viability (or oxygen consumption rate) of the cells or tissue equivalents to be seeded; (4) the size (diameter) of a cell or tissue equivalent; (5) the oxygen partial pressure (pO_2) at the target transplant site; (6) the thicknesses of the scaffold and any encapsulant; (7) the oxygen permeabilities of the materials used in the scaffold and any encapsulant; and (8)

the presence or absence and the thickness of a fibrotic capsule, which is dependent on the target transplant site, the TE construct materials and delivery of anti-proliferative agents (either local or systemic). Nearly all of these design parameters can be modified in some way. Of particular interest are strategies to improve oxygen transport properties in the materials used and to enhance local delivery of oxygen at the transplant site of the graft or device.

Abbreviations (Text)

^{19}F-MRI	fluorine-19 magnetic resonance imaging
^{19}F-MRS	fluorine-19 magnetic resonance spectroscopy
ATP	adenosine triphosphate
B_0	external magnetic field
COV	coefficient of variation
DNA	deoxyribonucleic acid
DTZ	diphenylthiocarbazone or dithizone
EM	electron microscopy
IE	islet equivalent
IT	islet transplant or transplantation
kgBW	kilogram of body weight
OCR	oxygen consumption rate
PFC	perfluorocarbon
pO_2	oxygen partial pressure
PP	pancreatic polypeptide
$R1$	longitudinal relaxation rate
SD	standard deviation
SE	standard error
$T1$	spin-lattice relaxation time
TE	tissue-engineered

Abbreviations (Formulaic)

α_i	oxygen solubility coefficient in constituent *i* [mol/cm^3/mm Hg]
$(\alpha D)_i$	oxygen permeability in constituent *i* [mol/cm/mm Hg/sec)]
D_i	oxygen diffusion coefficient in constituent *i* [cm^2/sec]
ΔP_i	oxygen partial pressure drop across constituent *i* [mm Hg]
ΔP_{max}	maximum oxygen partial pressure drop across half-thickness of TE graft or device [mm Hg]
ϵ_i	void (non-cellular, non-viable) volume fraction in constituent *i*
ϵ_{PFC}	volume fraction of perfluorocarbon in scaffold
K_m	Michaelis-Menten constant [mol/L or mol/cm^3]
L_i	distance from axisymmetry to surface of constituent *i* for planar geometry [cm]
L_{cyl}	length of TE graft or device with cylindrical geometry [cm]
N_0	total number of cells or tissue equivalents
$(OCR)_i$	oxygen consumption rate per unit volume of cells or tissue in constituent *i* [mol/cm^3/sec]
P_c	critical or minimum oxygen partial pressure to maintain cell viability or function [mm Hg]
P_{ext}	external oxygen partial pressure [mm Hg]
P_i	oxygen partial pressure in constituent *i* [mm Hg]
P_{si}	oxygen partial pressure at the surface of constituent *i* [mm Hg]
ρ	ratio of oxygen permeabilities of dispersed and continuous phases in a composite material
R_i	distance from axisymmetry to surface of constituent *i* for cylindrical or spherical geometry [cm]

$(SA)_1$	surface area of TE graft or device [cm^2]
V_i	rate of oxygen depletion per unit volume in constituent *i* [$mol/cm^3/sec$)]
ζ_1	seeding density of cells or tissue equivalents per unit volume of scaffold [$cells/cm^3$ or tissue equivalents/cm^3 or islet equivalents/cm^3]

Introduction

Tissue engineering is an interdisciplinary field combining engineering, biology and medicine for the purpose of developing bioartificial substitutes that can be transplanted to restore function of diseased tissue [309; 310]. For most tissue engineering applications, there are a minimum number of cell or tissue equivalents that would need to be transplanted in order to achieve the desired therapeutic outcome. This requirement will increase when there is cell or tissue loss during the posttransplant course, and can result from inflammation, immune rejection, or nutrient and oxygen deficiency. The number of cells or tissue equivalents that can be seeded into a tissue-engineered (TE) graft or device is in particular constrained by the availability of oxygen [311], and this constraint can be mitigated by appropriate design considerations. It is critically important to eliminate oxygen deprivation as this can reduce necrotic cell and tissue death, which in turn would minimize inflammation and immune rejection [312; 313]. In addition to reducing irreversible cell and tissue injury, improved local oxygen supply may be necessary to establish normal functioning of the transplanted cells or tissue. For example, pancreatic β-cells can survive down to oxygen partial pressures (pO_2) near-zero (~0.1 mm Hg), but insulin secretory capacity can be negatively affected at much higher pO_2 (>30 mm Hg) [87; 169; 314]. Another important consideration is the acceptable size (surface area) of a transplantable TE graft or device. Assuming a constant seeding density of cells or tissue equivalents, which should not exceed the maximum seeding density allowable given other design constraints, a higher required loading dose will result in a larger TE graft or device. In some cases, the required loading dose to achieve a therapeutic outcome would require transplantation of a TE graft or device that is prohibitively large.

For the reasons cited, oxygen transport is critical and must be considered when designing and fabricating a TE graft or device. There are a number of design parameters that need to be defined when developing a TE construct for a particular application, some which can be defined in part from values found in literature, and others which depend on characterization of the exact materials, and cells or tissue that are used in the construction of the TE graft or device. These design parameters include (but are not limited to): (1) the number and volume of the cells or tissue equivalents to be seeded; (2) the composition (including purity) of the cells or tissue equivalents to be seeded; (3) the viability (or oxygen consumption rate) of the cells or tissue equivalents to be seeded; (4) the size (diameter) of a cell or tissue equivalent; (5) the pO_2 at the target transplant site; (6) the thicknesses of the scaffold and any encapsulant; (7) the oxygen permeabilities of the materials used in the scaffold and any encapsulant; and (8) the presence or absence and the thickness of a fibrotic capsule, which is dependent on the target transplant site, the TE construct materials and delivery of anti-proliferative agents (either local or systemic). Nearly all of these design parameters can be modified in some way. Of particular interest is enhancing local oxygen supply at the transplant site and improving the oxygen transport properties in the materials used in the TE graft or device. Examples describing the impact of improved oxygen delivery on cell or tissue loading and TE graft or device size will be shown.

These principles apply virtually to all applications of tissue engineering, though this review and discussion is principally focused on the most promising approaches and methods for characterizing design parameters, and the design strategy for TE graft or devices in islet transplantation (IT).

General Design Considerations

Prior to designing a TE graft or device, several design parameters need to be defined. First, the amount, type and viability of the cells or tissue equivalents seeded into a graft or device needs to be accurately quantified. The currently used gold standard is visual counting, but this is technique is subject to inter-operator variability and can be inaccurate. Techniques based on direct measurements of DNA or nuclei may be the most accurate. Quantification of cell types is primarily important for heterogeneous cell or tissue preparations that contain multiple cell types. For example, islet preparations do not only contain (insulin-secreting) β-cells, but can have varying amounts of other cellular components (exocrine, other endocrine [α-, δ-, PP-], etc.) which lower the therapeutic quality of the preparation. Accurate assessment of cell viability is paramount. Techniques are currently available for direct measurement of oxygen consumption rate (OCR), which is a strong indicator of viability and a parameter important to the determination of cell or tissue loading within a TE graft or device. Second, accurate measurements of the local, steady-state pO_2 at the proposed site should be taken prior to any extravascular transplant, because vascularization does not occur immediately (10-14 days) and some sites may not be suitable from the standpoint of oxygenation. This information is required to ensure that the cells or tissue equivalents seeded within a TE graft or device have enough oxygen to remain viable during the entire post-transplant course. OCR and pO_2 measurements in tandem provide the basic information necessary to match oxygen demand with supply. Third, implants (whether prostheses, devices or grafts) usually induce inflammation in the days following surgery, which in some cases persists and results in the formation of an avascular fibrotic capsule. A fibrotic capsule itself can consume oxygen (contains 5-30% volume fraction of viable fibroblasts) and also represents an oxygen transfer resistance, which can severely affect oxygen delivery

to the cells or tissue of the TE graft or device. Given that many factors related to the material, shape, surface chemistry and transplant site contribute to the degree and nature of a foreign body reaction, each individual graft or device should be evaluated for whether it induces fibrotic capsule formation, how thick the capsule becomes and how much of the capsule is comprised of cells. Finally, it is important to consider ways available to enhance oxygenation of the TE graft or device. Possible strategies may involve improving native vascularization, exogenous oxygen delivery, and enhancing oxygen permeability in the materials used for the construction of the TE graft or device. Each of these design parameters is discussed in greater detail below within the context of IT, and it is shown how this information can be used to design a TE islet graft or device that enables adequate oxygen delivery to the islet graft. It should be noted that these general principles could be applied to virtually any type of TE graft or device design.

Methods for Measurement of Design Parameters for Islet Transplantation

Quantity, Composition, and Viability

Newer technologies have enabled direct and accurate measurement of the amount [81; 83], purity or composition [81; 85; 315] and viability [54; 81; 97; 98; 121] of a cellular or tissue preparation. These measurements are necessary in order to design and construct a TE graft or device with appropriate consideration for oxygen transport or supply limitations.

In the case of characterization of an islet preparation, and as discussed in *Chapter 3*, methods for direct quantification of either DNA content or nuclei counts are considered the most accurate since 1 cell or islet equivalent (IE, defined as a spheroidal cell

aggregate with an average diameter of 150 μm and containing about 1600 cells) have a reliably constant amount of genetic material, and the 2 measurements (DNA content and nuclei counts) are linearly proportional to each other [81]. DNA content measurements or nuclei counts are more accurate than visual counting (the current standard in the field) since they are less operator-dependent [81]. **Table 5-1** summarizes DNA content values on a per cell or IE basis, as described in literature.

For applications that involve cellular aggregates or tissue equivalents, in which the smallest, single unit of biological material is composed of >1 cell and which may contain cells of varying types, it is critical to accurately characterize their composition. This is particularly true for pancreatic islet preparations, whose purity are known to vary widely [217], especially in the case of clinical (human islet) preparations [217]. Pancreatic islet preparations contain a number of different cell types, including endocrine, exocrine, ductal, stromal, neuronal, leukocytic and endothelial, of which all cell types except endocrine are considered impurities. Furthermore, it may be prudent to characterize the proportion of β-cells (versus non-β-cells, or α-, γ- and pancreatic polypeptide [PP] cells) within the endocrine fraction to more accurately estimate the therapeutic value of the preparation. Pisania *et al.* reported results of a comprehensive study during which they quantified the number and volume fractions using electron microscopy and calculations, respectively, of the different cell types present in 33 freshly isolated human islet preparations [85]. Some of these results are reproduced in **Tables 5-2** and **5-3** for reference. The estimated average cell volumes used to convert number fractions to volume fractions are found in **Table 5-4**. The current standard employed for characterization of the purity in an islet preparation is staining with diphenylthiocarbazone (DTZ), a zinc-specific red dye that stains cells containing insulin

granules, followed by light microscopic evaluation [316]. However, this technique has been shown to consistently overestimate islet purity [81; 85]. Furthermore, as with visual counting, this technique is subjective and susceptible to inter-operator variability [217]. A better method to characterize the purity of an islet preparation may be by point counting morphometric analysis [81; 85], which has been shown to be correlate strongly with the more rigorous morphological assessment by electron microscopy [85]. Another technique that may be better involves immunohistochemistry followed by confocal laser scanning microscopy [315], though this technique involves 24-hour incubations with each primary and secondary antibodies rendering its pre-IT utility impractical.

As important as the quantity and composition of a cell or tissue preparation is the viability of that preparation. As discussed in *Chapter 3*, there are many assays of islet viability that have been studied, many involving direct detection of cell death indicators (vis-à-vis increased cell membrane permeability, caspase activation, phosphatidylserine externalization, DNA fragmentation) or mitochondrial dysfunction (vis-à-vis decreased mitochondrial membrane polarization, reduction potential, adenosine triphosphate (ATP) content, or OCR) [54]. Unfortunately, many of these have been shown incapable of detecting early irreversible cell injury or predicting outcomes post-IT. The most promising of these assays are believed to be the ones that detect mitochondrial dysfunction, as these events occur early during the cell death process [54; 317]. More specifically, recent data have shown that direct measurements of total OCR in a transplantable preparation (proportional to the amount of viable tissue to be transplanted) and OCR normalized to DNA content (OCR/DNA) (a measure of fractional viability) are capable of predicting outcomes following rat [120; 121], porcine [98], and human [91; 97; 99; 122] IT into the kidney capsule of diabetic nude mice (i.e., nude mouse bioassay). The nude

mouse bioassay has been found to be predictive of clinical islet transplant outcomes [89]. However, unlike the nude mouse bioassay, the OCR and OCR/DNA measurements can be performed prospectively and the information is available before the clinical transplantation needs to be done. Consequently, prospective measurements of transplanted OCR and OCR/DNA (in combination) have been observed to predict insulin independence in porcine-to-nonhuman primate (xenogeneic) islet transplantation (*unpublished observations*). Furthermore, initial clinical data with both autologous and allogeneic ITs have shown that transplanted OCR alone (not in combination with OCR/DNA) may be sufficient in predicting diabetes reversal [318]. Additionally, these results and observations may suggest that information regarding β-cell functional capacity (such as glucose-stimulated insulin secretion) may not be necessary to predict outcomes after IT. In addition to its predictive value, direct and accurate measurement of OCR is needed to design a TE graft or device, since the oxygen supply is usually limited and the magnitude of the oxygen sink is proportional to the number and viability of the cells or tissue equivalents to be seeded. OCR and/or OCR/DNA values obtained from the laboratory can be used with diffusion-reaction calculations to frame the dimensions and determine the maximum seeding density of the cells or tissue within a TE graft or device.

Native Oxygen Supply

Prior to transplantation of any TE graft or device it is important to quantify the available oxygen supply at the targeted transplant site. For this reason, the unknown pO_2 within the current clinical IT site of the liver has in part provided impetus for the theoretical work presented in *Chapter 4*. However, obtaining accurate *in vivo* pO_2 measurements is not a trivial matter.

There are several methods commonly employed to measure *in vivo* pO_2. The most common method utilizes polarographic needle electrodes. This technique works on the principle that electrical current generated at the cathode is proportional to the pO_2 at the cathode tip. The cathode tip is calibrated *in vitro* by exposing the cathode tip to buffered aqueous solution that is bubbled with gases of known pO_2. Although the method is simple, it has several limitations including that the measurements are affected by other factors in the local environment (pH, salinity and ionic strength) and may bias readings if performed over a longer period of time since the electrode tip consumes oxygen [319]. The insertion of the electrode tip itself is invasive and can cause tissue injury, and requires surgical exposure to access deeper structures. Smaller microelectrode tips (<10 μm) can be used, but these smaller tips are mechanically fragile and more susceptible to stray electrical currents [319]. However, these have been used to measure the pO_2 at several prospective islet transplant sites [202; 216]. Another commonly employed method involves optical fibers and fluorescence-based probes, similar technology as is used in the some of the systems used to measure OCR [54; 91; 97; 98; 121; 122]. The optical fiber carries light to a fluorophore coating at a probe tip, which generates fluorescence and is carried back to the spectrometer [319]. Different systems correlate different properties of the fluorescence (i.e., intensity, lifetime) with the pO_2 at the probe tip. To obtain a pO_2 measurement the probe tip must be inserted into the tissue-of-interest and the probe tips are relatively large (>200 μm), so they are more invasive than measurements with the polarographic electrode. However, unlike the polarographic electrodes, the fluorophore does not consume oxygen [319]. The main limitations of this technique are its invasiveness and attrition of the fluorophore coating, which requires maintenance (re-application). This problem can be minimized by covering the

fluorophore with a semi-permeable membrane, but this will slow the measurement response time. Both polarographic electrodes and fiberoptic oxygen sensors have another important limitation in that they provide single point measurements of pO_2 and are unable to account for oxygen gradients which may be present or for differences in the pO_2 between different compartments (intracellular, interstitial, intravascular).

Another type of pO_2 measurement utilizes fluorine magnetic resonance spectroscopy (^{19}F-MRS) or imaging (^{19}F-MRI). A main advantage of any MRS or MRI technique is that they are non-invasive. ^{19}F-MRS and ^{19}F-MRI exhibit additional advantages that make them attractive tools for *in vivo* measurement-taking, including: 1) the high detection sensitivity of the fluorine-19 nucleus (relative to other detectable nuclei like carbon-13, oxygen-17, sodium-23, or phosphorus-31) which is due to a strong magnetic moment – similar in magnitude to hydrogen-1; and 2) an otherwise low fluorine-19 background signal in the human body. Given these qualities, injection or implantation of fluorinated compounds has been a strategy used by many to introduce *in vivo* contrast detectable by ^{19}F-MRS or ^{19}F-MRI [217]. One of the most commonly used fluorine-rich compounds are perfluorocarbons (PFCs), which have a high fluorine content, are generally considered bio-inert, are highly hydrophobic and have high oxygen solubility (10-40 times higher than water).

The key relationship that enables pO_2 estimation by ^{19}F-MRS and ^{19}F-MRI is the linear correlation between the inverse of the spin-lattice relaxation time ($T1$), which is referred to as the spin-lattice relaxation rate ($R1$), and pO_2. The theoretical basis for this is elaborated on in *Chapter 6*. The correlation between $R1$ and pO_2 has been confirmed experimentally in numerous instances [56; 320; 321; 322; 323; 324; 325; 326; 327; 328;

329; 330; 331; 332; 333; 334; 335; 336] and has enabled the minimally-invasive estimation of pO_2 at the site(s) of injected [321; 322; 328; 329; 331; 333; 335; 337; 338; 339; 340; 341; 342; 343; 344], implanted [332; 334; 336; 345], or otherwise sequestered [324; 325; 327; 329; 330; 346; 347] PFC *in vivo*. ^{19}F-MRS or ^{19}F-MRI has been employed in research for its prospective use with IT [56; 334; 336].

If an intervention (e.g., pre-vascularization, supplementary *in situ* oxygenation) were to enhance the available oxygen supply, then the timing and magnitude of any changes in local pO_2 at the prospective transplant site should be measured, as such an intervention may impact the design of the TE graft of device. Researchers have developed methods to help facilitate better and more rapid vascularization of islets post-IT. Some of these methods have involved arteriovenous shunting [348; 349; 350; 351], controlled drug release of pro-angiogenic factors from polymeric devices/constructs [352; 353; 354; 355; 356; 357], prevascularization of tissue-engineered chambers at extrahepatic sites of transplant [348; 349; 350; 351; 352; 355; 356; 357; 358; 359; 360; 361; 362], co-transplantation of endothelial cells [357] or their progenitors [363], and the transfection of genes directly involved in vasculogenesis [229; 364], just to name a few.

There have not been many studies performed to quantify the *in vivo* pO_2 at prospective IT sites using any of the aforementioned techniques, but selected results from several studies are summarized in **Table 5-5**.

Fibrotic Capsule Formation

It is also important to determine whether the TE graft or device will stimulate a foreign body reaction and to characterize the extent of fibrotic capsule formation, as this would negatively affect TE graft oxygenation. A fibrous capsule arises from a chronic inflammatory reaction towards an implant, and may occur following transplantation of a TE graft or device. The fibrous capsule is typically characterized by an avascular layer composed of dense connective tissue and fibroblasts near the surface of the implant and a vascularized layer composed of loose connective tissue containing fibroblasts and new blood vessels that is separated from the implant by the avascular layer [207; 220]. The composition and thickness of the fibrotic capsule is dependent on numerous factors specific to the TE graft or device, including: (1) materials used, and their microarchitecture and porosity; (2) size of the graft or device; (3) shape of the graft or device; (4) the transplant site; (5) surface topography and chemistry; and (6) presence or absence of leachable substances or agents that may modulate a local fibrotic reaction [217; 365; 366; 367; 368; 369; 370]. Since fibrotic capsule formation is dependent on factors unique to the TE graft or device and its application, it is important to characterize the thickness of the avascular part of the capsule, the volume fraction of the fibroblasts (and other cells, like macrophages and foreign-body giant cells) within the fibrotic capsule, and the distance of the nearest blood vessels, since all of these affect the diffusion distance from the oxygen supply as well as the pO_2 at the surface of the TE graft or device.

Therapeutic Dose

The most important step in designing a TE graft or device is to determine the minimum required dose of cells or tissue equivalents that need to be transplanted in order to

achieve the desired post-transplant outcome. The required dose will impact the maximum (or allowable) seeding density of cells or tissue equivalents within the scaffold material or device, which will directly impact the minimum size (surface area) of the TE graft or device. For example, assuming an average islet quality, the minimum required dose to consistently achieve diabetes reversal is approximately 5000 IEs per kilogram of body weight (kgBW) for clinical auto-IT [183; 184], 10,000 IEs per kgBW for clinical allo-IT [43; 44; 45; 46; 68; 184], and 25,000 IEs per kgBW for xeno-IT (porcine-to-non-human primate) [371; 372]. These doses have been determined empirically through years of experience with intraportal IT. It is conceivable that the required islet dose could be reduced by transplanting islets at an extrahepatic site since there is evidence suggesting that the liver is not the optimal site for IT [217], and this is in part the focus of discussion in the previous chapter (*Chapter 4*). Also, even though the prescribed doses have been based primarily on the quantity of islets required to achieve the desired outcome (insulin independence), the quality of the preparation is possibly more critical [54; 55; 81; 97; 121]. However, examples that illustrate the relationship between required islet dose and minimum TE graft or device size are given following presentation of a generalized mathematical model used in the calculation of the maximum islet seeding density or loading.

We have now discussed the importance of characterizing the cell or tissue preparation for quantity, composition and viability, the pO_2 at the prospective transplant site, and the fibrogenicity of the TE graft or device following transplantation. Any information about the mass transfer properties (i.e., solubilities, diffusivities) is valuable to the design since these properties will influence the oxygen delivery to the cells or tissue that is seeded in the TE graft or device. Additionally, incorporation of immunomodulatory drugs,

angiogenic or anti-proliferative co-factors, imaging agents may have an effect on the thickness and composition of a fibrotic capsule, the nearness and density of the local blood supply, and the oxygen transport properties in the bulk material(s) – and their potential impact on the design should be considered. As much information regarding these design parameters should be gathered to best optimize the TE graft or device design. **Figure 5-1** summarizes the generalized strategy that is proposed when designing a TE graft or device. The next section of this *Chapter* focuses on presenting a generalized mathematical model for calculating the maximum cell or tissue seeding density, a quantity which is proportional to the minimum TE graft or device size.

General Mathematical Model and Assumptions

An engineered construct can be designed to account for the provision of oxygen delivery. Many TE grafts or devices rely on passive diffusion of oxygen from the surface and require that the seeding densities of cells or tissue remain low enough to prevent formation of hypoxic or anoxic regions, and thus to prevent early (<14 days) loss of cells or tissue. The maximum seeding density of the cells or tissue is determined from a number of design parameters, and can be calculated from diffusion-reaction theory. These calculations can help ensure that the cells or tissue receive adequate oxygenation based on the constraints inherent to an application. The generalized mathematical theory has been previously developed by Avgoustiniatos and Colton [207; 373], but the model has been simplified to involve only equations relevant to the TE graft or device design and to highlight some key design considerations. Regardless of the device geometry (planar, cylindrical, spherical), the TE graft or device can be represented schematically by a generalized arrangement of layers and it depicted in **Figure 5-2**. The generalized TE graft or device can be represented by 4 constituents, the cell or tissue

equivalent (constituent 0), the scaffold (constituent 1 or layer 1, which is the material into which the cells or tissue equivalents are seeded), the encapsulant (constituent 2 or layer 2, if included in the design), and the fibrotic capsule (constituent 3 or layer 3, if it exists). The basis of the diffusion-reaction theory arises from the mass conservation equation, which in its general form accounts for steady-state diffusion and oxygen consumption (reaction) within each constituent *i* (**Equation 5-4**):

(5-4) $$(\alpha D)_i \frac{\mathrm{d}^2\mathrm{P_i}}{\mathrm{dx}^2} = V_i$$

where $(\alpha D)_i$ is the oxygen permeability (which is the product of oxygen solubility and diffusion coefficients), P_i is the pO_2, and V_i is the rate of oxygen depletion per unit volume in constituent *i*. In this model, the analysis involves one dimension (*x*) since the geometry is symmetric about a plane (planar), line (cylindrical) or point (spherical). The OCR within each constituent *i* is modeled by assuming Michaelis-Menten kinetics (**Equation 5-5**) at a pO_2 that is much higher than the (K_m/α_i) value, which represents the pO_2 at which OCR is reduced by 50% (or the half-maximum value) (**Equation 5-6**):

(5-5) $$V_i = (OCR)_i(1-\epsilon_i)\frac{P_i}{\left(\frac{K_m}{\alpha_i}\right)+P_i}$$

(5-6) $$V_i = (OCR)_i(1-\epsilon_i)$$

where $(OCR)_i$ is the maximum volumetric OCR of cells or tissue in constituent *i*, which can be directly measured by conventional methods [54; 98], and ϵ_i is the non-viable void fraction in constituent *i*. At least in this case, modeling oxygen consumption as a zero-

order reaction is reasonable since the (K_m/α_i) for islets is believed to be very low (~0.1 mm Hg) and has been shown experimentally [98].

As illustrated in the schematic (*Figure 5-2*), the TE graft or device should be designed such that a cell or tissue equivalent located along the axisymmetry of the TE graft or device, which represents the largest distance that a single cell or tissue equivalent can be from the oxygen source, is expected to be fully oxygenated. The presence or absence of additional mass transfer resistances (such as an encapsulant or fibrotic capsule) will also impact oxygenation, and they need to be characterized to optimize the TE graft or device design.

The TE graft or device can be modeled with the following assumptions:

1. Steady-state oxygen transport and consumption;
2. The oxygen source is represented by the external pO_2 (P_{ext}) and is at the surface of the outermost constituent;
3. No oxygen flux across the axis of symmetry;
4. A cell or tissue equivalent is spherical with an average radius represented by R_0;
5. Cells or tissue equivalents are homogeneously distributed throughout the scaffold (Layer 1), with an average cell or tissue volume fraction represented by $(1-\epsilon_1)$;
6. The scaffold has a uniform half-thickness of L_1 (planar) or R_1 (cylindrical or spherical) and exhibits characteristic oxygen permeability in the scaffold material represented by $(\alpha D)_1$;
7. The encapsulant (Layer 2) has a uniform half-thickness of $(L_2 - L_1)$ or $(R_2 - R_1)$ and represents only a mass transfer resistance (no oxygen-consuming cells or

tissue) and exhibits characteristic oxygen permeability in the encapsulant material represented by $(\alpha D)_2$;

8. Fibroblasts are homogeneously distributed throughout the fibrotic capsule (Layer 3), with an average cell volume fraction represented by $(1-\epsilon_3)$;
9. The fibrotic capsule (Layer 3) has a uniform half-thickness of $(L_3 - L_2)$ or $(R_3 - R_2)$ and exhibits a characteristic oxygen permeability represented by $(\alpha D)_3$, which is the product of the oxygen solubility and diffusivity in connective tissue;
10. The cells or tissue equivalents seeded in the scaffold (Layer 1) or the fibroblasts residing in the fibrotic capsule consume oxygen at a characteristic rate given by $(OCR)_1$ (cells or tissue equivalents) or $(OCR)_3$ (fibroblasts).

The optimized form of the graft or device depends on key design parameters related to the following (the asterisk indicates that the design parameter is modifiable):

Graft or device size

Thickness*

Transplant site

External pO_2*

Material properties

Oxygen solubility*

Oxygen diffusivity*

Cells or tissue

Cell or tissue volume fraction (or void volume fraction)*

Viability (or oxygen consumption rate)

Size of cell or tissue equivalent

The overall size of the graft or device is related to the seeding density, but ultimately depends on the required dose of cell or tissue equivalents needed to achieve the desired therapeutic outcome. Modifiable design parameters and their impact on the design, and key strategies to increase seeding density and decrease size are depicted in **Figure 5-3**.

Each layer of the graft or device represents an oxygen transfer resistance that is associated with a characteristic pO_2 drop ($\Delta P_i = P_{si} - P_{s(i-1)}$). The final pO_2 drop that needs to be accounted for is into the cell or tissue equivalent located at the axisymmetry, which cannot exceed ($\Delta P_0 = P_{s0} - P_c$), where P_{s0} is the pO_2 at the surface of that cell or tissue equivalent and P_c is the critical pO_2 that represents the minimum allowable to sustain either viability or function, which may differ depending on the cell type and design requirements. For example, in the case of IT, the β-cells can survive down to very low pO_2 (~0.5 mm Hg) [167], but second-phase insulin secretion is severely reduced at much higher pO_2 (5-10 mm Hg) [87; 164; 169; 314]. The sum total of pO_2 drops (ΔP_{total}) through each layer must be less than the difference between the external (at the surface of the outermost layer) and critical pO_2 values (**Equation 5-6**).

(5-6) $$\Delta P_{max} = \Delta P_0 + \Delta P_1 + \Delta P_2 + \Delta P_3 < P_{ext} - P_c$$

Regardless of TE graft or device geometry, the pO_2 drop across a cell or tissue equivalent is calculated with the following (**Equation 5-7**):

(5-7) $$\Delta P_0 = \frac{(OCR)_0 R_0^2}{6(\alpha D)_0}$$

The pO_2 drop across each layer can be calculated for each of three geometries and the detailed theory is presented by Avgoustiniatos and Colton [207]. The equations have been reduced for all three geometries (planar, cylindrical, and spherical) and for each of the three layers (scaffold, encapsulant, and fibrotic capsule), as based on the schematic shown in *Figure 5-2*, and are shown below (**Equations 5-8** through **5-16**).

Planar

(5-8) $$\Delta P_1 = \frac{(OCR)_0(1-\epsilon_1){L_1}^2}{2(\alpha D)_1}$$

(5-9) $$\Delta P_2 = \frac{(OCR)_0(1-\epsilon_1)(L_2-L_1)L_1}{(\alpha D)_2}$$

(5-10) $$\Delta P_3 = \frac{(OCR)_3(1-\epsilon_3)(L_3-L_2)^2}{2(\alpha D)_3} + \frac{(OCR)_0(1-\epsilon_1)(L_3-L_2)L_1}{(\alpha D)_3}$$

Cylindrical

(5-11) $$\Delta P_1 = \frac{(OCR)_0(1-\epsilon_1){R_1}^2}{4(\alpha D)_1}$$

(5-12) $$\Delta P_2 = \frac{(OCR)_0(1-\epsilon_1){R_1}^2}{2(\alpha D)_2}\ln\left(\frac{R_2}{R_1}\right)$$

(5-13) $$\Delta P_3 = \frac{(OCR)_3(1-\epsilon_3)}{2(\alpha D)_3}\left[\frac{({R_3}^2-{R_2}^2)}{2} - {R_2}^2\ln\left(\frac{R_3}{R_2}\right)\right] + \frac{(OCR)_0(1-\epsilon_1)\cdot{R_1}^2}{2(\alpha D)_3}\ln\left(\frac{R_3}{R_2}\right)$$

Spherical

(5-14) $$\Delta P_1 = \frac{(OCR)_0(1-\epsilon_1){R_1}^2}{6(\alpha D)_1}$$

(5-15) $$\Delta P_2 = \frac{(OCR)_0(1-\epsilon_1){R_1}^3}{3(\alpha D)_2}\left(\frac{1}{R_1}-\frac{1}{R_2}\right)$$

(5-16) $$\Delta P_3 = \frac{(OCR)_3(1-\epsilon_3)}{3(\alpha D)_3}\left[\frac{{R_3}^2-{R_2}^2}{2}-{R_2}^2\left(1-\frac{R_2}{R_3}\right)\right]+\frac{(OCR)_0(1-\epsilon_1){R_1}^3}{3(\alpha D)_3}\left(\frac{1}{R_2}-\frac{1}{R_3}\right)$$

The cell or tissue volume fractions (relative to the total volume of the scaffold) can be estimated for each of the geometries using the following (**Equations 5-17** through **5-19**):

Planar

(5-17) $$(1-\epsilon_1) = \frac{2\pi N_0 {R_0}^3}{3L_1(SA)_1}$$

Cylindrical

(5-18) $$(1-\epsilon_1) = \frac{4N_0{R_0}^3}{3R_1X_1}$$

Spherical

(5-19) $$(1-\epsilon_1) = N_0\left(\frac{R_0}{R_1}\right)^3$$

where N_0 is the total number of cells or tissue equivalents seeded into a scaffold, $(SA)_1$ is the surface area of a planar graft or device, and X_1 is the length of a cylindrical graft or device.

These basic equations can be used to help guide TE graft or device design, and to answer relevant questions regarding the impact of different design parameters (i.e., thicknesses, external pO_2, oxygen permeabilities, etc.) on cell or tissue equivalent seeding density and graft or device size.

Application of Theory to Tissue-Engineered Graft or Device Design

A critical barrier for translating successful TE strategies from rodent or smaller animal models to humans is scaling. As indicated previously, assuming that an islet preparation is of average quality, it has been determined that approximately 10,000 IEs per kgBW are required to reverse diabetes following clinical allo-IT, meaning that 700,000 IEs need to be transplanted into a 70-kg recipient. The required dose is very large and it could itself be reduced given that the human pancreas has >1-1.5 million islets and between 5-30% of the total islet mass is required to maintain normoglycemia [198; 374]. Nevertheless, we consider the currently required dose. The required dose is important since it is proportional to the volume of cells or tissue to be transplanted, which will correlate with the allowable seeding density and ultimately the dimensions of the TE graft or device.

Seeding density and size

Consider a planar device seeded with islets and with no encapsulant or fibrotic capsule. In this case, the R_0 = 75 μm (average radius of an IE), the $(OCR)_0 = 2 \cdot 10^{-8}$ mol/cm^3/sec (representative viability of an islet preparation), the P_{ext} = 40 mm Hg (representative of measured pO_2 values in the intraperitoneal cavity, see *Table 5-5*), the P_c = 0.1 mm Hg (critical pO_2 for islet cell survival), and a reasonable scaffold half-thickness of L_1 = 0.1 cm

(schematic shown in **Figure 5-5**). All other model parameters, including oxygen permeabilities, are summarized in **Table 5-6**. The seeding density can be estimated and is dependent on the islet dose, the TE graft or device thickness and surface area (**Equation 5-20**), and represents the maximum number of IEs that can be seeded into a known scaffold volume.

(5-20) $$\zeta_1 = \frac{N_0}{2(SA)_1 L_1}$$

For this case, to estimate the approximate surface area, *Equations 5-6*, *5-7*, *5-8* and *5-17* are combined and re-arranged to solve for $(SA)_1$ (**Equation 5-21**):

Planar device, no encapsulant or fibrotic capsule

(5-21) $$(SA)_1 = \frac{\pi N_0 R_0 L_1}{(\alpha D)_1 \left[\frac{3\Delta P_{max}}{(OCR)_0 {R_0}^2} - \frac{(\propto D)_1}{2(\propto D)_0}\right]}$$

For a TE graft or device to be seeded with 700,000 IEs, the maximum seeding density would be low (≤5027 IEs/cm^3) and the surface area would have to be prohibitively large for transplant into a human recipient (≥696.0 cm^2). For reference, the surface area of a standard sheet of printer paper is 603.2 cm^2. The seeding density would further decrease and the surface area would increase with poorer oxygen supply, an immunoisolation barrier (encapsulant) or fibrotic capsule. Assuming the same external pO_2 as in the previous example (P_{ext} = 40 mm Hg), analysis can be done to account for the presence of an encapsulant and fibrotic capsule (schematic shown in **Figure 5-6**). In this case, to estimate the approximate surface area, *Equations 5-6*, *5-7*, *5-8*, *5-9*, *5-10* and *5-17* are combined and re-arranged to solve for $(SA)_1$ (**Equation 5-22**):

Planar device, with encapsulant and fibrotic capsule

(5-22) $$(SA)_1 = \frac{(OCR)_0 \pi N_0 {R_0}^3 \left[\frac{L_1}{(\alpha D)_1} + \frac{2(L_2 - L_1)}{(\alpha D)_2} + \frac{2(L_3 - L_2)}{(\alpha D)_3}\right]}{3\left[\Delta P_{max} - \frac{(OCR)_3 (1-\epsilon_3)(L_3 - L_2)^2}{2(\alpha D)_3} - \frac{(OCR)_0 {R_0}^2}{6(\alpha D)_0}\right]}$$

The addition of a relatively thin (100-μm) encapsulant and a fully-developed (100-μm, 10% cell volume fraction) fibrotic capsule results in the maximum seeding density being significantly reduced (≤1668 IEs/cm^3) and the required surface area almost tripling in size (≥2098.1 cm^2). In the previous two examples, the critical pO_2 was nearly zero (P_c = 0.1 mm Hg) and reflects the minimum pO_2 required to prevent islet cell death. However, insulin secretion is affected at much higher pO_2 and this should be accounted for in the design. The design objective may be to minimize islet cell death during the first few weeks posttransplant, with the intent that full function is reestablished at the time of completed neovascularization (1-2 weeks later). However, this may never occur. Consequently, in some cases, it may be prudent to account for the possibility that oxygen supply may not improve or may be transiently lowered in the peritransplant period (due to active inflammation). This can be done by increasing the minimum pO_2 requirement, which will reduce the maximum pO_2 drop that is allowable, which in turn will lower the maximum seeding density and increase the required size. Consider the previous scenario, except with the critical pO_2 being changed from 0.1 to 10 mm Hg. For a planar TE graft or device with no encapsulant or fibrotic capsule and seeded with 700,000 IEs, the maximum seeding density is ≤3106 IEs/cm^3 (~38% lower) and the minimum surface area is ≥1126.8 cm^2 (~62% larger). For the same TE graft or device with an encapsulant and fibrotic capsule, the maximum seeding density is ≤546 IEs/cm^3 (~67% lower) and the minimum surface area is ≥6413.3 cm^2 (~306% larger). These

analyses serve to illustrate the importance of oxygenation for TE graft or device design, and of determining appropriate design constraints. The calculations also highlight the importance of accurately characterizing the number of IEs and their viability (OCR) in an islet preparation, and the available external pO_2 – which may change with time post-transplant and which may differ depending on transplant site. With the currently required islet dose and under reasonable conditions, these calculations suggest that the required size of a planar TE graft or device is not practical for human transplant. Oxygen transfer does depend partly on geometry and improves with increasing surface area-to-volume ratio; planar (~$1/L_1$), cylindrical (~$2/R_1$), and spherical (~$3/R_1$). However, a change to a different geometry will still require a very large TE graft or device. There are several strategies that can be employed to significantly reduce the size of the TE graft or device, including increasing the local oxygen supply and improving the oxygen transfer.

Increased oxygen supply

The oxygen supply at or near the TE graft or device can be improved in a number of ways, including increasing the local vascular density [217] or *in situ* oxygen generation by electrochemistry [375], photosynthesis [376] or oxygen-generating biomaterials [377]. The effect of improved oxygenation on both islet seeding density and TE graft or device surface area can be estimated by adjusting the external pO_2 in the model; **Figures 5-7** and **5-8** illustrate estimates of seeding density and surface area in a planar TE graft or device, with increasing external pO_2 (P_{ext} = 25-760 mm Hg, range) and at two different critical pO_2 values, representing the lower threshold for islet cell death (P_c = 0.1 mm Hg) and healthy insulin secretion (P_c = 10 mm Hg). The estimates are also tabulated in **Tables 5-7** (no encapsulant or fibrotic capsule) and **5-8** (with encapsulant and fibrotic capsule). For a TE graft or device with no encapsulant or fibrotic capsule (*Figure 5-5*,

schematic representation) and the low critical pO_2 (0.1 mm Hg), an increase in the external pO_2 from 40 to 100 (arterial pO_2) or 305 mm Hg (achievable with *in situ* oxygen generation) increases the seeding density by 3.3 or 11.2 times, corresponding to a percent decrease in surface area of 69.8% (≥210.0 cm^2) or 91.1% (≥62.0 cm^2), respectively. If the same TE graft or device is considered except at the higher critical pO_2 (10 mm Hg), an increase in external pO_2 from 40 to 100 or 305 mm Hg increases the seeding density by 4.7 or 17.6 times, corresponding to a percent decrease in surface area of 78.9% (≥237.3 cm^2) or 94.3% (≥64.2 cm^2), respectively. An increase of external pO_2 can have a profound impact on the size of the TE graft or device, and could reasonably reduce the surface area from larger than a sheet of printer paper (≥600 cm^2) to smaller than a post-it note (≤60 cm^2).

Another relevant question is whether or not increasing the external pO_2 could sufficiently reduce the size of a TE graft or device if the oxygen source was separated from the cells or tissue by an encapsulant and fibrotic capsule. For a TE graft or device with an encapsulant and fibrotic capsule (*Figure 5-6*, schematic representation) and the low critical pO_2 (0.1 mm Hg), an increase in the external pO_2 from 40 to 100 or 305 mm Hg increases the seeding density by 5.1 or 19.0 times, corresponding to a proportional percent decrease in surface area of 80.3% (413.2 cm^2) or 94.7% (110.4 cm^2), respectively. If the same TE graft or device is considered except at a higher critical pO_2 (10 mm Hg), an increase in external pO_2 from 40 to 100 or 305 mm Hg increases the seeding density by 13.5 or 56.0 times, corresponding to a proportional percent decrease in surface area of 92.6% (476.3 cm^2) or 98.2% (114.4 cm^2), respectively. These calculations indicate that the size of a TE graft or device can be dramatically reduced by improved external oxygen supply, even with an encapsulant and fibrotic capsule. In

these examples, the encapsulant was relatively thin (100-um) and increasing the thickness would result in increased net oxygen transfer resistance into the TE graft or device. However, the majority of the pO_2 drop occurs in the avascular fibrotic capsule – which has a large cell volume fraction (10%) composed primarily of fibroblasts – suggesting the importance of preventing foreign body reaction at the surface of the TE graft or device.

Improved oxygen transfer

Oxygen delivery can be improved by materials engineering to reduce mass transfer resistances or by incorporation of substances that have higher oxygen permeability. One strategy is to incorporate PFCs – which have 10-40 times higher oxygen permeability than water [378] – into the TE graft or device scaffold [56; 379; 380]. Incorporation of PFCs can increase the effective oxygen permeability of a material. The magnitude of this increase can be estimated using the Maxwell relationship (**Equations 5-23** and **5-24**), which describes the effective oxygen permeability in a composite material containing two phases, one that is dispersed and one that is continuous. In this case, the dispersed phase is the PFC and the continuous phase is TE scaffold material, both of which have different oxygen permeability.

(5-23) $$\frac{(\alpha D)_{1,eff}}{(\alpha D)_1} = \frac{2 - 2\epsilon_{PFC} + \rho(1 + 2\epsilon_{PFC})}{2 + \epsilon_{PFC} + \rho(1 + \epsilon_{PFC})}$$

(5-24) $$\rho = \frac{(\alpha D)_{PFC}}{(\alpha D)_1}$$

where $(\alpha D)_{1,eff}$ is the effective oxygen permeability of the composite material, ϵ_{PFC} is the volume fraction of PFC, and ρ is the ratio of oxygen permeabilities of the two phases. Using the Maxwell relationship, incorporation of 5%, 10%, 20%, 30% and 50% PFC by volume is estimated to increase the oxygen permeability of a hydrogel-based scaffold by 1.2, 1.3, 1.7, 2.2 and 2.9 times, respectively. Depending on the case, this may have utility in improving oxygen transport into a TE graft or device.

Consider a planar TE graft seeded with islets and with no encapsulant or fibrotic capsule. The same constants will be assumed as before (**Table 5-6**). The difference in this case is the incorporation of PFC into the scaffold material of the TE graft (depicted as emulsified spherical droplets in **Figure 5-9**). Changes in the maximum islet seeding density and minimum TE graft surface area can be calculated using *Equations 5-20*, *5-21*, *5-23* and *5-24*. For example, assuming a P_{ext} = 40 mm Hg and P_c = 0.1 mm Hg, the maximum islet seeding density increases (216%) from 5027 to 10,876 IEs/cm^3 and the minimum surface area decreases (54%) from 696.2 to 321.8 cm^2 by incorporating 30% PFC by volume into the scaffold. If the same TE graft or device has an encapsulating layer and fibrotic capsule, the maximum islet seeding density increases (146%) from 1668 to 2433 IEs/cm^3 and the minimum surface area decreases (31%) from 2098.1 to 1,438.8 cm^2 by incorporating 30% PFC by volume into the scaffold. An increase to the P_{ext} can be combined with incorporation of PFC to reduce the TE graft size. For example, consider a TE graft with no encapsulant or fibrotic capsule with a P_{ext} = 305 mm Hg and P_c = 0.1 mm Hg. In this case, the maximum islet seeding density increases (216%) from 56,452 to 121,951 IEs/cm^3 and the minimum surface area decreases (54%) from 62.0 to 28.7 cm^2 by incorporating 30% PFC by volume into the scaffold. If the same TE graft or device has an encapsulating layer and fibrotic capsule, the maximum islet seeding

density increases (146%) from 31,703 to 46,235 IEs/cm^3 and the minimum surface area decreases (31%) from 110.4 to 75.4 cm^2 by incorporating 30% PFC by volume into the scaffold.

When compared with increases to the external oxygen supply, these improvements are modest. For example, a TE graft with no encapsulant or fibrotic capsule and with P_c = 0.1 mm Hg has a calculated surface area of 696.2 cm^2 at P_{ext} = 40 mm Hg and 0% v/v PFC, 321.8 cm^2 at P_{ext} = 40 mm Hg and 30% v/v PFC, 62.0 cm^2 at P_{ext} = 305 mm Hg and 0% PFC, and 28.7 cm^2 at P_{ext} = 305 mm Hg and 30% PFC. This indicates that an attainable increase in P_{ext} markedly reduces the TE graft size (>ten-fold), but solely incorporating PFC does not (~two-fold). The relative impact of increased oxygen permeability in the TE scaffold is further minimized when an encapsulant and/or fibrotic capsule is present. However, different applications may require the use of both strategies – such as when the external pO_2 requirement is limited or has been optimized for a particular type or cell or tissue, and additional size reduction can be accomplished by incorporation of substances like PFC. Another potential benefit of incorporation of PFC into a TE graft or device is its detection via ^{19}F-MRS or ^{19}F-MRI, which can be used to measure the average pO_2 in the vicinity of the cells or tissue [56; 334; 336].

The effects of increasing the scaffold oxygen permeability by incorporation of PFC is illustrated in **Figures 5-10**, **5-12** and **5-14** (maximum seeding density) and **Figures 5-11**, **5-13** and **5-15** (minimum surface area), are shown at different external pO_2 values (P_{ext} = 40, 100 and 305 mm Hg) and with or without an encapsulant and fibrotic capsule. **Tables 5-9**, **5-10**, **5-11**, **5-12**, **5-13** and **5-14** summarize the values presented in *Figures 5-10* through *5-15*.

Conclusion

This review and discussion is meant to highlight the importance of oxygenation in the design of TE graft or devices. Transplanted cells or tissues that are not immediately revascularized are susceptible to death if the oxygen supply and transport (by diffusion) is not adequate. By the time new blood vessels grow into the graft or near the device to provide adequate oxygen supply, many of the cells may be lost. This can be in part prevented with design of a TE graft or device with appropriate consideration for the available oxygen provision. This design process should involve accurate characterization of cell and tissue quantity, composition, and viability, as well as the pO_2 at the prospective transplant site. Fibrotic capsule formation can have a profound effect on oxygen delivery and needs to be evaluated for any application. Along with a determination of the required therapeutic dose, all of these factors contribute to the maximum cell or tissue seeding density and minimum TE graft or device size, which are important practical considerations for human transplant. In applications that currently require high doses of viable cells or tissue, the TE graft or device size can be reduced by increasing the local oxygen supply and transport.

Table 5-1: DNA content on a per cell or islet equivalent basis

Cell or Islet Type	DNA Content	Ref.
Rat α-cell	7.3 pg/cell	[381]
Rat β-cell	5.7 pg/cell	[381]
Rat islet	6.4-6.5 pg/cell	[83]
Human islet	6.6-6.9 pg/cell	[83; 86]
Human or porcine islet	10.4 ng/IE	[98]

Abbreviations: DNA, deoxyribonucleic acid; IE, islet equivalent.

Table 5-2: Cell number fraction estimates[a] from Pisania *et al*. [85]

Cell type	Mean (± SE)	Range	COV
Islet[b]	0.48 ± 0.03	0.13-0.85	0.31
β-	0.36 ± 0.02	0.13-0.64	0.35
Non-β- (α, γ, ε, PP)	0.13 ± 0.10	0.04-0.27	0.44
β- (within islet only)	0.74 ± 0.02	0.41-0.84	0.13
Non-islet[c]	0.52 ± 0.03	0.03-0.83	0.29
Acinar	0.25 ± 0.02	0.05-0.42	0.40
Duct	0.23 ± 0.02	0.02-0.38	0.37
Other	0.04 ± 0.004	0.004-0.12	0.64

[a]Based on electron microscopic evaluation with 33 freshly isolated human islet preparations.
[b]Not including acinar, ductal or other (neuronal, leukocytic, endothelial) cells.
[c]Acinar, ductal, and other cells.
Abbreviations: COV, coefficient of variation; PP, pancreatic polypeptide; SE, standard error.

Table 5-3: Volume fraction estimates and number of cells per islet equivalent from Pisania *et al*. [85]

Cell type	Mean (± SE)	Range	COV
Islet (EM)[a]	0.52 ± 0.03	0.20-0.89	0.31
Islet (DTZ)[b]	0.68 ± 0.03	0.30-0.95	0.26
Number of cells per IE			
Total	1560 ± 20	1430-1980	0.07
β-	1140 ± 15	837-1260	0.07

[a]Based on EM analysis and converted from number fraction data.
[b]Based on DTZ staining.
Abbreviations: COV, coefficient of variation; DTZ, diphenylthiocarbazone; EM, electron microscopy; IE, islet equivalent; PP, pancreatic polypeptide; SE, standard error.

Table 5-4: Cell volume and radii estimated from Pisania *et al*. [85]

Cell type	Native pancreas		Freshly isolated	
	Volume (μm^3)	Radius (μm)[c]	Volume (μm^3)	Radius (μm)[c]
Islet[a]				
β-	1000	6.2	950	6.1
Non-β- (α, γ, ε, PP)	400	4.6	400	4.6
Non-islet[b]				
Acinar	1550	7.2	1200	6.6
Duct	200	3.6	200	3.6
Other	200	3.6	200	3.6

[a]Not including acinar, ductal or other (neuronal, leukocytic, endothelial) cells.
[b]Acinar, ductal, and other cells.
[c]Calculated from cell volume data (assuming that the cells are spherical).

Table 5-5: Selected measurements of *in vivo* pO_2 at prospective islet transplant sites

Transplant site	Model	Method	Range and/or Mean±SD pO_2 [mm Hg]	Ref.
Intrahepatic				
	Rat	Clark microelectrode	3-4[a]	[202]
Intramuscular				
	Rat	Fluorine spectroscopy	Air: 41±10[b] Oxygen: 70±23[b] Hypoxic: 7±6[b]	[331]
	Rat	Fluorine spectroscopy	Air: 18±16 (day 2), 5±11 (day 90)[c] Oxygen: 237±61 (day 2), 12±7 (day 90)[c]	[332]
Intraperitoneal				
	Rat	Fluorine spectroscopy	Air: 52±7[b] Oxygen: 88±14[b] Hypoxic: 19±7[b]	[331]
	Rat	Fluorine spectroscopy	Air: 26±34 (day 1), 21±13 (day 54)[d] Oxygen: 56±62 (day 1), 69±40 (day 54)[d]	[332]
	Mouse	Fluorine spectroscopy	16-213[e]	[334]
	Mouse	Fluorine spectroscopy	51-58[f]	[336]
Pancreatic				
Islet	Rat	Clark microelectrode	37-42[a]	[202]
Acinar	Rat	Clark microelectrode	26-33[a]	[202]
Renal				
Subcapsular	Rat	Fluorine spectroscopy	Air: 8-33 and 17±9[g] Oxygen: 24-75 and 43±20[g]	[332]
Cortical	Rat	Clark microelectrode	13-14[a]	[202]
Spleen				
	Rat	Clark microelectrode	28-32 (non-diabetic), 18-22 (diabetic)[a]	[202]

[a]Estimated from bar graph (*Figures 1* or *3* of reference) for parenchymal pO_2 measurements in non-diabetic and diabetic animals. Unless indicated, pO_2 values were similar for non-diabetic and diabetic animals.
[b]Taken after injection of neat PFC into *quadriceps femoris* or intraperitoneal cavity of 3 animals breathing ambient air (pO_2 ~ 160 mm Hg), oxygen (pO_2 ~ 760 mm Hg), or hypoxic gas mixture (pO_2 ~ 76 mm Hg).
[c]Taken at days 2 and 90 after implantation of alginate beads containing PFC into *quadriceps femoris* of 7 animals breathing ambient air (pO_2 ~ 160 mm Hg) or oxygen (pO_2 ~ 760 mm Hg).
[d]Taken at days 1 and 54 after implantation of alginate beads containing PFC into intraperitoneal cavity of 13-15 animals breathing ambient air (pO_2 ~ 160 mm Hg) or oxygen (pO_2 ~ 760 mm Hg).
[e]Taken on days 0, 1, 2, 6 and 7 after implantation of alginate beads containing PFC into intraperitoneal cavity of 3-6 animals breathing carbogen (pO_2 ~ 720 mm Hg).
[f]Taken on days 1, 8 and 16 after implantation of alginate beads containing PFC (and no cells) into intraperitoneal cavity of 4 animals breathing oxygen (pO_2 ~ 760 mm Hg).
[g]Taken over 4-month period following implantation of alginate beads containing emulsified PFC in 6 animals breathing ambient air (pO_2 ~ 160 mm Hg) or oxygen (pO_2 ~ 760 mm Hg).
Abbreviations: PFC, perfluorocarbon; pO_2, oxygen partial pressure; SD, standard deviation.

Table 5-6: Summary of model constants and selected variables used in examples presented in *Chapter 5*, unless otherwise specified in the text

Description	Formulaic Abbreviation	Prescribed Value	Units	Reference(s)
Half-thickness				
Scaffold	L_1	0.10	cm	-
Encapsulant	(L_2-L_1)	0.01	cm	-
Fibrotic capsule	(L_3-L_2)	0.01	cm	[207]
Radius of IE	R_0	0.0075	cm	[81]
External pO_2	P_{ext}	40	mm Hg	Table 5-6
Critical pO_2				
Non-viable	P_c	0.1	mm Hg	[207]
Non-functional	P_c	10	mm Hg	[87]
Oxygen permeability				
Islet	$(\alpha D)_0$	$1.34\cdot10^{-14}$	mol/cm/mm Hg/sec	[163]
Scaffold (0% v/v PFC)	$(\alpha D)_1$	$3.43\cdot10^{-14}$	mol/cm/mm Hg/sec	[207]
Scaffold (5% v/v PFC)	$(\alpha D)_{1,\,eff}$	$3.93\cdot10^{-14}$	mol/cm/mm Hg/sec	-
Scaffold (10% v/v PFC)	$(\alpha D)_{1,\,eff}$	$4.49\cdot10^{-14}$	mol/cm/mm Hg/sec	-
Scaffold (20% v/v PFC)	$(\alpha D)_{1,\,eff}$	$5.78\cdot10^{-14}$	mol/cm/mm Hg/sec	-
Scaffold (30% v/v PFC)	$(\alpha D)_{1,\,eff}$	$7.42\cdot10^{-14}$	mol/cm/mm Hg/sec	-
Scaffold (50% v/v PFC)	$(\alpha D)_{1,\,eff}$	$9.94\cdot10^{-14}$	mol/cm/mm Hg/sec	-
Encapsulant	$(\alpha D)_2$	$3.43\cdot10^{-14}$	mol/cm/mm Hg/sec	[382; 383]
Fibrotic capsule	$(\alpha D)_3$	$1.34\cdot10^{-14}$	mol/cm/mm Hg/sec	[207]
Perfluorocarbon	$(\alpha D)_{PFC}$	$1.42\cdot10^{-12}$	mol/cm/mm Hg/sec	[378]
Volume fraction				
Fibroblasts	$(1-\epsilon_3)$	0.1	-	[207]
Viability				
Volumetric OCR (islet)	$(OCR)_0$	$2.00\cdot10^{-8}$	$mol/cm^3/sec$	[121]
Volumetric OCR (fibroblasts)	$(OCR)_3$	$3.00\cdot10^{-8}$	$mol/cm^3/sec$	[207]

Abbreviations: IE, islet equivalent; OCR, oxygen consumption rate; PFC, perfluorocarbon; pO_2, oxygen partial pressure.

Table 5-7: Summary of estimated islet seeding density and TE graft or device surface area for planar geometry with increasing external pO_2 and no encapsulant or fibrotic capsule

P_{ext} (mm Hg)	P_c = 0.1 mm Hg		P_c = 10 mm Hg	
	ρ_1 [IEs/cm^3]	$(SA)_1$ [cm^2]	ρ_1 [IEs/cm^3]	$(SA)_1$ [cm^2]
25	2121	1653.7	195	17903.7
40	5027	696.2	3106	1126.8
55	7938	440.9	6017	581.7
70	10849	322.6	8926	392.1
85	13758	254.4	11836	295.7
100	16667	210.0	14749	237.3
225	40936	85.5	39019	89.7
305	56452	62.0	54517	64.2
455	85575	40.9	83732	41.8
760	144628	24.2	142857	24.5

Abbreviations: IE, islet equivalent; P_{ext}, external pO_2; P_c, critical pO_2; ρ_1, seeding density in scaffold; $(SA)_1$, surface area of TE graft or device; TE, tissue-engineered.

Table 5-8: Summary of estimated islet seeding density and TE graft or device surface area for planar geometry with increasing external pO_2, an encapsulant and fibrotic capsule

P_{ext} (mm Hg)	P_c = 0.1 mm Hg		P_c = 10 mm Hg	
	ρ_1 [IEs/cm^3]	$(SA)_1$ [cm^2]	ρ_1 [IEs/cm^3]	$(SA)_1$ [cm^2]
25	-	-	-	-
40	1668	2098.1	546	6413.3
55	3369	1038.9	2246	1558.0
70	5070	690.4	3947	886.0
85	6770	517.0	5648	619.7
100	8470	413.2	7348	476.3
225	22639	154.6	21525	162.6
305	31703	110.4	30594	114.4
455	48747	71.8	47619	73.5
760	83333	42.0	82160	42.6

Abbreviations: IE, islet equivalent; P_{ext}, external pO_2; P_c, critical pO_2; ρ_1, seeding density in scaffold; $(SA)_1$, surface area of TE graft or device; TE, tissue-engineered.

Table 5-9: Summary of estimated islet seeding density and TE graft or device surface area for planar geometry with increasing volume fraction of perfluorocarbon in the scaffold, a low external pO_2 (40 mm Hg), and no encapsulant or fibrotic capsule

ϵ_{PFC}	P_c = 0.1 mm Hg		P_c = 10 mm Hg	
	ρ_1 [IEs/cm^3]	$(SA)_1$ [cm^2]	ρ_1 [IEs/cm^3]	$(SA)_1$ [cm^2]
0	5027	696.2	3106	1126.8
0.05	5765	607.1	3562	982.6
0.1	6578	532.1	4064	861.2
0.2	8481	412.7	5240	667.9
0.3	10876	321.8	6720	520.8
0.5	14577	240.1	9009	388.5

Abbreviations: IE, islet equivalent; P_{ext}, external pO_2; P_c, critical pO_2; ρ_1, seeding density in scaffold; $(SA)_1$, surface area of TE graft or device; TE, tissue-engineered.

Table 5-10: Summary of estimated islet seeding density and TE graft or device surface area for planar geometry with increasing volume fraction of perfluorocarbon in the scaffold, a low external pO_2 (40 mm Hg), and with an encapsulant and fibrotic capsule

ϵ_{PFC}	P_c = 0.1 mm Hg		P_c = 10 mm Hg	
	ρ_1 [IEs/cm^3]	$(SA)_1$ [cm^2]	ρ_1 [IEs/cm^3]	$(SA)_1$ [cm^2]
0	1668	2098.1	546	6413.3
0.05	1803	1941.1	591	5933.6
0.1	1935	1809.1	633	5530.1
0.2	2189	1598.9	716	4887.3
0.3	2433	1438.8	796	4398.1
0.5	2703	1294.9	884	3958.2

Abbreviations: IE, islet equivalent; P_{ext}, external pO_2; P_c, critical pO_2; ρ_1, seeding density in scaffold; $(SA)_1$, surface area of TE graft or device; TE, tissue-engineered.

Table 5-11: Summary of estimated islet seeding density and TE graft or device surface area for planar geometry with increasing volume fraction of perfluorocarbon in the scaffold, an intermediate external pO_2 (100 mm Hg), and no encapsulant or fibrotic capsule

ϵ_{PFC}	P_c = 0.1 mm Hg		P_c = 10 mm Hg	
	ρ_1 [IEs/cm^3]	$(SA)_1$ [cm^2]	ρ_1 [IEs/cm^3]	$(SA)_1$ [cm^2]
0	16667	210.0	14749	237.3
0.05	19115	183.1	16916	206.9
0.1	21807	160.5	19294	181.4
0.2	28112	124.5	24876	140.7
0.3	36045	97.1	31905	109.7
0.5	48343	72.4	42787	81.8

Abbreviations: IE, islet equivalent; P_{ext}, external pO_2; P_c, critical pO_2; ρ_1, seeding density in scaffold; $(SA)_1$, surface area of TE graft or device; TE, tissue-engineered.

Table 5-12: Summary of estimated islet seeding density and TE graft or device surface area for planar geometry with increasing volume fraction of perfluorocarbon in the scaffold, an intermediate external pO_2 (100 mm Hg), and with an encapsulant and fibrotic capsule

ϵ_{PFC}	P_c = 0.1 mm Hg		P_c = 10 mm Hg	
	ρ_1 [IEs/cm^3]	$(SA)_1$ [cm^2]	ρ_1 [IEs/cm^3]	$(SA)_1$ [cm^2]
0	8470	413.2	7348	476.3
0.05	9155	382.3	7942	440.7
0.1	9823	356.3	8522	410.7
0.2	11115	314.9	9642	363.0
0.3	12350	283.4	10716	326.6
0.5	13725	255.0	11905	294.0

Abbreviations: IE, islet equivalent; P_{ext}, external pO_2; P_c, critical pO_2; ρ_1, seeding density in scaffold; SA_1, surface area of TE graft or device; TE, tissue-engineered.

Table 5-13: Summary of estimated islet seeding density and TE graft or device surface area for planar geometry with increasing volume fraction of perfluorocarbon in the scaffold, an high external pO_2 (305 mm Hg), and no encapsulant or fibrotic capsule

ϵ_{PFC}	P_c = 0.1 mm Hg		P_c = 10 mm Hg	
	ρ_1 [IEs/cm^3]	$(SA)_1$ [cm^2]	ρ_1 [IEs/cm^3]	$(SA)_1$ [cm^2]
0	56452	62.0	54517	64.2
0.05	64695	54.1	62500	56.0
0.1	73840	47.4	71283	49.1
0.2	95109	36.8	92105	38.0
0.3	121951	28.7	117845	29.7
0.5	163551	21.4	158371	22.1

Abbreviations: IE, islet equivalent; P_{ext}, external pO_2; P_c, critical pO_2; ρ_1, seeding density in scaffold; SA_1, surface area of TE graft or device; TE, tissue-engineered.

Table 5-14: Summary of estimated islet seeding density and TE graft or device surface area for planar geometry with increasing volume fraction of perfluorocarbon in the scaffold, an high external pO_2 (305 mm Hg), and with an encapsulant and fibrotic capsule

ϵ_{PFC}	P_c = 0.1 mm Hg		P_c = 10 mm Hg	
	ρ_1 [IEs/cm^3]	$(SA)_1$ [cm^2]	ρ_1 [IEs/cm^3]	$(SA)_1$ [cm^2]
0	31703	110.4	30594	114.4
0.05	34280	102.1	33050	105.9
0.1	36765	95.2	35461	98.7
0.2	41617	84.1	40138	87.2
0.3	46235	75.7	44586	78.5
0.5	51395	68.1	49575	70.6

Abbreviations: IE, islet equivalent; P_{ext}, external pO_2; P_c, critical pO_2; ρ_1, seeding density in scaffold; $(SA)_1$, surface area of TE graft or device; TE, tissue-engineered.

Figure Captions

Figure 5-1: Schematic of generalized strategy for optimization of tissue-engineered (TE) graft or device design. Prior to transplantation of any TE graft or device, several design parameters need to be defined. The cell or tissue equivalents should be accurately characterized for quantity, composition and viability. The prospective transplant site should be evaluated for their native oxygen supply. Materials and any drugs, co-factors or agents that are incorporated into a TE graft or device should be evaluated for impact on local inflammation and fibrotic capsule formation at the proposed site of transplant. The materials should also be characterized for their oxygen permeability. Finally, the appropriate therapeutic dose needs to be defined, and depends on the quantity, composition and viability of the cells or tissue equivalents available for transplant. All information regarding design parameters is used to optimize cell or tissue seeding density and TE graft or device size. If the TE graft or device size is too large for a particular application, then additional strategies are employed to increase oxygenation or possibly the potency of the cell or tissue preparation.

Figure 5-2: Generalized arrangement of constituents or layers in an idealized tissue-engineered (TE) graft or device, including the cell or tissue of interest (Constituent 0), the biomaterial scaffold (Constituent 1 or Layer 1), an encapsulant (Constituent 2 or Layer 2), and a fibrotic capsule (Constituent 3 or Layer 3), each with characteristic dimensions represented by L_i (for planar geometry) or R_i (for cylindrical or spherical geometry). The TE graft or device may be designed such that a cellular or tissue equivalent located along the axis of symmetry (which represents the worst-case scenario) is able to obtain adequate oxygenation. Key modifiable design parameters are indicated in **blue** and they represent the external pO_2 (P_{ext}), characteristic size of cellular or tissue

equivalent (assumed to be spherical, with radius R_0), characteristic half-thicknesses of each layer (L_i-L_{i-1} or R_i-R_{i-1}), oxygen solubility (α_i) and diffusivity (D_i) specific to each constituent, the oxygen consumption rate (OCR) of the cells or tissue [$(OCR)_0$] and fibroblasts in the fibrotic capsule [$(OCR)_3$], and the non-viable void fraction (the volume fraction of the layer that does not contain cells or tissue) in the scaffold (ϵ_1) and fibrotic capsule (ϵ_3). P_c is the minimum critical pO_2 and may represent the pO_2 at which cells or tissue become non-viable (e.g., P_c = 0.1 mm Hg) or non-functional (e.g., P_c = 10 mm Hg), and its value depends on the other design requirements.

Figure 5-3: Modifiable design parameters and their impact on tissue-engineered (TE) graft or device design, and key strategies to increase seeding density and decrease size. Design parameters determined at the time of TE graft or device design help define the required oxygen need and the available oxygen supply, which determines the maximum allowable cell or tissue seeding density. The required therapeutic dose of cells or tissue will largely determine the overall size of the TE graft or device. Seeding density and size are inversely correlated and strategies exist to optimize them.

Figure 5-4: Illustration depicting a planar tissue-engineered (TE) graft or device containing 700,000 islet equivalents (IEs; 1 IE is equal to the amount of cells in a spherical cellular aggregate of 150-μm diameter and containing approximately 1600 cells) and the approximate size (surface area) required for avoidance of oxygen deprivation with an assumed *in vivo* pO_2 of 40 mm Hg. The required size of the TE graft or device increases with decreasing available pO_2, the need for encapsulation, and fibrotic capsule formation.

Figure 5-5: Schematic depicting cross-section through planar tissue-engineered graft or device seeded with islets only.

Figure 5-6: Schematic depicting cross-section through planar tissue-engineered graft or device seeded with islets, and designed with an immunisolation barrier (encapsulant) and with a fibrotic capsule on the exterior.

Figure 5-7: Theoretical maximum islet seeding densities within a planar tissue-engineered graft or device with increasing external pO_2 (25-760 mm Hg). White bars indicate islet seeding density for a critical pO_2 of 0.1 mm Hg, whereas gray bars indicate islet seeding density for a critical pO_2 of 10 mm Hg. Bars containing stripes indicate the islet seeding density for the same TE graft or device except with the presence of a 100-μm encapsulant and 100-μm fibrotic capsule; note the decrease in maximum seeding density due to decreased oxygen supply and transport at the surface of the scaffold.

Figure 5-8: Theoretical minimum tissue-engineered (TE) graft or device surface area for planar geometry with increasing external pO_2 (25-760 mm Hg). White bars indicate the surface area for a critical pO_2 of 0.1 mm Hg, whereas gray bars indicate the surface area for a critical pO_2 of 10 mm Hg. Bars containing stripes indicate the surface area for the same TE graft or device except with the presence of a 100-μm encapsulant and 100-μm fibrotic capsule; note the decrease in minimum surface area due to decreased oxygen supply and transport at the surface of the scaffold. The asterisk indicates that under the prescribed conditions a TE graft or device could not be designed without the formation of an anoxic region.

Figure 5-9: Schematic depicting cross-section through planar TE graft or device seeded with islets and perfluorocarbon, and designed with immunisolation barrier (encapsulant) and covered with fibrotic capsule on the exterior.

Figure 5-10: Theoretical maximum islet seeding densities within a planar tissue-engineered graft or device with increasing volume fraction of perfluorocarbon (0-0.50) and with an external pO_2 of 40 mm Hg. White bars indicate islet seeding density for a critical pO_2 of 0.1 mm Hg, whereas gray bars indicate islet seeding density for a critical pO_2 of 10 mm Hg. Bars containing stripes indicate the islet seeding density for the same TE graft or device except with the presence of a 100-μm encapsulant and 100-μm fibrotic capsule; note the decrease in maximum seeding density due to decreased oxygen supply and transport at the surface of the scaffold.

Figure 5-11: Theoretical minimum tissue-engineered (TE) graft or device surface area for planar geometry with increasing volume fraction of perfluorocarbon (0-0.50) and with an external pO_2 of 40 mm Hg. White bars indicate the surface area for a critical pO_2 of 0.1 mm Hg, whereas gray bars indicate the surface area for a critical pO_2 of 10 mm Hg. Bars containing stripes indicate the surface area for the same TE graft or device except with the presence of a 100-μm encapsulant and 100-μm fibrotic capsule; note the decrease in minimum surface area due to decreased oxygen supply and transport at the surface of the scaffold.

Figure 5-12: Theoretical maximum islet seeding densities within a planar tissue-engineered graft or device with increasing volume fraction of perfluorocarbon (0-0.50) and with an external pO_2 of 100 mm Hg. White bars indicate islet seeding density for a

critical pO_2 of 0.1 mm Hg, whereas gray bars indicate islet seeding density for a critical pO_2 of 10 mm Hg. Bars containing stripes indicate the islet seeding density for the same TE graft or device except with the presence of a 100-μm encapsulant and 100-μm fibrotic capsule; note the decrease in maximum seeding density due to decreased oxygen supply and transport at the surface of the scaffold.

Figure 5-13: Theoretical minimum tissue-engineered (TE) graft or device surface area for planar geometry with increasing volume fraction of perfluorocarbon (0-0.50) and with an external pO_2 of 100 mm Hg. White bars indicate the surface area for a critical pO_2 of 0.1 mm Hg, whereas gray bars indicate the surface area for a critical pO_2 of 10 mm Hg. Bars containing stripes indicate the surface area for the same TE graft or device except with the presence of a 100-μm encapsulant and 100-μm fibrotic capsule; note the decrease in minimum surface area due to decreased oxygen supply and transport at the surface of the scaffold.

Figure 5-14: Theoretical maximum islet seeding densities within a planar tissue-engineered graft or device with increasing volume fraction of perfluorocarbon (0-0.50) and with an external pO_2 of 100 mm Hg. White bars indicate islet seeding density for a critical pO_2 of 0.1 mm Hg, whereas gray bars indicate islet seeding density for a critical pO_2 of 10 mm Hg. Bars containing stripes indicate the islet seeding density for the same TE graft or device except with the presence of a 100-μm encapsulant and 100-μm fibrotic capsule; note the decrease in maximum seeding density due to decreased oxygen supply and transport at the surface of the scaffold.

Figure 5-15: Theoretical minimum tissue-engineered (TE) graft or device surface area for planar geometry with increasing volume fraction of perfluorocarbon (0-0.50) and with an external pO_2 of 100 mm Hg. White bars indicate the surface area for a critical pO_2 of 0.1 mm Hg, whereas gray bars indicate the surface area for a critical pO_2 of 10 mm Hg. Bars containing stripes indicate the surface area for the same TE graft or device except with the presence of a 100-μm encapsulant and 100-μm fibrotic capsule; note the decrease in minimum surface area due to decreased oxygen supply and transport at the surface of the scaffold.

Figure 5-1

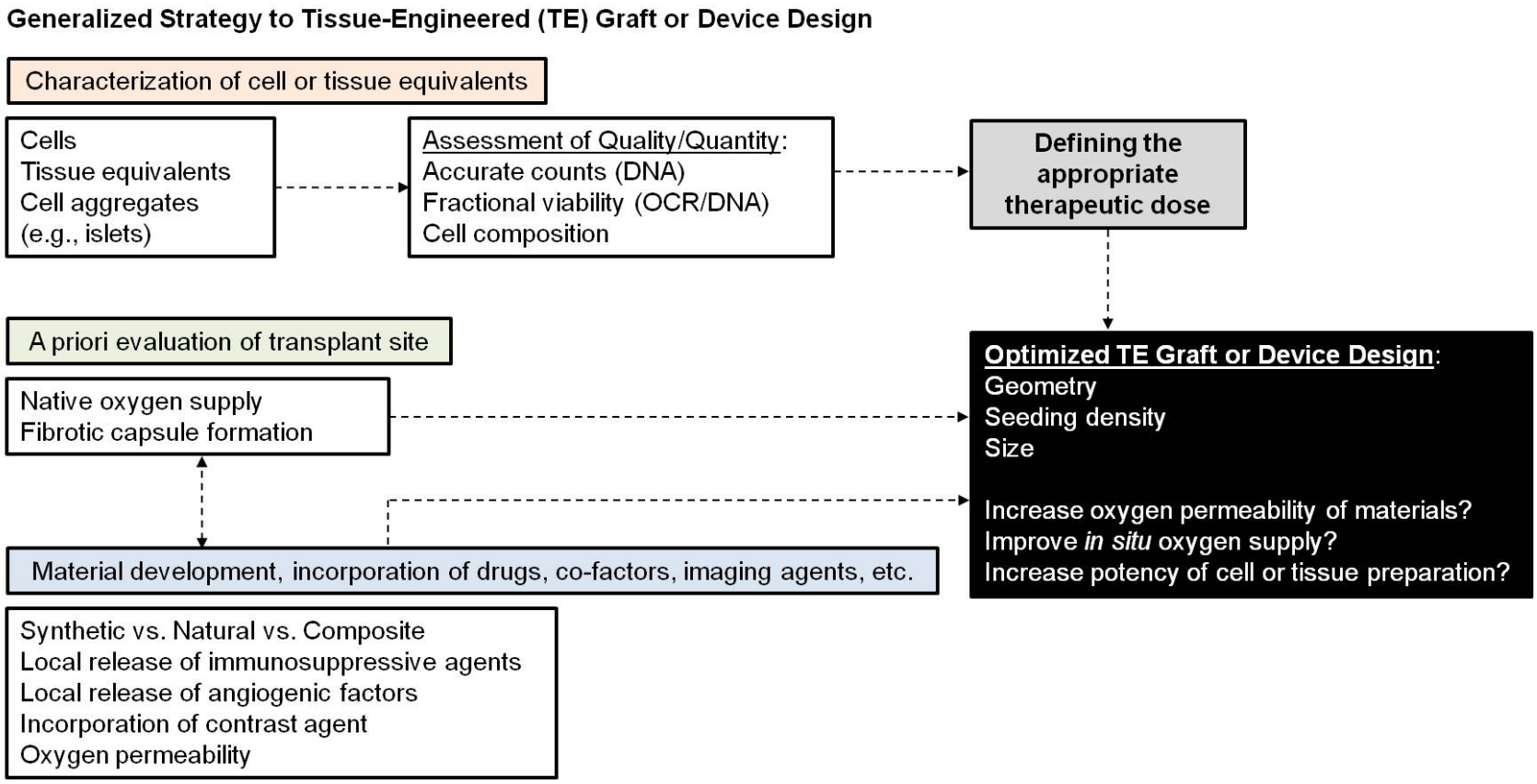
Generalized Strategy to Tissue-Engineered (TE) Graft or Device Design
Characterization of cell or tissue equivalents
Cells
Tissue equivalents
Cell aggregates
(e.g., islets)
Assessment of Quality/Quantity:
Accurate counts (DNA)
Fractional viability (OCR/DNA)
Cell composition
Defining the appropriate therapeutic dose
A priori evaluation of transplant site
Native oxygen supply
Fibrotic capsule formation
Optimized TE Graft or Device Design:
Geometry
Seeding density
Size
Increase oxygen permeability of materials?
Improve in situ oxygen supply?
Increase potency of cell or tissue preparation?
Material development, incorporation of drugs, co-factors, imaging agents, etc.
Synthetic vs. Natural vs. Composite
Local release of immunosuppressive agents
Local release of angiogenic factors
Incorporation of contrast agent
Oxygen permeability

Figure 5-2

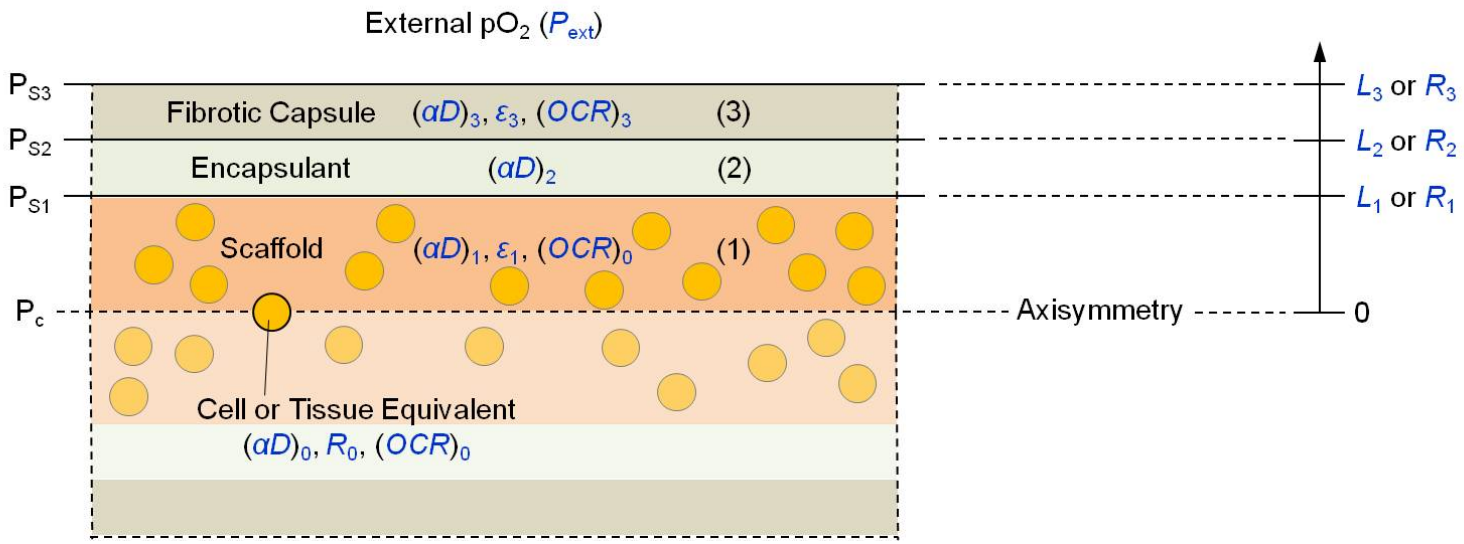
External pO2 (Pext)
PS3
PS2
PS1
Pc
Fibrotic Capsule
(αD)3, ε3, (OCR)3
(3)
Encapsulant
(αD)2
(2)
Scaffold
(αD)1, ε1, (OCR)0
(1)
Cell or Tissue Equivalent
(αD)0, R0, (OCR)0
Axisymmetry
L3 or R3
L2 or R2
L1 or R1
0

Figure 5-3

Modifiable Design Parameters and Relative Impact on Design

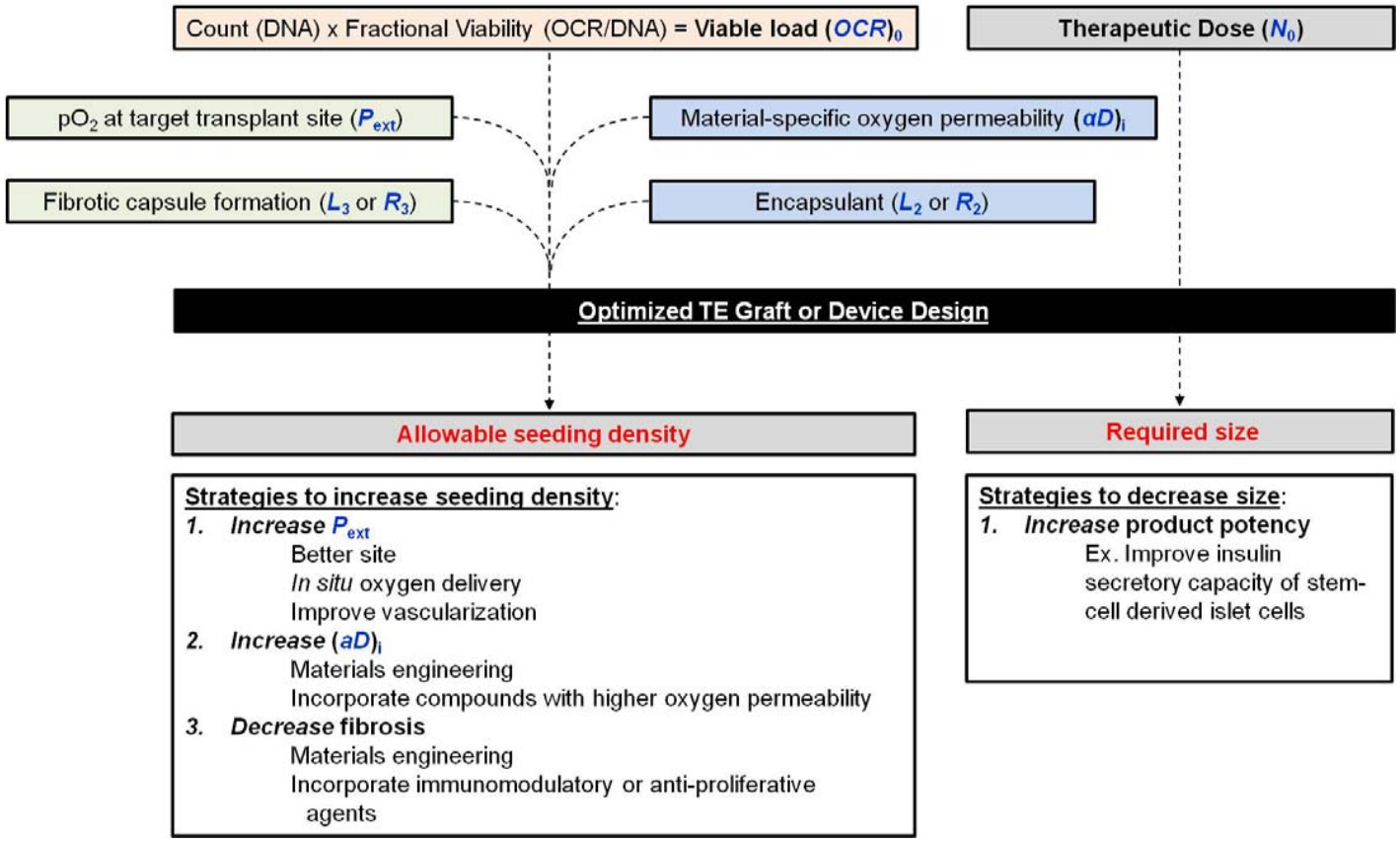

Figure 5-4

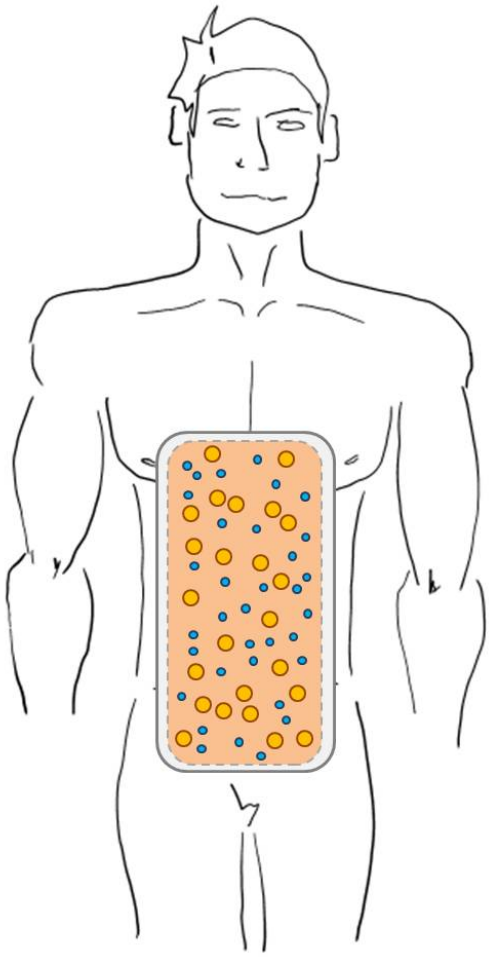

Figure 5-5

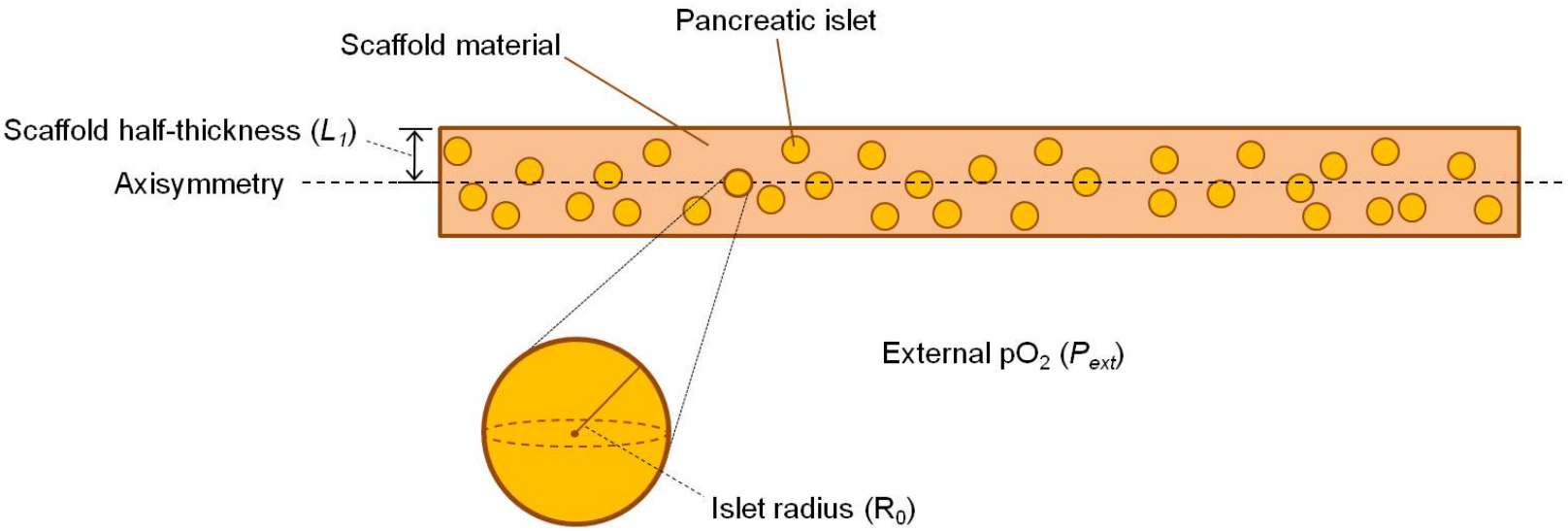
Pancreatic islet
Scaffold material
Scaffold half-thickness (L_1)
Axisymmetry
External pO_2 (P_{ext})
Islet radius (R_0)

Figure 5-6

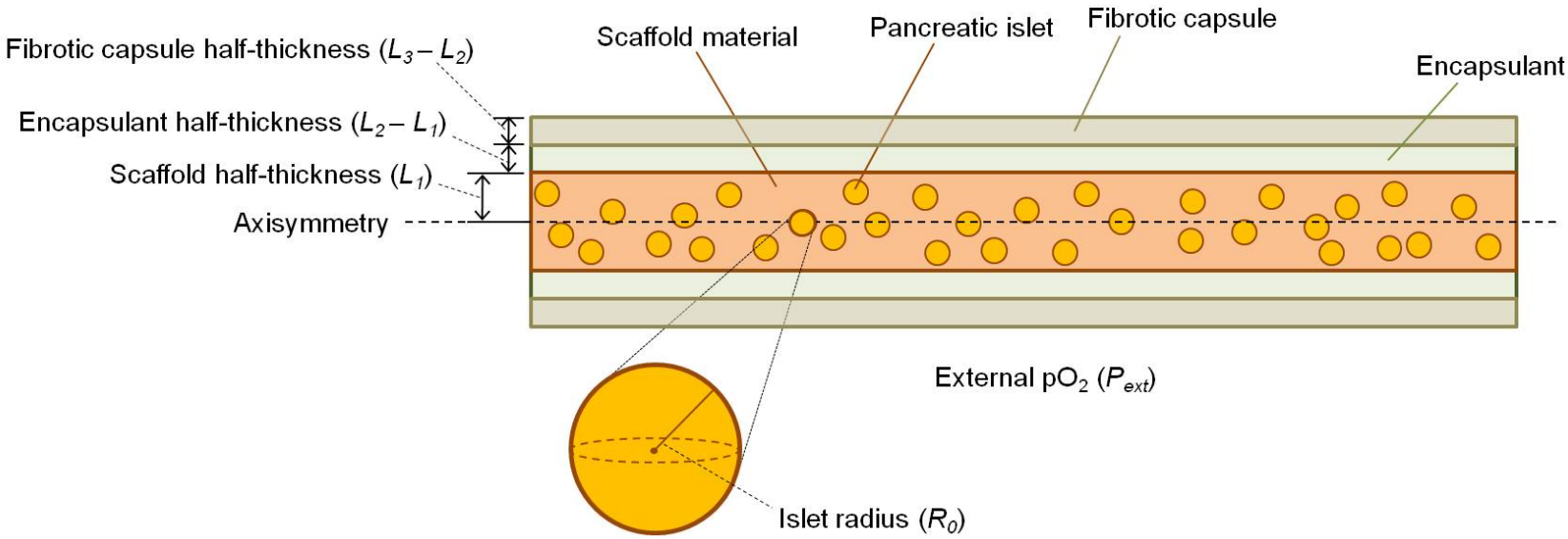
Fibrotic capsule half-thickness ($L_3 - L_2$)
Encapsulant half-thickness ($L_2 - L_1$)
Scaffold half-thickness (L_1)
Axisymmetry
Scaffold material
Pancreatic islet
Fibrotic capsule
Encapsulant
External pO_2 (P_{ext})
Islet radius (R_0)

Figure 5-7

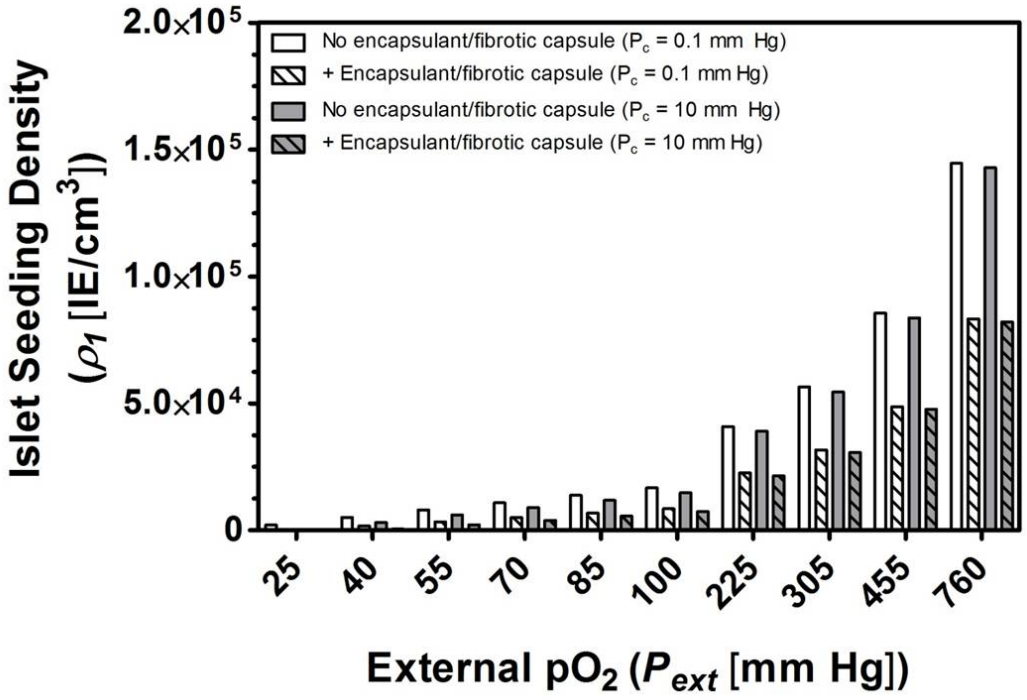
No encapsulant/fibrotic capsule (P_c = 0.1 mm Hg)
+ Encapsulant/fibrotic capsule (P_c = 0.1 mm Hg)
No encapsulant/fibrotic capsule (P_c = 10 mm Hg)
+ Encapsulant/fibrotic capsule (P_c = 10 mm Hg)
Islet Seeding Density (ρ_1 [IE/cm^3])
2.0×10^5
1.5×10^5
1.0×10^5
5.0×10^4
0
25
40
55
70
85
100
225
305
455
760
External pO$_2$ (P_{ext} [mm Hg])

Figure 5-8

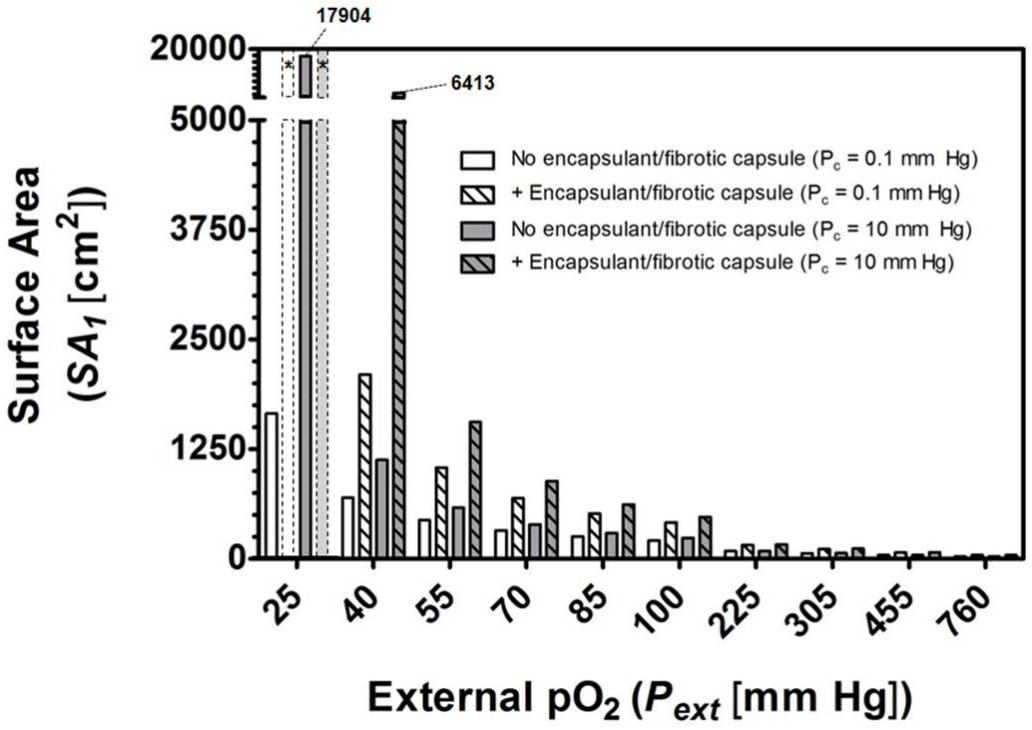
17904
6413
20000
5000
3750
2500
1250
0
Surface Area
(SA_1 [cm^2])
No encapsulant/fibrotic capsule (P_c = 0.1 mm Hg)
+ Encapsulant/fibrotic capsule (P_c = 0.1 mm Hg)
No encapsulant/fibrotic capsule (P_c = 10 mm Hg)
+ Encapsulant/fibrotic capsule (P_c = 10 mm Hg)
25
40
55
70
85
100
225
305
455
760
External pO_2 (P_{ext} [mm Hg])

Figure 5-9

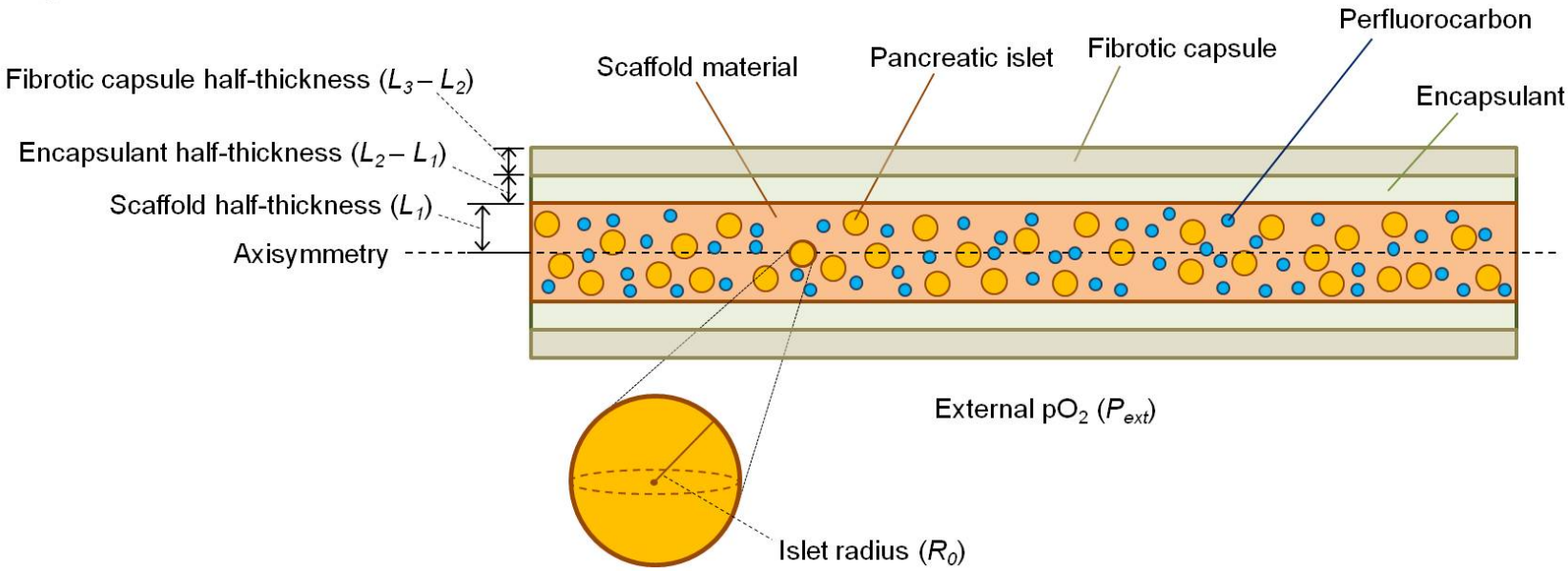
Fibrotic capsule half-thickness ($L_3 - L_2$)
Encapsulant half-thickness ($L_2 - L_1$)
Scaffold half-thickness (L_1)
Axisymmetry
Scaffold material
Pancreatic islet
Fibrotic capsule
Perfluorocarbon
Encapsulant
External pO_2 (P_{ext})
Islet radius (R_0)

Figure 5-10

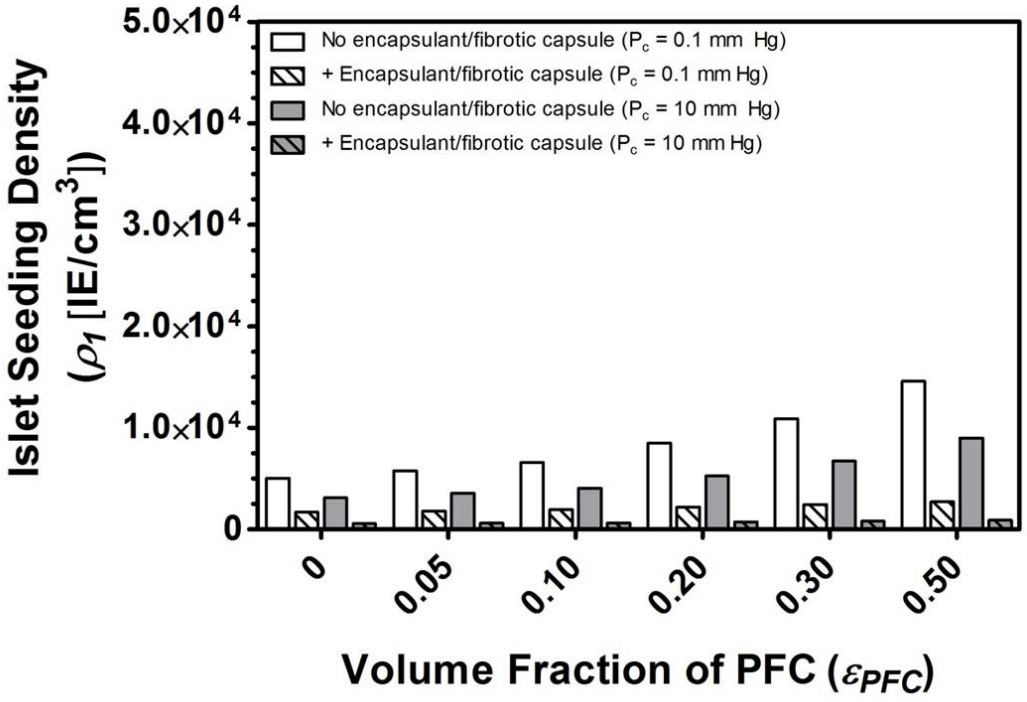
No encapsulant/fibrotic capsule (P_c = 0.1 mm Hg)
+ Encapsulant/fibrotic capsule (P_c = 0.1 mm Hg)
No encapsulant/fibrotic capsule (P_c = 10 mm Hg)
+ Encapsulant/fibrotic capsule (P_c = 10 mm Hg)
Islet Seeding Density (ρ_1 [IE/cm^3])
5.0×10^4
4.0×10^4
3.0×10^4
2.0×10^4
1.0×10^4
0
0
0.05
0.10
0.20
0.30
0.50
Volume Fraction of PFC (ε_{PFC})

Figure 5-11

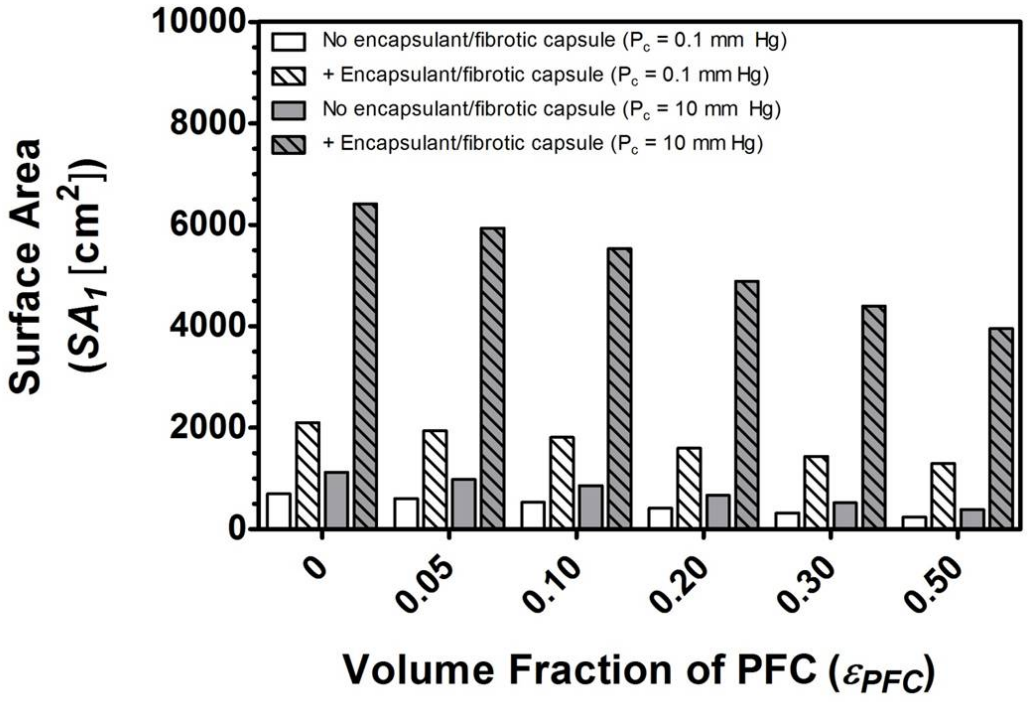
No encapsulant/fibrotic capsule (P_c = 0.1 mm Hg)
+ Encapsulant/fibrotic capsule (P_c = 0.1 mm Hg)
No encapsulant/fibrotic capsule (P_c = 10 mm Hg)
+ Encapsulant/fibrotic capsule (P_c = 10 mm Hg)
Surface Area (SA_1 [cm^2])
10000
8000
6000
4000
2000
0
0
0.05
0.10
0.20
0.30
0.50
Volume Fraction of PFC (ε_{PFC})

Figure 5-12

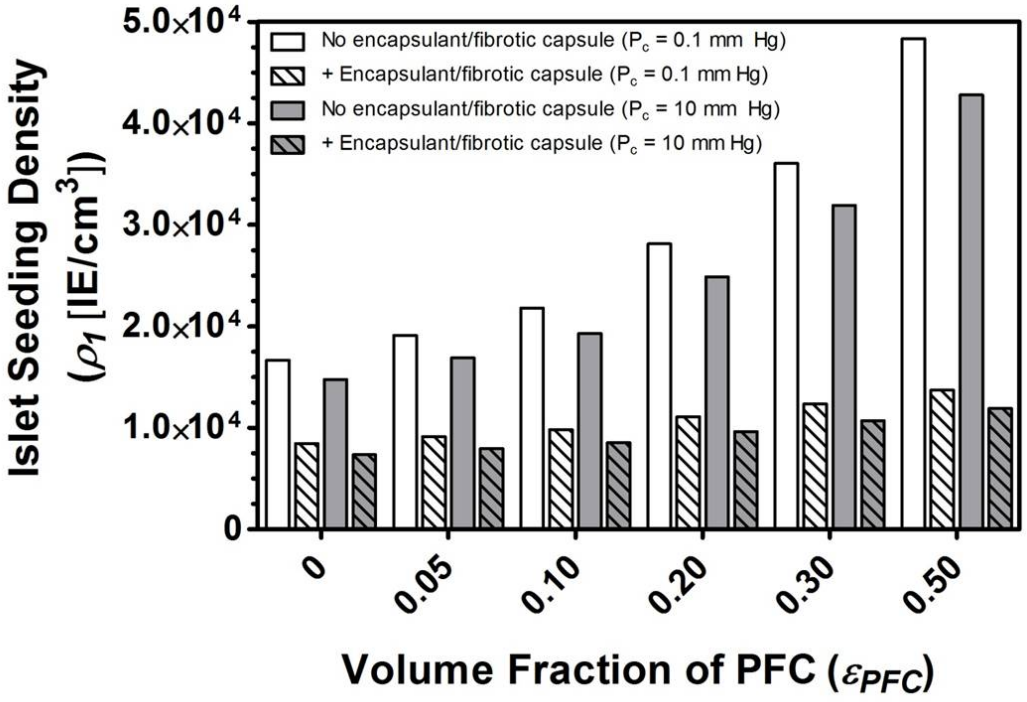
No encapsulant/fibrotic capsule (P_c = 0.1 mm Hg)
+ Encapsulant/fibrotic capsule (P_c = 0.1 mm Hg)
No encapsulant/fibrotic capsule (P_c = 10 mm Hg)
+ Encapsulant/fibrotic capsule (P_c = 10 mm Hg)
Islet Seeding Density (ρ_1 [IE/cm^3])
5.0×10^4
4.0×10^4
3.0×10^4
2.0×10^4
1.0×10^4
0
0
0.05
0.10
0.20
0.30
0.50
Volume Fraction of PFC (ε_{PFC})

Figure 5-13

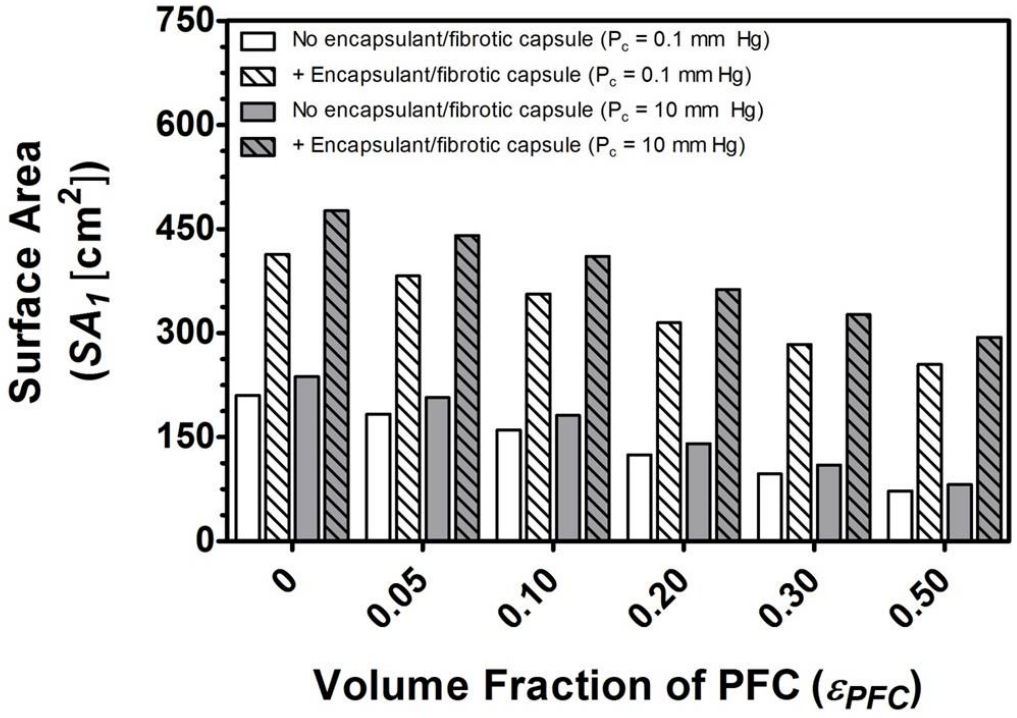
No encapsulant/fibrotic capsule (P_c = 0.1 mm Hg)
+ Encapsulant/fibrotic capsule (P_c = 0.1 mm Hg)
No encapsulant/fibrotic capsule (P_c = 10 mm Hg)
+ Encapsulant/fibrotic capsule (P_c = 10 mm Hg)
Surface Area (SA_1 [cm^2])
750
600
450
300
150
0
0
0.05
0.10
0.20
0.30
0.50
Volume Fraction of PFC (ε_{PFC})

Figure 5-14

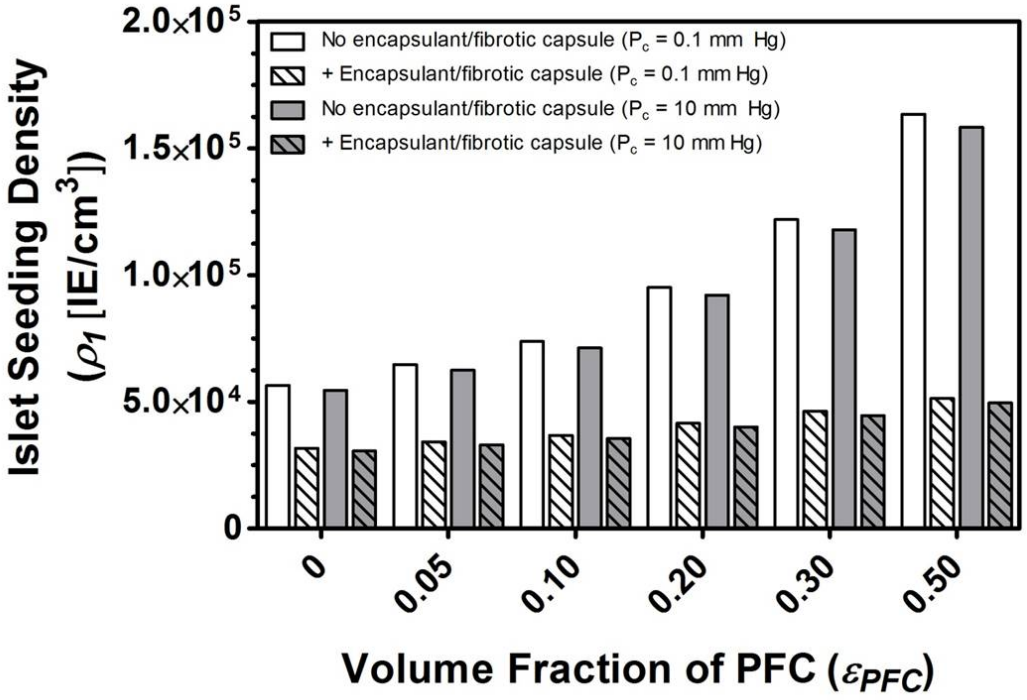
No encapsulant/fibrotic capsule (P_c = 0.1 mm Hg)
+ Encapsulant/fibrotic capsule (P_c = 0.1 mm Hg)
No encapsulant/fibrotic capsule (P_c = 10 mm Hg)
+ Encapsulant/fibrotic capsule (P_c = 10 mm Hg)
Islet Seeding Density (ρ_1 [IE/cm^3])
2.0×10^5
1.5×10^5
1.0×10^5
5.0×10^4
0
0
0.05
0.10
0.20
0.30
0.50
Volume Fraction of PFC (ε_{PFC})

Figure 5-15

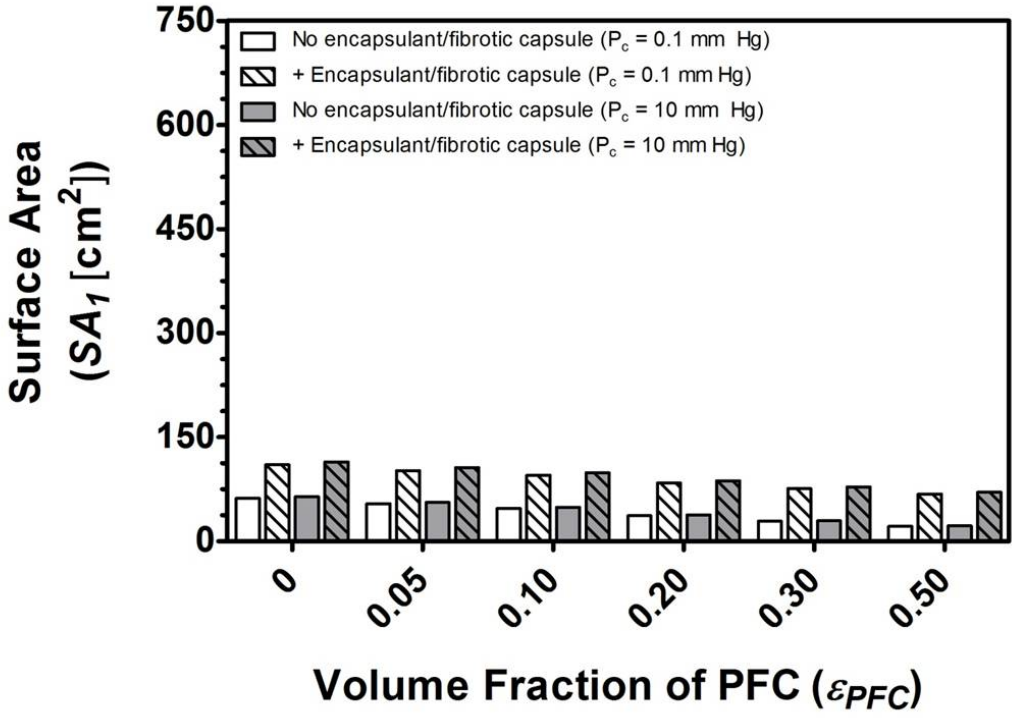
No encapsulant/fibrotic capsule (P_c = 0.1 mm Hg)
+ Encapsulant/fibrotic capsule (P_c = 0.1 mm Hg)
No encapsulant/fibrotic capsule (P_c = 10 mm Hg)
+ Encapsulant/fibrotic capsule (P_c = 10 mm Hg)
Surface Area (SA_1 [cm^2])
750
600
450
300
150
0
0
0.05
0.10
0.20
0.30
0.50
Volume Fraction of PFC (ε_{PFC})

CHAPTER 6: **Assessment of Tissue-Engineered Islet Graft Viability by Fluorine Magnetic Resonance Spectroscopy**

Suszynski T.M., Avgoustiniatos E.S., Stein S.A., Falde E.J., Hammer B.E., Papas K.K. Assessment of tissue-engineered islet graft viability by fluorine magnetic resonance spectroscopy. Transplant Proc. 43(9): 3221-3225 (2011)

Permission to reproduce the above publication was given by *Elsevier*, and the agreement (license number: 2924361380000) is found in Appendix 6-1.

Summary

Despite significant progress in the last decade, islet transplantation remains an experimental therapy for a very limited number of patients with type 1 diabetes. Tissue-engineered approaches may provide promising alternatives to current clinical protocol and would benefit greatly from concurrent development of graft quality assessment techniques. This study was designed to evaluate whether tissue-engineered islet graft viability can be assessed by using fluorine magnetic resonance spectroscopy (^{19}F-MRS) to non-invasively measure pO_2 and to then calculate islet oxygen consumption rate (*OCR*) from those measurements. Scaffolds composed of porcine plasma were seeded with human islets and perfluorodecalin and each graft was covered with the same volume of culture media in Petri dishes. Four scaffolds were seeded with different numbers (0-8000) of islet equivalents (IEs) aliquoted from the same islet preparation. Run order was randomized and grafts were examined by ^{19}F-MRS at 37°C using a 5T spectrometer and a single-loop surface coil placed underneath each graft. A standard inversion recovery sequence was used to obtain a characteristic ^{19}F spin-lattice relaxation time (*T*1), which was converted to a steady-state average pO_2 estimate using a previously determined linear calibration (R^2 = 1.000). Each condition was assessed with replicate ^{19}F-MRS measurements (n = 6-8). Grafts exhibited an IE dose-dependent increase in *T*1 and decrease in pO_2 estimates. From the difference between scaffold pO_2 estimates and ambient pO_2, the islet preparation *OCR* was calculated to be 95 ± 12 (mean ± SE) nmol/min/mg DNA using theoretical modeling. This value compares well with *OCR* values measured using established methods for human islet preparations. ^{19}F-MRS can be used for the non-invasive pre- and possibly post-transplant assessment of tissue-engineered islet graft viability by estimating the amount of viable, oxygen-consuming tissue in a scaffold.

Abbreviations (Text)

^{19}F-MRS	fluorine magnetic resonance spectroscopy
B_0	external magnetic field
CL	calibration line
DNA	deoxyribonucleic acid
IT	islet transplantation
IE	islet equivalent
OCR	oxygen consumption rate
PETG	glycol-mediated polyethylene terephthalate
PFC	perfluorocarbon
PFD	perfluorodecalin
pO_2	oxygen partial pressure
RFU	relative fluorescence unit
SE	standard error
$T1$	spin-lattice relaxation time
$T2$	spin-spin relaxation time
$R1$	spin-lattice relaxation rate
TE	tissue-engineered

Abbreviations (Formulaic)

a	thickness of anoxic region in graft [cm]
α_{PFC}	oxygen solubility coefficient for perfluorocarbon [mol/cm^3/mm Hg]
$(\alpha D)_1$	oxygen permeability in the viable/non-anoxic region of the graft [mol/cm/mm Hg/sec]
$(\alpha D)_2$	oxygen permeability in the aqueous media [mol/cm/mm Hg/sec]
$(\alpha D)_{S,eff}$	effective oxygen permeability in the scaffold [mol/cm/mm Hg/sec]
$(\alpha D)_M$	oxygen permeability in the aqueous media [mol/cm/mm Hg/sec]
$(\alpha D)_S$	oxygen permeability in the scaffold [mol/cm/mm Hg/sec]
dP/dx	oxygen flux [mm Hg/cm]
ΔP_{max}	maximum pO_2 drop across media layer and scaffold [mm Hg]
ΔP_M	pO_2 drop across media layer [mm Hg]
ΔP_S	pO_2 drop across scaffold [mm Hg]
DNA_{IE}	deoxyribonucleic acid content in islet equivalent [ng]
ϵ_i	viable islet volume fraction
ϵ_{PFC}	perfluorocarbon volume fraction in scaffold
$K_{m,i}$	Michaelis-Menten constant for islet oxygen consumption rate
L_1	graft thickness [cm]
L_2	distance between top of media layer and bottom of Petri dish [cm]
L_M	media layer thickness [cm]
L_S	scaffold thickness [cm]
M_Z	longitudinal magnetization
N_{IE}	number of islet equivalents
$(OCR)_i$	volumetric islet oxygen consumption rate [mol/cm^3/sec]
OCR/DNA	oxygen consumption rate normalized to DNA content [nmol/min/mg DNA]

P_1	local graft pO_2 in viable/non-anoxic region [mm Hg]
$P_{avg,1}$	average graft pO_2 in viable/non-anoxic region [mm Hg]
P_A	ambient (external) pO_2 [mm Hg]
P_C	critical pO_2 [mm Hg]
P_{PFC}	pO_2 in the perfluorocarbon [mm Hg]
P_S	average scaffold pO_2 [mm Hg]
P_{S1}	pO_2 at the surface of the graft (at the graft-media layer interface) [mm Hg]
P_{S2}	pO_2 at the surface of the media layer [mm Hg]
Φ	Thiele modulus
$R1_a$	longitudinal relaxation rate for nuclei exposed to no oxygen (anoxia) [sec^{-1} or $msec^{-1}$]
$R1_e$	effective longitudinal relaxation rate [sec^{-1} or $msec^{-1}$]
$R1_p$	longitudinal relaxation rate for nuclei exposed to oxygen (paramagnetic) [sec^{-1} or $msec^{-1}$]
ρ	ratio of oxygen permeability in perfluorocarbon versus scaffold material
R_{IE}	radius of islet equivalent [cm]
R_S	radius of cylindrically-shaped scaffold [cm]
$T1_a$	spin-lattice relaxation time for nuclei exposed to no oxygen (anoxia) [sec or msec]
$T1_e$	effective spin-lattice relaxation time [sec or msec]
$T1_p$	spin-lattice relaxation time for nuclei exposed to oxygen (paramagnetic) [sec or msec]
V_1	rate of oxygen depletion per unit volume in the scaffold [$mol/cm^3/sec$]
X	molar fraction of oxygen

Introduction

Widespread utilization of islet transplantation (IT) in the treatment of type 1 diabetes has yet to be achieved [50; 384; 385] despite significant progress in the field over the last decade [52; 68; 184; 386; 387; 388]. Intraportal delivery of islets may not be the most optimal approach and development of tissue-engineered (TE) strategies for extrahepatic IT may present promising long-term opportunity [389; 390]. Ultimately, the liver may not provide the best environment for healthy engraftment of transplanted islet tissue for a number of reasons that include (but are not limited to): (1) higher concentrations of orally-administered immunosuppressants [147; 273], which are known to impair normal insulin secretory function [148; 275] and islet re-vascularization [149; 278]; (2) intraportal thrombus formation and the associated inflammatory reaction, which is believed to contribute to early islet loss [208; 247; 250]; (3) poor re-establishment of the surrounding extracellular matrix, which is believed to adversely affect islet survival [107; 150]; and (4) poor oxygenation due to the mixed arterial and portal circulation [206] and presence of significant oxygen gradients within the hepatic parenchyma [153], which are believed to be of particular importance given the poor capacity of islets to undergo anaerobic metabolism [158] and their general susceptibility to hypoxic stress [131; 204].

Current efforts in islet graft tissue engineering have been accompanied by inconsistent outcomes when translated into small or large animal transplant models – and these efforts may have been stunted by an inability to accurately assess the quality of such a graft both pre- and post-transplantation. Improved methods for the quality assessment of an islet product prior to transplantation have enabled more accurate characterization of islet viability and potency [54]. Many of the most promising methods involve quantification of oxygen consumption [91; 97; 98; 99; 120; 121; 122]. However, these

techniques have yet to be extended to assessing the quality of TE islet grafts. Herein we present preliminary data on the use of fluorine magnetic resonance spectroscopy (^{19}F-MRS) in the assessment of TE islet graft viability by non-invasively measuring oxygen partial pressure (pO_2) and then using these measurements to estimate islet oxygen consumption rate (OCR).

Methods

Engineered scaffold design and fabrication

Human islets were isolated at the University of Pennsylvania and shipped to our institution (as part of the Integrated Islet Distribution Program) following 3 days of post-isolation culture. Upon arrival, islets were transferred into silicone rubber membrane culture flasks (Wilson-Wolf Manufacturing Corp., New Brighton, MN) and cultured at 22°C and 5% CO_2 for an additional 2 days. On the day of experimentation, approximately 14,000 islet equivalents (IEs) were aliquoted into a 15 mL conical tube (BD Biosciences, Franklin Lakes, NJ) and allowed to settle by gravity. The supernatant was decanted and the islet pellet was reconstituted in fresh CMRL 1066 culture media (Mediatech, Inc., Manassas, VA; supplemented with HEPES buffer, heparin, and human serum albumin) to a total suspension volume of 180 µL. Engineered scaffolds were constructed by combining fresh commercially-available porcine plasma (Sigma-Aldrich, St. Louis, MO) dissolved in calcium-free Krebs buffer solution, 30% v/v perfluorodecalin (PFD; Fluoromed, L.P., Round Rock, TX), and varying volumes of well-mixed islet suspension (amounting to 2000, 4000, and 8000 IEs) in 3.5-cm diameter Petri dishes (~10 cm^2 area), mixing, and then crosslinking using 5% v/v topical bovine thrombin solution (King Pharmaceuticals, Bristol, TN; 1000 U/mL). Each scaffold was covered with 1 mL of culture media (height ~0.1 cm). An additional control scaffold was constructed in

the same manner only without the addition of islet suspension. The grafts were cultured at 37°C for a few hours prior to experimentation to allow oxygen profiles to reach steady-state.

Fluorine magnetic resonance spectroscopy

^{19}F-MRS spectra were obtained at 5T using an APOLLO spectrometer (Tecmag Inc., Houston, TX) and a custom-built single-loop surface coil. Each sample was placed on top of the surface coil and centered within the bore of the magnet. Temperature was controlled using a custom-built water jacket and all measurements were performed at 37°C. A standard inversion recovery sequence was used to estimate fluorine-19 spin lattice relaxation time (*T*1) values corresponding to inversion of the singlet peak in the PFD spectrum. Data were obtained using the NTNMR software (Tecmag Inc., Houston, TX) and inversion recovery curves were fit using a custom routine generated in Matlab® R2008a v 7.6.0 (Mathworks, Natick, MA). **Equation 6-1** represents the generalized solution to the Bloch equation for relaxation of longitudinal magnetization (M_z), where *A*, *B*, and *T*1 are fitting constants that are obtained from the analysis.

$$M_z = A \cdot \left(1 - 2e^{-t/T1}\right) + B \qquad \text{(6-1)}$$

The characteristic *T*1 for each of the conditions was converted to a steady-state average pO_2 estimate (in the scaffold) using a previously determined linear calibration (pO_2 [mm Hg] = $8.96 \cdot 10^5/T1$ [ms] – 213; R^2 = 1.000). Each scaffold was assessed in replicate (n = 6-8).

Mathematical modeling

The graft was modeled at steady-state and as a diffusion-reaction system seeded with a known volume fraction of homogeneously distributed oxygen-consuming tissue. Oxygen was assumed to diffuse from the ambient air at the surface of the media layer (P_A = 160 mm Hg at x = 0 cm). Since the Petri dish is impermeable to gas transport, a zero flux boundary condition was imposed at the bottom of the scaffold material (dP/dx = 0 at x = 0.4 cm). Each graft was modeled as a one-dimensional slab of engineered tissue with constant thickness. It was assumed that the islet tissue is consuming oxygen with zero-order kinetics, which has been shown to be a reasonable assumption for most conditions involving $pO_2 >> K_m \sim 0.5$ mm Hg [207; 373].

Assuming that no anoxic core develops at the bottom of the scaffold (which was warranted by the tissue volume fractions used), the generalized solution for estimating the volumetric *OCR* (mol/cm^3/s) is given by **Equation 6-2**, where P_A (mm Hg) is the ambient (surface) pO_2, P_S (mm Hg) is the average steady-state scaffold pO_2 (obtained from ^{19}F-MRS), L_M (cm) is the thickness of media, L_S (cm) is the thickness of the scaffold, ϵ_i (dimensionless) is the islet volume fraction in the scaffold, $(\alpha D)_M$ (mol/cm/s/mm Hg) is the permeability of oxygen in culture media at 37°C, and $(\alpha D)_S$ (mol/cm/s/mm Hg) is the effective permeability of oxygen in the scaffold at 37°C [207].

$$(OCR)_i = \frac{P_A - P_S}{\left(\frac{L_S L_M}{(\alpha D)_M} + \frac{{L_S}^2}{3(\alpha D)_S}\right) \cdot \epsilon_i} \qquad (6\text{-}2)$$

The effective permeability of oxygen in the scaffold was estimated using the Maxwell relationship [207], which accounts for the contribution of the dispersed phase (i.e., PFD)

to the overall permeability. This adjustment is important given the high oxygen solubility of perfluorocarbons. The islet volume fraction was estimated from the islet volume and the scaffold volume [81] and is calculated by **Equation 6-3**, where N_{IE} is the total number of IEs per scaffold, R_{IE} (cm) is the radius of an IE, and R_S (cm) is the radius of the cylindrically-shaped scaffold.

(6-3) $$\epsilon_i = \frac{4{R_{IE}}^3 N_{IE}}{3{R_S}^2 L_S}$$

The volumetric *OCR* in units of mol/cm^3/s (from *Equation 6-2*) can be converted using **Equation 6-4** to *OCR* normalized to DNA in units of nmol/min/mg DNA – which are the standard units of *OCR/DNA* and a routinely measured islet quality read-out in our laboratory [97; 98; 121] – by assuming a DNA content per IE of DNA_{IE} = 10.4 ng/IE [81]:

(6-4) $$OCR/DNA = (OCR)_i \cdot \frac{4\pi}{3}(75 \cdot 10^{-4})^3 \cdot \frac{60 \cdot 10^6 \cdot 10^9}{10.4} \sim (OCR)_i \cdot (1.0195 \cdot 10^{10})$$

Table 6-1 summarizes the values of constant parameters used in the theoretical diffusion-reaction model.

Figure 6-1 illustrates a schematic of the theoretical model system, highlighting key dimensions and boundary conditions.

Results

Scaffolds exhibited an IE dose-dependent increase in $T1$ and a corresponding decrease in steady-state pO_2 estimates (**Table 6-2**).

From the difference between scaffold pO_2 measurements and ambient pO_2 (P_A - P_S), we calculated the islet preparation OCR to be 95 ± 12 (mean ± SE [nmol/min/mg DNA]) using the aforementioned equations. This value compares well with OCR values measured using established methods for human islet preparations [97].

Discussion

Engineered strategies for extrahepatic IT provide appealing alternatives to intraportal infusion – which is the currently-performed clinical protocol. Despite the optimism, localized transplantation of a graft seeded with islets has not progressed into clinical application, partly due to: (1) inadequate consideration of oxygen diffusion limitations in the early post-transplant period; (2) a lack of available tools for the accurate, quantitative, and non-invasive assessment of TE islet graft quality; and (3) failure to appreciate the problems associated with scaling-up designs that work well in rodents but would require very large volumes in larger mammals. These data represent preliminary results in developing ^{19}F-MRS as a technique that may enable non-invasive quality assessment of TE grafts based on direct measurements of pO_2 and estimates of OCR.

Given the inherent inaccuracies with visual counts and preparing aliquots of islets, it is important to use in future studies more accurate measures (e.g., spectrofluorometric DNA quantification) to determine the amount of islet tissue seeded into scaffolds. Additionally, comparisons between direct measurements of *OCR/DNA* with the standard

method on the islet preparation [97; 98; 121] prior to seeding into scaffolds will enable further validation of this ^{19}F-MRS method. Future work may also involve comparing analytical calculations of *OCR* with solutions generated using finite element methods that relax the homogeneity assumption. It is expected that these types of simulations would yield more accurate estimates of *OCR*, yet may require a more complete understanding of the spatial distribution of islets within the scaffold – particularly in the direction of oxygen diffusion. Nevertheless, this study highlights the prospective utility of ^{19}F-MRS for measuring islet viability at any point following graft construction, which includes during culture and possibly engraftment. ^{19}F-MRS may help guide development of new TE approaches to IT and enable meaningful graft monitoring before and after transplantation.

Conclusions

^{19}F-MRS can be used for the non-invasive pre- and possibly post-transplant assessment of TE islet graft viability by estimating the amount of viable, oxygen-consuming tissue in a scaffold. If better non-invasive methods for islet graft quality assessment are developed, TE approaches and extrahepatic IT may become more feasible in the clinical setting.

Supplementary Methods

Mathematical Theory

Consider the schematic in *Figure 6-1*, depicting a TE graft containing viable islet tissue (orange circles) and emulsified perfluorocarbon (PFC, blue circles), which is cultured in a gas-impermeable Petri dish with a thin layer of aqueous medium on top.

The islet graft can be modeled with the following assumptions:

1. Steady-state oxygen transport and consumption;
2. The oxygen source is represented by the external pO_2 (P_M) which is at the surface of the culture media and is equal to the ambient pO_2 of the surrounding air [boundary condition 1: P_A = ~160 mm Hg, at x = 0];
3. No oxygen flux at the bottom of the scaffold since the Petri dish is gas-impermeable [dP/dx = 0 at x = 0.4 cm];
4. Islets are homogeneously distributed throughout the scaffold material, with an average cell or tissue volume fraction represented by ϵ_i;
6. The scaffold has a uniform thickness of L_S and exhibits characteristic oxygen permeability in the scaffold material represented by $(\alpha D)_S$;
10. The islet equivalents seeded in the scaffold material consume oxygen at a characteristic volumetric rate given by $(OCR)_i$, which can be converted to *OCR/DNA* as described by *Equation 6-4*.

The Thiele modulus – which represents the ratio of the relative rates of oxygen diffusion and consumption – is used to calculate the pO_2 drop across the media (**Equation 6-5**) and scaffold layers (**Equation 6-6**).

(6-5) $$\Delta P_M = \frac{(OCR)_i \epsilon_i L_S L_M}{(\alpha \mathcal{D})_M}$$

(6-6) $$\Delta P_S = \frac{(OCR)_i \epsilon_i {L_S}^2}{2(\alpha \mathcal{D})_{S,eff}}$$

where $(OCR)_i$ is the volumetric islet oxygen consumption rate, ϵ_i is the volume fraction of viable islets within the scaffold, L_s is the thickness of the scaffold, L_M is the thickness of the media layer, $(\alpha D)_M$ is the oxygen permeability of the aqueous media, and $(\alpha D)_{S,eff}$ is the effective oxygen permeability of the scaffold material, which has been modified by the inclusion of PFC (a material of higher oxygen permeability) and whose contribution can be accounted for by the Maxwell relationship as described in *Chapter 5*. Briefly, incorporation of PFCs can increase the effective oxygen permeability of a material. The magnitude of this increase can be estimated using the Maxwell relationship (**Equations 6-7** and **6-8**), which describes the effective oxygen permeability in a composite material containing two phases, one that is dispersed and one that is continuous. In this case, the dispersed phase is the PFC and the continuous phase is the scaffold material, both of which have different oxygen permeability.

(6-7) $$\frac{(\alpha D)_{S,eff}}{(\alpha D)_S} = \frac{2 - 2\epsilon_{PFC} + \rho(1 + 2\epsilon_{PFC})}{2 + \epsilon_{PFC} + \rho(1 + \epsilon_{PFC})}$$

(6-8) $$\rho = \frac{(\alpha D)_{PFC}}{(\alpha D)_S}$$

where $(\alpha D)_{S,eff}$ is the effective oxygen permeability of the composite scaffold material, ϵ_{PFC} is the volume fraction of PFC, and ρ is the ratio of oxygen permeabilities of the two phases.

For a TE scaffold homogeneously distribute with viable islet tissue, the following **Equation 6-9** can be used to estimate the average scaffold pO_2:

(6-9) $$P_A = \frac{\int P dx}{\int dx} = P_S - \frac{(OCR)_i \epsilon_i}{2(\alpha \mathcal{D})_{S,eff}} \left[\frac{\int_0^{L_S} (L_S{}^2 - x^2) dx}{\int_0^{L_S} dx} \right]$$

which can simplify to the following (**Equation 6-10**):

(6-10) $$P_A = P_S - \frac{(OCR)_i \epsilon_i L_S{}^2}{3(\alpha \mathcal{D})_{S,eff}}$$

The media layer represents an oxygen transport resistance and can be described by the following (**Equation 6-11**):

(6-11) $$P_S = P_M - \frac{(OCR)_i \epsilon_i L_S L_M}{(\alpha \mathcal{D})_M}$$

Equation 6-11 can be substituted into *Equation 6-10*, and solved for $(OCR)_i$ to yield *Equation 6-2*. The volumetric OCR for the islet tissue can be converted to *OCR/DNA* as described above (*Equations 6-3* and *6-4*).

One of the key assumptions in this theoretical analysis is that there is no anoxic region in the scaffold. For the scaffold of the geometry shown in *Figure 6-1*, the maximum number of islets that can be seeded into the graft can be calculated by indicating that the maximum pO_2 drop across the media and scaffold layers cannot exceed the available oxygen supply, which in this case is represented by the ambient pO_2 at the surface of the media layer (**Equation 6-12**).

(6-12) $$\Delta P_{max} = \Delta P_M + \Delta P_S$$

By combining *Equations 6-3*, *6-5*, *6-6* and *6-12* and re-arranging to solve for the maximum number of islets (**Equation 6-13**):

(6-13) $$N_{IE} = \frac{3\Delta P_{max} {R_S}^2 L_S}{4(OCR)_i \left[\frac{L_S L_M}{(\alpha D)_M} + \frac{{L_S}^2}{2(\alpha D)_{S,eff}}\right] \cdot {R_{IE}}^3}$$

Prior to seeding into a TE scaffold, the OCR/DNA measurement of an islet preparation can be made using conventional methods [97; 98] and it can be converted to $(OCR)_i$ using *Equation 6-4*. For example, with an average porcine islet preparation of $(OCR)_i$ of $2 \cdot 10^{-8}$ mol/cm^3/sec (corresponding to an OCR/DNA of ~200 nmol/min/mg DNA), the maximum number of islets that can be seeded into the TE graft shown in *Figure 6-1* can be calculated using *Equation 6-13* to be ~8700 IEs. Since the average human islet preparation has an $(OCR)_i$ that is roughly half of that characteristic for porcine islet preparations (or an OCR/DNA of ~100 nmol/min/mg DNA), the maximum number of islets that can be seeded is ~16,400 IEs. All of the data collected to validate the ^{19}F-MRS

method for determining the TE graft viability has been generated using numbers of IEs that would not result in the formation of an anoxic region.

In the case of human islets (OCR/DNA ~100 nmol/min/mg DNA) or porcine islets (OCR/DNA ~200 nmol/min/mg DNA) of average viability, seeding the TE scaffold shown in *Figure 6-1* with >16,400 (human) or >8700 (porcine) IEs would likely result in the formation of an anoxic region. The size of this anoxic region can be characterized using diffusion-reaction equations, some of which are presented in *Chapter 5*. For these examples, consider the schematic in **Figure 6-2**, which depicts three regions for this system (culture media [Layer 2], viable [Layer 1] and anoxic [Layer 0] regions).

The conservation equation describing steady-state oxygen diffusion and consumption within the viable region can be described (**Equation 6-14**).

(6-14) $$(\alpha D)_1 \frac{\mathrm{d}^2 \mathrm{P}_1}{\mathrm{dx}^2} = V_1$$

where $(\alpha D)_1$ is the oxygen permeability, V_1 is the volumetric oxygen depletion rate, and P_1 is the local $p\mathrm{O}_2$ in layer 1.

As described in *Chapter 5*, the oxygen depletion rate is entirely determined by the oxygen consumption rate of the islets seeded within the scaffold, and can be estimated by Michaelis-Menten kinetics (**Equation 6-15**).

(6-15) $$V_1 = (OCR)_i \epsilon_i \frac{P_1}{K_{m,i} + P_1}$$

where $(OCR)_i$ is the volumetric islet oxygen consumption rate, ϵ_i is the viable islet volume fraction, P_1 is the local pO_2 in the scaffold, and $K_{m,i}$ is the Michaelis-Menten constant for islet tissue.

At lower pO_2 levels [$P_1 << K_{m,i}$], the oxygen-depletion rate exhibits first-order dependence (**Equation 6-16**).

(6-16) $$V_1 = (OCR)_i \epsilon_i \frac{P_1}{K_{m,i}}$$

At higher pO_2 levels [$P_1 >> K_{m,i}$], the oxygen-depletion rate exhibits zero-order dependence (Equation 6-17).

(6-17) $$V_1 = (OCR)_i \epsilon_i$$

Since the $K_{m,i}$ is believed to be very low (~0.5 mm Hg [207]), using zero-order kinetics to describe the oxygen-depletion rate in the scaffold is reasonable.

The constitutive species conservation equation must be solved for the media and viable region. There are three boundary conditions. Firstly, at the interface between the viable and anoxic regions, there is no oxygen flux [$dP/dx = 0$, at $x = 0$], and this is due to the combination of no oxygen consumption in the anoxic region and the impermeable solid-bottom of the Petri dish. Secondly, the pO_2 at the top of the culture media is determined by the external pO_2 [$P_{S2} = 160$ mm Hg, at $L_2 = 0.4$ cm]. Thirdly, the flux at the interface

between the culture media and the viable region [L_1 = 0.3 cm] are also equal. The solution for the pO_2 profile in the viable region [$a \leq x \leq L_1$] in terms of P_{S1} (**Equation 6-18**) and the equation describing the thickness of the anoxic region [a] (**Equation 6-19**) is given herein:

(6-18) $$\left(\frac{P_1}{P_{S1}}\right) = 1 - \left[\frac{V_1 {L_1}^2}{2(\alpha D)_1 P_{S1}}\right]\left\{1 - \left(\frac{x}{L_1}\right) - 2\left(\frac{a}{L_1}\right)\left(1 - \frac{x}{L_1}\right)\right\}$$

(6-19) $$\left(\frac{a}{L_1}\right) = 1 - \left[\frac{2(\alpha D)_1 (P_{S1} - P_C)}{V_1 {L_1}^2}\right]^{1/2}$$

The quantity found in the right-hand side of *Equation 6-19* is the square of the Thiele modulus (**Equation 6-20**).

(6-20) $$\varphi^2 = \left[\frac{V_1 {L_1}^2}{(\alpha D)_1 (P_{S1} - P_C)}\right]$$

To calculate the thickness of the anoxic region from *Equation 6-19*, P_{S1} must be calculated using **Equations 6-21** and **6-22**.

(6-21) $$P_{S1} = P_{S2} - \Delta P_2$$

where

(6-22) $$\Delta P_2 = \frac{1}{(\alpha D)_2}[V_1 (L_2 - L_1)(L_1 - a)]$$

Equation 6-22 can be substituted into *Equation 6-21*, and the values for a and P_{S1} are determined by solving *Equations 6-19* and *6-21* implicitly.

The volume-averaged pO_2 ($P_{avg,1}$) in the scaffold can also be calculated using the generalized **Equation 6-23**, where $P_1(x)$ is derived from *Equation 6-18*.

(6-23) $$P_{avg,1} = \frac{\int P_1(x)dx}{\int dx}$$

The bounds of integration are at the surface of the scaffold [$P_1(x) = P_{S1}$, at $x = L_1$] and at the edge of the anoxic region [$P_1(x) = 0$, at $x = a$], and the average pO_2 for the viable region is given by **Equation 6-24**.

(6-24) $$P_{avg,1} = \frac{P_{S1}\int_a^{L_1} dx - \left[\frac{V_1 {L_1}^2}{2(\alpha D)_1}\right]\left\{\int_a^{L_1}\left[1 - \frac{x^2}{{L_1}^2} - 2\left(\frac{a}{L_1}\right)\left(1 - \frac{x}{L_1}\right)\right]\right\}}{\int_a^{L_1} dx}$$

Integrating and simplifying *Equation 6-24* yields **Equation 6-25**.

(6-25) $$P_{avg,1} = \frac{P_{S1}(L_1 - a) - \left[\frac{V_1 {L_1}^2}{(\alpha D)_1}\right]\left\{\frac{L_1}{3} - a + \frac{a^2}{L_1} - \frac{a^3}{3{L_1}^2}\right\}}{(L_1 - a)}$$

Fluorine magnetic resonance spectroscopy

^{19}F-MRS can be used to non-invasively estimate the average pO_2 within a TE graft. The basis for this technique stems from the unique physicochemical properties of both PFCs and oxygen. Since molecular oxygen is paramagnetic, it shortens both spin-lattice ($T1$)

and spin-spin (*T*2) relaxation times for any nucleus. Other moieties (such as ions, proteins, etc.) can affect *T*1 and *T*2, but since PFCs are hydrophobic most of these will not dissolve in PFC and thus will be excluded from interaction with the fluorine-19 nuclei in PFC [321; 328]. *T*1 and *T*2 are also dependent on temperature and the magnitude of the external magnetic field (B_0), but under experimental conditions both are controlled. Consequently, the *T*1 and *T*2 relaxation effects of oxygen can be isolated and it has been determined that the longitudinal relaxation rate (*R*1, which is the inverse of *T*1 or equal to 1/*T*1) is linearly proportional to the pO_2 in the vicinity of the fluorine-19 nuclei in the sample of interest. The theoretical basis for this relationship was developed by Parhami and Fung in the early 1980s [320]. The fluorine-19 nuclei in PFC can be segregated into two sub-populations, those that are exposed to molecular oxygen and those that are not. The ones that are not exposed to oxygen have a characteristic longitudinal relaxation rate of $1/T1_a$ (or $R1_a$, where the subscript '*a*' is in reference to anoxia) [320]. The fluorine nuclei that are within the vicinity of molecular oxygen have a different, apparent longitudinal relaxation rate of $1/T1_a + 1/T1_p$, where $1/T1_p$ (or $R1_p$) is the paramagnetic contribution of oxygen to the overall relaxation rate [320]. Because oxygen molecules quickly diffuse throughout the PFC, the effective relaxation rate (denoted $1/T1_e$ or $R1_e$) is simply a weighted molar average for each type of fluorine-19 nucleus (**Equation 6-26**), which can be simplified (**Equation 6-27**) [320]:

(6-26) $$\frac{1}{T1_e} = (1 - X)\frac{1}{T1_a} + X\left(\frac{1}{T1_a} + \frac{1}{T1_p}\right)$$

(6-27) $$\frac{1}{T1_e} = \frac{1}{T1_a} + \frac{x}{T1_p}$$

The variable '*X*' is simply the molar fraction of oxygen. Like aqueous solvents, PFC dissolves oxygen and obeys Henry's Law. Consequently, each PFC has a characteristic oxygen solubility coefficient (α_{PFC}). As a result, *Equation 6-27* can be simplified further (**Equation 6-28**):

(6-28) $$\frac{1}{T1_e} = \frac{1}{T1_a} + \frac{\alpha_{PFC} \cdot P_{PFC}}{T1_p}$$

From *Equation 6-28*, it can be demonstrated that a plot of $1/T1_e$ versus pO_2 (P_i) should be linear, described by a y-intercept of $1/T1_a$ and a slope of $\alpha_{PFC}/T1_p$. Since each chemically-equivalent fluorine-19 nucleus lies in a unique position within the PFC molecule, each such fluorine nucleus has a unique resonance and relaxation properties. Therefore, each fluorine nucleus is affected differently by the presence of oxygen and that is reflected in differences in the $T1_e$. The characteristic relaxation sensitivity of an individual fluorine-19 nucleus to oxygen can sometimes be referred to as the '*R*1 sensitivity' and can be expressed as the slope of the plotted pO_2 versus $R1_e$ calibration line divided by the y-intercept (or $\alpha_{PFC} \cdot T1_a/T1_p$). More commonly, however, the slope is an indicator of the oxygen relaxation effects on a specific fluorine-19 resonance. It is important to mention that temperature can also affect the relaxation properties of fluorine nuclei and that these effects may [323; 324] or may not [322] be linear, and may depend on the temperature range of interest, the magnetic field strength, and the PFC involved. Consequently, the selected PFC should be evaluated for its temperature sensitivity using the magnet that will be used for *in vivo* experiments. This is particularly important if accurate pO_2 estimates need to be made and temperature cannot be measured. Mason *et al.* discussed that temperature and pO_2 can be simultaneously estimated using

separate *R*1 measurements at two different resonance frequencies corresponding to two different fluorine-19 nuclei located in the same PFC molecule. This technique requires generating separate *R*1 versus pO_2 and temperature calibrations for each of the resonance frequencies, and solving a system of linear equations [324].

In our studies, all measurements were done under controlled and monitored conditions at physiological temperature (37°C) and at constant external magnetic field strength (5 T). To generate a calibration line for PFD at 37°C and 5 T, PFD was added into gas-impermeable 2.0-mL containers and pre-bubbled at 4-5 different samples with different gases or gas mixtures containing varying proportions of oxygen (100, 21, 5, 1 and 0%) for >30 minutes at a gas flow rate of ≥5 mL/min (**Figure 6-3**). A water jacket maintained the temperature within the bore of the magnet to about ±0.2°C. The sample was placed over a 6-cm diameter single-loop, custom-built surface coil and centered within the bore of the magnet. The singlet peak in the PFD spectrum was identified and a standard inversion recovery sequence was used to obtain characteristic *T*1 values for each pre-bubbled sample. Inversion recovery curves were fit to the Bloch equation using a custom routine generated in Matlab® R2008a v 7.6.0 (Mathworks, Natick, MA). **Appendix 6-2** summarizes the related equations and shows a representative curve fitting. *R*1 values at each pO_2 were plotted to yield a linear calibration (CL1, **Figure 6-4**). A second calibration line (CL2, **Figure 6-5**) under the same conditions (37°C, 5 T) was prepared to confirm the correlation obtained in the first calibration line. An adjustment was made to account for the absolute humidity [6.6-6.8 g/m^3] (water vapor pressure) in the room in which the ambient air samples were prepared, and adjusted the ambient air sample to Both calibration lines were used to convert subsequent *R*1 measurements to compare the validity of each pO_2 estimate.

To determine whether the pO_2 estimates obtained via ^{19}F-MRS reflect the minimum, maximum, volume- or weighted-average pO_2 in a sample, an experiment was conducted in which two gas-impermeable containers containing equal volumes of PFD were placed over the surface coil separately and together (**Figure 6-6**). The first container (Sample A) was equilibrated with ambient pO_2 (158.2 mm Hg) and the second container (Sample B) was pre-bubbled with argon gas for >30 minutes (pO_2 = 0 mm Hg). The results of this experiment indicated that when samples A and B were interrogated together via ^{19}F-MRS the estimated pO_2 reflected a volume-average pO_2. Since the magnetic resonance facility was located off-site and the time from pre-bubbling samples to measurement-taking could exceed 3-4 hours, it was important to ensure that the containers being used were indeed gas-permeable. Another experiment was conducted in which two gas-impermeable containers containing equal volumes of PFD were examined separately over the course of up to two days following preparation of samples. The first container was equilibrated with ambient pO_2 (158.2 mm Hg) and the second container was pre-bubbled with pure oxygen gas for >60 minutes (pO_2 = 760 mm Hg). Pure oxygen gas was chosen since it provided the greatest difference between the ambient pO_2 and the pO_2 within the PFD in the second container – which would impose the largest driving force (gradient) for oxygen to leak out of the container. The results of this experiment showed no differences in $T1$ measurements in either the control or pre-oxygenated samples for up to 48 hours post-bubbling (**Figure 6-7**). The next section summarizes supplementary results in using ^{19}F-MRS in assessing the viability of TE islet grafts, obtained since the publication of Suszynski *et al*. [56].

Supplementary Results and Discussion:

The results published in Suszynski *et al*. [56] were reproduced several times using human (n = 3) and porcine (n = 1) islet preparations (unpublished). There were no differences in the methods from prior description [56], except that the number of islets seeded into each graft were determined by DNA quantification instead of visual counting, which has been validated to be much more accurate [81], and that each preparation was characterized for OCR/DNA using the stirred microchamber [98]. DNA was quantified using fluorospectrophotometry (Quant-IT PicoGreen dsDNA assay kit, Invitrogen, Eugene, OR) [55] using a SpectraMax M5 plate reader (Molecular Devices, Sunnyvale, CA). OCR/DNA measurements were generally performed before ^{19}F-MRS measurements were taken (1.5-6.5 hours prior to experimentation). For each experiment, the TE islet grafts were constructed at the same time as described previously [56] and the ^{19}F-MRS measurement run order was randomized in each case. A schematic illustrating the nature of a pO_2 estimate obtained via ^{19}F-MRS for a TE islet graft and the factors that affect the estimate is shown in **Figure 6-8**.

Assessment of human islet TE grafts via ^{19}F-MRS and theory: Three different human islet preparations were used for three separate experiments. Each preparation containing 9000-15,000 IEs (based on DNA quantification) was aliquoted proportionally (based on volume of suspension) into 2-4 TE grafts, and each experiment involved an additional TE scaffold containing no islet tissue (summary of conditions and run order in **Table 6-3**). The number of IEs used in an experiment was different when comparing experiments since the availability of human islets was different in each case. Data ($T1$, $R1$, and pO_2 estimates) from these three experiments are summarized in **Table 6-4**.

Mean (± standard error, SE) *R*1 values and the corresponding pO_2 estimates (as calculated using CL1 and CL2) are also shown graphically in **Figures 6-9**, **6-10**, and **6-11** to illustrate the dose-dependent relationship between number of IEs seeded and these metrics. OCR/DNA measurements obtained for each preparation prior to seeding and OCR/DNA estimates derived from ^{19}F-MRS and theoretical analysis [56] for these three experiments are summarized in **Table 6-5**. The OCR/DNA estimates are comparable to the OCR/DNA measurements, but there are differences.

Explanations that may account for some of these differences include: (1) inaccuracy of model assumptions (islet and PFC homogeneity, media layer and scaffold thickness); (2) inaccuracy of model constants (effective oxygen permeability of scaffold); (3) aliquoting error; (4) loss of islet tissue during experimentation; (5) temperature fluctuations. Loss of islet tissue during experimentation is unlikely since the ^{19}F-MRS measurements were taken within 8 hours of OCR/DNA measurements, and *T*1 values did not change and were stable (standard error ~ $5\text{-}10 \cdot 10^{-3}$ s) once each TE graft equilibrated in temperature and reached steady-state. Temperature fluctuations were unlikely since the water-jacketing system within the bore of the magnet was insulated; all measurements were confirmed to be taken at 37.0°C using multiple fiberoptic temperature probes and/or standard mercury thermometer. There was a transient period that occurred following the placement of a sample into the magnet during which *T*1s would lengthen until they reached a steady-state in usually 45-60 minutes. This transient period was attributable to the difference in temperature between room (~23°C) and within the water jacket/bore (37°C), and in part reflects the difference in islet OCR at these two different temperatures; the OCR is ~3.1 times lower at room temperature than at physiologic temperature if OCR exhibits temperature dependence described by the Arrhenius

equation [$OCR \sim \exp(-1/RT)$, where R is the universal gas constant and T is temperature in degrees Kelvin]. Islet distribution is difficult to determine, and it may be impossible to accurately characterize their homogeneity within the graft – particularly since islets are inherently inhomogeneous in both composition and size. PFC distribution appears homogeneous (**Figure 6-12**, light micrograph) throughout the scaffold material even though PFD has a density two times that of water and may be that larger emulsified droplets are found at the bottom of each graft. Inaccurate estimates of media layer and graft thickness can have an impact on the OCR/DNA estimate, with the media layer thickness having the greater possible effect. For example, if the media layer was one-half times the expected thickness (~0.05 cm) then the estimated OCR/DNA would increase by ~50%. If the media layer was two times the expected thickness (0.2 cm) then the estimated OCR/DNA would decrease by ~40%. In contrast, if the graft was one-half times the expected thickness (~0.15 cm) then the estimated OCR/DNA would increase by ~20%. If the graft was two times the expected thickness (0.6 cm), then the estimated OCR/DNA would decrease by 25%. It is more likely that the media layer varied in thickness since the graft thickness may not be uniform from the center to the edges of the Petri dish (**Figure 6-13** and **6-14**, micro-CT images). Surface tension effects may have also contributed to the non-uniformity of the media layer. It is unlikely that the actual thickness of the graft was different from the expected thickness since the surface area of the Petri dish (~10 cm^2) and the volume of the graft material (scaffold, PFC, islets; ~3 cm^3) were both fairly constant. An inaccurate value for the effective oxygen permeability within the graft may affect the OCR/DNA estimate. For example, if the oxygen permeability was one-half times the expected value (and equal to that in water at 37°C), then the OCR/DNA estimate would decrease by ~25%. If the oxygen permeability was two times the expected value, then the OCR/DNA estimate would

increase by ~20%. Upon transfer of graft material from the microcentrifuge tube (in which plasma, PFC and islets are mixed) to the Petri dish, it may be that the more dense PFC is preferentially left behind – which would lower the effective oxygen permeability within the graft. Aliquoting error or inaccurate islet counts would significantly impact OCR/DNA estimates and are the primary subject of the supplementary experiment presented in the next sub-section.

Assessment of porcine islet TE graft via ^{19}F-MRS and theory: A porcine islet preparation was used for an experiment, primarily to illustrate the potential impact of inaccurate counts and aliquoting error on outcomes. The islet preparation contained ~12,000 IEs (based on DNA counts performed several days prior to experimentation) and was aliquoted proportionally (based on volume of suspension) into 3 TE grafts. There was also an additional TE scaffold prepared which contained no islet tissue (summary of conditions and run order in *Table 6-3*). Data ($T1$, $R1$, and pO_2 estimates) from this experiment is summarized in **Table 6-6**. Mean (± SE) $R1$ values and the corresponding pO_2 estimates (as calculated using CL1 and CL2) are also shown graphically in **Figure 6-15** to illustrate that, in this case, there was no dose-dependent relationship between number of IEs seeded and either of these metrics. Not surprisingly, OCR/DNA measurements obtained prior to seeding was not comparable with OCR/DNA estimates derived from ^{19}F-MRS and theoretical analysis [56], and are presented in **Table 6-7**. Since the data did not reflect expected outcomes and because inaccurate counts and aliquoting error were suspected, samples from the preparation prior to aliquoting were analyzed for DNA content and a protocol was developed to process the islet TE graft for DNA content. The mean (± SE) number of IEs in the preparation based on DNA quantification was found to be 7923 (± 888), much lower than the expected number of

IEs available for this study (~12,000 IEs). Following the ^{19}F-MRS experiment, each sample was transported from the MR facility to the Schulze Diabetes Institute and sonicated using standard protocol that was modified to ensure all DNA would be retrieved (ten times at 11% amplitude for 15 seconds). After sonication, the graft material was transferred to a capped plastic test tube (each of which was massed prior to use) using a 1000-µL pipette. Each Petri dish was then twice washed with 500-µL detergent solution, and the post-wash solution was collected and combined with the sonicated graft material. Once all material was successfully retrieved, the test-tube was capped, mixed, massed and placed into a -20°C freezer. The same modified protocol was repeated for each graft. The scaffold containing no IEs was also processed for DNA analysis to determine if the PFD (or any other material) generates background autofluorescence signal that would confound the measurements obtained via the spectrofluorometric DNA assay. **Figure 6-16** illustrates representative photographs of the Petri dish (graft) immediately following experimentation, sonication and DNA recovery. Each condition was assessed at 20X dilution (from stock sample) and the mean (± SE) RFU values are presented in **Table 6-8**.

In order to calculate the DNA content per graft, an accurate pooled volume from the post-sonicated sample needed to be measured or estimated. Since volumetric measurements (such as by using a pipette to determine volume of sample) were determined to be inaccurate due to the viscosity of the sample and difficulty in being able to remove all material from a test tube, samples were massed and the masses were converted volumes using presumed densities. Both the mass of the empty capped test tube and the total mass of a capped test tube and sample were measured. These measurements are summarized in **Table 6-9**. Mass measurements were converted to

volume estimates by sub-dividing the aqueous and PFC components of each sample and assuming that densities to be 1.000 and 1.917 g/mL for the two components, respectively. A summary of the estimated masses for all components for each sample are presented in **Table 6-10**. Since the total measured (actual) mass of each sample (*Table 6-9*) and the total estimated mass of each sample (*Table 6-10*) are not equal, it was assumed that difference represents the amount of scaffold material that was lost during the recovery, that equal proportions of both aqueous and PFC components were lost and that no detergent was lost from the sample (since detergent is added as the final wash step following sonication). Consequently, the recovered masses of each scaffold can be estimated and these values are shown in **Table 6-11**, and then converted to volumes as shown in **Table 6-12**. The calculated pooled sample volumes (*Table 6-12*) were used in conjunction with DNA measurements to estimate the total number of IEs in each sample. **Table 6-13** summarizes the estimated number of IEs per graft, as determined by post-experimentation DNA analysis on the grafts material. To more accurately estimate OCR/DNA of the islet preparation using ^{19}F-MRS and theory, the initial count estimates were replaced by the more reliable counts based on DNA (**Figure 6-17**) and the theoretical calculations can be performed again, and are presented in **Table 6-14**. The mean (± SE) estimated OCR/DNA for the islet graft was 195.0 (± 10.9) and 197.2 (± 11.0) nmol/min/mg DNA when using CL1 and CL2, respectively, which is remarkably comparable to the actual OCR/DNA measurements for the islet preparation [190.1 (± 8.9) nmol/min/mg DNA]. These data indicate that DNA measurements performed prior to seeding is important to ensure that the correct number of IEs is added into a TE graft. Nevertheless, aliquoting error may still occur and may account for some inaccuracy in the method used for estimation of OCR/DNA [56]. It

should be noted that the method based on ^{19}F-MRS and theory may enable detection of suspected aliquoting error after a TE graft is constructed.

Table 6-1: Values of constants used for theoretical modeling.

Constant	Units	Value	Reference
P_A	mm Hg	160	-
L_M	cm	0.1	-
L_S	cm	0.3	-
$(\alpha D)_M$	mol/(cm·s·mm Hg)	$3.53 \cdot 10^{-14}$	[207]
$(\alpha D)_S$	mol/(cm·s·mm Hg)	$7.06 \cdot 10^{-14}$	[207]
R_S	cm	1.75	-
R_{IE}	cm	0.0075	-
N_{IE}	-	2000, 4000, 8000	-
DNA_{IE}	ng	10.4	[81]

Abbreviations: P_A, ambient (or surface) oxygen partial pressure (pO_2); L_M, thickness of culture media layer; L_S, thickness of scaffold; $(\alpha D)_M$, oxygen permeability in culture media; $(\alpha D)_S$, oxygen permeability in scaffold; R_S, radius of scaffold; R_{IE}, radius of islet equivalent (IE); N_{IE}, number of IEs seeded into scaffold; DNA_{IE}, DNA content per IE.

Table 6-2: *T*1 values and pO_2 estimates for scaffolds seeded with varying numbers of human IEs (Suszynski *et al*. [56])

IEs per Scaffold	*T*1 Measured [s]	pO_2 Estimate, P_S [mm Hg]
0	1.866 ± 0.019	160
2000	1.942 ± 0.033	145
4000	2.081 ± 0.053	121
8000	2.181 ± 0.094	106

*T*1 values are presented as mean ± standard error.
Abbreviations: *IE*, islet equivalent; pO_2, oxygen partial pressure; P_S, scaffold pO_2; *T*1, spin lattice relaxation time.

Table 6-3: Summary of conditions and run order in supplementary experiments of assessment of human islet graft viability via ^{19}F-MRS

Experiment	Conditions [number of IEs seeded per scaffold]	Run Order [by Condition]
S-H1	0, 4000, 8000	1: 8000, 2: 4000, 3: 0
S-H2	0, 3000, 6000	1: 3000, 2: 6000, 3: 0
S-H3	0, 1000, 2000, 4000, 8000	1: 2000, 2: 4000, 3: 1000, 4: 8000, 5: 0

Abbreviations: ^{19}F-MRS, fluorine magnetic resonance spectroscopy; IE, islet equivalent.

Table 6-4: Summary of data (*T*1, *R*1 and pO_2 estimates) from supplementary experiments involving human islet tissue-engineered grafts

Experiment	Condition [IEs/graft]	*T*1 [s]	*R*1 [s^{-1}]	pO_2 Estimate [mm Hg]
S-H1	0	1.966 ± 0.004	0.509 ± 0.001	158.2
	4000	2.295 ± 0.007	0.436 ± 0.001	107.4
	8000	2.408 ± 0.015	0.415 ± 0.003	93.2
S-H2	0	1.908 ± 0.005	0.524 ± 0.001	158.2
	3000	2.051 ± 0.007	0.488 ± 0.002	132.7
	6000	2.293 ± 0.011	0.436 ± 0.002	96.9
S-H3	0	1.924 ± 0.004	0.520 ± 0.001	158.2
	1000	1.966 ± 0.006	0.509 ± 0.002	150.6
	2000	1.975 ± 0.004	0.506 ± 0.001	149.0
	4000	2.114 ± 0.008	0.473 ± 0.002	125.7
	8000	2.476 ± 0.008	0.404 ± 0.001	77.7

*T*1 and *R*1 values are presented as mean ± standard error.
pO_2 estimates are derived of calibration line 1 (*Figure 6-4*).
Abbreviations: IE, islet equivalent; pO_2, oxygen partial pressure; *R*1, spin-lattice relaxation rate; *T*1, spin-lattice relaxation time.

Table 6-5: Summary of actual and estimated OCR/DNA from supplementary experiments involving human islet tissue-engineered grafts

Experiment	Number of Grafts [*N*]	Actual OCR/DNA [nmol/min/mg DNA]	Estimated OCR/DNA [nmol/min/mg DNA]
S-H1	2	57.1 ± 7.2	135.8 ± 29.9
S-H2	2	73.7 ± 1.3	121.8 ± 11.5
S-H3	4	68.7 ± 13.5	78.5 ± 14.9

OCR/DNA measurements were obtained using the stirred microchamber method [98]. OCR/DNA estimates were obtained using ^{19}F-MRS and theoretical analysis [56].
Abbreviations: ^{19}F-MRS, fluorine magnetic resonance spectroscopy; DNA, deoxyribonucleic acid; OCR, oxygen consumption rate.

Table 6-6: Summary of data (*T*1, *R*1 and pO_2 estimates) from supplementary experiment involving porcine islet tissue-engineered grafts

Experiment	Condition [IEs/graft]	*T*1 [s]	*R*1 [s^{-1}]	pO_2 Estimate [mm Hg]
S-P1	0	1.787 ± 0.017	0.560 ± 0.005	158.2
	2000	1.918 ± 0.004	0.521 ± 0.001	131.5
	4000	1.976 ± 0.008	0.506 ± 0.002	120.9
	8000	1.890 ± 0.018	0.529 ± 0.005	136.9

*T*1 and *R*1 values are presented as mean ± standard error.
pO_2 estimates are derived of calibration line 1 (CL1, *Figure 6-4*).
Abbreviations: IE, islet equivalent; pO_2, oxygen partial pressure; *R*1, spin-lattice relaxation rate; *T*1, spin-lattice relaxation time.

Table 6-7: Summary of actual and estimated OCR/DNA from supplementary experiments involving porcine islet tissue-engineered grafts

Experiment	Number of Grafts [*N*]	Actual OCR/DNA [nmol/min/mg DNA]	Estimated OCR/DNA [nmol/min/mg DNA]
S-P1	3	190.1 ± 8.9	113.8 ± 37.1

OCR/DNA measurements were obtained using the stirred microchamber method [98]. OCR/DNA estimates were obtained using ^{19}F-MRS and theoretical analysis [56].
Abbreviations: ^{19}F-MRS, fluorine magnetic resonance spectroscopy; DNA, deoxyribonucleic acid; OCR, oxygen consumption rate.

Table 6-8: Mean (± SE) raw and adjusted RFU values from DNA analysis of tissue-engineered scaffolds following experimentation.

Condition [IEs/graft]	Raw Signal [RFUs]	Adjusted Signal [RFUs][a]
0	86.5 (± 0.5)	-
2000	561.2 (± 3.8)	474.7 (± 3.8)
4000	656.2 (± 3.2)	569.7 (± 3.2)
6000	440.4 (± 1.1)	353.7 (± 1.1)

[a]Adjusted for by subtracting mean RFU signal corresponding to autofluorescence from raw RFU signal.
Abbreviations: DNA, deoxyribonucleic acid; IE, islet equivalent; RFU, relative fluorescence units; SE, standard error.

Table 6-9: Mass measurements of test tubes and samples for each condition.

Condition [IEs/graft]	Mass of test tube [g]	Mass of test tube + sample [g]	Total mass of sample [g][a]
0	3.6169	8.2014	4.5845
2000	3.4419	7.5974	4.1555
4000	3.5370	7.7424	4.2054
6000	3.5869	8.2557	4.6688

[a]The total mass of the sample was calculated by subtracting the mass of the test tube from the mass of the test tube and sample.
Abbreviations: IE, islet equivalent.

Table 6-10: Summary of estimated masses for all components of each sample.

Condition [IEs/graft]	Aqueous component [g]					PFC component [g]	Total mass [g]
	Plasma	ME199 media	Detergent	Thrombin	Islet suspension	PFD	
0	2.1	1.0	1.0	0.075	0.0	1.73	4.90
2000	2.1	1.0	1.0	0.075	0.0165	1.73	4.91
4000	2.1	1.0	1.0	0.075	0.033	1.73	4.93
6000	2.1	1.0	1.0	0.075	0.050	1.73	4.95

Abbreviations: IE, islet equivalent; PFC, perfluorocarbon; PFD, perfluorodecalin.

Table 6-11: Recovered masses for each scaffold

Condition [IEs/graft]	Total mass of graft and test tube [g]	Mass of graft only [g]	Mass fraction of aqueous components	Mass of aqueous components [g]	Mass of PFC component [g]
0	4.5845	3.5845	0.6479	2.3225	1.2620
2000	4.1555	3.1555	0.6491	2.0482	1.1073
4000	4.2054	3.2054	0.6503	2.0843	1.1210
6000	4.6688	3.6688	0.6515	2.3901	1.2787

Abbreviations: IE, islet equivalent; PFC, perfluorocarbon.

Table 6-12: Recovered volumes (in units mL) for each graft

Condition [IEs/graft]	Volume of aqueous scaffold	Volume of PFC scaffold	Volume of scaffold	Pooled volume of sample
0	2.3225	0.6583	2.9808	3.9808
2000	2.0482	0.5776	2.6258	3.6258
4000	2.0844	0.5848	2.6692	3.6692
8000	2.3901	0.6670	3.0572	4.0571

Abbreviations: IE, islet equivalent; PFC, perfluorocarbon.

Table 6-13: Total number of IEs per graft as determined by DNA analysis

Expected number of IEs (Pre-experimentation)	Actual Number of IEs (Post-experimentation)
0	0
2000	1846
4000	2245
6000	1535

Abbreviations: DNA, deoxyribonucleic acid; IE, islet equivalents.

Table 6-14: Theoretical values of OCR/DNA derived from ^{19}F-MRS and theory following correction with more accurate IE counts based on DNA post-experimentation

Expected count [IEs/graft]	Actual count by DNA [IEs/graft]	OCR/DNA (via CL1) [nmol/min/mg DNA]	OCR/DNA (via CL2) [nmol/min/mg DNA]
0	0	0	0
2000	1846	188.3	190.4
4000	2245	216.3	218.8
6000	1535	180.4	182.4
Mean ± SE		195.0 ± 10.9	197.2 ± 11.0

Abbreviations: ^{19}F-MRS, fluorine magnetic resonance spectroscopy; CL, calibration line; DNA, deoxyribonucleic acid; IE, islet equivalent; OCR, oxygen consumption rate; SE, standard error.

Figure Captions

Figure 6-1: Schematic illustrating the design of the tissue-engineered graft containing scaffold material (crosslinked plasma), emulsified perfluorocarbon (represented by the smaller, darker circles) and human pancreatic islets (represented by the larger, lighter circles), and also highlighting boundary conditions used in the diffusion-reaction model. Variables presented in this *Figure* are defined in the *Mathematical modeling* sub-section of the *Methods*. *Abbreviations*: ^{19}F-MRS, fluorine magnetic resonance spectroscopy; d*P*/d*x*, oxygen flux; L_M, thickness of culture media layer; L_S, thickness of scaffold; P_A, ambient (and media surface) oxygen partial pressure (pO_2); P_S, average scaffold pO_2; $T1$, spin-lattice relaxation time.

Figure 6-2: Schematic illustrating the generalized design of the theoretical model system for the tissue-engineered islet graft, featuring three distinct regions (culture media [Layer 2], viable [Layer 1] and anoxic [Layer 0] regions).

Figure 6-3: Schematic illustrating ^{19}F-MRS characterization of perfluorocarbon (PFC) in terms of oxygen sensitivity ($R1$ vs. pO_2). (A) PFCs (like perfluorodecalin, PFD) are added into gas-impermeable container, pre-bubbled with varying gas mixtures containing different but known pO_2 (100%, 21%, 5%, 1% and 0% oxygen) and then sealed; (B) The sample is centered within/onto an appropriately-sized radiofrequency coil and placed into a magnet; (C) A ^{19}F-spectrum is generated and the singlet is identified; (D) Standard inversion recovery is performed using this singlet peak and these data are fitted to an exponential function (derived of the Bloch equation) to yield a spin lattice relaxation rate ($R1$) which is characteristic for each PFC at a specific pO_2; (E) The measurements are repeated at different pO_2 to create a linear calibration that

relates the relaxation rate ($R1$, which is $1/T1$) to pO_2. *Abbreviations*: ^{19}F-MRS, fluorine magnetic resonance spectroscopy; PFC, perfluorocarbon; PFD, perfluorodecalin; pO_2, oxygen partial pressure; $R1$, spin-lattice relaxation rate; $T1$, spin-lattice relaxation time.

Figure 6-4: Calibration line 1 (**CL1**) for perfluorodecalin at 37°C and 5 T. The resulting equation is linear [$R1 = 0.00144 \cdot pO_2 + 0.351$] and exhibits a strong correlation between $R1$ and pO_2 [$R^2 = 1.000$]. Five different samples were used, each pre-bubbled for >30 minutes at ≥5 mL/min using gases or gas mixtures characterized by different pO_2 values (0, 7.6, 38.0, 158.2, 760 mm Hg). *Abbreviations*: CL, calibration line; pO_2, oxygen partial pressure; $R1$, spin-lattice relaxation rate.

Figure 6-5: Calibration line 2 (**CL2**) for perfluorodecalin at 37°C and 5 T. The resulting equation is linear [$R1 = 0.00142 \cdot pO_2 + 0.340$] and exhibits a strong correlation between $R1$ and pO_2 [$R^2 = 0.999$]. Four different samples were used, each pre-bubbled for >30 minutes at ≥5 mL/min using gases or gas mixtures characterized by different pO_2 values (7.6, 38.0, 158.2, 760 mm Hg). *Abbreviations*: CL, calibration line; pO_2, oxygen partial pressure; $R1$, spin-lattice relaxation rate.

Figure 6-6: Schematic of experimental methods and summary of results for experiment performed to determine whether pO_2 estimate obtained from ^{19}F-MRS analysis is reflective of the minimum, maximum, volume-averaged or weighted-average pO_2 in a sample. Two samples were prepared by filling two separate containers with equal volumes of perfluorodecalin (PFD). Sample A was not pre-bubbled and was equilibrated with ambient air (pO_2 = 158.2 mm Hg), whereas Sample B was pre-bubbled for >60 minutes with pure argon gas (pO_2 ~ 0 mm Hg). Each sample was placed onto a single-

loop, custom-built surface coil and interrogated separately and together via ^{19}F-MRS as described previously [56]. Combining the two samples yielded a pO_2 estimate that was close to the arithmetic mean of the individual measurements of the two samples. Abbreviations: ^{19}F-MRS, fluorine magnetic resonance spectroscopy; PFD, perfluorodecalin; pO_2, oxygen partial pressure.

Figure 6-7: Summary of results from experiment showing that perfluorodecalin (PFD) pre-bubbled with pure oxygen gas and sealed in a glycol-modified polyethylene terephthalate (PETG) container does not equilibrate quickly with the ambient atmosphere. One sample of PFD (experimental) was pre-bubbled with pure oxygen gas for >60 minutes for ≥5 mL/min, and another sample (control) was not pre-bubbled but was equilibrated with ambient air. $R1$ measurements and pO_2 estimates are relatively stable during ~48-hour period of ^{19}F-MRS interrogation, indicating that the PETG containers are able to prevent gas leakage from sample over a reasonable time frame. *Abbreviations*: ^{19}F-MRS, fluorine magnetic resonance spectroscopy; PETG, glycol-modified polyethylene terephthalate; PFD, perfluorodecalin; pO_2, oxygen partial pressure; $R1$, spin-lattice relaxation rate.

Figure 6-8: Schematic illustrating the nature of a pO_2 estimate obtained via ^{19}F-MRS for a tissue-engineered (TE) islet graft and the factors that affect the estimate. The estimated obtained from the ^{19}F-MRS analysis represents the volume-averaged pO_2 in a TE graft, which is affected by the external (ambient) oxygen supply, the thickness of the media layer and scaffold, the amount of oxygen-consuming tissue in the graft, and the volume fraction of perfluorocarbon in the scaffold. *Abbreviations*: ^{19}F-MRS, fluorine magnetic resonance spectroscopy; pO_2, oxygen partial pressure; TE, tissue-engineered.

Figure 6-9: *R*1 and pO_2 results from supplementary experiment with human islets (S-H1). Estimates of pO_2 were performed using calibration lines 1 (*Figure 6-4*) and 2 (*Figure 6-5*), and the values are shown above each condition. Bars indicate mean values and error bars indicate standard error of the mean. *Abbreviations*: CL, calibration line; IE, islet equivalent; pO_2, oxygen partial pressure; *R*1, spin-lattice relaxation rate.

Figure 6-10: *R*1 and pO_2 results from supplementary experiment with human islets (S-H2). Estimates of pO_2 were performed using calibration lines 1 (*Figure 6-4*) and 2 (*Figure 6-5*), and the values are shown above each condition. Bars indicate mean values and error bars indicate standard error of the mean. *Abbreviations*: CL, calibration line; IE, islet equivalent; pO_2, oxygen partial pressure; *R*1, spin-lattice relaxation rate.

Figure 6-11: *R*1 and pO_2 results from supplementary experiment with human islets (S-H3). Estimates of pO_2 were performed using calibration lines 1 (*Figure 6-4*) and 2 (*Figure 6-5*), and the values are shown above each condition. Bars indicate mean values and error bars indicate standard error of the mean. *Abbreviations*: CL, calibration line; IE, islet equivalent; pO_2, oxygen partial pressure; *R*1, spin-lattice relaxation rate.

Figure 6-12: Light micrograph illustrating emulsified perfluorocarbon droplets within the scaffold material of an islet tissue-engineered graft. Note the relative homogeneous distribution of the droplets, but which vary in size (in the ~100s of microns).

Figure 6-13: Micro-CT reconstruction of a representative islet tissue-engineered graft. Note the unevenness of the surface of the graft and the non-uniform thickness (more thin near the center of the graft). Resolution is 36-μm.

Figure 6-14: Micro-CT images of a representative islet tissue-engineered graft. Note the non-uniform thickness (more thin near the center of the graft). Resolution is 36-μm. The hypointense regions appear to indicate material of less density, but it is unclear whether islets and/or perfluorocarbon droplets can be visualized.

Figure 6-15: *R*1 and pO_2 results from supplementary experiment with porcine islets (S-P1) before correction of IE counts with post-experimentation DNA content measurements. Estimates of pO_2 were performed using calibration lines 1 (*Figure 6-4*) and 2 (*Figure 6-5*), and the values are shown above each condition. The number of IEs per scaffold is the expected number of IEs as based on DNA counts performed several days prior to experimentation. Bars indicate mean values and error bars indicate standard error of the mean. *Abbreviations*: CL, calibration line; DNA, deoxyribonucleic acid; IE, islet equivalent; pO_2, oxygen partial pressure; *R*1, spin-lattice relaxation rate.

Figure 6-16: Photographs illustrating a tissue-engineered islet graft before (A) and after sonication (B), and after the graft material is collected for DNA quantification. *Abbreviation*: DNA, deoxyribonucleic acid.

Figure 6-17: *R*1 and pO_2 results from supplementary experiment with porcine islets (S-P1) after correction of IE counts with post-experimentation DNA content measurements. Estimates of pO_2 were performed using calibration lines 1 (*Figure 6-4*) and 2 (*Figure 6-5*),

and the values are shown above each condition. The number of IEs per scaffold is the expected number of IEs as based on DNA counts performed several days prior to experimentation. Bars indicate mean values and error bars indicate standard error of the mean. *Abbreviations*: CL, calibration line; DNA, deoxyribonucleic acid; IE, islet equivalent; pO_2, oxygen partial pressure; $R1$, spin-lattice relaxation rate.

Figure 6-1

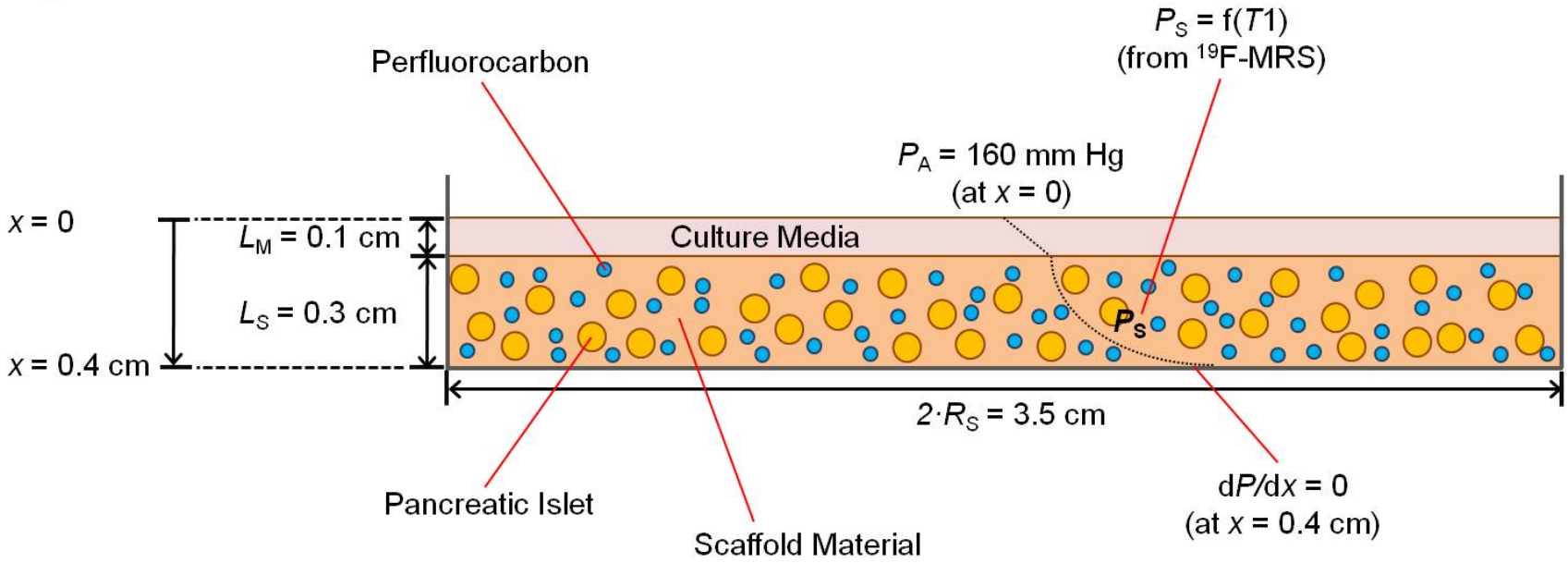
Perfluorocarbon
P_S = f($T1$)
(from ^{19}F-MRS)
P_A = 160 mm Hg
(at x = 0)
x = 0
L_M = 0.1 cm
Culture Media
L_S = 0.3 cm
P_S
x = 0.4 cm
$2 \cdot R_S$ = 3.5 cm
Pancreatic Islet
Scaffold Material
dP/dx = 0
(at x = 0.4 cm)

Figure 6-2

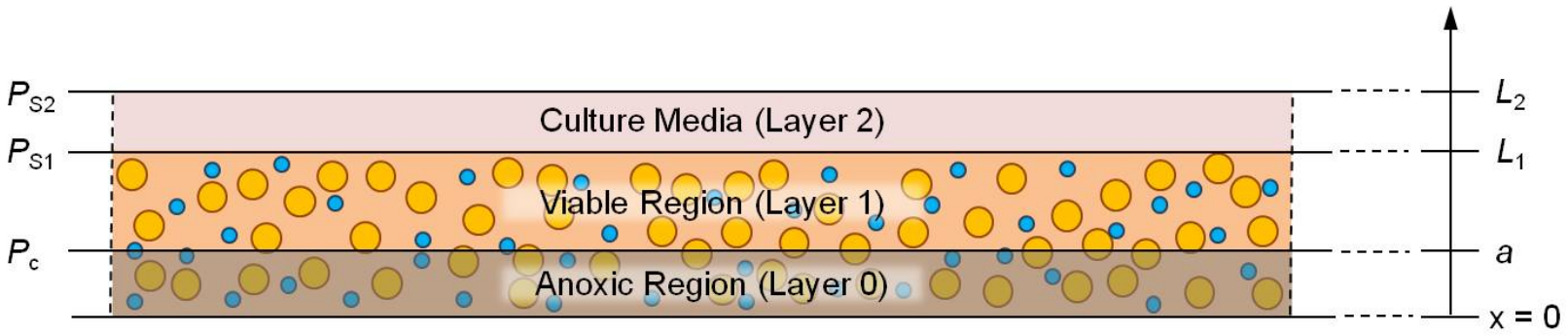
P_{S2}
P_{S1}
P_c
Culture Media (Layer 2)
Viable Region (Layer 1)
Anoxic Region (Layer 0)
L_2
L_1
a
x = 0

Figure 6-3: Characterization of PFC via ^{19}F-MRS and generation of *R*1 vs. pO_2 calibration line

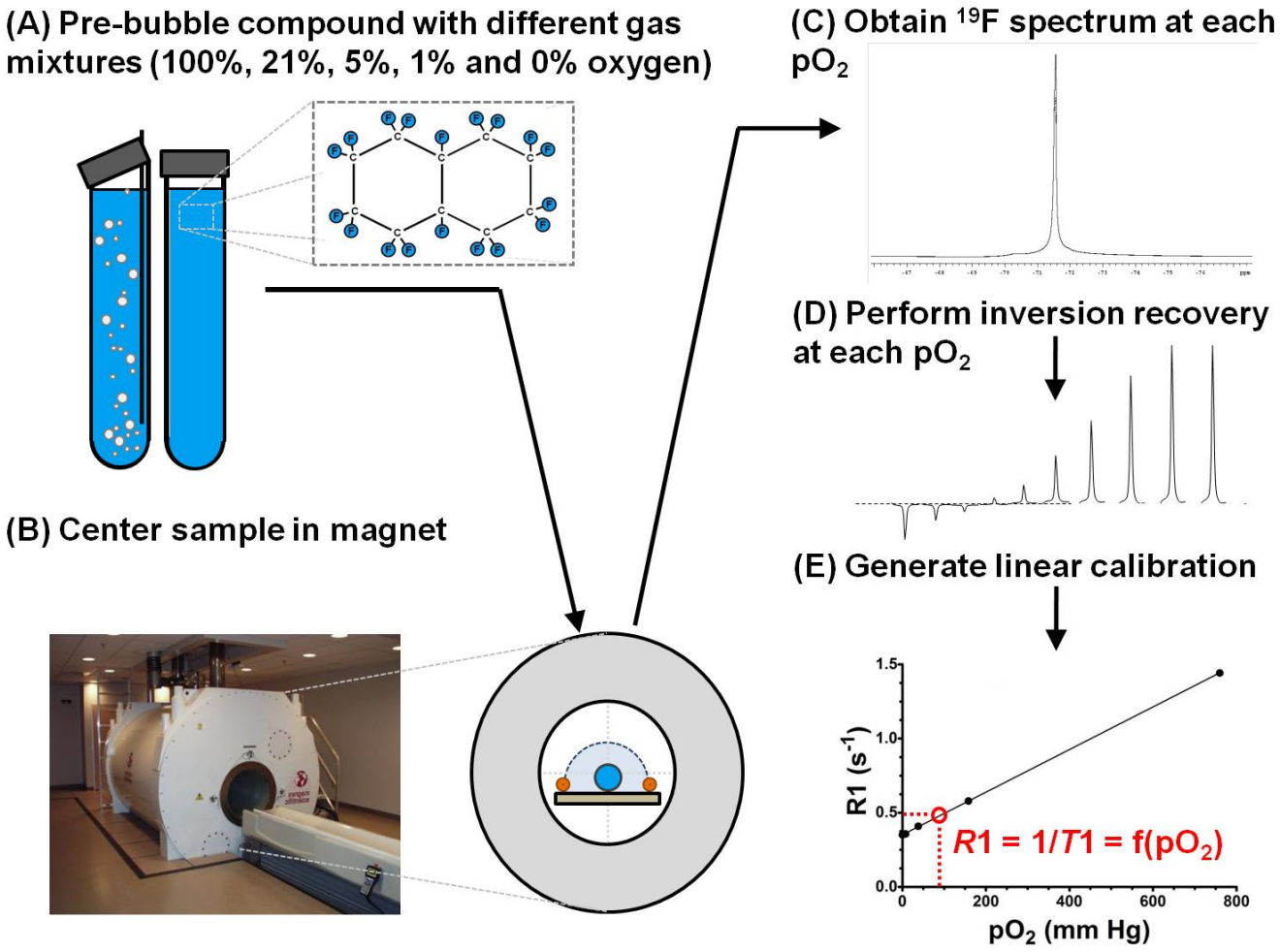

Figure 6-4: CL1 (PFD at 37°C and 5 T)

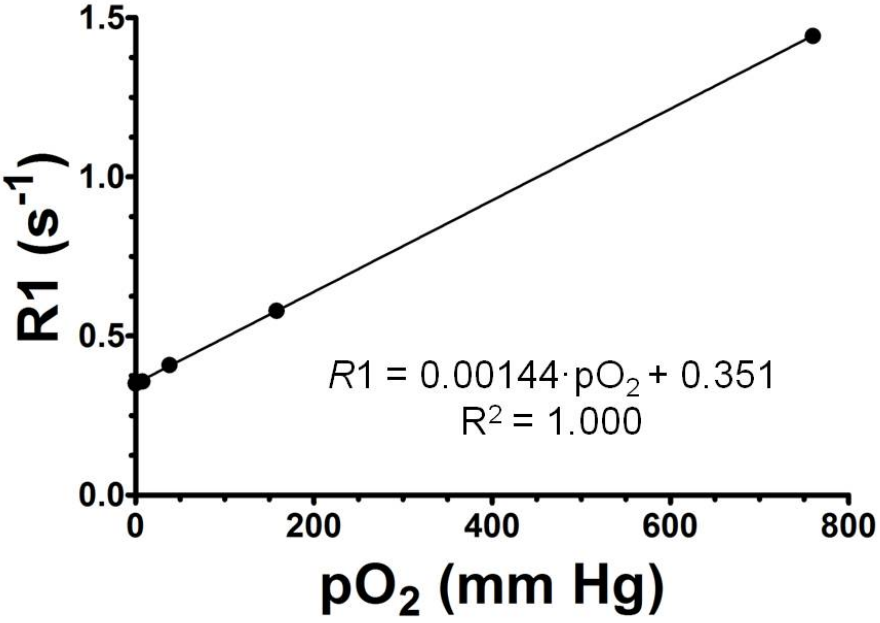

Figure 6-5: CL2 (PFD at 37°C and 5 T)

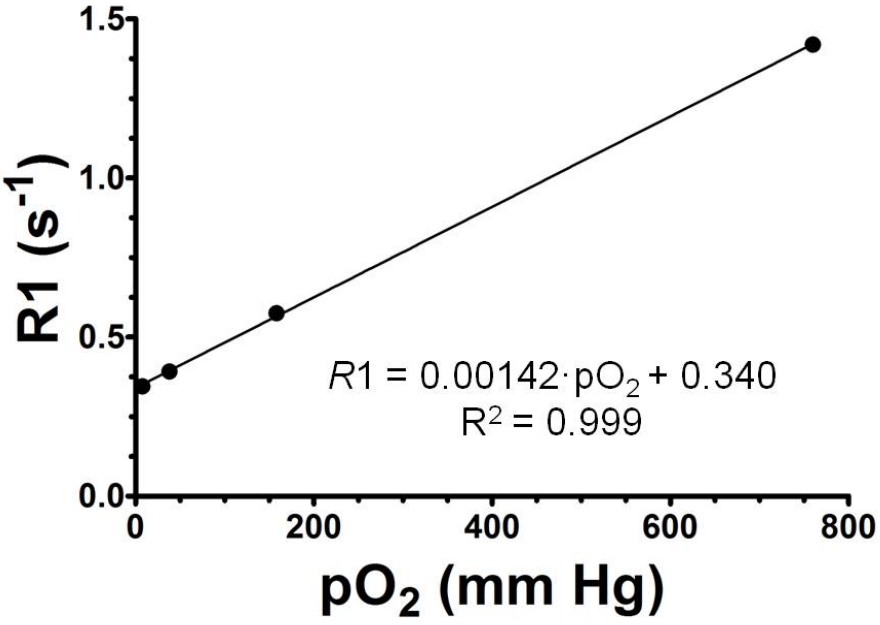

Figure 6-6: Volume-averaged pO_2 estimate via ^{19}F-MRS

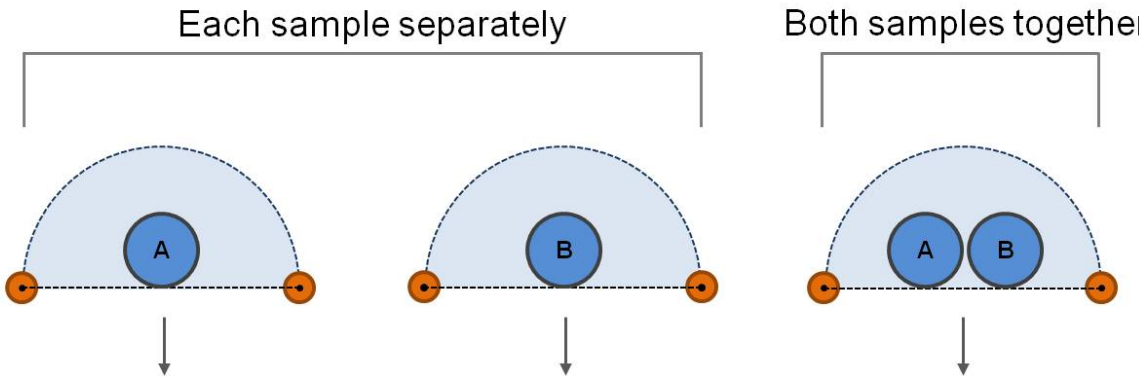

Expected pO_2:	158.2 mm Hg	0 mm Hg	79.0 mm Hg
Actual pO_2:	158.2 mm Hg	0 mm Hg	75.3 mm Hg

Figure 6-7: Gas-impermeability of PETG containers

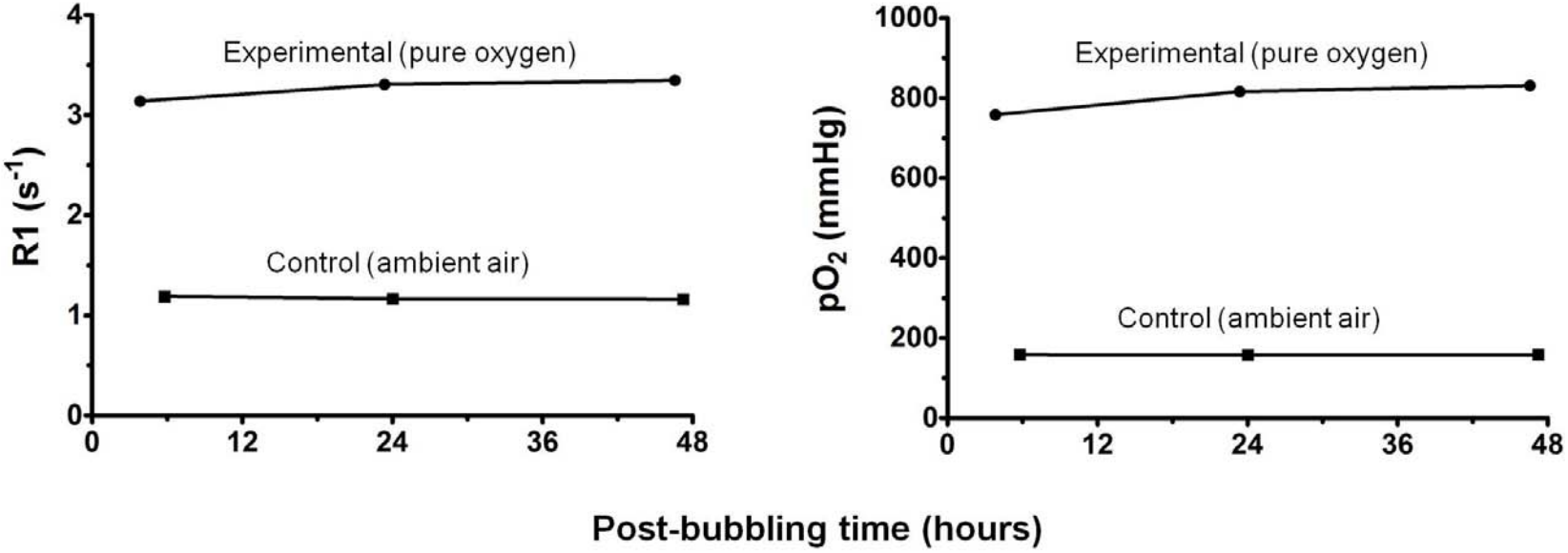

Figure 6-8: pO_2 estimate in TE islet graft via ^{19}F-MRS and theory

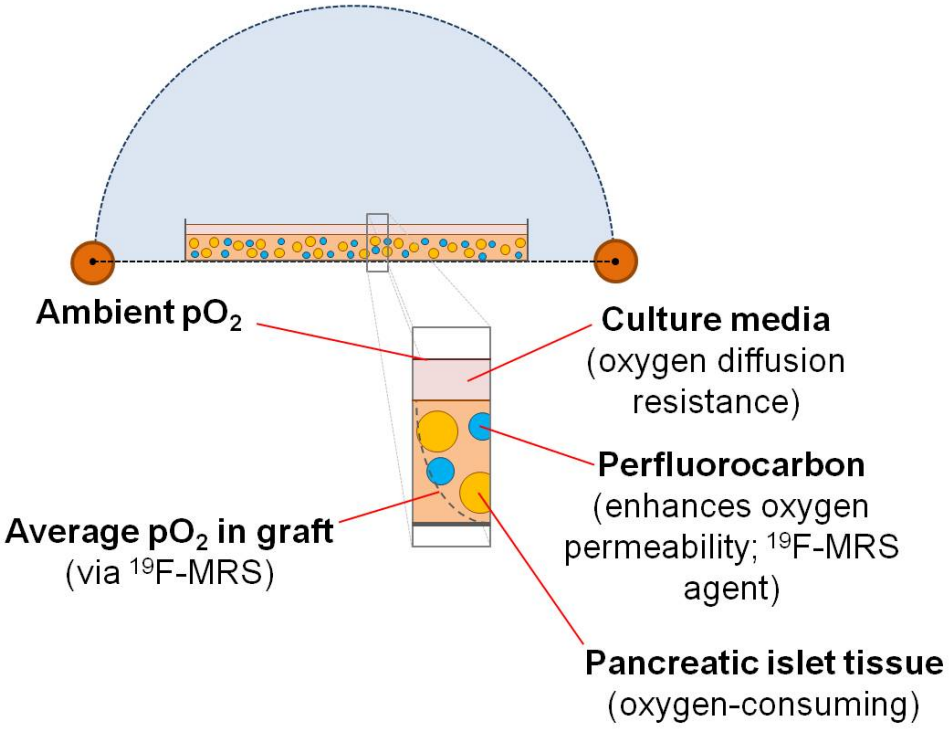

Figure 6-9: *R*1 and pO_2 results from supplementary experiment with human islet preparation (S-H1)

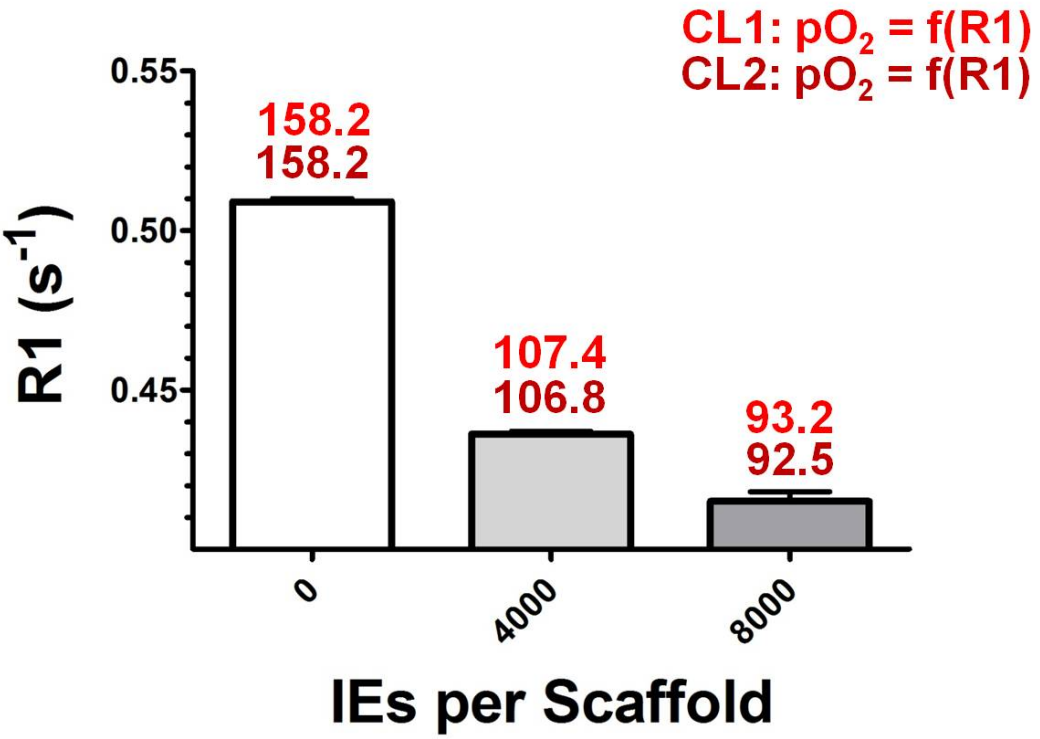

Figure 6-10: *R*1 and pO_2 results from supplementary experiment with human islet preparation (S-H2)

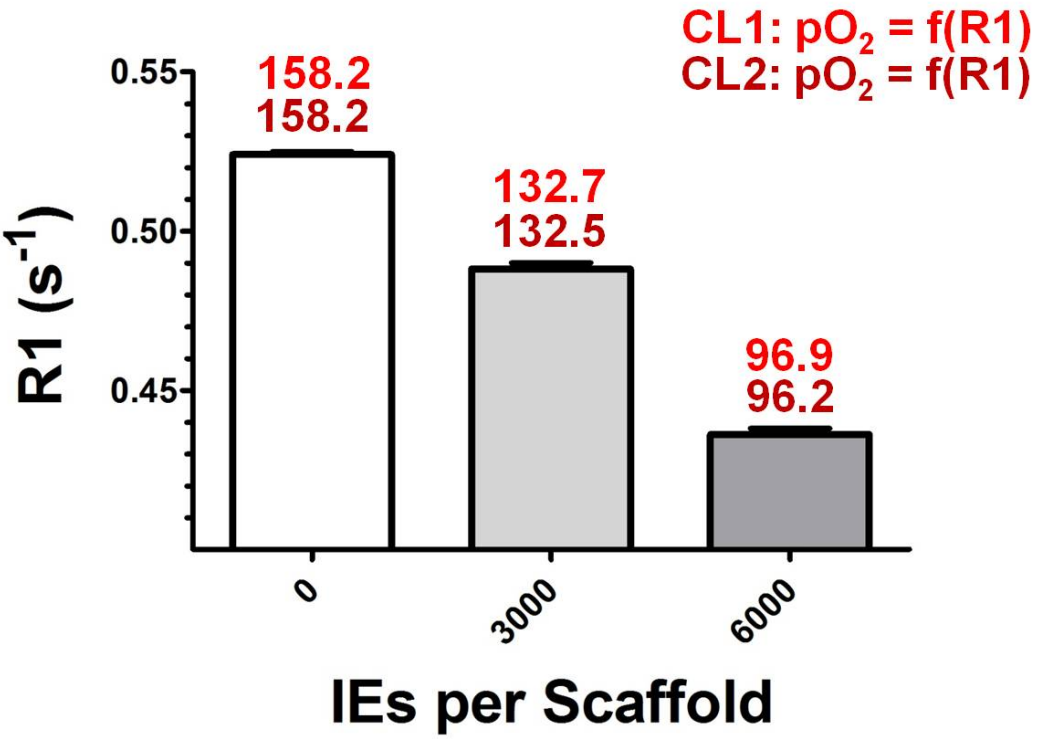

Figure 6-11: *R*1 and pO_2 results from supplementary experiment with human islet preparation (S-H3)

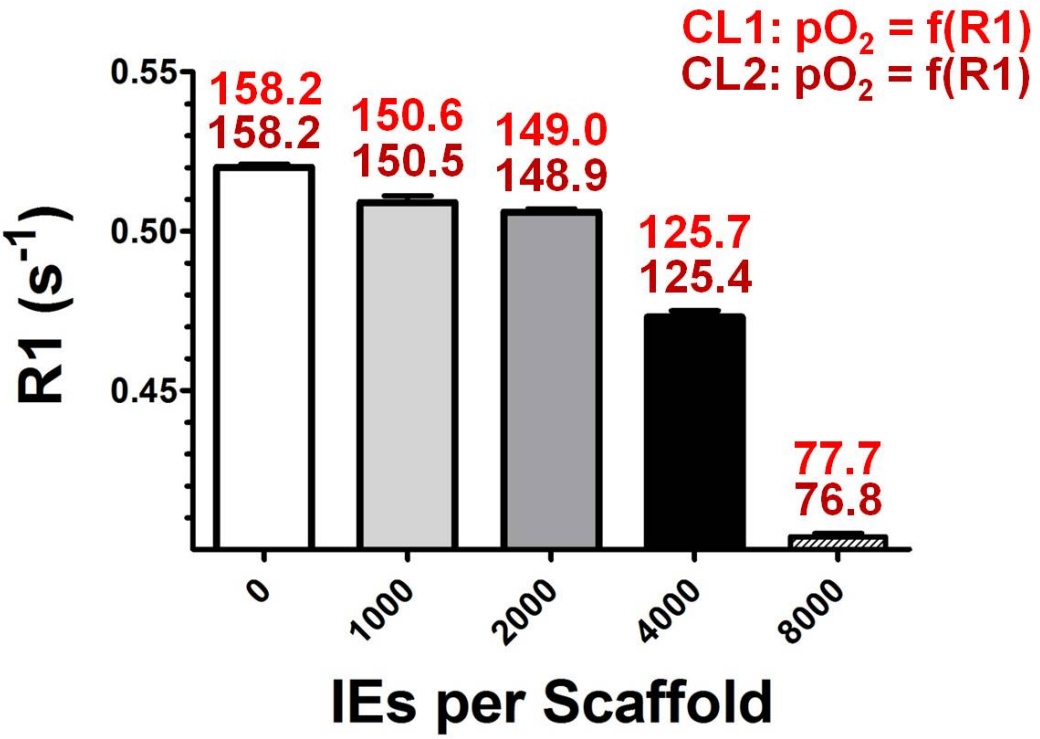

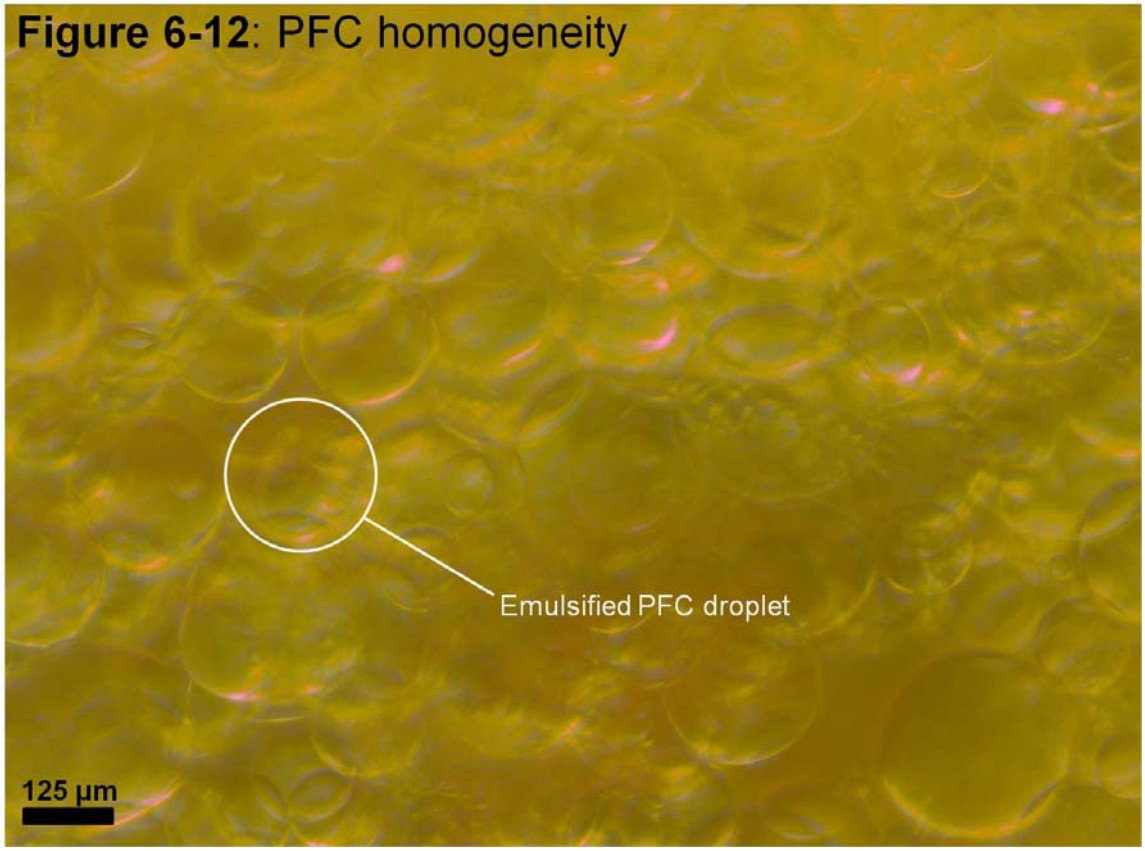
Figure 6-12: PFC homogeneity
Emulsified PFC droplet
125 µm

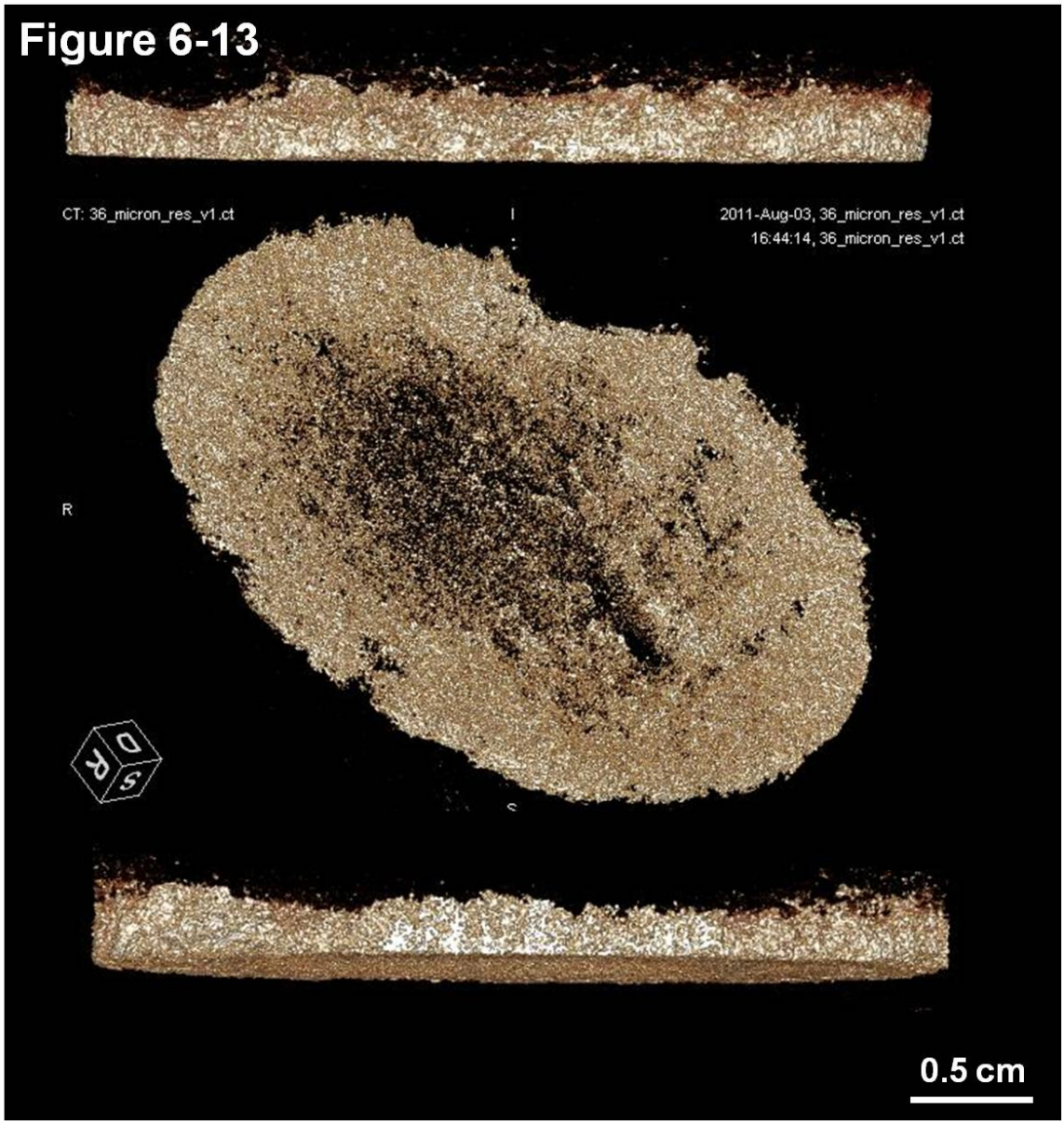
Figure 6-13
CT: 36_micron_res_v1.ct
2011-Aug-03, 36_micron_res_v1.ct
16:44:14, 36_micron_res_v1.ct
R
0.5 cm

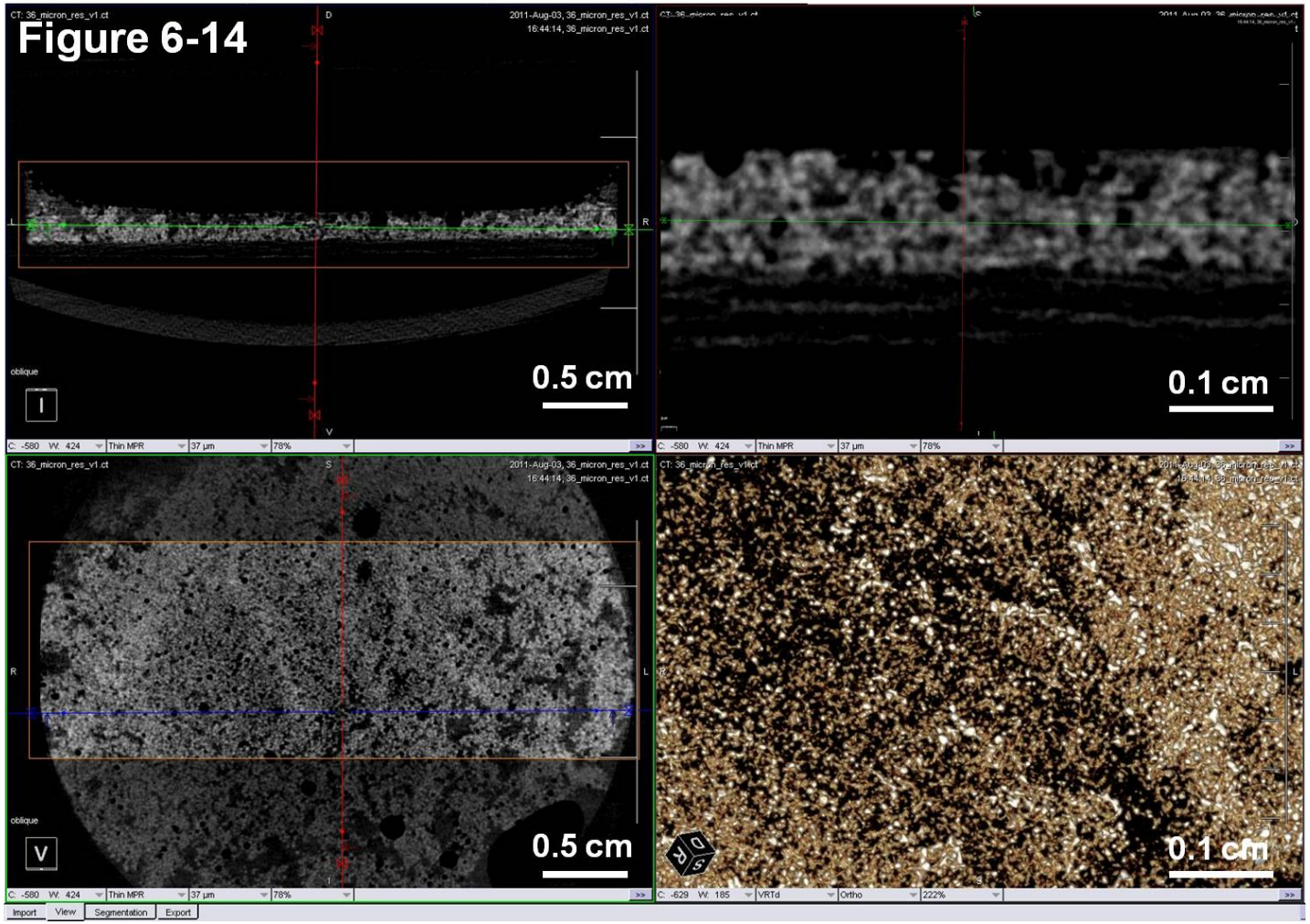
Figure 6-14
0.5 cm
0.1 cm
0.5 cm
0.1 cm
Import
View
Segmentation
Export

Figure 6-15: *R*1 and pO_2 results from supplementary experiment with human islet preparation (S-P1, Pre-DNA re-adjustment)

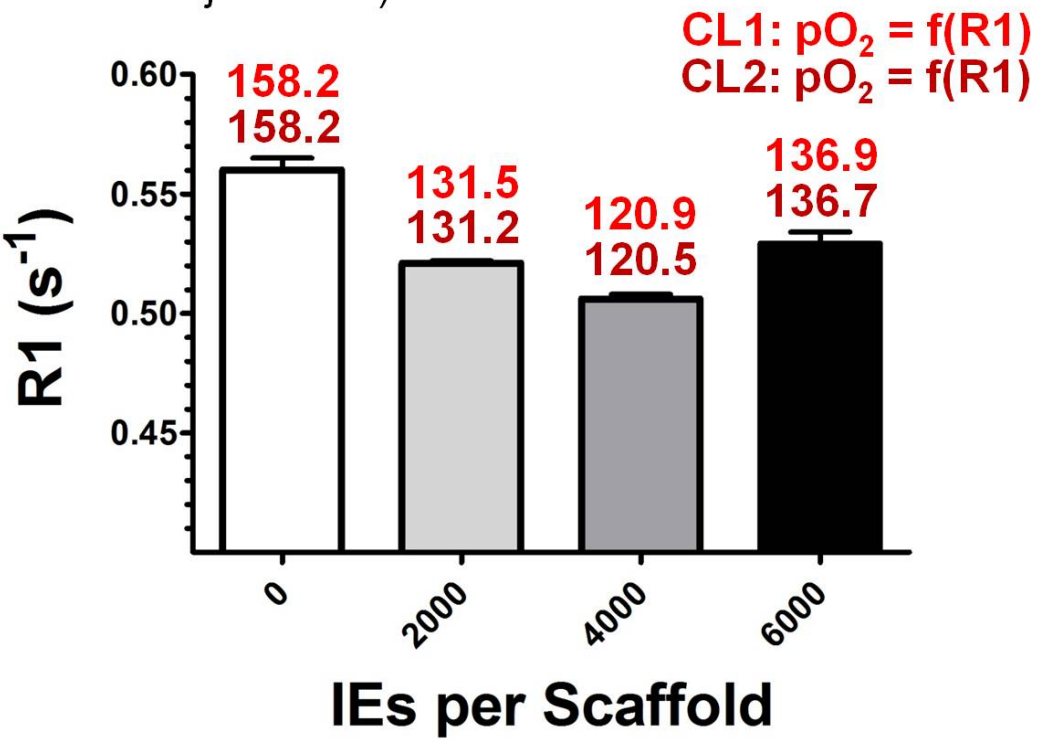

Figure 6-16: DNA collection protocol

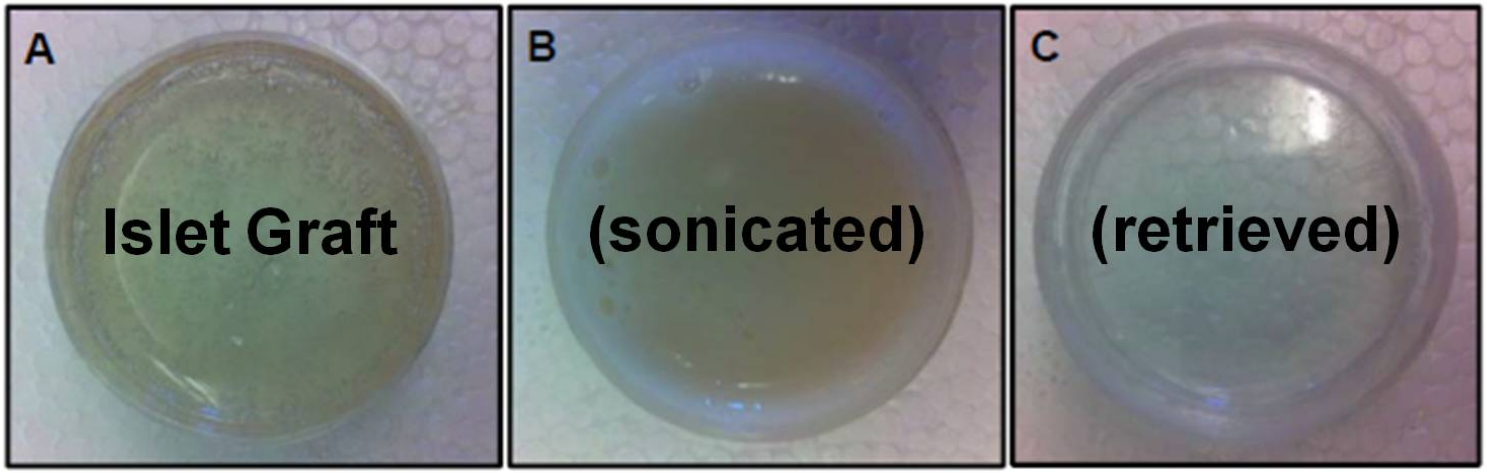

Figure 6-17: *R*1 and pO_2 results from supplementary experiment with human islet preparation (S-P1, Post-DNA re-adjustment)

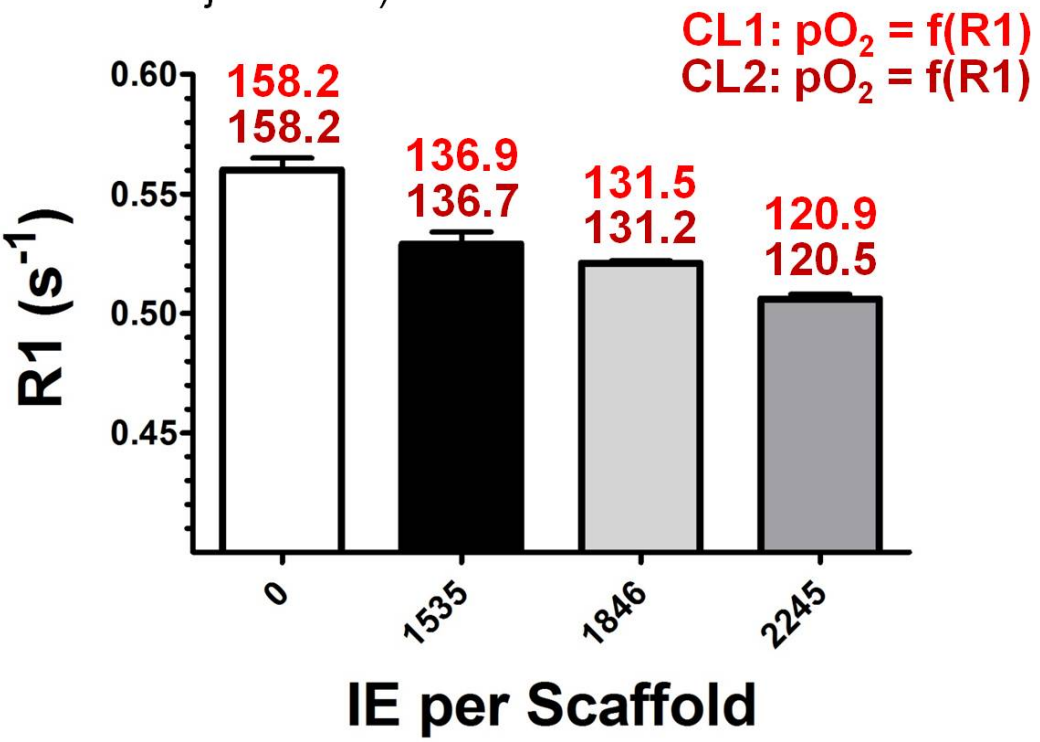

CHAPTER 7: Other Related Work

Summary

Work presented in this thesis has largely focused on the pancreatic islet product quality assessment, possible limitations of the current clinical islet transplant site (intrahepatic), and design, fabrication and assessment of tissue-engineered islet grafts or devices to be transplanted at alternative sites (extrahepatic). However, islet transplantation will only become more widely available if current islet product manufacturing and transplant is improved. Given the complexity of the approach, it is critically important to improve each step of the process that is involved, including pancreas procurement, preservation and assessment, and islet isolation, purification, culture, shipping, assessment and transplant. All of these areas may impact the quantity and quality of the islets retrieved from a pancreas, and the method and location of transplant will affect the clinical outcomes. Some this work is presented in this final chapter.

Abbreviations

ADP	adenine diphosphate
AMP	adenine monophosphate
A-PSF	anterograde persufflation
ATP	adenine triphosphate
AUC	area-under-the-curve
CPB	cardiopulmonary bypass
CPS	cold preservation solution
CT	celiac trunk
DCD	donation after cardiac death
GSIS	glucose-stimulated insulin secretion
HE	Hematoxylin and eosin
HMP	hypothermic machine perfusion
IE	islet equivalent
IT	islet transplantation
MP	microparticle
MS	magnetic separation
OCR	oxygen consumption rate
OCR/DNA	oxygen consumption rate normalized to DNA content
POD	post-operative day
PSF	persufflation
QMS	quadrupole magnetic sorting
R-PSF	retrograde PSF
SCS	static cold storage
SE	standard error

SMA	superior mesenteric artery
SOD	superoxide dismutase
TLM	two-layer method
UNOS	United Network for Organ Sharing
UW	University of Wisconsin solution
WIT	warm ischemia time

Persufflation (or Gaseous Oxygen Perfusion) as a Method of Organ Preservation

Suszynski T.M., Rizzari M.D., Scott III W.E., Tempelman L.A., Taylor M.J., Papas K.K. Persufflation (or gaseous oxygen perfusion) as a method of organ preservation. Transplant Proc. 43(9): 3221-3225 (2011)

Permission to reproduce the above publication was given by *Elsevier*, and the agreement (license number: 2924380328935) is found in Appendix 7-1.

Abstract

Improved preservation techniques have the potential to improve transplant outcomes by better maintaining donor organ quality and by making more organs available for allotransplantation. Persufflation, (PSF, gaseous oxygen perfusion) is potentially one such technique that has been studied for over a century in a variety of tissues, but has yet to gain wide acceptance for a number of reasons. A principal barrier is the perception that *ex vivo* PSF will cause *in vivo* embolization post-transplant. This review summarizes the extensive published work on heart, liver, kidney, small intestine and pancreas PSF, discusses the differences between anterograde and retrograde PSF and between PSF, and other conventional methods of organ preservation (static cold storage, hypothermic machine perfusion). Prospective implications of PSF within the broader field of organ transplantation and in the specific application with pancreatic islet isolation and transplant are also discussed. Finally, key issues that need to be addressed before PSF becomes a more widely utilized preservation strategy are summarized and discussed.

Introduction

The advancement of allotransplantation over the past half century has stimulated the development of techniques for whole organ preservation, especially in the face of common logistical challenges inherent in the delivery of the therapy (such as the need for transportation and coordination of operating times). In addition to preserving the function and viability of cadaveric organs accepted via standard criteria, improved organ preservation has the potential to increase the fraction of marginal organs used for transplant [391; 392]. It is generally believed that improved preservation techniques should contribute to improved maintenance of organ quality, minimize ischemia-reperfusion injury and result in more successful transplant outcomes with the consequence that substantial research effort has focused on optimizing organ preservation protocols.

A key area of research interest lies in the optimization of oxygen delivery during hypothermic preservation. It has been shown that conventional static cold storage (SCS) techniques may not provide sufficient oxygen to the core of a larger organ [392; 393], and only oxygenate to a maximum depth of a millimeter from the surface [394]. Efforts to improve the oxygen solubility of cold preservation solutions by using perfluorocarbons have proven largely ineffective, because these methods still rely on oxygen delivery by passive diffusion from the surface [395]. Even hypothermic machine perfusion (HMP), which has been designed to deliver cold preservation solution into the organ via the native vasculature, may deliver inadequate oxygen to an organ during preservation, particularly when the perfusate is not saturated with oxygen at a higher than atmospheric pO_2 [61; 396; 397]. It is in this regard that persufflation (PSF), or gaseous oxygen perfusion, may provide additional advantages as compared to either SCS or HMP (see

Table 7-1 for more detailed comparison of the advantages and disadvantages between SCS, HMP and PSF). PSF is not a new concept but can be considered an emerging technique for current-day organ preservation and deserves considerable attention for a variety of compelling reasons, including the unique capability to deliver oxygen gas or gas mixture directly into an organ by using the native vasculature. When compared with SCS and HMP, PSF may represent the best opportunity to fully oxygenate an entire, human-sized organ. This review details the historical development of PSF with heart, kidney, liver, small intestine and pancreas and discusses the differences between the two main approaches for PSF (anterograde versus retrograde). We also discuss the future research landscape for PSF in relation to established methods of preservation and describe some of the important issues that need to be addressed before the technique becomes more widely accepted.

Early History with Persufflation

PSF was first discovered in 1902 by Rudolf Magnus, when he made an unexpected observation while perfusing an isolated cat heart with defibrinated blood [398]. The reservoir storing liquid perfusate emptied inadvertently and was not re-filled immediately. Since compressed oxygen gas was used to pressurize the reservoir, the gas was pulled into the perfusion circuit and into the heart. Magnus observed that the heart continued to contract rhythmically for nine minutes during PSF. This initial observation prompted the initiation of a series of more extensive studies designed to elucidate the utility of PSF in preserving cardiac function. Magnus illustrated that it was possible to maintain a beating heart in bradycardia during 69 minutes of PSF and that reperfusion of blood through the coronaries restored a normal heart rate (80 bpm). Interestingly, Magnus persufflated the cat heart with gaseous hydrogen and showed that it still beat at 20 minutes of treatment.

Furthermore, he tried coronary persufflation with gaseous carbon dioxide and was able to demonstrate, unlike either oxygen or hydrogen gas, that the heart stops after just minutes. Even though Magnus' findings were intriguing at the time, it was not until the mid-1950s that the significance of his studies was appreciated.

With the advent of clinical transplant on the near horizon [399; 400], a group at McGill University in Montreal discovered in 1954 that PSF could preserve spinal reflexes in frogs and active cardiac and skeletal muscle contractions in rabbits [401; 402]. Their first paper highlighted the benefits of PSF versus liquid perfusion in a frog spinal reflex model [401]. The authors showed that peripheral nerve reflexes and muscle contractions were preserved for up to 6-8 hours when the gaseous oxygen was delivered into the systemic circulation. This paper described the significant benefit of PSF over liquid perfusion, citing the lack of edema formation and improved oxygenation. The authors even replaced oxygen gas with nitrogen gas to illustrate how anoxia eliminated these reflex activities. In a related, follow-up study the same group showed that a rabbit heart and skeletal muscle (tibialis anterior muscle) could be preserved with minimal depreciation of function during about 3 hours of PSF [402].

These early reports establishing the potential virtues of PSF for improved organ preservation set the scene for exploration in a variety of tissues and organs.

Whole Organ Persufflation

Heart

Although the earliest studies of PSF were focused on the heart, research in heart PSF had subsided for about three decades (1960s-1990s) in favor of research in liver and

kidney PSF. More recently, cardiac PSF has been rekindled and several studies have been published in which PSF was used prior to transplant, including the use of PSF to preserve hearts having suffered short periods of warm ischemia. Collectively, these studies have at least established that cardiac PSF is technically possible and that it can preserve heart tissue.

The advent of cardiopulmonary bypass (CPB) in the mid-1950s provided impetus for exploring the use of PSF. In 1959, Sabiston *et al*. at Johns Hopkins explored the use of PSF in conjunction with CPB [403]. In the first set of experiments, hearts from medium-sized dogs were cannulated at the coronary ostia, flushed with pre-oxygenated normal saline, then persufflated with humidified gaseous carbogen (a mixture of 95% O_2 and 5% CO_2). This approach, generally termed anterograde PSF (A-PSF), contrasts with retrograde PSF (R-PSF) which would be tried in the heart [404; 405] and subsequently in the kidney [406; 407]. Hearts maintained at 37°C continued to beat for an average duration of 5.1 hours (2.5-8 hours, range). Cardiac contractility remained strong for the first 2-3 hours and then gradually weakened. In some cases, the electrical activity of the heart continued for periods up to 4 hours following cessation of a visible heartbeat. The second set of experiments examined *in situ* A-PSF of the heart. Once the heart had been isolated from the systemic circulation, A-PSF was performed for 25-30 minutes. A normal hemodynamic response was restored in 9 of 12 animals and some animals maintained a heartbeat for 48 hours following the reestablishment of native coronary circulation. This study established the use of PSF in cardiac surgery by showing that oxygen gas can be used by the heart and that coronary blood flow may be reestablished after PSF. In 1960, a follow-up study introduced the concept of R-PSF [405]. At the time, retrograde perfusion of oxygenated blood via the coronary sinus was used to maintain a

heartbeat and protect the heart from anoxia for short periods of time during open aortic valve procedures [408; 409]. Talbert *et al*. used this knowledge, along with their previous work on A-PSF, to investigate whether R-PSF could be performed successfully in the heart. In their experiments, the coronary sinus was cannulated in 7 canine hearts, flushed with normal saline and started on R-PSF. These organs maintained a beat for an average duration of 3.5 hours (2-4 hours, range). In 3 separate hearts, the anterior cardiac veins were additionally cannulated and persufflated. These organs maintained a visible beat for an average duration of 5.5 hours and up to 7 hours. They noted that cardiac activity remained strong over the first 2 hours of experimental conditions and then gradually became weaker until ventricular fibrillation or complete asystole had occurred. Talbert compared the R-PSF with A-PSF and determined that the heartbeat was visibly weaker and sustained for a shorter period of time using the retrograde approach. Nevertheless, they concluded that oxygen gas can be delivered retrogradely and that the method exhibits some efficacy.

In 1966, the Talbert *et a*l. concept of R-PSF was applied by Camishion *et al*. [404]. They noted that continuous blood perfusion during open aortic valve procedures was cumbersome due to the obstruction of the surgical field caused by cannulation of the coronary vessels from within the aorta. Consequently, they tried to determine whether animals could survive CPB by using R-PSF of the coronary sinus as the main preservation technique. This was investigated by repeating previous work by Talbert *et al*. on *in situ* R-PSF using a similar canine model [405]. They reported that each of 10 canine hearts maintained a sinus rhythm for at least 31 minutes while being retrogradely persufflated. Following the loss of a sinus rhythm, 8 animals maintained a nodal or ventricular rhythm for up to 7 hours and 2 animals developed and sustained ventricular

fibrillation for up to 6 hours. When hearts were persufflated with nitrogen gas, sinus rhythm was maintained for 5 minutes or less and a visible beat was lost in all 10 animals within an average duration of 11 minutes and no longer than 25 minutes. When persufflation was switched to oxygen gas, a 30-fold increase in the tissue partial oxygen tension of the hearts was observed almost immediately. In 2 animals, asystole was converted to a persistent ventricular rhythm. In a second experimental study, the coronary sinus in 20 porcine and 10 canine hearts were cannulated and animals were placed on CPB using R-PSF for 1 hour. During CPB, 25 of 30 animals maintained sinus rhythm for the entire hour. Of the remaining 5 animals, all developed ventricular fibrillation after an average of 30 minutes and one spontaneously reverted to a nodal rhythm after 20 minutes of sustained ventricular fibrillation. Following removal of CPB, 22 of 30 animals remained in sinus rhythm. Four animals with ventricular fibrillation were converted electrically to sinus rhythm, 3 animals developed fibrillation after reperfusion, all of which could be converted electrically to sinus rhythm. The remaining animal exhibiting nodal rhythm converted to normal sinus rhythm spontaneously following cessation of CPB. After re-establishment of native coronary blood flow, mean aortic blood pressure was maintained between 60-120 mm Hg and central venous pressures remained 4.4-14.7 mm Hg in all animals. Of the 30 experimental animals in the second group, only one exhibited signs of heart failure postoperatively. This animal developed severe pulmonary edema following transfusion of 2500 mL of blood for ongoing hemorrhage. From the vantage point of a contemporary understanding of shock and transfusion medicine, it is conceivable that this animal may have developed a variant of acute respiratory distress syndrome or transfusion-related acute lung injury, which may have been misinterpreted as pulmonary edema from congestive heart failure – though the true pathology will never be known. Nevertheless, these studies illustrated that a

heart could be preserved by PSF during CPB and that these organs recovered their function following reperfusion. No evidence of air embolization was found in the brain or viscera of any experimental animal. The authors commented on the fundamental difference between gas embolization and PSF; gas emboli are small bubbles that may occlude smaller vessels, whereas PSF is characterized by the free flow of a gas within the system. This distinction is still not fully appreciated by the clinical community and services to highlight that this will need to continue to be proven experimentally. Camishion *et al*. also raised the possibility of using this preservation technique for the maintenance of donor hearts in cardiac transplant, even before the first successful heart transplant was performed in South Africa a few years later [410].

Also in 1966, Gabel *et al*. examined the physiology of the persufflated heart by using juvenile feline hearts that were anterogradely persufflated with gaseous carbogen mixture (95% O_2, 5% CO_2) via cannulae secured in the proximal aorta and compared with controls perfused with substrate-free Krebs solution [411]. They found that the heart rate in persufflated hearts declined rapidly over the first hour and then declined more slowly over the next 9 hours, whereas the heart rate in the liquid-perfused heart exhibited a steady decline over the entire experimental period. Contractility measurements under A-PSF showed an initial rise in contractile force during the first 20 minutes and subsequent fall after 4 hours. The persufflated hearts reached 50% of the initial contractile force after 7 hours, whereas liquid-perfused hearts declined to 50% of initial contractile force in only 80 minutes. Metabolic studies revealed that glycogen, carbohydrate, lactate, and pyruvate levels decreased rapidly in the persufflated heart, but when these hearts were treated with pharmacologic agents they responded as expected. In addition, they found that rhythm changes in the A-PSF model reproducibly

occurred above a certain threshold PSF pressure. Gabel *et al*. concluded that persufflated hearts exhibited stronger contractile forces, performed more work and were slower to fail than the hearts perfused with liquid. They theorized that oxygen gas allowed an increase in cardiac work, even though oxygen supply is not traditionally considered a major determinant of work capacity. It may be that cardiac oxygen extraction is altered when oxygen is delivered by PSF or that simply more oxygen is delivered using PSF. Another hypothesis emerging from these findings was that, in the case of PSF, active metabolites equilibrate solely between the extracellular fluid and the intracellular space, as opposed to being flushed away by a liquid perfusate.

Lochner *et al*. subsequently studied the metabolism and function of anterogradely persufflated guinea pig and rat hearts [412]. Hearts were persufflated with carbogen gas mixture (95% O_2, 5% CO_2) at 37°C for 1 hour. With persufflated hearts, the peak systolic pressures and the first derivative of the left ventricular systolic pressure decreased, while exhibiting very little change in the heart rate. This seemed to indicate that the persufflated heart could continue to generate hemodynamic work. In a few of the hearts, A-PSF time was extended to 2 hours, resulting in no additional decreases in heart rate, left ventricular systolic pressure and its first temporal derivative, or isovolumetric work. Isovolumetric work and the first derivative of left ventricular systolic pressure following PSF were calculated to be 16.4% and 18.4% of values characteristic for liquid-perfused hearts, respectively. Measurements of tissue creatine phosphate and ATP were similar between the PSF and liquid perfusion groups. This led the authors to suggest that the decrease in cardiac work was likely not due to a lack of available cellular energy. They also discovered that work capacity could be enhanced by increasing the PSF pressure or the diastolic filling pressure.

Following these early studies, there was a gap of several decades during which no work was published on the gaseous perfusion of hearts. It was not until the late 1990s that interest in cardiac PSF rekindled, largely as a result of the successful application of PSF in other organs, in particular the kidney and liver. What had been previously referred to as ‘gaseous oxygen perfusion’ was eventually termed ‘persufflation’ by Denecke [413]. After pursuing extensive work in kidneys and livers, Fischer’s group in Cologne explored cold preservation via cardiac PSF in 1998 [414]. Porcine hearts were flushed and stored at 0-1°C using three different methods: (1) SCS using modified Euro-flush solution with glutathione (based on Euro-Collins solution); (2) SCS with University of Wisconsin (UW) solution ; and (3) A-PSF via the ascending aorta in combination with SCS using Histidine-Tryptophan-Ketoglutarate solution modified by adding hyaluronidase. The overall mean preservation time was 14.5 hours. Hearts were orthotopically transplanted into recipient pigs of comparable body weight using standard CPB, reperfused on CPB using whole blood for an average of 154 minutes before being weaned off CPB to allow the hearts to take over normal circulation. Following transplantation, hemodynamic parameters were measured to estimate cardiac function and serum creatine kinase values were obtained as an indicator of myocardial damage. Prior to sacrificing the porcine recipient, left ventricular biopsies were performed to estimate myocardial water content and ATP levels. Persufflated hearts exhibited stroke work similar to preoperative values, whereas comparable measurements could not be obtained in static cold-stored organs due to severe arrhythmia and ventricular dyskinesia. Measurements of cardiac output, left ventricular systolic pressure and its first temporal derivative revealed that the persufflated hearts fared significantly better than hearts stored in modified Euro-flush solution alone and had better cardiac output than hearts stored in UW solution alone.

Equivalent creatine kinase levels between each group indicated that the degree of cellular damage using A-PSF may have been similar to conventional SCS. However, persufflated hearts exhibited significantly higher ATP levels than UW/Euro-flush solution-stored hearts. Collectively, these data seem to indicate that A-PSF may permit superior recovery of post-transplant heart function compared with SCS using either UW or modified Euro-flush solution. Importantly, myocardial water content measurements indicated that there was significantly less myocardial edema with A-PSF than static UW solution alone. Decreased myocardial edema is a distinct benefit of PSF, as it is known that tissue edema can significantly impair cardiac function [415]. A follow-up study examined the effects of A-PSF on myocardial tissue quality and post-transplant cardiac function by comparing against SCS in Histidine-Tryptophan-Ketoglutarate solution with and without hyaluronidase [416]. The cohort of hearts preserved by coronary A-PSF showed significantly higher left ventricular systolic pressure and its first temporal derivative, and cardiac output compared to hearts preserved by SCS with Histidine-Tryptophan-Ketoglutarate solution, but not when modified with hyaluronidase. Persufflated hearts maintained normal circulatory function for longer when compared to either SCS methodology. Additionally, tissue ATP levels were significantly higher in transplanted hearts following A-PSF than after SCS only. Post-transplant myocardial water content was not elevated in persufflated hearts over controls.

Up to this point, most of the research into cardiac PSF had thus far involved experimental operations with hearts experiencing no “down-time” or conventional warm ischemia as experienced with donation after cardiac death (DCD). The opportunity to resuscitate DCD hearts inspired the Cologne group to study PSF following warm ischemic damage. Thus, Yotsumoto *et al*. studied the effects of several hypothermic

preservation techniques on post-transplant cardiac function following a mean warm ischemia time (WIT) of 16.7 minutes in a porcine autotransplant model [417]. Three hours of A-PSF was compared with SCS, with an additional set of controls not damaged by warm ischemia and also stored in Histidine-Tryptophan-Ketoglutarate solution modified with hyaluronidase. As with previous studies examining the effects of preservation on heart function, a number of physiologic parameters were recorded and samples were taken to assess the metabolic recovery of the cardiac tissue. It was reported that control and persufflated hearts were completely weaned from CPB within 2 hours of transplantation, whereas the static cold-stored hearts exhibited significantly diminished functional recovery. Near the end of the 3-hour reperfusion period – cardiac output, left ventricular contractility, and the relaxation velocity were significantly higher in the A-PSF group as compared to SCS. It appeared that persufflated DCD hearts had functional outcomes similar to hearts procured from heart-beating donors using conventional storage methods. Importantly, Troponin T levels were significantly higher under SCS than for undamaged controls and hearts preserved by A-PSF at 1 hour after reperfusion. These data indicate that A-PSF may limit myocardial injury incurred during WIT. The authors noted that the transplant field is reluctant to adopt PSF as a legitimate cardiac preservation technique largely due to concerns about resulting endothelial damage. More recent studies have shown that the coronary arteries of porcine hearts following 3 hours of oxygen A-PSF had normal functioning endothelium post-transplant [418; 419; 420]. Additionally, hearts transplanted following 14 hours of A-PSF exhibited no topographic signs of endothelial damage, as assessed by scanning electron microscopy [420]. Fischer has recently reviewed work done by his group, and has described the detailed experimental approach in which A-PSF is recommended as the preferred method [421]. Collectively, these works have shown that cardiac PSF has

considerable potential as an emerging preservation technique, and **Table 7-2** summarizes the published work on heart PSF presented in this review.

Kidney

The initial studies with kidney PSF occurred in the 1960s, shortly after the early development of heart PSF. It was in the kidney that PSF has been most extensively evaluated, likely because the vascular anatomy and associated transplant models are considered to be most straightforward (amongst the major transplantable organs). Following an initial study by Talbert *et al*. at Johns Hopkins in the 1960s [422], most all work on kidney PSF was performed by Fischer, Isselhard and others in Cologne, Germany. Early research efforts were comprehensive in developing the technical aspects of PSF (including optimization of flow pressures, oxygen partial pressures, temperature, and type of approach – whether anterograde or retrograde – used during kidney PSF) by evaluating their effects on the bioenergetic status and function post-reperfusion. The groundwork produced by the researchers in Cologne stimulated interest in the field and by the 1980s a number of other institutions had initiated studies to explore the value of kidney PSF.

The initial study by Talbert *et al*. involved *in situ* PSF of 7 canine kidneys [422] and showed that A-PSF with gaseous carbogen mixture (95% O_2 and 5% CO_2) could be used to preserve kidney function for 4 hours. A-PSF was performed by feeding a catheter through the left iliac artery and positioning it at the renal artery. Once the catheter was appropriately positioned and the proximal renal artery around the catheter was sealed, the left renal vein was clamped distally and the left gonadal vein was divided and used for drainage. Once the blood was flushed using normal saline, A-PSF

was started at a pressure of 120-150 mm Hg (to expel the liquid perfusate) and gradually decreased to 80-100 mm Hg. The left kidney was persufflated for 2-4 hours, flushed with normal saline until no visual evidence of gas appeared in the venous effluent and then renal blood flow was re-established. This was performed by pulling back on the renal arterial catheter, removing the renal venous clamp and ligating the proximal stump of the left gonadal vein. The animals were then monitored for up to a year. The study included two sets of controls. In the first set, 4 dogs had the left renal artery isolated and clamped for 2 hours, while in the second set of controls the left renal artery was cannulated, flushed and the renal circulation was re-established after 2 hours of warm ischemia. Compared to controls, persufflated kidneys functioned for some time after the treatment. Renal function was determined primarily through intravenous pyelography and also by assessing left kidney function following contralateral nephrectomy. Furthermore, histologically, most of the persufflated kidneys exhibited some signs of tubular atrophy and scarring, but these findings were considered minimal in comparison with ischemic controls. The authors concluded that PSF has the potential to prevent the harmful consequences of warm ischemia and that the afforded protective effects are likely a result of tissue being able to utilize and survive by consumption of gaseous oxygen. They noted that simply clearing the renal vasculature of blood (to prevent coagulation during the ischemic period) was not enough to preserve organ function. These findings are highly significant in that PSF kept kidneys alive during 2 hours of WIT.

It would be 10 years before these encouraging observations reported by Talbert *et al*. were pursued further by others. In 1971, Denecke developed an *in situ* canine renal ischemia model [413], similar to the one developed by Talbert *et al*. [422]. This study involved comparison between hypothermic A-PSF at 100 mm Hg and SCS. Kidneys

undergoing either treatment were initially flushed clear of blood by perfusion with an unspecified crystalloid solution. Following 4 hours of A-PSF or SCS, contralateral nephrectomy was performed and circulation to the remaining experimental kidney was re-established. It was reported that A-PSF was actually more harmful to the kidneys than SCS alone; 4 of 5 dogs had died within 7 days, while the remaining dog survived but exhibited marked uremia. Of the 3 dogs having their kidneys preserved by SCS, all survived. Additionally, it was determined that persufflated kidneys had difficulty maintaining normal blood flow following the treatment, with perfusion having decreased to roughly one-third of normal. Moreover, despite an increase in tissue levels of ATP during A-PSF, the ATP levels quickly diminished following reperfusion. The authors postulated that as a result of enhanced oxygenation, the renal vasculature had responded reflexively by increasing the resistance to flow, thereby decreasing global reperfusion of the kidney. As far as we are aware, further evidence has not been provided to substantiate this claim. In our opinion, the physiological response invoked to explain these observations does not seem tenable under hypothermic conditions. It is more likely that the decrease in perfusion may have been related to vascular damage caused by hyperoxia and elevated PSF pressures. On a historical note, this was the first time that the term 'persufflation' was substituted for gaseous oxygen perfusion.

Follow-up studies resulting from this original report are important for addressing the largely unexpected outcome that A-PSF had a distinctly detrimental outcome as compared with R-PSF. Isselhard and his collaborators spearheaded a series of studies that examined the differences between A-PSF and R-PSF [406; 407; 423; 424; 425; 426], which is PSF by delivering the gas in the direction opposite to physiologic flow (starting at the venous end). Historically, the technique of R-PSF also involved the introduction of

small, pin-pricks into the surface of the organ – to facilitate gas efflux as illustrated in **Figure 7-1**. In these studies, the effects of SCS, A-PSF and R-PSF on the bioenergetic profile of canine kidneys throughout preservation and after reperfusion were explored using their established *in situ* model. The degradation rate of high-energy phosphates at 37°C, 26°C and 6°C in canine kidneys was studied to better understand the effect of hypothermia on ATP, ADP and AMP levels. Furthermore, they measured the levels of high-energy phosphates and lactate in kidneys undergoing A-PSF and R-PSF using pure gaseous oxygen (100% O_2), 40% oxygen gas (mixed with 55% N_2 and 5% CO_2), and room air (21% O_2) to also study the effects of delivered oxygen concentration. A-PSF was performed at 60 or 100 mm Hg and R-PSF at 30 or 60 mm Hg. To study the impact of preservation protocol on metabolic status, renal cortical biopsies were taken at various time-points before and during preservation and after blood flow had been re-established. ATP depletion rate dropped by a factor of 2 and nearly 10 for kidneys preserved at 26°C and 6°C, respectively, as compared with measurements at 37°C. These findings confirmed that hypothermia diminishes the pace of energy utilization during storage. In the same study, Isselhard *et al*. were able to illustrate that the operational pressures of both A-PSF and R-PSF needed optimization for the best outcomes. ATP levels during R-PSF at 26°C and for 8 hours were strongly dependent on the driving pressures, averaging 81% and 98% of control values at 30 and 60 mm Hg. They also reported that R-PSF was generally better at the lower pressure (30 mm Hg) than A-PSF at either 60 or 100 mm Hg, based on these metabolic assays. It also appeared that lowering the PSF pressure from 100 to 60 mm Hg during A-PSF had a stronger, negative effect on ATP metabolism than lowering the PSF pressure from 60 to 30 mm Hg during R-PSF. The authors specifically stated that pressures below 60 mm Hg were unable to sustain adequate gas flow during A-PSF and they also pointed out

that the rate at which ATP was degraded increased inversely with gaseous oxygen concentration. Not surprisingly, lactate levels rose as the oxygen concentration decreased (from 100% to 40% and 21%) in both A-PSF (at 60 mm Hg) and R-PSF (at 30 mm Hg), but more dramatically during A-PSF. A remarkable accomplishment was the demonstration that ATP levels were maintained at 40% and 30% of control values under A-PSF (at 60 mm Hg, 66 hours) and R-PSF (at 30 mm Hg, 72 hours) at 6°C, respectively. In contrast, during SCS – ATP levels were reduced to negligible levels within minutes. The investigators noted that despite an ability to maintain a healthy bioenergetic status in preserved kidneys by PSF, the energy disparity (between utilization and production) remains during hypothermic storage and is only slowed down.

Further studies by this group remained focused on the important differences between A-PSF and R-PSF, by assessing their effects on renal bioenergetic status and function after reperfusion [407; 423]. I*n situ* A-PSF (at 90-100 mm Hg) was performed on canine kidneys for 4 hours at 6°C. Following the preservation period, a contralateral nephrectomy was carried out and the treated kidneys were reperfused. These persufflated kidneys were compared with healthy control kidneys and kidneys preserved by SCS for 4 hours and at 6°C. In summary, it was shown that A-PSF was better at maintaining ATP levels than SCS alone. However, once blood flow was restored, kidneys preserved by A-PSF fared no better. Sixty minutes after reperfusion, static cold-stored kidneys restored their ATP to levels comparable to those achieved following A-PSF. It was observed that kidneys preserved by A-PSF exhibited healthy levels of ATP during the first 30 minutes of reperfusion, but that deterioration quickly ensued. The authors attributed this fall in ATP to the development of poor intrarenal blood flow following reperfusion and speculated that the cause was damage inflicted on glomerular

vessels during A-PSF. *In vivo* renal function studies yielded findings that supported the belief that filtration had been most affected. Within 8 days, all dogs having a kidney preserved by A-PSF had died, while all dogs in the SCS control group survived. A progressive decline in renal function was documented through failing urine production, uremia and systematic elevation in serum creatinine. The glomerular filtration rate and renal plasma flow had dropped drastically by post-operative day (POD) 2 in all animals that died following A-PSF. Following this study, Isselhard pursued an identical study using R-PSF and, in contrast to A-PSF, R-PSF for 4 hours at 30 mm Hg did not result in the same deterioration in kidney function. ATP levels remained similar after 60 minutes of reperfusion, were no different from healthy controls, and better than static cold-stored controls. Furthermore, serum urea and creatinine values were generally lower following R-PSF than with SCS, but remained above baseline at POD 10. Glomerular filtration rate and renal plasma flow were normalized by POD 2 in persufflated kidneys, but static cold-stored kidneys did not fully normalize until POD 21, highlighting the accelerated recovery of renal function following R-PSF. As a direct result of these studies, the Cologne group primarily adopted R-PSF as the most promising of these approaches.

In the mid-to-late 1970s, Fischer's group contributed some of the most fundamental work on kidney PSF. In 1978, Fischer *et al*. presented a study in which the functional recovery of kidneys was documented after 2 or 30 minutes of WIT and following 24 hours of R-PSF, all of which preceded heterotopic autotransplantation into dogs [427]. For this, the authors developed a unique model where a contralateral nephrectomy was not used to isolate the functional output of each kidney – rather the preserved kidney was by transplanted into the collar region while the contralateral kidney was left in the retroperitoneum. It was demonstrated that 24 hours of R-PSF, in the presence of up to

30 minutes of WIT, was capable of preserving post-transplant renal function. Key measurable parameters of kidney function were glomerular filtration rate and renal plasma flow during a 3-hour period following transplantation. In kidneys subjected to only 2 minutes of WIT, the persufflated and autotransplanted kidney exhibited mean glomerular filtration rate and renal plasma flow that were 46% and 56% of the healthy contralateral kidney, respectively. Similarly, in kidneys undergoing 30 minutes of WIT – the preserved kidney had mean values of glomerular filtration rate and renal plasma flow that were 32% and 49% of the healthy control during the observation period. These results demonstrated that *ex vivo*, hypothermic R-PSF for 24 hours can preserve renal function in the face of considerable WIT (30 minutes). At the same time, Isselhard suggested that the duration of cold preservation by R-PSF could possibly be extended even further, up to 48 hours [428] – leading to a new line of investigation. In summary, they found that R-PSF maintained ATP levels for up to 120 hours. A more significant finding was that the effect of 30 minutes of WIT did not have as profound an effect on the ability of R-PSF to resuscitate the organ. ATP levels were monitored for 72 hours and were maintained at levels comparable to kidneys not damaged by warm ischemia. As cold ischemia time was prolonged, the capacity for aerobic metabolism measurably decreased but it was apparent that R-PSF may extend the life of kidneys during cold preservation.

At this point, the reported merits of PSF had not been tried clinically. However, in 1975, Flatmark *et al.* described a short study in which they reported their experiences with the accidental gas perfusion of human kidneys during HMP [429]. These kidneys were preserved in SCS (at 4°C, for 4-7.5 hours), transported from the site of procurement and then started on machine perfusion (at 8-10°C, with the perfusate equilibrated to 66% N_2,

33% O_2 and 1% CO_2) once received at their institution in Oslo. At some time after the start of HMP (between 3-12.5 hours), leaks were discovered near the oxygenator, which allowed air to be pulled into the flow circuit. In each of 4 kidneys the leak persisted and these organs were persufflated with air for about 60-120 minutes. Once the leak was identified, liquid perfusion was re-established and continued for the remainder of cold preservation, or 2-18.5 hours. Each kidney was subsequently transplanted, with all producing urine immediately and most achieved healthy renal function by 4 weeks post-operatively. One of the 4 patients unfortunately died, but the cause of death was not reported. In conclusion the authors stated that PSF (which they referred to as 'massive gas embolization') for up to 2 hours did not adversely affect post-transplant renal function. This was the first time that PSF was performed on human organs, albeit inadvertently.

The significant contributions of the Cologne group provided impetus for other investigators to pursue this field of investigation. In Australia, Ross and Escott explored 24-hour PSF on canine kidneys following 30 minutes of WIT and the effects of PSF on heterotopic autotransplant outcomes [430; 431]. These studies were focused on how the composition of the gaseous perfusate affected post-transplant renal function and survival. Also, these investigators tried persufflating via the ureter for the first time. Three interesting observations were reported: Firstly, that R-PSF was better at preserving renal function than A-PSF, as measured by serum creatinine values post-transplant. Secondly, that carbogen (95% O_2, 5% CO_2) may be better than pure oxygen gas (100% O_2) in normalizing renal function post-transplant. Thirdly, that ureteral PSF may work, but that it needs further exploration. Another puzzling finding was the relatively high incidence of intravascular thrombosis in all groups studied. They had postulated that it may have

been due to endothelial damage resulting from a gas-drying effect, yet the greatest incidence of thrombosis occurred in the group receiving humidified pure oxygen gas. Traumatic damage to the vasculature may have been an alternative explanation. An explanation not explicitly considered was the possibility of endothelial damage resulting from hyperoxia.

During this same era, Pegg and his group in Cambridge, England published a series of studies exploring the utility of PSF in kidney preservation. This group developed a fairly elaborate canine autotransplantation model that they used to examine the effects of varying lengths of WIT (30 and 60 minutes) in combination with R-PSF for 24 or 48 hours duration [432; 433; 434]. They also explored the differences between pure oxygen, air, nitrogen and helium PSF on post-transplant renal function and survival (for up to 3 months). It was reported that no kidney transplanted after 60 minutes of WIT and 24 hours of SCS was able to sustain recipient survival. On the contrary, R-PSF with pure oxygen gas was capable of sustaining long-term renal function and survival in most recipients. When air was substituted for oxygen, kidneys remained functioning, but the survival rates decreased. R-PSF with nitrogen and helium gases generated results similar to kidneys preserved by SCS. Kidneys that had undergone 30 minutes of WIT and 48 hours of cold ischemia time performed significantly better post-transplant, particularly if they had been persufflated; most animals (80% of group) survived R-PSF, while only a single animal (20% of group) survived following transplantation of a control kidney. Another noteworthy finding was that they were not able to establish any differences in total adenine nucleotide content between persufflated and control kidneys, or between kidneys persufflated for 24 versus 48 hours or with different gases. One explanation is that the authors do not report ATP, ADP or AMP levels, but rather total

adenine nucleotide content, which is the sum of these three; it is possible that the individual ATP and ADP fluctuations are masked by their summation. It is also important to note that the R-PSF pressures used in their study were particularly low, which may have resulted in inadequate PSF of the entire organ. This may be corroborated by the better outcomes using pure oxygen gas rather than air. Since the total adenine nucleotide content measurements are derived from tissue processed following biopsy, it is possible that the sampled regions of the kidney were poorly persufflated or that these samples do not reflect real-time total adenine nucleotide content levels because the tissue processing involves several steps and takes some time. Nevertheless, these data are compelling because the authors raise very reasonable questions regarding the interpretation of ATP and ADP measurements and their use as accurate predictors of metabolic quality in organ preservation. It has been widely appreciated that high energy phosphates recycle rapidly and that a single measurement is only a snapshot into the tissue metabolic status that does not necessarily provide information regarding the ability of tissue to recover from an insult [55].

The Cambridge group also published a follow-up pilot study in which a number of DCD human kidneys were persufflated prior to transplantation and compared with static cold-stored kidneys post-transplant in a paired fashion (meaning that each donor provided one kidney for R-PSF and another for SCS) [434]. The average WIT was 55 minutes, whereas the average cold ischemia time was 21.5 hours. The persufflated organs performed better post-transplant, exhibiting a mean (± standard deviation) onset of function at 8.4 (± 2.6) days versus 13.9 (± 1.4) days in the paired controls. Furthermore, the reported mean serum creatinine levels at POD 15 were 457 μM and 826 μM for the R-PSF and SCS groups, respectively. It was also explained that cyclosporine was

largely omitted from the immunosuppressive regimen in order to limit the impact of calcineurin inhibitor-associated nephropathy on the study results. Even so, of the 6 recipients having received cyclosporine, 4 of them received a kidney that was preserved by R-PSF. This first clinical study exploring R-PSF in preserving DCD kidneys illustrated that: 1) R-PSF can be executed within the current clinical infrastructure, including timeframe; and 2) R-PSF also exhibits the ability to resuscitate organs that have suffered from significant warm ischemia. Collectively, these two observations suggest that R-PSF may be easily implemented and could make more DCD organs suitable for transplant.

In an attempt to further elucidate the mechanism of preservation by PSF, Pegg *et al*. carried out an interesting study in 1989 in which they compared 24 hours of SCS to 24 hours of R-PSF following 60 minutes of WIT in an *ex vivo* rabbit kidney model [432]. Their hypothesis was that gaseous oxygen PSF enables continued aerobic respiration and that hypothermic conditions only slow the rates governing energy turnover. They studied ATP levels following R-PSF in conjunction with pharmacologic treatment with ouabain or cyanide/iodoacetate. Concomitant administration of ouabain, a potent sodium pump inhibitor, led to elevated ATP levels over R-PSF controls, which exhibited significantly higher ATP levels if compared with kidneys preserved by SCS. Conversely, treatment with cyanide/iodoacetate resulted in a fall of ATP, below levels present in static cold-stored kidneys. These measurements confirmed that if oxygen is available, even as a gas at low temperatures, it will be consumed by viable tissue. If pumps that consume ATP, like the Na^+/K^+-ATPase, are actively blocked, ATP levels will transiently rise, suggesting that 'new' ATP has been produced. On the contrary, if the electron transport chain is inhibited, then the capacity to generate ATP drops and the available oxygen supply will not be consumed. These findings provided insight into the

mechanistic principles governing oxygen consumption. Histology and electron microscopy revealed that renal tissue after R-PSF exhibited cellular damage over smaller foci and were largely surrounded by healthy tissue. Intriguingly, electron micrographs were capable of discriminating between the “orthodox” (or energized) mitochondrial configuration present in persufflated samples and the “condensed” (de-energized) mitochondria of the cold-stored tissues [432]. As a whole, these findings support the belief that R-PSF can maintain renal tissue viability and prevent irreversible injury during prolonged cold storage.

During this time, Stowe *et al*. at the Cleveland Clinic pursued *ex vivo* R-PSF in conjunction with a canine autotransplantation model [435]. After resecting the left kidney and flushing immediately with chilled lactated Ringers solution, R-PSF was performed for 48 hours (at 4-5°C and 7-10 mm Hg). Two days following the start of cold preservation, a contralateral nephrectomy was performed and the preserved kidney was transplanted heterotopically. Only 25% of animals that were autotransplanted with kidneys preserved by SCS or R-PSF survived to POD 22. In addition to comparing R-PSF with SCS, 3 animals received an intramuscular dose (500 mg) of deferoxamine mesylate. All 3 animals receiving a kidney preserved by R-PSF and treated with intramuscular deferoxamine mesylate survived to POD 22. In general, persufflated kidneys exhibited better overall renal function than static cold-stored kidneys. Though the total number of transplants was low, it appeared that deferoxamine mesylate contributed to an elevated survival rate post-transplant. The authors postulated that this was possibly due to free radical-scavenging activity in deferoxamine mesylate.

Several years later, Kootstra's group at the University Hospital in Maastricht addressed the question of whether the presence of adenosine benefits the quality of warm ischemically-damaged (30 minutes of WIT) and preserved rat kidneys during both R-PSF and SCS. Yin *et al*. used UW solution containing exogenous adenosine and UW solution with no adenosine [436]. All kidneys, whether preserved by 24 hours of R-PSF or SCS, were flushed with either of these UW solutions. In brief, they determined that regeneration of ATP was not affected by the presence of adenosine in UW solution. The authors postulated that since the levels of hypoxanthine (degradation product of adenosine) were significantly higher in renal tissue preserved with exogenous adenosine than in tissue without, that most of the additionally available adenosine was degraded in the tissue and not used in the direct replenishment of ATP. However, hypoxanthine levels were significantly lower in persufflated kidneys than in static cold-stored kidneys, which were also flushed with adenosine-containing UW solution. Alternatively, it may be that adenosine found in the preservation solutions may not be able to cross the plasma membranes of viable cells. The authors also went further by transplanting 20 kidneys, 10 from each of the R-PSF and SCS groups. They reported that none of the rats transplanted with static cold-stored kidneys survived, whereas 3 of the rats transplanted with retrogradely persufflated kidneys survived an observation period of 2 weeks. Because the survival rates between the two groups were not significantly different, they concluded that singular measurements of ATP during the preservation period may not predict survival outcomes. These conclusions were similar to those generated at Cambridge [433]. However, a point of caution must be raised regarding the choice in animal model. In general, PSF (or HMP, for that matter) will impart its greatest benefit if an organ is large and cannot obtain adequate oxygen by passive diffusion from the surface alone. In other words, success in a rat model may not be comparable to the

human clinical situation because of significant size disparity. This scaling problem has already been encountered when comparing the rat and porcine pancreata during SCS [394]. Rat data must be interpreted with appreciation for oxygen transport limitations, especially when trying to translate outcomes from animal models into the clinical arena.

Finally, more recently, Treckmann built upon the work of his predecessors and published studies that highlight the promising prospects of clinical PSF [437; 438]. In 2006, Treckmann *et al*. used a porcine autotransplantation model to show that R-PSF of kidneys damaged by significant WIT, when compared with conventional SCS, may yield improved survival [438]. Left kidneys from porcine donors were clamped off *in situ* for 60-120 minutes of WIT, resected, flushed anterogradely, preserved by R-PSF or SCS for 4 hours and autotransplanted. They demonstrated that all animals transplanted with persufflated kidneys after 60 minutes of WIT survived the 7-day observation period, with robust renal function. Animals receiving a similarly-treated kidney but stored by SCS survived in 57.1% of cases. This paired comparison was also performed for both 90 and 120 minutes of WIT, but did not reveal strong differences between R-PSF and SCS, at least in terms of post-transplant survival. It is important to note that only the persufflated kidneys received a pre-treatment of superoxide dismutase (SOD), which had been determined from their earlier liver work, to help protect against the oxidative damage caused by hyperoxia and reperfusion [439]. A follow-up study compared R-PSF and HMP, using the same porcine autotransplant model; 13 kidneys were resected following 60 minutes of WIT and preserved by SCS, HMP or R-PSF following pre-treatment with SOD [437]. Results showed that all indicators of renal function were significantly better in persufflated kidneys versus machine-perfused and static cold-stored kidneys at POD 7. Recipient survival after 7 days was 57%, 60% and 100% after transplantation of kidneys

preserved by SCS, HMP and R-PSF, respectively. These results in the larger animal model suggest that R-PSF is a promising way to maintain organ quality in DCD kidneys, particularly because R-PSF was directly compared against the already clinically-accepted HMP and performed comparably if not better. The collective work performed on kidney PSF has been summarized in **Table 7-3**.

Liver

PSF was tested for the first time in rat livers around 1980 by Fischer's group at the University of Cologne [440], but was not studied in depth (by the same group) until the 1990s. Initial work revolved around establishing that livers damaged by prolonged WIT could be resuscitated using R-PSF. Each liver in the R-PSF cohort was flushed with cold preservation solution and R-PSF was performed by administering gaseous oxygen at 18-30 mm Hg via a hepatic vein, while providing an escape route for the gas by introducing small, pin-sized holes on the liver surface. They reported that 24 hours of R-PSF resulted in no detectable lactate accumulation, but a substantial decrease in glycogen content.

It was during this period that anti-oxidants were identified and used to provide additional value in preservation using R-PSF, by conferring improved hepatocellular integrity and function following reperfusion [439]. In the 1990s, the same group had begun to translate some of their *in vitro* studies using small animal (rat) and, shortly thereafter, large animal (pig) liver transplant models. They showed that poorer quality livers could be revived to function successfully post-transplant. As recently as 2008, the same researchers showed that clinical PSF is possible; having a cohort of 5 patients transplanted with persufflated livers and showing no adverse effects and strong graft function [441].

Another interesting niche for PSF has been in the conditioning of a liver near the end of the preservation period, in so-called end- or post-ischemic conditioning [442]. As it stands, liver PSF is actively being explored and the preceding three decades of work highlights some of the reasons why.

In 1993, Minor *et al*. studied reperfusion injury in the rat liver following an ischemic period during preservation [439]. They procured a number of rat livers, flushed sequentially with lactated Ringers and Euro-Collins solutions via the hepatic vein, and bathed the organ in Krebs-Henseleit solution at 37°C for 60 minutes. After the controlled duration of WIT, the liver was submerged in Euro-Collins solution at 4°C and stored for another 60 minutes. Following static storage alone, the organs underwent normothermic (37°C) R-PSF for 30 minutes and were subsequently flushed with lactated Ringers solution. Persufflated organs received some combination of anti-oxidant pre-treatment; either a bolus injection of allopurinol prior to ischemia and/or the addition of allopurinol or SOD into the flush solution. At the end of the 2.5-hour treatment, the liver was flushed with lactated Ringers solution via the infrahepatic caval vein. The effluent was collected and analyzed for ATP and total adenine nucleotide content. The authors also determined the amount of malondialdehyde accumulated (via free radical-induced lipid peroxidation) and the amounts of liver enzymes released by damaged hepatic parenchyma. It was reported that R-PSF of the liver was capable of partially reversing ATP levels after 120 minutes of combined warm and cold ischemia. Additionally, it was shown that pre-treatment with anti-oxidants decreased the degree of lipid peroxidation and improved ATP recovery with R-PSF. Samples from persufflated livers pre-treated with allopurinol/SOD revealed that gaseous PSF alone can harm the liver due to oxidative

damage, but also highlighted the potential of anti-oxidant administration as an adjunctive therapy.

In a follow-up study, the same group showed that early administration of R-PSF reduces lipid peroxidation and may actually suppress the adverse effects of free-radical damage [443]. The authors speculated that immediate PSF may prevent damage by enabling the preservation of free-radical scavenging activity, which itself can require energy. Two years later this concept was studied in more depth using a rat liver reperfusion model [444; 445]. The effect of R-PSF in suppressing ischemia reperfusion injury was compared to preservation with 48 hours of SCS in UW solution at 4°C and followed by a 30 minute period of re-warming with normal saline at 25°C. Reperfusion consisted of pre-oxygenated (95% O_2, 5% CO_2), re-circulating Krebs-Henseleit solution delivered through the portal vein for up to 45 minutes. The effluent was analyzed and it was reported that endothelial and hepatic parenchymal damage was lowered and that activation of Kupffer cells had been reduced in livers that had been persufflated. These findings suggested that R-PSF may avoid disturbances in perfusion (like higher portal venous pressures) that result from damage to vessels. In addition, ATP concentrations were higher in persufflated livers than in static cold-stored livers and, at different times throughout the reperfusion, comparable to fresh control livers that were not subjected to cold storage. It was interesting to note that livers preserved by R-PSF exhibited significantly greater ATP levels as compared to reference values obtained from native rat liver [444].

These studies were extended to evaluate whether R-PSF in combination with SOD pre-conditioning would resuscitate the DCD rat liver, harvested after 30 minutes of WIT [446].

Livers are known to be poorly resistant to warm ischemic damage [447]. In fact, post-transplant outcomes following DCD transplant have been strongly tied to the extent of warm ischemic injury [447; 448; 449]. In this study, DCD livers preserved for 24 hours with R-PSF appeared to be healthier when compared with livers preserved by SCS in UW solution. The degree of lipid peroxidation was found to be lower in the R-PSF cohort. Interestingly, bile production and ATP levels were higher, while endothelial damage and portal perfusion pressures were lower than even fresh controls following 45 minutes of reperfusion with pre-oxygenated Krebs-Henseleit solution. It appeared that the putative, harmful effects of high oxygen concentrations during R-PSF could be prevented with the help of anti-oxidant treatment and resuscitation of livers from DCD was possible using R-PSF.

In 1997, Minor *et al*. introduced a novel rat liver transplant model in which rat livers were preserved with SCS alone or R-PSF [450]. The hypotheses they tested was the proposal that R-PSF limited proteolytic degradation of the liver, believed to contribute to hepatocellular injury during SCS, and that R-PSF would result in improved post-transplant indicators such as decreased plasma levels of malondialdehyde, decreased alanine aminotransferase, increased bile production and increased hepatic tissue perfusion. Proteolysis was estimated by a measured tissue content of free L-alanine. Twenty-four hours of SCS in UW solution resulted in significantly higher concentrations of free L-alanine than fresh (non-stored) controls, while R-PSF seemed to prevent some proteolysis. Following *in vivo* reperfusion, Minor *et al*. reported that both the static cold-stored only and persufflated livers experienced decreased hepatic perfusion initially, but that the persufflated organs exhibited an overall better recovery. Furthermore, plasma levels of malondialdehyde and alanine aminotransferase were significantly lower in the

livers having undergone R-PSF, but still elevated in both, while hepatic bile production was significantly increased in persufflated livers and comparable to fresh controls. It was concluded that R-PSF may help the ischemic liver obviate some of the ill-effects of hypoxia (like activation of cytosolic proteases and autolysis) by maintaining a more favorable metabolic condition. The authors reiterated that protecting tissue from oxidative damage necessitates sufficient energetic support, fueled by an adequate oxygen supply.

In the same year, Minor *et al*. examined the effect of lower pressure (9 mm Hg) versus higher pressure (18 mm Hg) R-PSF and the use of both pure gaseous oxygen and air [451]. The effectiveness and homogeneity of the R-PSF was studied by detecting autofluorescence of nicotinamide adenine dinucleotide [452; 453; 454], accumulated primarily in anoxic tissue. The reason why R-PSF was traditionally performed at 18 mm Hg of pressure was arbitrary; it had been determined that it was the pressure required for visual detection of bubbles escaping from the surface of the perforated liver. Nonetheless, interrogation at 1 and 24 hours after the start of cold preservation revealed that R-PSF at 9 and 18 mm Hg resulted in a comparable and significant decrease in nicotinamide adenine dinucleotide over static cold-stored controls. On the other hand, R-PSF with air at 18 mm Hg did not decrease detected nicotinamide adenine dinucleotide levels below those detected in livers on SCS, suggesting that air may not provide adequate oxygen during liver PSF.

Following the extensive studies in rat livers, translation of PSF into a larger animal model was the next step. In 1998, Minor *et al*. described work in which recipients were allotransplanted with DCD porcine livers following 1of 2 preservation protocols [455]. All

livers were harvested after 45 minutes of *in situ* WIT in a non-heparinized donor. Using the first protocol, the donor livers were flushed with heparinized normal saline and UW solution via the portal vein and stored on UW solution at 4°C for 4-5 hours. With the second protocol, the donor livers were also flushed with heparinized normal saline and UW solution, but the last 100 mL of UW solution used to flush the liver was spiked with SOD. Following the flush, R-PSF was initiated via the inferior vena cava for 4-5 hours. After the period of cold preservation, the stored livers were orthotopically transplanted into recipients. Shortly following transplantation, it was determined that SCS alone was not able to adequately preserve DCD livers; all 5 recipients died in the early post-transplant course. On the other hand, all livers stored by R-PSF were capable of normalizing ammonia levels by POD 1 and aspartate aminotransferase plasma levels by POD 7.

In a follow-up paper, the same investigators again compared SCS and R-PSF/SOD preservation by measuring plasma levels of aspartate aminotransferase, alanine aminotransferase, lactate dehydrogenase and clotting times at 1-hour post-transplant, with the primary endpoint of recipient survival at POD 5 [456]. DCD livers underwent 60 minutes of WIT prior to 4 hours of SCS with UW solution or R-PSF and pre-treatment with SOD. All DCD transplants were compared with control livers resected and transplanted immediately following cardiac arrest. They reported that UW-stored livers fared poorly post-transplant, accounting for significantly higher plasma hepatic enzyme levels, lactate dehydrogenase and prolongated partial thromboplastin time, suggesting that the liver had incurred significant hepatocellular injury during the preservation. Additionally, all of the animals receiving such livers died within 3 hours of reperfusion. On the contrary, animals receiving livers preserved by R-PSF/SOD survived the

observation period. Impressively, it was stated that persufflated porcine DCD livers performed comparably to fresh livers during the post-transplant course. Since very few DCD livers are transplanted nowadays, making more DCD livers available for transplant would reduce the numbers of patients on liver transplant waiting lists.

Around the same time PSF was being used in the resuscitation of DCD livers, Minor *et al*. explored an interesting application of PSF in pre-conditioning the long-term, static cold-stored liver for reperfusion [442]. In their first study on this topic, rat livers were subjected to either 48 hours of SCS on UW solution or 47 hours of SCS on UW solution followed by R-PSF for 60 minutes. Each of the organs were then warmed and reperfused *in vitro* for 45 minutes. Following reperfusion, livers conditioned (with R-PSF) fared significantly better – exhibiting decreased parenchymal enzyme levels and portal venous pressures, and improved bioenergetic status. It is believed that the delivery of gaseous oxygen prior to reperfusion may prevent edema formation due to the improvement in metabolic condition of the organ. Additionally, it may be that free-radical scavenging activity has been depressed during SCS and that pre-conditioning for reperfusion using PSF helps provide the oxygen necessary for replenishment of such activity [442; 457].

The concept of using PSF to pre-condition for reperfusion was studied more than a decade later with the preservation of fatty rat livers [457]. In these most recent studies, R-PSF for 90 minutes following 20 hours of SCS decreased hepatic parenchymal enzyme release, lipid peroxidation, cellular apoptosis and autophagy, and improved the functional clearance of ammonia, microscopic morphology and overall metabolic status of these livers as compared with unconditioned livers. These preliminary studies

illustrate that post-ischemic conditioning of preserved organs prior to transplant is an area meriting further study.

With anti-oxidant therapy having already been explored for use with PSF [439; 446; 455; 456], it became apparent that continued success using PSF in preservation may require protection against reperfusion injury. In 2003, Lauschke *et al*. studied the effect of administering taurine or SOD prior to R-PSF [458]. These studies employed a DCD rat model in which the livers were resected following 60 minutes of WIT and preserved either by SCS in UW solution, by R-PSF/taurine, or by R-PSF/SOD for 24 hours. Following the preservation period, livers were reperfused *in vitro* using Krebs-Henseleit solution maintained at 37°C for 45 minutes. Analysis of the effluent at the end of the reperfusion period revealed that livers treated with anti-oxidant exhibited decreased enzyme release and portal vascular resistance, and increased bile production. Interestingly, taurine and SOD appeared to have a similar protective effect for DCD livers in the face of ischemia-reperfusion. Future work to enhance the successful application of PSF for all organs of interest may require the identification of the appropriate anti-oxidant, dose(s) and schedule.

Most recently, Treckmann and colleagues have taken a major step, by translating R-PSF into the human clinical setting. In 2008, they reported from a pilot study using R-PSF to resuscitate 5 DCD human livers between April 2004 and March 2005 [441]. These donor cadaveric livers were estimated to have undergone anywhere from 20-60 minutes of WIT and the donors had expired after failed attempts at cardiopulmonary resuscitation or having experienced prolonged periods of hypoperfusion (<60 mm Hg). It is also important to note that these donor livers were rejected for transplant by at least three

different centers. The livers were procured off-site, perfused with UW solution and Histidine-Tryptophan-Ketoglutarate solution, and then shipped to the transplant center. After establishing recipient consent, the livers were additionally flushed with UW solution containing N-acetylcysteine and were retrogradely persufflated at 18 mm Hg for 70-200 minutes prior to orthotopic transplantation. The results of the transplants were encouraging in all cases. All patients survived and none of the patients required a re-transplant; all patients were alive, with strong graft function, at a minimum of 2 years follow-up. Histologic evaluation was performed on biopsies taken immediately prior to and after R-PSF, and directly following reperfusion. Analysis revealed that R-PSF did not appear to cause any vascular damage to the liver. Additionally, it was shown that PSF had recovered ATP levels by 2-5 times the pre-PSF measurements. These data are highly encouraging, especially considering the potential impact that PSF could have in expanding DCD liver transplantation. **Table 7-4** summarizes the published work on liver PSF presented in this review.

Small Bowel and Pancreas

To date, the pancreas and small intestine have not been studied extensively as targets of PSF. In 1997, Minor *et al*. published the only known work on luminal gas oxygenation of the small bowel [459]. Rat jejunal segments (15-cm in length) along with the vascular pedicle were harvested and stored in UW solution at 4°C for 18 hours and half of the experimental organs underwent low-pressure, luminal gas oxygenation. Following the experimental storage period, intestinal absorption was estimated by introducing galactose into the lumen and measuring concentrations in portal venous effluent. Collecting the total luminal effluent and subtracting the known inflow volume was used to measure the net influx of water into the intestinal lumen. Results showed significantly

increased accumulation of hypoxanthine in the small bowel segments with SCS alone. ATP, creatine phosphate and total adenine nucleotide content were significantly higher in the group undergoing luminal gas oxygenation versus SCS alone and resembled values from rat intestine *in vivo*. However, intestinal carbohydrate absorption was found to be severely impaired in both static cold-stored and gas oxygenated jejunal segments, even though gas oxygenation significantly improved post-ischemic absorption when compared to SCS. The net secretion of water into the gut lumen was significantly lower following gas oxygenation than SCS, reflecting less damage to intestinal villi. The authors noted that luminal gas oxygenation of the intestine could be improved by the introduction of supplements to the cold preservation solution, such as glutamine, an important substrate for intestinal mucosal cells. Although unique opportunities exist for the preservation of the small intestine using intraluminal gas oxygenation (a variant to intravascular PSF), this area of research has remained largely unexplored.

In contrast to small bowel intraluminal gas oxygenation, pancreas PSF has started to attract more interest in recent years. Currently, it is widely regarded that improvements in organ preservation may have a positive impact on pancreatic islet isolation and transplant outcomes [393]. For some time, the two-layer method (TLM) was considered the state-of-the-art for pancreas preservation before islet isolation. This has recently been challenged by studies showing that islet isolation outcomes are equivalent when comparing TLM and conventional SCS [460; 461]. It is likely that the inefficiency of oxygen delivery by passive diffusion from the organ surface alone is responsible for the limited efficacy of TLM in preserving larger organs [63; 394].

Over the last several years, PSF has been identified as a possible improvement to the current pancreas preservation protocol, particularly before islet isolation. Our research group is currently studying PSF of the pancreas to parallel our concurrent interests in pancreas HMP [462; 463] and have recently published several works on A-PSF of porcine pancreata for the purposes of improving whole organ and islet quality [62; 63]. In one study [63], human and porcine pancreata were preserved using TLM or A-PSF at 4°C. A-PSF was performed via the superior mesenteric artery and either the splenic artery (human) or the celiac trunk (pig). Following procurement, the organs were imaged by conventional MRI and ATP levels and ATP-to-inorganic phosphate ratios were estimated using ^{31}P-NMR spectroscopy. MRI revealed well-distributed areas of negative contrast throughout all persufflated pancreata, indicating the homogeneous presence of gas within the organ. Rat pancreata preserved by TLM showed relatively high ATP levels, though ATP levels were nearly undetectable in porcine pancreata preserved with TLM. In contrast, human pancreata preserved by A-PSF exhibited ATP-to-inorganic phosphate ratios similar to those observed in the rat pancreata on the TLM. Additionally, when A-PSF was stopped, ATP-to-inorganic phosphate ratios quickly declined to undetectable levels, similar to porcine organs preserved by TLM. When A-PSF was re-started, ATP levels rose again. In another study, DCD porcine pancreata were procured and the splenic lobe was separated from the connecting and duodenal lobes [62] – the anatomy being described previously [64]. The duodenal lobe was isolated following 1.5-2 hours of SCS and served as a first control, while the connecting lobe was stored on TLM for 24 hours and at 4°C to serve as a second control. Splenic lobes were submerged in cold preservation solution and preserved by A-PSF using a custom-designed, portable electrochemical oxygen concentrator (Giner Inc, Newton, MA) via the celiac trunk and superior mesenteric artery for 24 hours and at 4°C. Biopsies from organs preserved by

A-PSF showed distended capillaries and less autolysis and necrosis when compared to organs preserved by TLM. In contrast, TLM-stored pancreata showed frequent pyknotic nuclei, indicating possible irreversible cellular damage. A follow-up study extended the comparison to porcine pancreatic isolation, having shown that 24 hours of A-PSF was better than the TLM in preserving islet morphology, viability and post-culture recovery (unpublished results). Collectively, these results illustrate the potential of A-PSF in improving tissue and islet quality in larger pancreata when compared with conventional preservation methods.

These early and promising results have established the need for more extensive studies since pancreas PSF represents a significant opportunity to improve both solid organ and islet preservation over the current techniques used in the field. Additionally, the portable electrochemical oxygen concentrator used in our studies may enable more widespread use of PSF, not just of the pancreas, since it provides a safe method of delivering gas (or gas mixtures) during transportation and especially during air travel. **Table 7-5** summarizes the published work on small intestine and pancreas PSF presented in this review.

A schematic of the key milestone events during the historical development and use of PSF is presented in **Figure 7-2**.

Comparison between Anterograde and Retrograde Persufflation

Earlier, we outlined that two main modes of PSF have been introduced and evaluated as a means of delivering oxygen to an organ. The relative merits of R-PSF versus A-PSF were not clearly established by earlier studies and it was not until the early 1970s that

studies were undertaken to directly compare the two methods in a single system (canine kidney) [406; 407; 423]. Isselhard *et al*. developed an *in situ* ischemia model to study the effects of SCS, A-PSF or R-PSF on canine kidney preservation. Initially, they claimed that adequate preservation of kidneys required oxygen gas pressures of at least 60 mm Hg for A-PSF and 30-60 mm Hg for R-PSF. Because the authors did not present data at lower PSF pressures, it is unclear what criteria were used to determine adequate oxygenation – whether it was visual detection of gas escaping the renal vein or puncture holes in the capsule, or whether it was based on measured ATP. Nevertheless, they showed that an increase from 60 to 100 mm Hg in A-PSF did not improve ATP levels. The investigators did not comment on whether these pressures were sufficient to maintain ATP levels at control levels. On the other hand, the metabolic profile improved with an increase from 30 to 60 mm Hg in R-PSF. After 8 hours of R-PSF at 60 mm Hg, the ATP levels were near that of healthy controls. When directly comparing A-PSF at 60 mm Hg and R-PSF at 30 mm Hg, the authors illustrated that ATP levels were maintained at similar levels and at similar points during cold preservation.

Subsequently, the research group extended their comparison between A-PSF and R-PSF to the reperfusion period. They showed that A-PSF (at 90-100 mm Hg) for 4 hours resulted in deterioration of renal function upon reperfusion, despite being able to maintain adequate levels of ATP throughout preservation. These results were in contrast to those obtained for R-PSF (at 30 mm Hg); R-PSF for 4 hours with reperfusion exhibited no such deterioration in function and resulted in faster restoration of normal kidney function when compared with static cold-stored kidneys. Additionally, glomerular filtration rate and renal plasma flow dropped in most kidneys preserved by A-PSF, whereas they had normalized by the second day after reperfusion in kidneys preserved

by R-PSF. The authors noted that systemic blood pressures immediately increased for both sets of animals following reperfusion, regardless of the preservation technique employed. However, in animals having a kidney preserved by A-PSF, the systemic blood pressures increased abruptly – until they normalized again after 40-60 minutes. Dramatic blood pressure increases were not seen with kidneys preserved by either SCS or R-PSF. It was unclear how A-PSF would cause such disparate change in systemic blood pressure – yet these physiologic changes may be attributable to either vascular spasm following the mechanical stresses of surgical manipulation or PSF, reflexive responses of systemic vessels to decreased renal perfusion (via the renin-angiotensin system) or vascular damage and dysfunction with possible thrombosis. In further investigations, these researchers decided to use an A-PSF pressure of 90-100 mm Hg, even though it was determined that lower pressures would suffice. It is very possible that the elevated PSF pressures may have damaged the renal vasculature. Aside from mechanical damage, elevated oxygen levels throughout the glomerular capillary beds may have created a favorable setting for free radical damage. This may not be the case during R-PSF, where the resistances to gas flow are 2-3 times lower and the regional oxygen concentrations are lower (as gas circumvents capillary beds and exits capsular veins). The authors have cited that histologic evidence points to more noticeable changes in the glomerular structure during A-PSF than R-PSF, but these data were unpublished and inconclusive.

In contrast, Fischer *et al*. described that A-PSF may not cause functional damage to the vasculature of an organ during preservation [419]. They described a study in which porcine hearts were subjected to 16 minutes of WIT and stored for 3.3 hours at 0-1°C by either SCS or coronary A-PSF and then orthotopically transplanted. It was shown that

nitric oxide production by coronary endothelium was not adversely affected by A-PSF (as compared with SCS) and the ability of the coronaries to dilate and contract was preserved during reperfusion. Notable differences between this study and past studies involving A-PSF were that A-PSF was performed on porcine hearts (rather than canine kidneys) and under lower PSF pressures (45 mm Hg). Clearly, differences between the organ models may have contributed to varying results using A-PSF.

Despite somewhat conflicting results between the experimental models, it is reasonably certain that optimizing the PSF technique for both perfusion pressures and oxygen concentrations is important in achieving the best preservation possible. It is also likely that the optimal PSF technique may be different for different organs. It may be that A-PSF under lower pressures and lower oxygen tension could yield comparable, if not better, outcomes than R-PSF. However, this scenario has remained largely unstudied. In the case of the kidney and liver, it appears that the Cologne group may have maximized success using R-PSF, but it seems A-PSF has not been fully optimized and may prove to be the better approach for certain organs or applications.

In a very recent review, Fischer recommends that the coronary oxygen PSF should be carried out by A-PSF via the coronary arteries with outflow of gas from the coronary sinus. Retrograde gas flow through the aorta to reach coronary arteries does not establish a retrograde PSF of the myocardium. In contrast, Fischer argues that PSF in organs like liver and kidney should not be established in an anterograde manner because entry of gas into the microvessels may block any reperfusion. Hence, R-PSF is recommended in these organs because gas never reaches the microvessels and leaves the organ via openings in capsular veins [421].

Table 7-6 summarizes some of the potential advantages and disadvantages with A-PSF and R-PSF.

Comparison between Hypothermic Machine Perfusion and Persufflation

HMP is a method of organ preservation that has recently seen a resurgence of interest and shown clinically to have significant benefits over conventional SCS of kidneys [391; 392; 464]. Kidneys preserved using HMP have shown better early graft function when compared with SCS [465; 466]. HMP has recently been recommended as the preferred preservation method for DCD and extended criteria donor kidneys [391; 392; 464; 467; 468]. Recently, data is emerging for clinical use of HMP in other organs. Guarrera *et al*. have shown excellent outcomes, including decreased length of hospital stay with the first human trial of HMP-preserved livers [469]. The scientific basis behind HMP is largely based on rapidly reducing and maintaining the core organ temperature during ischemia. The potential for delivering nutrients, removing harmful waste products, extending cold preservation times, maintaining a patent vascular bed and being able to prospectively monitor whole organ viability during preservation, are all potential benefits of HMP . Potential disadvantages of HMP may include excessive damage to the vascular endothelium as a result of fluid shear and hydrostatic pressures, inadequate oxygen solubility of the perfusate, the possibility that vital or protective substrates of metabolism are continually removed via the circulation, the development of edema detrimental to the organ and the increased cost relative to SCS and possibly PSF. A summary of the advantages and disadvantages of SCS, HMP and PSF can be found in *Table 8-1*.

Very few studies have directly compared HMP and PSF, yet some work exists in this regard. Within the last 10 years, So and Fuller compared SCS, HMP, and R-PSF in the preservation of rat livers [470]. The organs were harvested and divided into three groups, all of which were stored at 4°C. Group 1 livers were preserved by SCS in non-oxygenated UW solution alone, Group 2 employed R-PSF with livers bathed in non-oxygenated UW solution, and Group 3 livers were preserved by HMP bathed in oxygenated UW solution. Tissue samples were obtained from livers at 2 and 24 hours of cold preservation and samples were analyzed for adenine nucleotide levels and glucose, lactate, ketone and alanine contents. At 2 hours, ATP levels were elevated in livers preserved by HMP and R-PSF, but were only statistically different from static cold-stored livers in the case of HMP. At 24 hours, the situation was different revealing that both HMP and R-PSF had the effect of significantly increasing ATP levels as compared with SCS. Lactate levels were initially elevated during SCS and R-PSF, but after 24 hours the lactate levels were comparable in livers preserved by HMP or R-PSF. Measured glucose contents were significantly higher during SCS and R-PSF than with HMP. Additionally, alanine levels were significantly elevated under R-PSF and ketone bodies were significantly lower with HMP at both time points. The authors concluded that both HMP and R-PSF could oxygenate a liver during long preservation times. Differences in early lactate measurements between the two groups were attributable to lactate being flushed out continuously during HMP. These are very relevant findings, because it may be that lactate is a beneficial substrate utilized by tissue during cold preservation. The authors noted that R-PSF did not appear to completely reverse the low ATP state of early ischemia as quickly as HMP, but these assertions are debatable. They believed that the metabolic resuscitation of organs following a period of hypoxia would require over 2 hours of PSF.

Along similar lines, Stegemann *et al*. recently published a study directly comparing the three modalities of cold preservation with DCD livers [471]. Following 30 minutes of WIT, rat livers were harvested and preserved for 18 hours using SCS, HMP or R-PSF. Organ viability was evaluated following *in vitro* reperfusion for 120 minutes with warm, oxygenated Krebs solution. Portal venous pressures were estimated during reperfusion and alanine aminotransferase, lactate/glutamate dehydrogenase levels were measured in the effluent. The degree of lipid peroxidation, metabolic status and cellular morphology were also studied. Hepatocellular damage was found to be greater during reperfusion in HMP-preserved livers versus those preserved by R-PSF. Glutamate dehydrogenase, an enzyme normally found within mitochondria, was shown to be elevated only during HMP. Histologic analysis of tissue biopsies paralleled the enzyme leakage data. Evidence of lipid peroxidation was similar between HMP and R-PSF, while the metabolic status of persufflated livers was better – as evidenced by significantly higher ATP levels during reperfusion. Finally, only after HMP did the portal venous pressures rise during reperfusion. In contrast, bile production rose significantly only after R-PSF. These data suggest that R-PSF may be a superior method of cold preservation for DCD livers. Longer term recovery of function was not studied during these experiments, yet it begs the question what happens to the organs following 2 hours of reperfusion. A limitation of this study was the use of a reperfusate that was not blood and did not contain any of the proteins (including clotting factors) typically found in plasma. It must be emphasized that there are a number of variables directly affecting the oxygen delivery to tissue by either HMP or PSF, including the fluid dynamic parameters, perfusate oxygen solubility and the patency of the intravascular flow path.

We reviewed earlier the most recent study by Treckmann *et al*., in which they compared SCS, HMP and R-PSF in porcine kidneys using an autotransplantation model [437]. Recipient survival at POD 7 was 100% after re-transplant of kidneys preserved by R-PSF, while only 57% by SCS and 60% by HMP. In animals re-transplanted with kidneys preserved by either SCS or HMP, plasma creatinine levels remained significantly elevated above baseline, whereas animals with persufflated kidneys maintained normal creatinine clearance. Significant proteinuria and increased lipid peroxidation was noted only after re-transplantation of HMP-preserved kidneys. Microscopic evaluation of tissue from explanted organs revealed that only persufflated kidneys were indistinguishable from healthy controls, which was not the case for kidneys preserved by SCS or HMP. Mild interstitial nephritis characterized static cold-stored kidneys, while HMP-preserved kidneys exhibited tubular protein deposits with signs of interstitial inflammation. The authors acknowledged certain limitations of their study, including the use of UW solution as the HMP perfusate instead of the gold-standard, Belzer machine perfusion solution. Another limitation of this study, as noted by the authors, were the relatively short preservation (4 hours) and monitoring (7 days post-operatively) times, which are not representative of standard practice. Future research might consider repeating this study using an allotransplant model to provide additional information, as acute rejection episodes have been linked to delayed graft function [472; 473], which in turn has been shown to be influenced by ischemia time and method of preservation [392; 472]. It is also noteworthy that only kidneys preserved by R-PSF received the anti-oxidant SOD, whereas the other two groups did not. This difference may have contributed to differences between HMP and R-PSF. Nevertheless, the authors concluded that R-PSF enhanced organ viability and function following a period of WIT in procured kidneys.

It remains difficult to appreciate the true benefit of PSF over HMP (or vice-versa), given the conflicting results amongst studies directly comparing the two techniques. What is clear is that the two modalities exhibit at least comparable potential, particularly with resuscitation of DCD kidneys and livers. Future studies are needed to better reveal the relative utility of each technique with regards to standard and expanded criteria organ preservation.

Prospective Implications for Persufflation in Transplantation

There is a clear longstanding discrepancy between the numbers of donor organs available for transplant and the numbers of prospective recipients on waiting lists. With the field of allotransplantation having come far over the last 60 years, an indisputable and persistent reality has been the shortage of donor organs. Many approaches have been levied in order to make more organs available for the donor pool, including the responsible expansion of acceptance criteria and improvements in organ preservation strategies. Some of these actions have yielded fruitful results and have helped prevent amplification of the problem. Data compiled by the United Network for Organ Sharing (UNOS) between 2001 and 2009 has illustrated both the promising and concerning trends (UNOS Data as of April 30th, 2010). Though the overall numbers of recipients on waiting lists have steadily decreased for heart, liver and simultaneous pancreas-kidney transplantation, the numbers of prospective kidney and pancreas transplant recipients have increased since 2001 by 38.9% and 22.3%, respectively. In the case of the kidney, the mean percent growth of the waitlist was 6.35% per year during this time span. In addition, most data indicate that the mean percent increase in the number of new patients added to a waitlist per year has increased during every year of this era, with the number of new kidney transplant candidates added at a mean rate of 5.2% annually

(with a range of 0.2%-11.0% per year). With kidney transplantation being the definitive treatment option for end-stage renal disease, it is no surprise that the candidate list is getting longer with every year.

Due to this increased demand for transplantable organs, the number of DCD transplants has been steadily increasing for both kidney (3.1% per year) and liver (3.5% per year). **Figure 7-3** depicts the trends in DCD transplants for liver, kidney, pancreas and simultaneous pancreas-kidney. The stark increase in the numbers of DCD kidney transplants over the last 6 years results from the more wide-spread utilization of HMP during preservation, illustrating that continued acceptance of newer preservation strategies can be a successful approach to make more organs available for transplant. Despite these efforts, many more organs could still be retrieved. In 2009, for example, the total number of DCD transplants only amounted to 8.2% of all performed solid organ transplants. Of all organs recovered for DCD transplant since 2001, 30.1% of livers, 21.4% of kidneys and 50.4% of pancreata were never transplanted. According to UNOS records, 17.2% of livers, 3.9% of kidneys and 11.5% of DCD pancreata that had been procured were discarded due to WIT beyond what was considered acceptable. In addition, many more organs were classified under an ‘other’ category, which suggests that some organs may have been discarded from consideration after having undergone unknown periods of WIT. Many of these consented organs could have been salvageable. It could be argued that the room for improvement is limited (based on these numbers alone). However, it is likely that many potential DCD organs are never procured because it is perceived that their poor quality does not merit the investment of resources required for their recovery. It is conceivable that improved preservation techniques could result in a lengthening of allowable ischemic times (particularly for heart, liver and pancreas),

possibly making previously unsuitable organs suitable for transplant. In other words, advancements in organ preservation may in fact accompany the expansion of donor organ criteria. The opportunity to resuscitate organs damaged by prolonged WIT and to better prevent their deterioration during storage should provide sufficient impetus to pursue the development of promising preservation strategies – like PSF. **Figure 7-4** illustrates the total DCD transplants been performed between 2001-2009 and further segregates them into the transplanted, recovered (but not transplanted) and possibly available (but not recovered) fractions. The numbers of organs that are possibly available but are never recovered have been estimated by assuming that each DCD kidney donor exhibits the potential to donate a liver and pancreas.

Even if improvements in preservation strategy do not lead to an immediate improvement in the number of transplantable organs, an incremental improvement in this area should be welcomed. Ultimately, the number of patients that die while waiting on transplant lists is the most important statistic. For instance, on an annual basis, 6.4% and 10.4% of potential transplant candidates for kidney and liver, respectively, do not survive long enough to make it to the operating room. Despite the recent strides made by the field of transplantation, many patients still never receive an opportunity to accept a potentially life-saving organ. In this light, seeking better ways to recover and preserve a greater number of suitable organs should continue to be a primary objective.

PSF has the potential to lengthen the allowable WIT and cold ischemia time for any organ, as supported by some of the studies reviewed herein. As described earlier in this section, there remains a unique opportunity to maximize the number of accepted DCD donors by rescuing these organs from incurring intolerable amounts of ischemic damage.

The case has been made that PSF may benefit heart, liver, kidney and pancreas transplant. A potential application that was only briefly discussed in this review is pancreas PSF before islet isolation. In addition to the unique susceptibility of the pancreas and the islets of Langerhans to ischemia [87; 158; 474; 475], islet cell transplantation poses additional challenges that are not seen in solid organ transplant. For instance, due to the complexity and expense associated with islet isolation, very few centers have the capacity to produce therapeutic preparations. Consequently, procured pancreata may need to be transported further in order to be processed for their islets. These additional travel considerations and distances may require longer preservation times (>12 hours). Studies performed at our institution have shown how pancreas PSF could be used to preserve human islets [62; 63]. Given the therapeutic promise of clinical islet cell transplantation [43; 44; 45; 46; 48; 50; 52; 371; 476; 477], exploring the utility of pancreas PSF is one of many efforts that are worthwhile.

To expand the acceptance and utilization of PSF in organ preservation, the technique must be developed further. Future work in PSF will involve: (1) optimization of technique and/or operational parameters so they are tailored to the tissue/organ-of-interest; (2) exploration of its use in conjunction with other preservation techniques (such as with HMP); or (3) as a method to condition organs prior to reperfusion; (4) direct comparison with other well-accepted preservation techniques; (5) development of portable PSF systems (like the electrochemical oxygen concentrator); (6) the identification of single or multiple pharmacologic agents used to prevent or reduce oxygenation and/or reperfusion injury; and (7) persuasion of the clinical community that *ex vivo* PSF is not the same as *in vivo* gas embolization – the two are fundamentally different from each other and (if

performed properly) PSF should not cause embolization. **Table 7-7** summarizes some of the keys areas of future work that may accompany an advancement of PSF.

We have attempted to demonstrate by the work presented in this review that oxygen gas delivered by PSF was found to be useable by a number of different types of tissues during hypothermic preservation. Hypothermic PSF has been shown to be capable of extending the allowable WIT and cold ischemia time and to be better in maintaining organ quality when compared with SCS and possibly HMP. The basis behind the intervention of PSF is to provide an adequate oxygen supply to an organ during preservation. Data collected over decades has confirmed that improved oxygenation is better for maintaining the quality of an organ and, in some cases, enables the recovery of reversibly-damaged tissue. Most of the studies presented in this review have demonstrated that PSF exhibits the capacity to improve the metabolic quality of tissue, as measured using a number of methods and in a variety of organs, and is poised for more research and clinical application.

Table 7-1: Potential advantages and disadvantages of hypothermic organ preservation techniques

Preservation technique	Advantages	Disadvantages
Static cold storage (SCS)	Easiest and cheapest to implement Simplest logistical considerations	Significant nutrient delivery and oxygen diffusion limitations Extends core organ warm ischemia time and characterized by slow, inhomogeneous cooling Cannot extend allowable cold ischemia time or resuscitate ischemically-damaged organs
Hypothermic machine perfusion (HMP)	Can efficiently deliver nutrients and oxygen into the core of the organ under appropriate conditions Can continuously clear waste products during preservation period Can extend preservation period up to 48-72 hours in kidneys and may in other organs May be able to monitor viability more easily	May increase risk of damage to vascular structures Can cause edema within organ ('perfusion nephropathy') Common perfusates have limited oxygen solubility, especially as compared with blood Perfusion pressures may damage endothelium (possibly affecting vascular function and/or inducing thrombosis) Useable substrates may be washed out Risk of transmitting reactive antibodies or pathogens may exist (if cryoprecipitated plasma is used) More challenging logistical considerations Fairly complicated and expensive technique to implement
Persufflation (PSF)	Can deliver more oxygen per gram tissue than SCS or HMP Gaseous perfusate has lower viscosity, may reach more regions of preserved organs and does not cause edema Can extend preservation time and may be able to resuscitate marginal organs May be able to monitor viability more easily May be simpler to implement than HMP	May increase risk of damage to vascular structures Depending on gaseous oxygen concentration, may induce hyperoxic damage in tissue Risk of damaging tissue by desiccation if gas is not properly humidified during long-term preservation PSF resembles iatrogenic gas embolization and challenges clinical dogma Cannot deliver nutrients like liquid perfusion and may be less efficient at removing waste products

Table 7-2: Summary of published work on heart PSF

Year	Author [Ref.]	Model(s)	Approach	WIT [min]	Duration of PSF [hours]	Gas used	Temp [°C]	Primary Endpoint
1902	Magnus R [398]	Cat	A-PSF	-	≤ 1.15	O_2, H_2, CO_2	24-28	Cardiac activity during PSF
1958	Burns B [402]	Rabbit	A-PSF	-	> 3	Carbogen[a], N_2,	37	Cardiac activity during PSF
1959	Sabiston D [403]	Dog	A-PSF	-	< 8	Carbogen[a], N_2	37	Cardiac activity during PSF and after reperfusion
1960	Talbert J [405]	Dog	R-PSF	-	2-7	Carbogen[a]	37	Cardiac activity during PSF and reperfusion
1966	Camishion R [404]	Dog, Pig	R-PSF	-	< 7	O_2, N_2	38	Cardiac activity during PSF
1966	Gabel L [411]	Cat	A-PSF	-	10	Carbogen[a]	40	Cardiac activity and metabolic profile during PSF
1968	Lochner A [412]	Guinea pig, Rat	A-PSF	-	< 1.5	Carbogen[a]	4-37	Cardiac activity, WOOCR and metabolic profile during PSF
1998	Kuhn-Regnier F [414]	Pig^{Tx}	A-PSF	-	14.5	O_2	0-1	Cardiac function and metabolic profile post-allotransplant
2000	Kuhn-Regnier F [416]	Pig^{Tx}	A-PSF	-	14.5	O_2	0-1	Cardiac function and metabolic profile post-allotransplant
2001	Fischer J [418]	Pig (DCD)	A-PSF	16	3.3	O_2	0-1	Coronary endothelial function
2003	Yotsumoto G [417]	Pig $(DCD)^{Tx}$	A-PSF	16.7	2.3	O_2	0-1	Cardiac function and metabolic profile post-allotransplant
2004	Kuhn-Regnier F [420]	Pig^{Tx}	A-PSF	-	14	O_2	0-1	Endothelial and myocardial cell function post-allotransplant
2004	Fischer J [419]	Pig (DCD)	A-PSF	16	3.3	O_2	0-1	Coronary endothelial function

[a]95% O_2, 5% CO_2
Abbreviations: A-PSF, anterograde persufflation; DCD, donation after cardiac death; PSF, persufflation; R-PSF, retrograde persufflation; Tx, specifies transplant model; WOOCR, whole organ oxygen consumption rate.

Table 7-3: Summary of published work on kidney PSF

Year	Author [Ref.]	Model	Approach	WIT [min]	Duration of PSF [hours]	Gas used	Temp [°C]	Primary Endpoint
1961	Talbert J [422]	Dog	A-PSF	-	2-4	Carbogen[a]	37	Renal function after reperfusion, gross and microscopic morphology
1971	Denecke H [413]	Dog	NS	-	4	O_2	6	Renal function and metabolic profile after PSF and during reperfusion
1972	Isselhard W [406]	Dog	A-PSF, R-PSF	-	2-72	O_2, Air, Mixture[b]	6, 26	Metabolic profile during PSF
1973	Isselhard W [423]	Dog	A-PSF	-	4	O_2	6	Renal function and metabolic profile after PSF and during reperfusion
1974	Isselhard W [407]	Dog	R-PSF	-	4	O_2	6	Renal function and metabolic profile after PSF and during reperfusion
1975	Flatmark A [429]	Human^{Tx}	A-PSF	-	1-2	Air	4	Renal function post-allotransplant
1978	Fischer J [427]	Dog^{Tx}	R-PSF	2, 30	24	O_2	6	Renal function post-autotransplant (into neck, with no contralateral native nephrectomy)
1978	Isselhard W [428]	Dog^{Tx}	R-PSF	30	24, 48, 72	O_2	NS	Renal function post-autotransplant
1979	Ross H [430]	Dog^{Tx}	A-PSF, R-PSF	30	24	O_2	NS	Renal function post-autotransplant
1982	Ross H [431]	Dog^{Tx}	R-PSF, Ureteral		48	O_2, Carbogen[a], Air	NS	Renal function post-autotransplant
1984	Rolles K [433]	Dog^{Tx}	R-PSF	30, 60	24, 48	O_2, Air, N_2, Helium	0-6	Renal function post-autotransplant
1986	Stowe N [435]	Dog^{Tx}	R-PSF	-	48	O_2	4-5	Renal function post-autotransplant
1989	Rolles K [434]	Human (DCD)^{Tx}	R-PSF	13-80	15-27	O_2	0	Renal function post-allotransplant
1989	Pegg D [432]	Rabbit	R-PSF	60	24	O_2	0	Mechanistic evaluation of oxygen utilization and morphology before and after PSF
1996	Yin M [478]	Rat (DCD)^{Tx}	R-PSF	30	24	O_2	4	Metabolic profile before and after PSF, renal function post-allotransplant, and evaluation of exogenous adenosine in CPS
2006	Treckmann J [438]	Pig^{Tx}	R-PSF	60, 90, 120	4	O_2	4	Renal function post-autotransplant
2009	Treckmann J [437]	Pig^{Tx}	R-PSF	60	4	O_2	4	Renal function post-autotransplant, comparison with HMP

[a]95% O_2, 5% CO_2
Abbreviations: DCD, donation after cardiac death; NS, not specified; PSF, persufflation; Tx, specifies transplant model.

Table 7-4: Summary of published work on liver PSF

Year	Author [Ref.]	Model	Approach	WIT [min]	Duration of PSF [hours]	Gas used	Temp [°C]	Primary Endpoint
1980	Fischer J [440]	Rat	R-PSF	-	24	O_2	6	Metabolic profile after PSF
1993	Minor T [439]	Rat	R-PSF	60	0.5	O_2, N_2	37	Hepatic injury and metabolic state before and after PSF, evaluation of anti-oxidant treatment after PSF
1994	Minor T [443]	Rat	R-PSF	60	1	O_2	4, 37	Hepatic injury, oxidative state and metabolic profile after reperfusion
1996	Minor T [445]	Rat	R-PSF	30[a]	48	O_2	4	Hepatic injury after reperfusion, endothelial activity and WOOCR
1996	Minor T [444]	Rat	R-PSF	30[a]	48	O_2	4	Metabolic profile after PSF and during reperfusion
1996	Minor T [446]	Rat (DCD)	R-PSF	30[a]	24	O_2	4	Hepatic injury and metabolic profile during reperfusion
1997	Minor T [450]	Rat^{Tx}	R-PSF	-	24	O_2	4	Assessment of proteolysis after PSF, hepatic function, perfusion, injury and oxidative state post-allotransplant
1997	Minor T [451]	Rat	R-PSF	-	24	O_2, Air	4	Hepatic oxygenation during PSF
1997	Minor T [453]	Rat (DCD)	R-PSF	60	2	O_2	12	Hepatic function, injury and metabolic profile after reperfusion
1997	Minor T [452]	Rat^{Tx}	R-PSF	-	24	O_2	4	Hepatic oxygenation during PSF, metabolic profile after PSF, hepatic injury post-allotransplant
1998	Minor T [454]	Rat	R-PSF	-	24	O_2, Air	4	Hepatic oxygenation before and after PSF
1998	Minor T [442]	Rat	R-PSF	30[a]	1	O_2	4	Hepatic function, injury and metabolic profile following post-ischemic conditioning using PSF and during reperfusion
1998	Minor T [455]	Pig (DCD)^{Tx}	R-PSF	45	4-5	O_2	4	Hepatic function, injury post-allotransplant
2001	Saad S [456]	Pig (DCD)^{Tx}	R-PSF	60	4	O_2	4	Hepatic function, injury post-allotransplant
2003	Lauschke H [458]	Rat (DCD)^{Tx}	R-PSF	60	24	O_2	4	Hepatic function, injury and oxidative state after reperfusion, evaluation of anti-oxidant pre-treatment during PSF
2008	Treckmann J [441]	Human (DCD)^{Tx}	R-PSF	20-60	1.2-3.3	O_2	4	Metabolic status before and after PSF, hepatic function and injury post-allotransplant
2009	Minor T [457]	Rat	R-PSF	20[a]	1.5	O_2	4	Hepatic function, injury, oxidative state and metabolic profile following post-ischemic conditioning using PSF and during reperfusion

[a]Re-warming period prior to reperfusion.
Abbreviations: DCD, donation after cardiac death; PSF, persufflation; Tx, signifies transplant model; WOOCR, whole organ oxygen consumption rate.

Table 7-5: Summary of published work on small intestine and pancreas PSF

Year	Author [Ref.]	Model	Approach	WIT [min]	Duration of PSF [hours]	Gas used	Temp [°C]	Primary Endpoint
Small intestine								
1997	Minor T [459]	Rat	Luminal	NS	18	O_2	4	Intestinal function and metabolic profile after PSF
Pancreas								
2010	Scott WE III [63]	Pig (DCD)	A-PSF	< 30	< 24	40% O_2	4	Metabolic quality during PSF, comparison with TLM
2010	Scott WE III [62]	Pig (DCD)	A-PSF	< 30	24	40% O_2	4	Histologic assessment after PSF, comparison with TLM

Abbreviations: DCD, donation after cardiac death; NS, not specified; PSF, persufflation; TLM, two-layer method.

Table 7-6: Potential advantages and disadvantages of A-PSF and R-PSF

Preservation technique	Advantages	Disadvantages
Anterograde persufflation (A-PSF)	Follows physiologic flow path	Elevated driving pressures may damage vascular function or endothelium
	May directly deliver gas to a greater part of the organ	May cause spastic or reflexive vascular changes, reducing blood flow to kidney and increasing systemic blood pressure
		May damage renal microvasculature and has resulted in poorer transplant outcomes
Retrograde persufflation (R-PSF)	Has been shown to sufficiently oxygenate and preserve various organs	Flow is in the opposite direction of physiological flow and highest pressures localized to thin-walled veins
		May require small punctures on surface of organ which could lead to bleeding upon reperfusion
	May require lower driving pressures	May not fully deliver oxygen-rich gas to all regions of the organ

Table 7-7: Areas of future work in PSF

Optimization of technique for specific tissue or organ, including: ▪ Development of surgical procurement protocol(s) ▪ Identification of appropriate approach (A-PSF, R-PSF or other) ▪ Minimization of required pressures ▪ Identification of appropriate gas or gas mixture (i.e., pO_2)
Direct comparisons between PSF and the state-of-the-art in preservation for a specific application
Exploration of utility in non-traditional applications, such as: ▪ Combination of PSF with other preservation strategies ▪ Use of PSF in post-ischemic conditioning
Continued development of a portable oxygen generator for PSF
Identification of appropriate strategy for the prevention of injury due to enhanced oxygenation during preservation or ischemia-reperfusion injury, including: ▪ Type of anti-oxidant(s), anti-apoptotic agent(s), or other drug(s) ▪ Dose of treatment(s) ▪ Schedule of treatment(s)
Elucidation of differences between PSF and gas embolization, which will include efforts to: ▪ Demonstrate negligible presence of gas following reperfusion of persufflated organ ▪ Maximize benefit to transplant community (e.g., extended allowable WIT and CIT) ▪ Maximize benefit to recipient of persufflated organ (e.g., lowered risk of delayed graft function) ▪ Establish that transplantation of persufflated organ carries limited risk of adverse clinical sequelae

Abbreviations: A-PSF, anterograde persufflation; CIT, cold ischemia time; pO_2, oxygen partial pressure; R-PSF, retrograde persufflation; WIT, warm ischemia time

Figure Captions (Suszynski *et al*. [57])

Figure 7-1: Cross-sectional illustration from the anterior view showing a native kidney (A) and kidneys being preserved by A-PSF (B) and R-PSF (C). Note the differences between A-PSF and R-PSF, in particular the relatively pronounced distension of the kidney during A-PSF and the capsular perforations only found with R-PSF – which allow for gas to escape during preservation and reduces overall resistance to gas flow. *Abbreviations*: A-PSF, anterograde persufflation; R-PSF, retrograde persufflation.

Figure 7-2: Historical timeline of significant contributions to the development of persufflation as a method of tissue and organ preservation.

Figure 7-3: Relative trends comparing number of donation after cardiac death (DCD) liver, kidney, simultaneous kidney/pancreas and pancreas transplants performed in the United States between 2001 and 2009. Data illustrates the increase in DCD liver and kidney transplants over the last six years, with the increase in the number of kidney transplants being due largely to improved preservation protocol, like hypothermic machine perfusion. Data was prepared by the United Network for Organ Sharing (UNOS) on April 30th, 2010.

Figure 7-4: Total numbers of donation after cardiac death (DCD) transplants performed in the United States between 2001 and 2009, further segregated into transplanted and recovered (but not transplanted fractions). Additionally, DCD donor livers and pancreata are often not recovered with DCD donor kidneys due to their true or perceived poor quality; these organs (represented by gray bars) are possibly available for recovery and

transplant, and may represent target organs for resuscitation via PSF. Data was prepared by the United Network for Organ Sharing (UNOS) on April 30th, 2010.

Abbreviations: DCD, donation after cardiac death; PSF, persufflation; UNOS, United Network for Organ Sharing.

Figure 7-1

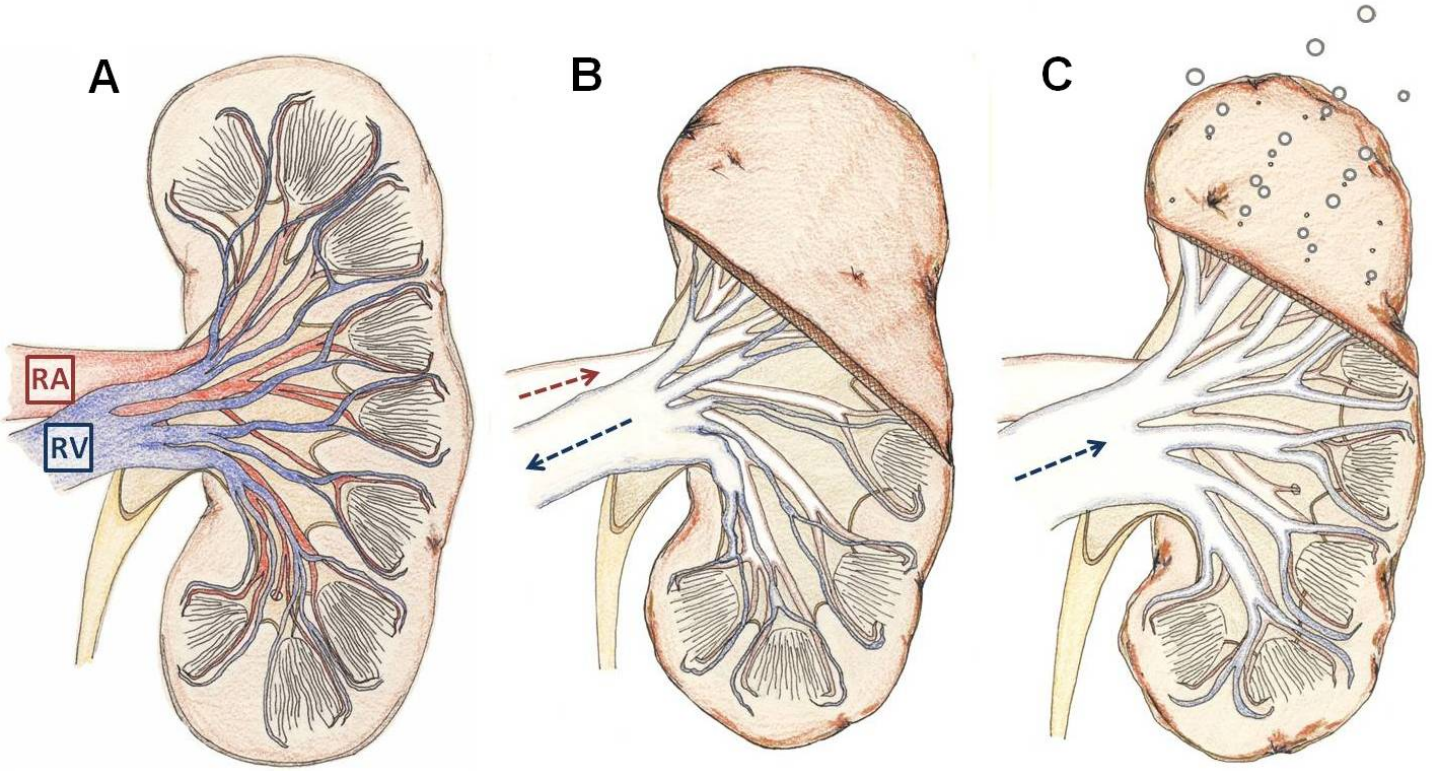

Figure 7-2

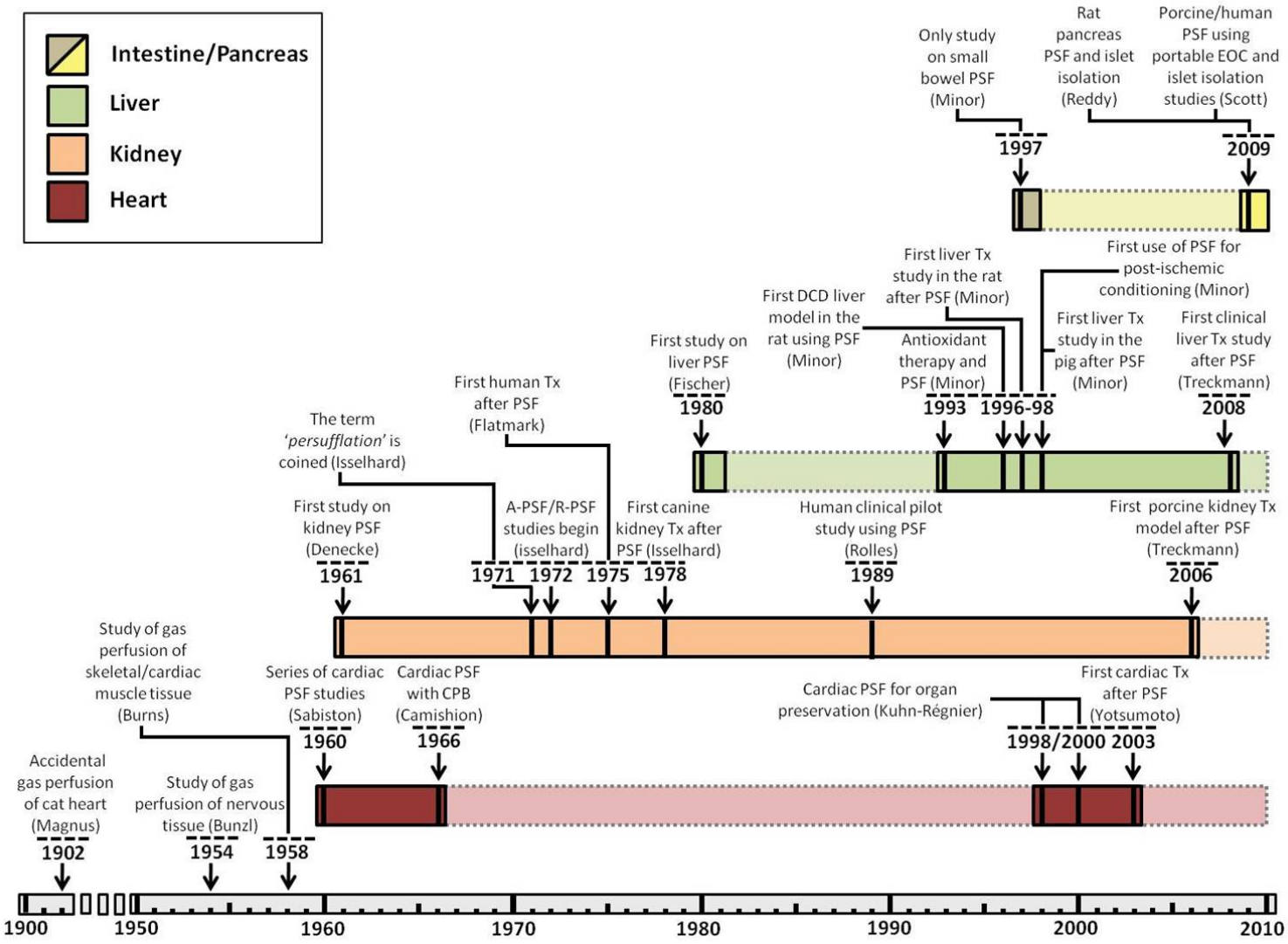
Intestine/Pancreas
Liver
Kidney
Heart
Only study on small bowel PSF (Minor)
Rat pancreas PSF and islet isolation (Reddy)
Porcine/human PSF using portable EOC and islet isolation studies (Scott)
1997
2009
First liver Tx study in the rat after PSF (Minor)
First use of PSF for post-ischemic conditioning (Minor)
First DCD liver model in the rat using PSF (Minor)
First liver Tx study in the pig after PSF (Minor)
First clinical liver Tx study after PSF (Treckmann)
First study on liver PSF (Fischer)
Antioxidant therapy and PSF (Minor)
1980
1993
1996-98
2008
First human Tx after PSF (Flatmark)
The term 'persufflation' is coined (Isselhard)
First study on kidney PSF (Denecke)
A-PSF/R-PSF studies begin (isselhard)
First canine kidney Tx after PSF (Isselhard)
Human clinical pilot study using PSF (Rolles)
First porcine kidney Tx model after PSF (Treckmann)
1961
1971
1972
1975
1978
1989
2006
Study of gas perfusion of skeletal/cardiac muscle tissue (Burns)
Series of cardiac PSF studies (Sabiston)
Cardiac PSF with CPB (Camishion)
Cardiac PSF for organ preservation (Kuhn-Régnier)
First cardiac Tx after PSF (Yotsumoto)
1960
1966
1998/2000
2003
Accidental gas perfusion of cat heart (Magnus)
Study of gas perfusion of nervous tissue (Bunzl)
1902
1954
1958
1900
1950
1960
1970
1980
1990
2000
2010

Figure 7-3

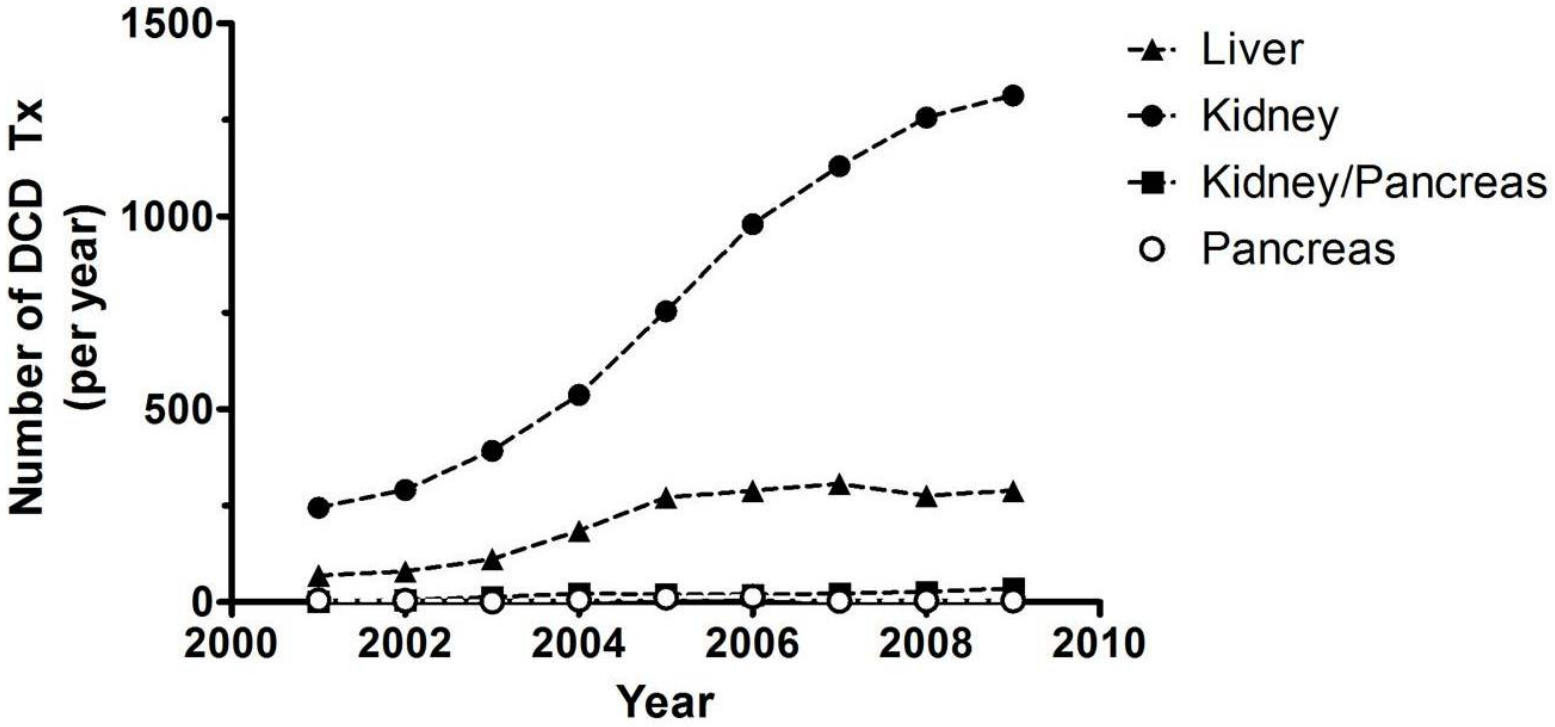
1500
1000
500
0
Number of DCD Tx
(per year)
2000
2002
2004
2006
2008
2010
Year
Liver
Kidney
Kidney/Pancreas
Pancreas

Figure 7-4

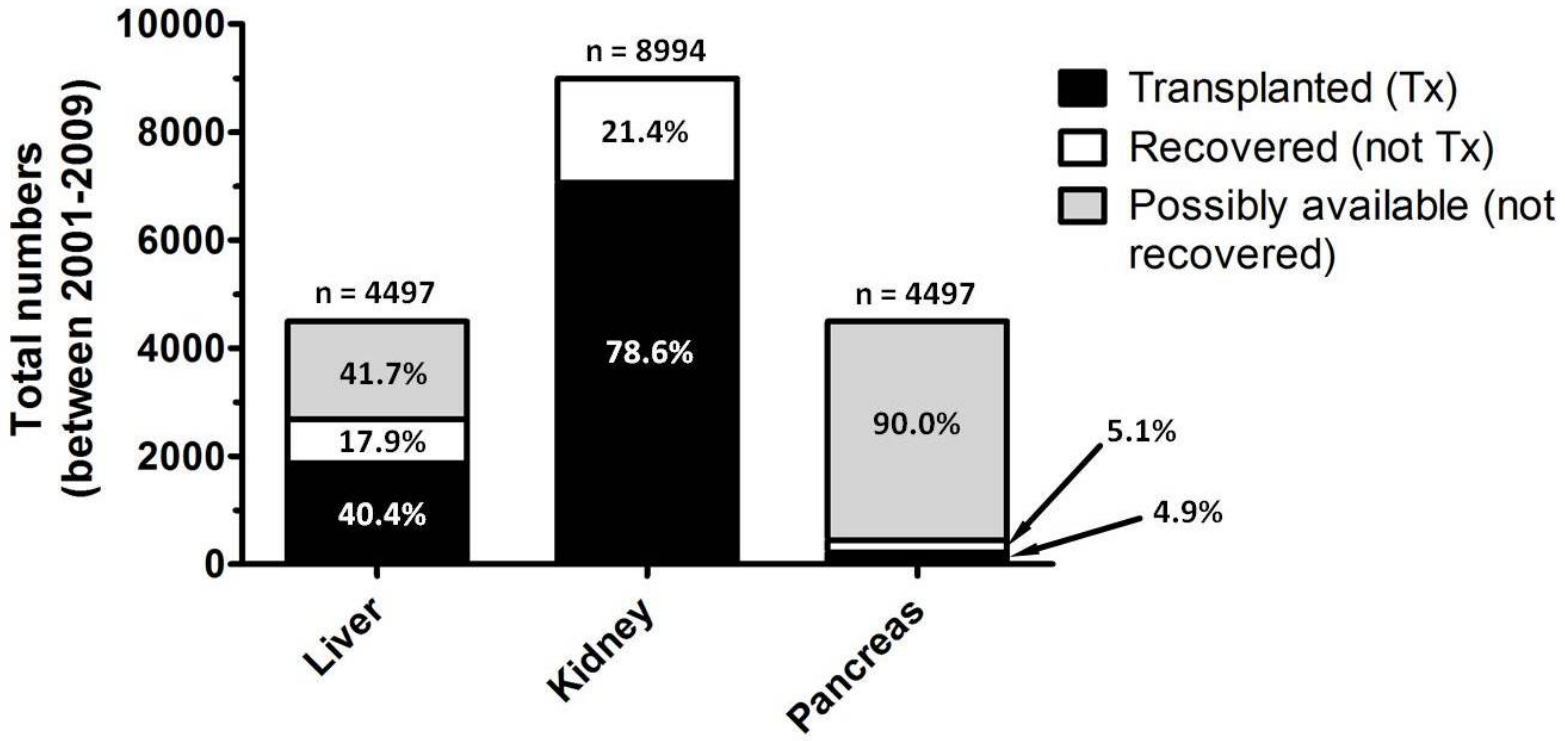
Total numbers (between 2001-2009)
10000
8000
6000
4000
2000
0
n = 4497
41.7%
17.9%
40.4%
n = 8994
21.4%
78.6%
n = 4497
90.0%
5.1%
4.9%
Liver
Kidney
Pancreas
Transplanted (Tx)
Recovered (not Tx)
Possibly available (not recovered)

Paramagnetic Microparticles Do Not Elicit Islet Cytotoxicity with Co-culture or Host Immune Reactivity after Implantation

Suszynski T.M., Rizzari M.D., Kidder L.S., Mueller K., Chapman C.S., Kitzmann J.P., Pongratz R.L., Cline G.W., Todd P.W., Kennedy D.J., O'Brien T.D., Avgoustiniatos E.S., Schuurman H.J., Papas K.K. Paramagnetic microparticles do not elicit islet cytotoxicity with co-culture or host immune reactivity after implantation. Xenotransplantation. 18(4): 239-244 (2011)

Abstract

Paramagnetic microparticles (MPs) may be useful in pancreatic islet purification, in particular purification of porcine islets as a potential xenotransplantation product. We assessed whether MPs affect islet function or induce an immune reaction following implantation. Porcine islets were co-cultured with 0, 500, and 1500 MPs per islet equivalent (IE) for 1 day and with 0 and 1500 MPs/IE for 7 days. Fractional viability was assessed using oxygen consumption rate normalized to DNA content (OCR/DNA), and after 7-day co-culture by perifusion glucose-stimulated insulin secretion (GSIS) and by transplantation under the renal capsule of diabetic nude mice. To assess immune reactivity, MPs (~10^7) were implanted under the renal capsule of C57BL/6 mice. No statistically significant differences were measured in OCR/DNA (mean ± standard error [SE]) following 1-day co-culture with 0, 500, or 1500 MPs/IE (243.3 ± 4.5, 211.3 ± 8.1, or 230.6 ± 11.3 nmol/min/mg DNA, respectively) or following 7-day co-culture with 0 or 1500 MPs/IE (248.5 ± 1.4 or 252.9 ± 4.7 nmol/min/mg DNA, respectively). GSIS was not affected by presence of MPs; first- and second-phase insulin area-under-the-curve (mean ± SE) reflected no statistically significant differences after 7-day co-culture between 0 and 1500 MPs/IE (8.36 ± 0.29 and 8.45 ± 0.70 pg/mL/min/ng DNA for first-phase; 69.73 ± 2.18 and 65.70 ± 4.34 pg/mL/min/ngDNA for second-phase, respectively). Islets co-cultured with MPs normalized hyperglycemia in diabetic nude mice, suggesting no adverse effects on *in vivo* islet function. Implantation of MPs did not elicit tissue injury, inflammatory change or immune reactivity. In summary, MPs do not adversely affect islet viability or function during co-culture, and MPs are not immune reactive following implantation.

Introduction

Pancreatic islet transplantation has considerable promise in reversing the diabetic state in patients with type 1 diabetes. However, consistent outcomes over the long-term have been largely elusive [43; 48; 52]. Among possible reasons for this is the need for transplantation of higher numbers of and better quality islets. It is widely accepted that a sufficient viable β-cell mass needs to be transplanted to normalize hyperglycemia [43] and that many of the islets residing in a pancreas are either never retrieved during isolation [479] or lost during manufacturing by processes inducing cell death [480]. In addition to the overall yield, purification may benefit posttransplant outcomes, because exocrine contaminants in islet preparations can induce undesired inflammatory and/or immunologic responses [102], and inhibit vascularization of the graft [481]. These experiences in transplantation using human islets directly apply as well to xenotransplantation using porcine islets considering the fact that manufacturing of porcine islets is more complicated and requires regulatory requirements such as good manufacturing practices.

A major step in current islet cell manufacturing is islet purification, which is a harsh technique that imparts prolonged exposure to proteolytic components of the digestion mixture, toxic substances like oxygen free radicals, and mechanical stresses [482]. Additionally, the centrifugation step takes considerable time, which lengthens the ischemic period for islets that are known to be poorly equipped to handle hypoxia [158]. Islet cell purification by centrifugation could be improved when it is replaced by selective magnetic separation, using magnetic labels that preferentially tag onto the surface of islets [483] or acinar tissue components [484], or that are entrapped within the tortuous microcapillary network of islets [485; 486; 487]. Rodent studies have provided early

proof-of-concept [485]; Donor pancreata could be infused with magnetic ferric oxide paramagnetic microparticles (MPs) which preferentially lodge within the capillary lumen of islets. Subsequent purification based on magnetic retraction decreases the time of the procedure 3-fold and results in improved islet morphology and viability while retaining insulin secretory function in the *in vitro* and *in vivo* settings. Furthermore, islets purified by magnetic retraction do not appear to stimulate an overt inflammatory response *in vivo,* despite the presence of ferric oxide MPs [485]. The evolution of magnetic retraction has led to the development of quadrupole magnetic sorting, a specialized technique that has recently been adopted for use with islets and which relies on the principle of applying a force against magnetically-labeled cells and/or aggregates of cells in order to pull them away from unlabeled tissue. The clear advantage of this technique has been described from a theoretical perspective [486]. A number of studies have shown the potential of separating magnetically-labeled islets by applying a external magnetic field [483; 484; 485; 486; 487], which have included separation of porcine islets [487].

Porcine islet cell manufacturing is receiving increasing interest because of the potential application of a porcine islet xenotransplantation product in patients with diabetes. This prompted us to initiate studies on using magnetic separation in the process of porcine islet cell manufacturing. We selected appropriate paramagnetic MPs of 4.5-μm diameter (Dynabead M450, Invitrogen Dynal, Oslo, Norway) for their ability to preferentially lodge within the microvasculature of porcine islets following embolization [485; 487], for their desired magnetic susceptibility [486; 487], and because of their track record with regulatory approval [488].

To address potential adverse side effects we conducted an exploratory study with the aim to examine potential effects of MPs on porcine islet viability and function during co-culture, and to examine for any tissue injury, inflammatory changes or immune reaction following implantation of large quantities of MPs. We used real-time insulin secretion as a read-out from *in vitro* evaluation and diabetes reversal in mice during *in vivo* assessment, as these allow for a most sensitive detection of effects manifested in pancreatic islet cell dysfunction.

Methods

Porcine pancreas procurement and islet isolation

Three Landrace sows, retired breeders aged 36-48 months and weighing 250-260 Kg, served as pancreas donors. Pancreas procurements and islet isolations were performed by the standard protocol used at the Schulze Diabetes Institute at the University of Minnesota [371]. Isolated porcine islets were cultured at 37°C in standard ME199 culture medium (Mediatech, Manassas, VA) supplemented with 10% heat-inactivated porcine serum. A total of 3 isolations were performed for this study.

Islet co-culture with and without MPs

MPs of 4.5-μm diameter (Dynabead M450) were obtained from Invitrogen Dynal (Oslo, Norway). Porcine islet aliquots from the same preparation were co-cultured with MPs at 0, 500, and 1500 MPs per islet equivalent (IE) for 1 day in 12-well culture plates (BD Biosciences, San Jose, CA). The dose levels were selected arbitrarily at 500 and 1500 MPs/IE, to maximize exposure while assessing for a dose-response and detection of an adverse effect. The number of IEs and the volume of ME199 medium were kept constant in each culture well. Islets from the same preparation were also co-cultured with MPs at

the higher dose (1500 MPs/IE) for 7 days. This condition was selected because a 7-day co-culture reflects the standard culture time during the islet cell manufacturing process and high doses were chosen to provide the best opportunity of detecting adverse effects. Preparations after co-culture were sampled for analysis of oxygen consumption rate (OCR) per DNA (or OCR/DNA), glucose-stimulated insulin secretion (GSIS) by perifusion, standard cytology, and some preparations were also assessed for their ability to reverse the diabetic state in nude mice by transplantation under the renal capsule.

Islet quality assessment

All quality assays were performed in triplicate, and results are presented as means ± standard error (SE). Preparations from a total of 3 islet isolations were used in these studies, with aliquots from each divided into untreated and MP-treated groups. OCR and DNA assays were conducted as described previously [98]; samples analyzed for OCR were subsequently assayed for quantification of DNA content. Cytologic preparations were stained by hematoxylin and eosin. For insulin staining, a polyclonal guinea pig antibody to porcine insulin (diluted 1:300, #A5064, Dako, Carpinteria, CA, USA) was applied using a Dako Autostainer, with detection using EnVision (Rb; Dako, Glostrup, Denmark) with diaminobenzidine chromogen (LSAB Kit, Dako). The negatively-stained control was generated using the same procedure described above, with the primary antibody omitted and substituted with an undiluted Supersensitive (Dako). The positively-stained control for insulin was performed on sections from a normal pancreas. Dynamic insulin secretory function (or GSIS) was assayed *in vitro* using a protocol described elsewhere [489], but modified slightly to enable use of a larger number of islets (approximately 300 IEs). The concentration of insulin in the supernatant was determined by enzyme-linked immunosorbent assay for porcine insulin (ALPCO

Diagnostics, Salem, NH). The basal glucose concentration was maintained at 2.5 mM, whereas the glucose stimulus consisted of a single-step increase in glucose concentration to 16.7 mM. Normally the insulin secretion into the supernatant follows a biphasic pattern and, for both patterns (first- and second-phase responses), the area-under-the-curve (AUC) was calculated using the linear trapezoidal rule.

Diabetes reversal in immune deficient mice

The procedure was performed as described previously [97]. In short, adult athymic nude mice were rendered diabetic by intraperitoneal streptozotocin injection (240 mg/kg body weight). Once hyperglycemia was established (at blood glucose levels >350 mg/dL for ≥2 consecutive days), approximately 2000 IEs after 7 days of culture ± 1500 MPs were transplanted in the renal subcapsular space, and glucose was monitored daily up to 33 days post-transplant. Diabetes reversal was defined as ≥2 consecutive days of glucose level ≤200 mg/dL. Animals exhibiting diabetes reversal were subjected to nephrectomy (which includes the removal of the transplant), and monitored afterwards for glucose to confirm for function of the graft. Each experimental group included 3 animals.

MP implantation in immune competent mice

All procedures involving animals were approved by the Institutional Animal Care and Use Committee at the University of Minnesota. Approximately 10^7 MPs were implanted underneath the renal capsule of C57BL/6 mice (n = 3), and controls received a sham operation (n = 3). Also, nude control mice (n = 3) were implanted with approximately 20,000 MPs. This implantation site was selected as this is mostly used for cell and tissue transplants in rodents. Three days after implantation, the animals were sacrificed and

the kidneys were resected, fixed in 10% buffered formalin and embedded in paraffin. Four-micron thick sections were stained with hematoxylin and eosin.

Statistical analysis

Data are presented as mean values ± SE. The difference between groups was analyzed using the paired two-tailed Student's t-test, with the level of significance set at $P < 0.05$.

Results

Effects of MPs on porcine islet fractional viability, cytology and insulin secretory function following co-culture

Table 7-8 shows OCR/DNA values for islet preparations co-cultured for 1 day with varying doses of MPs (0, 500, and 1500 MPs/IE). There were no statistically significant differences detected between the three dose levels. **Table 7-9** summarizes the fractional viability as expressed in OCR/DNA from untreated and MP-treated islet preparations following 7-day co-culture. MPs had no statistically significant effect on the OCR/DNA. **Figure 7-5** illustrates cytology of porcine islets following 7-day co-culture with 1500 MPs/IE, with MPs highlighted (in red) in the islet periphery. Islets exhibited normal cytology after co-culture and without indication of damage or cytotoxicity.

Figure 7-6 shows the GSIS of islet preparations after a 7-day co-culture, and illustrates the lack of a deleterious effect on secretory function in the presence of 1500 MPs/IE. After a glucose stimulus, the insulin concentration in the culture supernatant increased and followed a biphasic pattern – reaching an initial peak of 0.9 to 1.4 pg/mL·ngDNA, which is a normal observation from our experience. MPs did not appear to adversely affect GSIS during the full period of the tracing – up to about 45 minutes after the initial

stimulus. There was no statistically significant difference between cultures (± 1500 MPs/IE) in measured insulin AUC for the first-phase (between 3-14 minutes after the glucose stimulus) and second-phase (between 14-65 minutes after the glucose stimulus) responses (*Table 2*).

Effects of MPs implanted under the renal capsule in C57BL/6 mice

To assess for potential adverse side effects *in vivo*, MPs were implanted at an excessive dose of approximately 10^7 MPs under the kidney capsule of immune competent C57BL/6 mice, and assessed 3 days later with histology. Control (sham-operated) and experimental group included 3 animals each. All cases exhibited similar histologic results (**Figure 7-7**). MPs were confined to the subcapsular space, with the capsule remaining intact and the kidney parenchyma exhibiting a normal appearance. There were no signs of any acute tissue damage or inflammatory lesion, including the absence of polymorphonuclear granulocytes or lymphocytes. Few macrophages were observed at scattered locations in some tissue sections. MPs were neither encapsulated by fibrosis nor did they initiate granuloma formation, as commonly seen with foreign body reactions. These observations suggest that the selected MP suspensions are biologically inert.

Therapeutic potency of porcine islets co-cultured with MPs and transplanted into diabetic nude mice

Immune deficient diabetic mice were transplanted with 2000 IEs cultured for 7 days ± 1500 MPs/IE, and subjected to a 33-day follow-up. Two of 3 animals in each cohort became normoglycemic within a few days of renal subcapsular transplantation. Following a subsequent nephrectomy, all normoglycemic animals quickly reverted back

to a hyperglycemic state. These data show that islets co-cultured with MPs are as efficacious as untreated islets in reversing hyperglycemia in the diabetic nude mouse.

Discussion

In this exploratory study the Dynabead M450 MPs selected for application in islet cell manufacturing do not elicit adverse effects on porcine islets during co-culture; MPs do not affect the cytologic picture of cultured islets (*Figure 8-5*), fractional viability as measured by OCR/DNA (*Table 8-8*), or influence insulin secretory function as measured directly by GSIS (*Figure 8-6*, *Table 8-8*). Furthermore, islets co-cultured with MPs were as capable of reversing hyperglycemia in the diabetic nude mouse model as control islets not cultured in the presence of MPs. These *in vivo* data are consistent with data from others [487], showing that 75% of untreated and 80% of MP-treated preparations normalized blood glucose levels in nude mice. There is a difference in experimental design – Shenkman *et al*. [487] infused MP suspensions directly through the vasculature during porcine pancreas procurement and prior to islet isolation, whereas in the present study islets were externally exposed to much larger doses of MPs during the culture period after isolation. It is important to note that the polymeric material contributing a significant mass fraction to these MPs is biologically inert and stable *in vivo*. Concerns about this aspect have been raised during the regulatory evaluation to determine whether these MPs are suitable for clinical use [488].

Implantation of large quantities of MPs under the renal capsule of immunocompetent mice did not elicit any tissue injury or inflammatory reaction, as evidenced by histology 3 days after implantation. These data are similar to data generated by others [485], on the absence of an inflammatory response after implantation of islets containing ferric oxide

MPs under the kidney capsule of rats. It is noteworthy that the quantities of MPs used in the present study were orders of magnitude beyond the quantities expected to accompany a transplanted islet preparation purified using magnetic sorting. From past experiences, only a handful (up to 10 or so) MPs entrap within a single islet. For instance, in the case of transplanting 2000 IEs under the renal capsule of a diabetic nude mouse, the maximum number of MPs present within and near the graft would be on the order of 10^4 MPs – which is at least a thousand-fold less than the amounts implanted per animal in this study (~10^7).

We conclude that MP suspensions exhibit no evident adverse side effects affecting the function of porcine islets *in vitro* or *in vivo*, and when administered alone do not evoke tissue injury, an inflammatory response or immune reaction under the kidney capsule of immune competent mice. These data open the possibility of further studies to address the potential use of MPs in the islet manufacturing process, with the perspective of obtaining both higher yields and higher quality of islets. Such studies are now underway, addressing both safety and the benefits for improved outcome in islet cell transplantation.

Conflict of Interest Disclosure

Dr Paul W Todd is an employee of Techshot, Inc – which subcontracted with the University of Minnesota within the NIDDK 2R44DK072647-02A1 award that provided funding for some of this research. Dr David J Kennedy is an employee of IKOTECH, LLC, which sells Quadrupole Magnetic Sorting equipment. All other authors of this manuscript have no conflicts of interest to disclose.

Table 7-8: OCR/DNA of islet preparations co-cultured with different proportions of microparticles for 1 day

Proportion [MPs/IE]	OCR/DNA [nmol/min/mgDNA]
0	243.3 ± 4.5
500	211.3 ± 8.1
1500	230.6 ± 11.3

Data presented are from 3 independent islet isolations (mean ± standard error).
Abbreviations: IE, islet equivalent; MP, microparticle; OCR/DNA, oxygen consumption rate normalized to DNA content.

Table 7-9: OCR/DNA and perifusion GSIS outcomes in islet preparations co-cultured with microparticles for 7 days

	OCR/DNA [nmol/min/mgDNA]	AUC[a] [pg/mL/min/ngDNA]	
Co-culture (MPs/IE)		First-phase	Second-phase
0	248.5 ± 1.4	8.36 ± 0.29	69.73 ± 2.18
1500	252.9 ± 4.7	8.45 ± 0.70	65.70 ± 4.34

Data presented are from 3 independent islet isolations (mean ± standard error).
[a]AUC was estimated from GSIS tracing shown in *Figure 8-6.*
Abbreviations: AUC, area-under-the-curve; GSIS, glucose-stimulated insulin secretion; IE, islet equivalent; MP, microparticle; OCR/DNA, oxygen consumption rate normalized to DNA content.

Figure Captions (Suszynski *et al*. [58])

Figure 7-5: Cytology of islets treated with paramagnetic MPs after 7-day co-culture. Most MPs (highlighted by red arrows) are located at the periphery of the islets. Islets are stained with hematoxylin and eosin (A) and for insulin (B) and appear unaffected by the presence of MPs. *Abbreviation*: MP, microparticle.

Figure 7-6: Perifusion GSIS tracing for both untreated and MP-treated porcine pancreatic islets after 7-day culture, depicting a biphasic insulin release profile in direct response to an increase in perfusate glucose concentration (from 2.5 mM to 16.7 mM). Data shown are mean values ± SE for 3 independent experiments. *Abbreviations*: GSIS, glucose-stimulated insulin secretion; MP, microparticle; SE, standard error.

Figure 7-7: Histology following implantation of approximately 10^7 paramagnetic MPs under the renal capsule of C57BL/6 mice. Sections were stained by hematoxylin and eosin and both low (A, bar = 200 μm) and high (B, bar = 50 μm) magnification images are presented. The renal capsule appears intact and MPs are confined to the subcapsular space. *Abbreviation*: MP, microparticle.

Figure 7-5

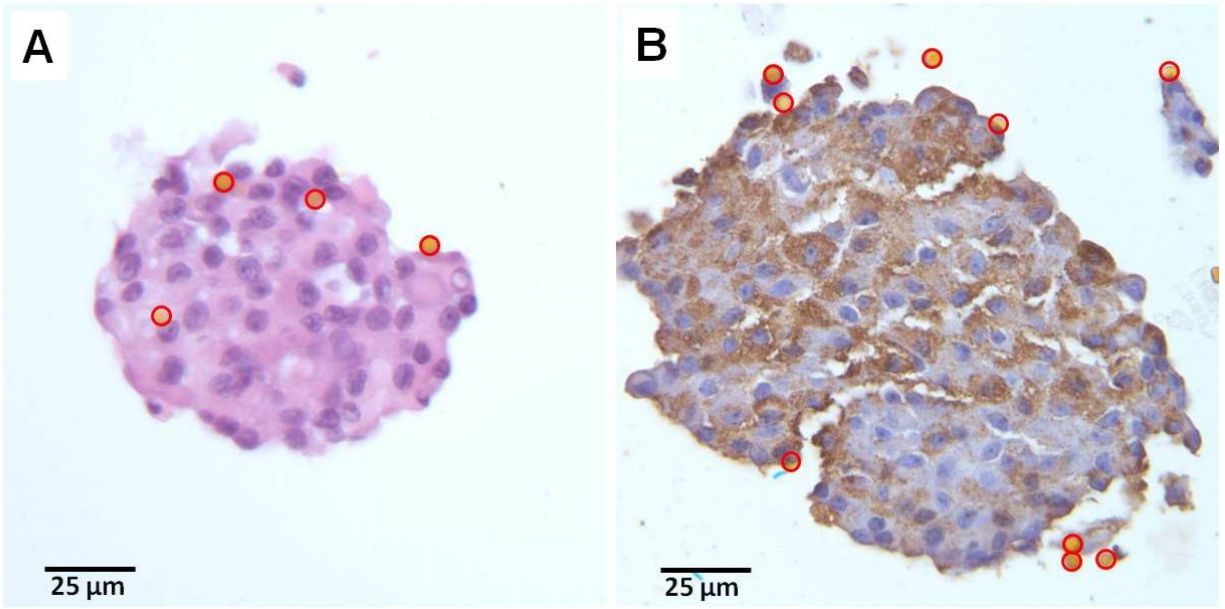

Figure 7-6

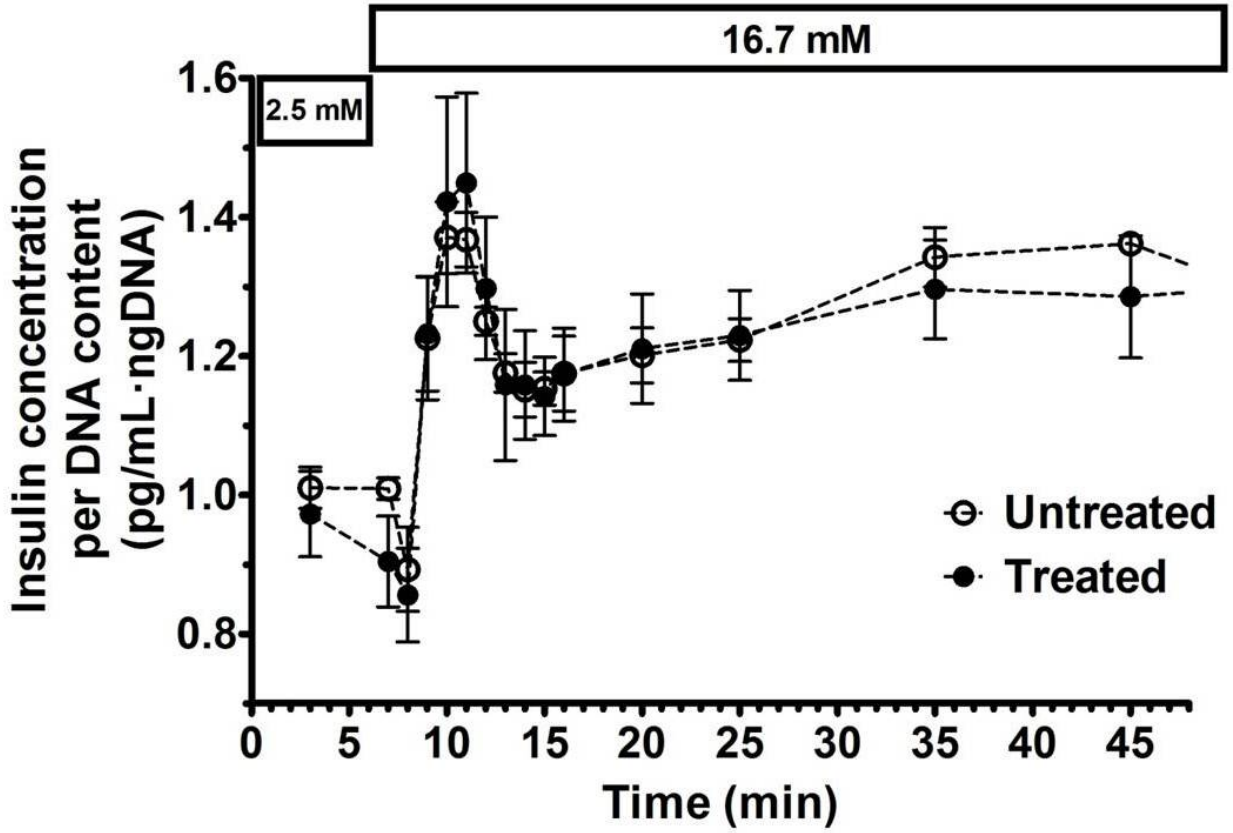
16.7 mM
2.5 mM
Insulin concentration per DNA content (pg/mL·ngDNA)
1.6
1.4
1.2
1.0
0.8
0
5
10
15
20
25
30
35
40
45
Time (min)
Untreated
Treated

Figure 7-7

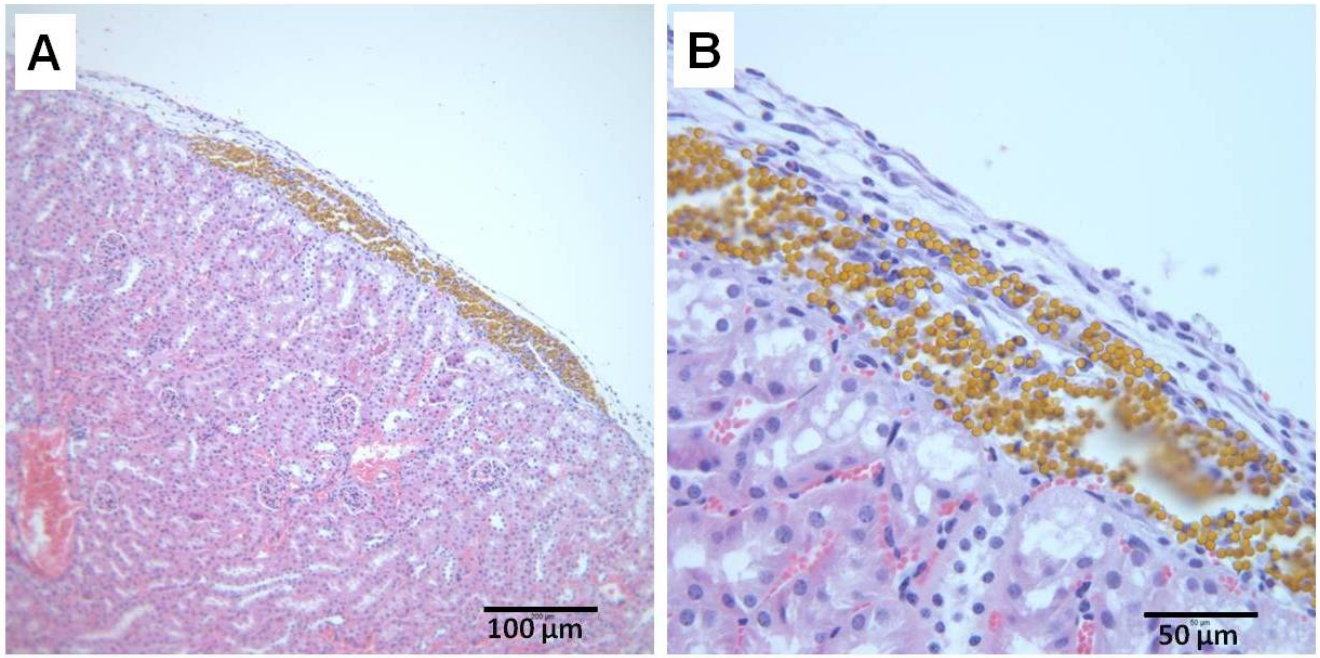

Surgical Protocol Involving the Infusion of Paramagnetic Microparticles for Preferential Incorporation within Porcine Islets

Rizzari M.D., Suszynski T.M., Kidder L.S., Stein S.A., O'Brien T.D., Sajja V.S., Scott III W.E., Kirchner V.A., Weegman B.P., Avgoustiniatos E.S., Todd P.W., Kennedy D.J., Hammer B.E., Sutherland D.E., Hering B.J., Papas K.K. Surgical protocol involving the infusion of paramagnetic microparticles for preferential incorporation within porcine islets. Transplant Proc. 42(10): 4209-4212 (2010)

Permission to reproduce the above publication was given by *Elsevier*, and the agreement (license number: 2924370837818) is found in Appendix 8-3.

Abstract

Despite significant advances, widespread applicability of islet cell transplantation remains elusive. Refinement of current islet isolation protocols may improve transplant outcomes. Islet purification by magnetic separation has shown early promise. However, surgical protocols must be optimized to maximize the incorporation of paramagnetic microparticles (MPs) within a greater number of islets. This study explores the impact of MP concentration and infusion method on optimizing MP incorporation within islets. Five porcine pancreata were procured from donors after cardiac death. Splenic lobes were isolated and infused with varying concentrations of MPs (8, 16, and 32 × 10^8 MPs/L of cold preservation solution) and using one of two delivery techniques (hanging bag versus hand-syringe). After procurement and infusion, pancreata were stored at 0°C to 4°C during transportation (less than 1 hour), fixed in 10% buffered formalin, and examined by standard magnetic resonance imaging (MRI) and histopathology. T2*-weighted MRI showed homogeneous distribution of MPs in all experimental splenic lobes. In addition, histologic analysis confirmed that MPs were primarily located within the microvasculature of islets (82% to 85%), with few MPs present in acinar tissue (15% to 18%), with an average of five to seven MPs per islet (within a 5-μm thick section). The highest MP incorporation was achieved at a concentration of 16 × 10^8 MPs/L using the hand-syringe technique. This preliminary study suggests that optimization of a surgical protocol, MP concentrations, and applied infusion pressures may enable more uniform distribution of MPs in the porcine pancreas and better control of MP incorporation within islets. These results may have implications in maximizing the efficacy of islet purification by magnetic separation.

Introduction

Islet transplantation (IT) has shown promise in the treatment of type 1 diabetes, but widespread applicability has not yet been achieved. Among the challenges limiting outcome is the inability to recover a sufficient amount of viable islets from a donor pancreas [47; 50; 479; 490]. Islet isolation techniques involving purification by magnetic separation (MS) have exhibited promise in obviating some of these challenges [483; 484; 485; 486; 487; 491]. Early studies in rodents have revealed the potential of using MS in conjunction with an intravascular infusion of paramagnetic microparticles (MPs) to preferentially label the islets [485]. Distribution of MPs throughout the entire human pancreas appears to be reproducible, but purification of this larger volume of tissue (following digestion) has thus far been limiting [491]. Quadrupole magnetic sorting (QMS) was primarily developed for single cell suspensions, but may represent the most promising technique for the MS of islets from acinar tissue, particularly in larger-sized organs. However, unlike the MP distribution achieved in human organs [491], the first attempts at infusing MPs into porcine pancreata have resulted in poor distribution [487]. With porcine xeno-IT having moved to the forefront of the field [371] and MS having shown considerable promise in improving islet isolation and purification over currently-used protocols [483; 484; 485; 486; 487; 491], improving MP distribution throughout the porcine pancreas and the fraction of total islets labeled with MPs represent two objectives for the successful application of QMS technology to porcine islet purification. New insight into the anatomical variability in porcine pancreatic vascular and ductal anatomy may provide an opportunity for improved surgical techniques accompanying MP infusion. Additionally, systematic investigation of selected surgical parameters may enable optimization of MP distribution and preferential incorporation of MPs within porcine islets. The objective of this preliminary study was to explore the impact of the

MP concentration in the perfusate and the infusion method used (either hanging bag or hand-syringe) during pancreas procurement on MP distribution and preferential islet labeling.

Methods

Porcine pancreas procurement and MP infusion

All procedures involving animals were approved by the Institutional Animal Care and Use Committee (IACUC) at the University of Minnesota. The porcine pancreas procurement was performed by standard protocol used at the Schulze Diabetes Institute and has been described elsewhere [64; 371]. Briefly, 5 pancreata were harvested from adult Landrace pigs following cardiac death using an *en bloc* technique. The posterior aorta was identified, longitudinally divided and both the celiac trunk (CT) and superior mesenteric artery (SMA) were cannulated. Distal splenic, gastric and hepatic vessels were clamped and 1 L of cold preservation solution (CPS, cold storage/purification stock solution containing 2% Pentastarch, Mediatech, Inc, Herndon, VA) was flushed into both the CT and SMA, simultaneously. During the flush, the main pancreatic duct was identified and cannulated just proximal to its insertion into the duodenum. Approximately 60 mL of CPS was then slowly infused over two minutes by hand-syringe into the main pancreatic duct. Following the flush, the pancreas was excised and divided into the combined connecting/duodenal lobes (control) and splenic lobe (experimental), all while taking care to preserve native vasculature. Varying concentrations of paramagnetic MPs (4.5 μm diameter, Dynabead M450, Invitrogen, Carlsbad, CA) suspended in 1 L of CPS were then infused into the splenic lobe only, via the CT and SMA by either hanging bag (gravity) or hand-syringe (applied pressure) infusion. Suspension concentrations of 8, 16 or 32 (x 10^8) MPs per L of CPS were used. Infusion of MP suspension was immediately

followed by a 1 L flush with CPS. All lobes were then submerged into CPS and stored at 0-4°C for transportation from the procurement facility (<1 hour). The splenic lobe was fixed with 180 mL of 10% buffered formalin injected via the CT and SMA and then all lobes were completely immersed in formalin.

MRI

Following complete formalin fixation (≥24 hours), pancreata underwent MRI. MRI was performed at 1.5 T with an APOLLO spectrometer (Tecmag Inc., Houston, TX, USA) and a custom-built 16-leg low-pass birdcage resonator (24 cm diameter, 20 cm in length). Images were obtained with a T2*-weighted true three-dimensional gradient echo sequence with one dimension frequency-encoded and the other two dimensions phase-encoded. A nonselective pulse was used to nutate the nuclei approximately 25 degrees during the scan. Typical acquisition parameters included a 9.6 msec acquisition time, 6.5 msec echo time, 120 msec repetition time, and a 20 cm x 10 cm x 5 cm field of view.

Histopathology

After MRI, biopsies were collected from several regions of the pancreas, embedded in paraffin and sectioned at 4 μm. Sections were examined using hematoxylin and eosin (HE) and insulin immunohistochemical stains. Sections were evaluated by an experienced histopathologist (T.D.O.) to estimate fraction of MP incorporation within islet and acinar tissues.

Results:

T2*-weighted MRI illustrated a uniform distribution of hypointense regions, indicating the presence of MPs throughout the experimental splenic lobe in all organs (**Figure 7-8**).

Histologic analysis confirms that MPs were found predominantly within islet microvasculature, with very few present in surrounding acinar tissue (**Figure 7-9**). Using varying MP concentrations and either hanging bag or hand-syringe infusion techniques has enabled MP incorporation in up to 90% of islets, as estimated by histology based on fraction of islets containing at least one MP. In the histologic sections examined, MPs were preferentially distributed within islets (82-85%) rather than acinar tissue (15-18%), with an average of 5-7 MPs per islet (within a 5 μm thick section). The highest MP incorporation within islets was achieved using the hand-syringe infusion technique with a concentration of 16 x 10^8 MPs per liter of CPS.

Discussion:

Islet cells endure significant stresses under current isolation protocols and many islets are either never recovered during isolation [479; 482] or are lost via a number of cell death processes [480; 482; 492; 493; 494]. Currently, few institutions are able to treat type 1 diabetes with islets from a single donor pancreas [47; 50]. Consequently, if more viable islets can be isolated per pancreas, there may be an opportunity to reduce the frequency of IT requiring multiple donors or to treat multiple patients with one donor [495]. Additionally, with porcine xeno-IT providing much hope [371], improving the porcine islet isolation process has become a worthwhile endeavor.

MS is a technique that may allow for isolation of superior quality islets. Using magnetic forces to preferentially separate islets from the acinar tissue of the pancreas following enzymatic digestion is attractive for several reasons. It may eliminate the use of continuous density gradient centrifugation, which imparts prolonged exposure to the harsh proteolytic components of digestion, toxic substances and mechanical stresses

[479; 482]. MS may also shorten isolation time and thereby minimize ischemia to islets, which are known to be particularly sensitive to hypoxia [87; 158; 169; 474]. The number of MPs required to achieve purification by QMS has been determined analytically based on fluid dynamics treatments and is largely a function of islet size and starting position in the fluid flow field [487; 496]. Islets that reach the QMS for purification are restricted to 500 μm in diameter and smaller by the mesh screen size used in the Ricordi chamber. All islets containing at least 10 MPs will have sufficient mobility for QMS purification. Purification of islets having less than 10 MPs is a function of size of the islet and relative starting position in the QMS magnetic field. When considering the 3-dimensional shape of a spherical islet, our data indicates that labeled islets will likely contain greater than 10 MPs, on average.

Shenkman and colleagues published results of preferential porcine islet labeling via MP infusion prior to separation by QMS [487]. They demonstrated that paramagnetic MPs were preferentially sequestered within the islet microvasculature. Islets undergoing MS from acinar and ductal tissue during isolation did not exhibit diminished viability. Despite being able to illustrate the potential applicability of QMS to porcine islet purification, they noted an inhomogeneous distribution of MPs throughout the pancreas as well as variable islet yields. Specifically, they described a narrow cylindrical region of infused MPs extending from the splenic lobe into the duodenal lobe with the highest concentrations in the region most proximal to the point of infusion at the CT. The inhomogeneous MP distribution in the porcine pancreas may have been due to the use of a donation after cardiac death model with poor flushing. Comprehensive characterization of the complex vascular and ductal anatomy of the porcine pancreas [64] and improvements in the procurement and flushing techniques [497] have created a new

opportunity to re-visit this problem. With a better understanding of porcine anatomy, surgical procurement and MP infusion techniques were substantially improved. In this preliminary study, we were able to show an improvement in the distribution of MPs throughout the experimental splenic lobe, as shown by MRI and histology, by adjusting the MP concentration and infusion pressure. Despite a limited number of organs studied, we have observed improvements in the distribution of MPs by using a manual hand-syringe infusion. Higher infusion pressures may allow for more homogeneous distribution of MPs throughout the porcine pancreas and improved sequestration of MPs within islet microvasculature. These early studies suggest that optimization of selected surgical procurement parameters may allow for better control of MP incorporation within islets. It is important to note that only splenic lobes were infused with MPs via the CT and SMA in this study, whereas entire pancreata were infused with MPs via the CT in the study published by Shenkman *et al*. [487]. Division of the pancreas and concomitant infusion of MPs via both the CT and SMA may have enabled better distribution of MPs throughout the splenic lobes.

Future studies will involve further optimization of surgical protocol, MP concentration and infusion pressures and techniques, including the use of machine perfusion and heart-beating porcine donors. It is conceivable that these techniques may be extended and optimized for use with human pancreata. In the past, QMS equipment had been largely used for single cell suspensions and was not initially developed to accommodate larger particles or cell aggregates (such as islets) or large suspension volumes, as is the case following the digestion of human or porcine pancreata. New QMS equipment has been developed that is capable of processing larger particles and volumes [486]. Future QMS studies will include the use of this new equipment. Additionally, methods for rapid and

quantitative assessment of bead incorporation in islets as opposed to acinar tissue are needed for optimizing bead infusion protocols. Histology is a useful tool but is neither rapid nor quantitative, especially for large organs. A new technique involving particle-tracking velocimetry may enable real time quantitative assessment of bead incorporation into islets versus acinar tissue in the raw pancreas digest and could be proven extremely valuable in optimizing the process.

Figure Captions (Rizzari MD *et al*. [59])

Figure 7-8: T2*-weighted MRI of the control connecting/duodenal lobe (above) and the experimental splenic lobe (below), in which infused MPs resulted in well-distributed hypointense regions. *Abbreviations*: MP, microparticle; MRI, magnetic resonance imaging.

Figure 7-9: Representative low and high magnification micrographs of an islet located in the experimental splenic lobe (distal region), illustrating minimal accumulation of MPs in the acinar tissue (A, HE) and significant accumulation within islet (B, HE). Representative high-magnification micrograph showing preferential seeding of MPs within capillaries of an islet located in the proximal splenic lobe, near the site of infusion at the celiac trunk (C, insulin). Insets in both high magnification images further illustrate presence of MPs specifically within capillaries (outlined by dotted black lines). Histological samples were taken from a splenic lobe infused with 16 x 10^8 MPs/L of cold preservation solution using the hand-syringe technique. *Abbreviations*: HE, hematoxylin and eosin; MP, microparticle.

Figure 7-8

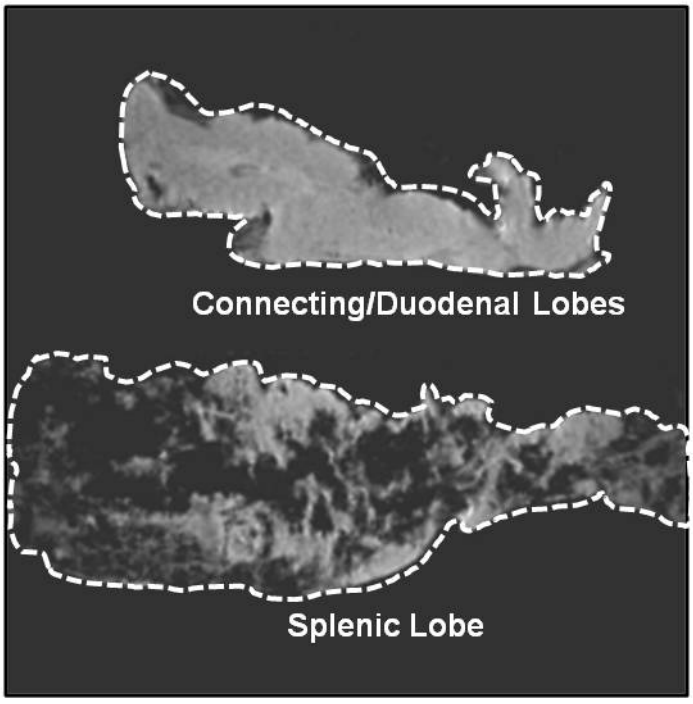

Figure 7-9

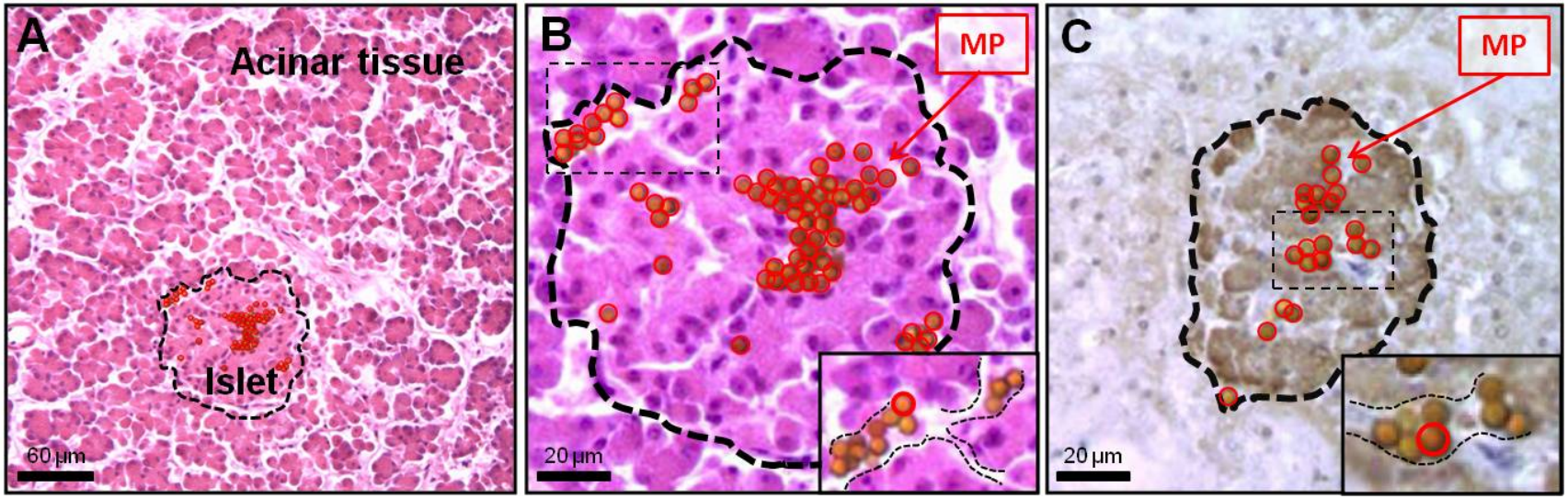

References

[1] S.B. Mohr, C.F. Garland, E.D. Gorham, and F.C. Garland, The association between ultraviolet B irradiance, vitamin D status and incidence rates of type 1 diabetes in 51 regions worldwide. Diabetologia 51 (2008) 1391-8.

[2] C.R. Cardwell, L.C. Stene, G. Joner, E.A. Davis, O. Cinek, J. Rosenbauer, J. Ludvigsson, C. Castell, J. Svensson, M.J. Goldacre, T. Waldhoer, J. Polanska, S.G. Gimeno, L.M. Chuang, R.C. Parslow, E.J. Wadsworth, A. Chetwynd, P. Pozzilli, G. Brigis, B. Urbonaite, S. Sipetic, E. Schober, C. Ionescu-Tirgoviste, C.E. de Beaufort, D. Stoyanov, K. Buschard, and C.C. Patterson, Birthweight and the risk of childhood-onset type 1 diabetes: a meta-analysis of observational studies using individual patient data. Diabetologia 53 (2010) 641-51.

[3] J.P. Crandall, W.C. Knowler, S.E. Kahn, D. Marrero, J.C. Florez, G.A. Bray, S.M. Haffner, M. Hoskin, and D.M. Nathan, The prevention of type 2 diabetes. Nat Clin Pract Endocrinol Metab 4 (2008) 382-93.

[4] V.S. Malik, B.M. Popkin, G.A. Bray, J.P. Despres, and F.B. Hu, Sugar-sweetened beverages, obesity, type 2 diabetes mellitus, and cardiovascular disease risk. Circulation 121 (2010) 1356-64.

[5] J.B. Meigs, P. Shrader, L.M. Sullivan, J.B. McAteer, C.S. Fox, J. Dupuis, A.K. Manning, J.C. Florez, P.W. Wilson, R.B. D'Agostino, Sr., and L.A. Cupples, Genotype score in addition to common risk factors for prediction of type 2 diabetes. N Engl J Med 359 (2008) 2208-19.

[6] M. Kaijser, A.K. Bonamy, O. Akre, S. Cnattingius, F. Granath, M. Norman, and A. Ekbom, Perinatal risk factors for diabetes in later life. Diabetes 58 (2009) 523-6.

[7] M. Oikarinen, S. Tauriainen, S. Oikarinen, T. Honkanen, P. Collin, I. Rantala, M. Maki, K. Kaukinen, and H. Hyoty, Type 1 diabetes is associated with enterovirus infection in gut mucosa. Diabetes 61 (2012) 687-91.

[8] D.G. Clayton, Prediction and interaction in complex disease genetics: experience in type 1 diabetes. PLoS Genet 5 (2009) e1000540.

[9] B.F. Voight, L.J. Scott, V. Steinthorsdottir, A.P. Morris, C. Dina, R.P. Welch, E. Zeggini, C. Huth, Y.S. Aulchenko, G. Thorleifsson, L.J. McCulloch, T. Ferreira, H. Grallert, N. Amin, G. Wu, C.J. Willer, S. Raychaudhuri, S.A. McCarroll, C. Langenberg, O.M. Hofmann, J. Dupuis, L. Qi, A.V. Segre, M. van Hoek, P. Navarro, K. Ardlie, B. Balkau, R. Benediktsson, A.J. Bennett, R. Blagieva, E. Boerwinkle, L.L. Bonnycastle, K. Bengtsson Bostrom, B. Bravenboer, S. Bumpstead, N.P. Burtt, G. Charpentier, P.S. Chines, M. Cornelis, D.J. Couper, G. Crawford, A.S. Doney, K.S. Elliott, A.L. Elliott, M.R. Erdos, C.S. Fox, C.S. Franklin, M. Ganser, C. Gieger, N. Grarup, T. Green, S. Griffin, C.J. Groves, C. Guiducci, S. Hadjadj, N. Hassanali, C. Herder, B. Isomaa, A.U. Jackson, P.R. Johnson, T. Jorgensen, W.H. Kao, N. Klopp, A. Kong, P. Kraft, J. Kuusisto, T. Lauritzen, M. Li, A. Lieverse, C.M. Lindgren, V. Lyssenko, M. Marre, T. Meitinger, K. Midthjell, M.A. Morken, N. Narisu, P. Nilsson, K.R. Owen, F. Payne, J.R. Perry, A.K. Petersen, C. Platou, C. Proenca, I. Prokopenko, W. Rathmann, N.W. Rayner, N.R. Robertson, G. Rocheleau, M. Roden, M.J. Sampson, R. Saxena, B.M. Shields, P. Shrader, G. Sigurdsson, T. Sparso, K. Strassburger, H.M. Stringham, Q. Sun, A.J. Swift, B. Thorand, et al., Twelve type 2 diabetes susceptibility loci identified through large-scale association analysis. Nat Genet 42 (2010) 579-89.

[10] J.C. Barrett, D.G. Clayton, P. Concannon, B. Akolkar, J.D. Cooper, H.A. Erlich, C. Julier, G. Morahan, J. Nerup, C. Nierras, V. Plagnol, F. Pociot, H. Schuilenburg, D.J. Smyth, H. Stevens, J.A. Todd, N.M. Walker, and S.S. Rich, Genome-wide association study and meta-analysis find that over 40 loci affect risk of type 1 diabetes. Nat Genet 41 (2009) 703-7.

[11] F.M. Allen, E. Stillman, and R. Fitz, Total dietary regulation in the treatment of diabetes, The Rockefellar Institute for Medical Research, New York, 1919.

[12] F.G. Banting, C.H. Best, J.B. Collip, W.R. Campbell, and A.A. Fletcher, Pancreatic Extracts in the Treatment of Diabetes Mellitus. Can Med Assoc J 12 (1922) 141-6.

[13] F.G. Banting, Early Work on Insulin. Science 85 (1937) 594-6.

[14] M. Bliss, The Discovery of Insulin, The University of Chicago Press, Chicago, IL, 1982.

[15] D.M. Nathan, Long-term complications of diabetes mellitus. N Engl J Med 328 (1993) 1676-85.

[16] The Diabetes Control and Complications Trial (DCCT). Design and methodologic considerations for the feasibility phase. The DCCT Research Group. Diabetes 35 (1986) 530-45.

[17] R. Klein, B.E. Klein, S.E. Moss, M.D. Davis, and D.L. DeMets, Glycosylated hemoglobin predicts the incidence and progression of diabetic retinopathy. JAMA 260 (1988) 2864-71.

[18] The effect of intensive treatment of diabetes on the development and progression of long-term complications in insulin-dependent diabetes mellitus. The Diabetes Control and Complications Trial Research Group. N Engl J Med 329 (1993) 977-86.

[19] P. Reichard, B.Y. Nilsson, and U. Rosenqvist, The effect of long-term intensified insulin treatment on the development of microvascular complications of diabetes mellitus. N Engl J Med 329 (1993) 304-9.

[20] Retinopathy and nephropathy in patients with type 1 diabetes four years after a trial of intensive therapy. The Diabetes Control and Complications Trial/Epidemiology of Diabetes Interventions and Complications Research Group. N Engl J Med 342 (2000) 381-9.

[21] Sustained effect of intensive treatment of type 1 diabetes mellitus on development and progression of diabetic nephropathy: the Epidemiology of Diabetes Interventions and Complications (EDIC) study. JAMA 290 (2003) 2159-67.

[22] D.M. Nathan, P.A. Cleary, J.Y. Backlund, S.M. Genuth, J.M. Lachin, T.J. Orchard, P. Raskin, and B. Zinman, Intensive diabetes treatment and cardiovascular disease in patients with type 1 diabetes. N Engl J Med 353 (2005) 2643-53.

[23] R.R. Holman, S.K. Paul, M.A. Bethel, D.R. Matthews, and H.A. Neil, 10-year follow-up of intensive glucose control in type 2 diabetes. N Engl J Med 359 (2008) 1577-89.

[24] I.H. de Boer, W. Sun, P.A. Cleary, J.M. Lachin, M.E. Molitch, M.W. Steffes, and B. Zinman, Intensive diabetes therapy and glomerular filtration rate in type 1 diabetes. N Engl J Med 365 (2011) 2366-76.

[25] M.E. Molitch, M. Steffes, W. Sun, B. Rutledge, P. Cleary, I.H. de Boer, B. Zinman, and J. Lachin, Development and progression of renal insufficiency with and without albuminuria in adults with type 1 diabetes in the diabetes control and complications trial and the epidemiology of diabetes interventions and complications study. Diabetes Care 33 (2010) 1536-43.

[26] P. Gaede, H. Lund-Andersen, H.H. Parving, and O. Pedersen, Effect of a multifactorial intervention on mortality in type 2 diabetes. N Engl J Med 358 (2008) 580-91.

[27] W.D. Kelly, R.C. Lillehei, F.K. Merkel, Y. Idezuki, and F.C. Goetz, Allotransplantation of the pancreas and duodenum along with the kidney in diabetic nephropathy. Surgery 61 (1967) 827-37.

[28] R.C. Lillehei, R.L. Simmons, J.S. Najarian, R. Weil, H. Uchida, J.O. Ruiz, C.M. Kjellstrand, and F.C. Goetz, Pancreatico-duodenal allotransplantation: experimental and clinical experience. Ann Surg 172 (1970) 405-36.

[29] D.E. Sutherland, Pancreas and islet transplantation. II. Clinical trials. Diabetologia 20 (1981) 435-50.

[30] J.S. Najarian, D.E. Sutherland, A.J. Matas, M.W. Steffes, R.L. Simmons, and F.C. Goetz, Human islet transplantation: a preliminary report. Transplant Proc 9 (1977) 233-6.

[31] D.E. Sutherland, A.J. Matas, and J.S. Najarian, Pancreatic islet cell transplantation. Surg Clin North Am 58 (1978) 365-82.

[32] D.E. Sutherland, A.J. Matas, F.C. Goetz, and J.S. Najarian, Transplantation of dispersed pancreatic islet tissue in humans: autografts and allografts. Diabetes 29 Suppl 1 (1980) 31-44.

[33] B.N. Gray, and E. Watkins, Jr., Prevention of vascular complications of diabetes by pancreatic islet transplantation. Arch Surg 111 (1976) 254-7.

[34] S.M. Mauer, M.W. Steffes, D.E. Sutherland, S. Najarian, A.F. Michael, and D.M. Brown, Studies of the rate of regression of the glomerular lesions in diabetic rats treated with pancreatic islet transplantation. Diabetes 24 (1975) 280-5.

[35] D.M. Thompson, I.S. Begg, C. Harris, Z. Ao, M.A. Fung, R.M. Meloche, P. Keown, G.S. Meneilly, R.J. Shapiro, S. Ho, K.G. Dawson, K. Al Ghofaili, L. Al Riyami, M. Al Mehthel, S.E. Kozak, S.O. Tong, and G.L. Warnock, Reduced progression of diabetic retinopathy after islet cell transplantation compared with intensive medical therapy. Transplantation 85 (2008) 1400-5.

[36] G.L. Warnock, D.M. Thompson, R.M. Meloche, R.J. Shapiro, Z. Ao, P. Keown, J.D. Johnson, C.B. Verchere, N. Partovi, I.S. Begg, M. Fung, S.E. Kozak, S.O. Tong, K.M. Alghofaili, and C. Harris, A multi-year analysis of islet transplantation compared with intensive medical therapy on progression of complications in type 1 diabetes. Transplantation 86 (2008) 1762-6.

[37] D.M. Thompson, M. Meloche, Z. Ao, B. Paty, P. Keown, R.J. Shapiro, S. Ho, D. Worsley, M. Fung, G. Meneilly, I. Begg, M. Al Mehthel, J. Kondi, C. Harris, B. Fensom, S.E. Kozak, S.O. Tong, M. Trinh, and G.L. Warnock, Reduced progression of diabetic microvascular complications with islet cell transplantation compared with intensive medical therapy. Transplantation 91 (2011) 373-8.

[38] R.W. Bilous, S.M. Mauer, D.E. Sutherland, J.S. Najarian, F.C. Goetz, and M.W. Steffes, The effects of pancreas transplantation on the glomerular structure of renal allografts in patients with insulin-dependent diabetes. N Engl J Med 321 (1989) 80-5.

[39] P. Fioretto, M.W. Steffes, D.E. Sutherland, F.C. Goetz, and M. Mauer, Reversal of lesions of diabetic nephropathy after pancreas transplantation. N Engl J Med 339 (1998) 69-75.

[40] W.R. Kennedy, X. Navarro, F.C. Goetz, D.E. Sutherland, and J.S. Najarian, Effects of pancreatic transplantation on diabetic neuropathy. N Engl J Med 322 (1990) 1031-7.

[41] R. Giannarelli, A. Coppelli, M.S. Sartini, M. Del Chiaro, F. Vistoli, G. Rizzo, M. Barsotti, S. Del Prato, F. Mosca, U. Boggi, and P. Marchetti, Pancreas transplant alone has beneficial effects on retinopathy in type 1 diabetic patients. Diabetologia 49 (2006) 2977-82.

[42] X. Navarro, D.E. Sutherland, and W.R. Kennedy, Long-term effects of pancreatic transplantation on diabetic neuropathy. Ann Neurol 42 (1997) 727-36.

[43] A.M. Shapiro, J.R. Lakey, E.A. Ryan, G.S. Korbutt, E. Toth, G.L. Warnock, N.M. Kneteman, and R.V. Rajotte, Islet transplantation in seven patients with type 1 diabetes mellitus using a glucocorticoid-free immunosuppressive regimen. N Engl J Med 343 (2000) 230-8.

[44] E.A. Ryan, J.R. Lakey, B.W. Paty, S. Imes, G.S. Korbutt, N.M. Kneteman, D. Bigam, R.V. Rajotte, and A.M. Shapiro, Successful islet transplantation: continued insulin reserve provides long-term glycemic control. Diabetes 51 (2002) 2148-57.

[45] E.A. Ryan, J.R. Lakey, R.V. Rajotte, G.S. Korbutt, T. Kin, S. Imes, A. Rabinovitch, J.F. Elliott, D. Bigam, N.M. Kneteman, G.L. Warnock, I. Larsen, and A.M. Shapiro, Clinical outcomes and insulin secretion after islet transplantation with the Edmonton protocol. Diabetes 50 (2001) 710-9.

[46] E.A. Ryan, B.W. Paty, P.A. Senior, D. Bigam, E. Alfadhli, N.M. Kneteman, J.R. Lakey, and A.M. Shapiro, Five-year follow-up after clinical islet transplantation. Diabetes 54 (2005) 2060-9.

[47] J.F. Markmann, S. Deng, X. Huang, N.M. Desai, E.H. Velidedeoglu, C. Lui, A. Frank, E. Markmann, M. Palanjian, K. Brayman, B. Wolf, E. Bell, M. Vitamaniuk, N. Doliba, F. Matschinsky, C.F. Barker, and A. Naji, Insulin independence following isolated islet transplantation and single islet infusions. Ann Surg 237 (2003) 741-9; discussion 749-50.

[48] T. Froud, C. Ricordi, D.A. Baidal, M.M. Hafiz, G. Ponte, P. Cure, A. Pileggi, R. Poggioli, H. Ichii, A. Khan, J.V. Ferreira, A. Pugliese, V.V. Esquenazi, N.S. Kenyon, and R. Alejandro, Islet transplantation in type 1 diabetes mellitus using cultured islets and steroid-free immunosuppression: Miami experience. Am J Transplant 5 (2005) 2037-46.

[49] B.J. Hering, Achieving and maintaining insulin independence in human islet transplant recipients. Transplantation 79 (2005) 1296-7.

[50] B.J. Hering, R. Kandaswamy, J.D. Ansite, P.M. Eckman, M. Nakano, T. Sawada, I. Matsumoto, S.H. Ihm, H.J. Zhang, J. Parkey, D.W. Hunter, and D.E. Sutherland, Single-donor, marginal-dose islet transplantation in patients with type 1 diabetes. JAMA 293 (2005) 830-5.

[51] M.D. Bellin, F.B. Barton, A. Heitman, J.V. Harmon, R. Kandaswamy, A.N. Balamurugan, D.E. Sutherland, R. Alejandro, and B.J. Hering, Potent induction immunotherapy promotes long-term insulin independence after islet transplantation in type 1 diabetes. Am J Transplant 12 (2012) 1576-83.

[52] M.D. Bellin, R. Kandaswamy, J. Parkey, H.J. Zhang, B. Liu, S.H. Ihm, J.D. Ansite, J. Witson, P. Bansal-Pakala, A.N. Balamurugan, K.K. Papas, D.E. Sutherland, A. Moran, and B.J. Hering, Prolonged insulin independence after islet allotransplants in recipients with type 1 diabetes. Am J Transplant 8 (2008) 2463-70.

[53] A. Frank, S. Deng, X. Huang, E. Velidedeoglu, Y.S. Bae, C. Liu, P. Abt, R. Stephenson, M. Mohiuddin, T. Thambipillai, E. Markmann, M. Palanjian, M. Sellers, A. Naji, C.F. Barker, and J.F. Markmann, Transplantation for type I diabetes: comparison of vascularized whole-organ pancreas with isolated pancreatic islets. Ann Surg 240 (2004) 631-40; discussion 640-3.

[54] K.K. Papas, T.M. Suszynski, and C.K. Colton, Islet assessment for transplantation. Curr Opin Organ Transplant 14 (2009) 674-82.

[55] T.M. Suszynski, G.M. Wildey, E.J. Falde, G.W. Cline, K.S. Maynard, N. Ko, J. Sotiris, A. Naji, B.J. Hering, and K.K. Papas, The ATP/DNA ratio is a better indicator of islet cell viability than the ADP/ATP ratio. Transplant Proc 40 (2008) 346-50.

[56] T.M. Suszynski, E.S. Avgoustiniatos, S.A. Stein, E.J. Falde, B.E. Hammer, and K.K. Papas, Assessment of tissue-engineered islet graft viability by fluorine magnetic resonance spectroscopy. Transplant Proc 43 (2011) 3221-5.

[57] T.M. Suszynski, M.D. Rizzari, W.E. Scott, 3rd, L.A. Tempelman, M.J. Taylor, and K.K. Papas, Persufflation (or gaseous oxygen perfusion) as a method of organ preservation. Cryobiology 64 (2012) 125-43.

[58] T.M. Suszynski, M.D. Rizzari, L.S. Kidder, K. Mueller, C.S. Chapman, J.P. Kitzmann, R.L. Pongratz, G.W. Cline, P.W. Todd, D.J. Kennedy, T.D. O'Brien, E.S. Avgoustiniatos, H.J. Schuurman, and K.K. Papas, Paramagnetic microparticles do not elicit islet cytotoxicity with co-culture or host immune reactivity after implantation. Xenotransplantation 18 (2011) 239-44.

[59] M.D. Rizzari, T.M. Suszynski, L.S. Kidder, S.A. Stein, T.D. O'Brien, V.S. Sajja, W.E. Scott, 3rd, V.A. Kirchner, B.P. Weegman, E.S. Avgoustiniatos, P.W. Todd, D.J. Kennedy, B.E. Hammer, D.E. Sutherland, B.J. Hering, and K.K. Papas, Surgical protocol involving the infusion of paramagnetic microparticles for preferential incorporation within porcine islets. Transplant Proc 42 (2010) 4209-12.

[60] T. Minor, W.E. Scott, 3rd, M.D. Rizzari, T.M. Suszynski, B. Luer, P. Efferz, K.K. Papas, and A. Paul, Energetic recovery in porcine grafts by minimally invasive liver oxygenation. J Surg Res (2012).

[61] B.P. Weegman, V.A. Kirchner, W.E. Scott III, E.S. Avgoustiniatos, T.M. Suszynski, J. Ferrer-Fabrega, M.D. Rizzari, L.S. Kidder, K. R, D.E. Sutherland, and K.K. Papas, Continuous real-time viability assessment of kidneys based on oxygen consumption. Transplant Proc 42 (2010) 2020-2023.

[62] W.E. Scott III, T.D. O'Brien, J. Ferrer-Fabrega, E.S. Avgoustiniatos, B.P. Weegman, T. Anazawa, S. Matsumoto, V. Kirchner, M. Rizzari, M.P. Murtaugh, T.M. Suszynski, T. Aasheim, L.S. Kidder, B.E. Hammer, S.G. Stone, L.A. Tempelman, D.E. Sutherland, B.J. Hering, and K.K. Papas, Persufflation improves pancreas preservation when compared with the two-layer method (TLM). Transplant Proc 42 (2010) 2016-2019.

[63] W.E. Scott III, B.P. Weegman, J. Ferrer-Fabrega, S.A. Stein, T. Anazawa, V. Kirchner, M. Rizzari, J. Stone, S. Matsumoto, B.E. Hammer, A.N. Balamurugan, L.S. Kidder, T.M. Suszynski, E.S. Avgoustiniatos, S.G. Stone, L.A. Tempelman, D.E. Sutherland, B.J. Hering, and K.K. Papas, Pancreas oxygen persufflation increases ATP levels as shown by nuclear magnetic resonance. Transplant Proc 42 (2010) 2011-2015.

[64] J. Ferrer, W.E. Scott, 3rd, B.P. Weegman, T.M. Suszynski, D.E. Sutherland, B.J. Hering, and K.K. Papas, Pig pancreas anatomy: implications for pancreas procurement, preservation, and islet isolation. Transplantation 86 (2008) 1503-10.

[65] E.S. Avgoustiniatos, B.J. Hering, P.R. Rozak, J.R. Wilson, L.A. Tempelman, A.N. Balamurugan, D.P. Welch, B.P. Weegman, T.M. Suszynski, and K.K. Papas, Commercially available gas-permeable cell culture bags may not prevent anoxia in cultured or shipped islets. Transplant Proc 40 (2008) 395-400.

[66] E.S. Avgoustiniatos, W.E. Scott III, T.M. Suszynski, H.J. Schuurman, R. Nelson, P.R. Rozak, K. Mueller, A.N. Balamurugan, J. Ansite, D. Fraga, A. Friberg, G.M.

Wildey, T. Tanaka, C. Lyons, D.E. Sutherland, B. Hering, and K.K. Papas, Supplements in human islet culture: human serum albumin is inferior to fetal bovine serum. Cell Transplant (in press) (2012).

[67] E.S. Avgoustiniatos, P.R. Rozak, K. Mueller, C. Lyons, W.E. Scott III, T.M. Suszynski, B.P. Perrault, E.J. Falde, J.P. Kitzmann, D.P. Welch, J.R. Wilson, A.N. Balamurugan, B. Hering, and K.K. Papas, Silicone rubber membrane devices allow islet culture at 20 times the standard surface density with no adverse effects on viability, recovery, or potency. Cell Transplant (submitted) (2012).

[68] A.M. Shapiro, C. Ricordi, B.J. Hering, H. Auchincloss, R. Lindblad, R.P. Robertson, A. Secchi, M.D. Brendel, T. Berney, D.C. Brennan, E. Cagliero, R. Alejandro, E.A. Ryan, B. DiMercurio, P. Morel, K.S. Polonsky, J.A. Reems, R.G. Bretzel, F. Bertuzzi, T. Froud, R. Kandaswamy, D.E. Sutherland, G. Eisenbarth, M. Segal, J. Preiksaitis, G.S. Korbutt, F.B. Barton, L. Viviano, V. Seyfert-Margolis, J. Bluestone, and J.R. Lakey, International trial of the Edmonton protocol for islet transplantation. N Engl J Med 355 (2006) 1318-30.

[69] P.Y. Benhamou, L. Milliat-Guittard, A. Wojtusciszyn, L. Kessler, C. Toso, R. Baertschiger, I. Debaty, L. Badet, A. Penfornis, C. Thivolet, E. Renard, F. Bayle, P. Morel, E. Morelon, C. Colin, and T. Berney, Quality of life after islet transplantation: data from the GRAGIL 1 and 2 trials. Diabet Med 26 (2009) 617-21.

[70] A. Hogan, A. Pileggi, and C. Ricordi, Transplantation: current developments and future directions; the future of clinical islet transplantation as a cure for diabetes. Front Biosci 13 (2008) 1192-205.

[71] B. Keymeulen, P. Gillard, C. Mathieu, B. Movahedi, G. Maleux, G. Delvaux, D. Ysebaert, B. Roep, E. Vandemeulebroucke, M. Marichal, P. In 't Veld, M.

Bogdani, C. Hendrieckx, F. Gorus, Z. Ling, J. van Rood, and D. Pipeleers, Correlation between beta cell mass and glycemic control in type 1 diabetic recipients of islet cell graft. Proc Natl Acad Sci U S A 103 (2006) 17444-9.

[72] C.B. Leitao, T. Tharavanij, P. Cure, A. Pileggi, D.A. Baidal, C. Ricordi, and R. Alejandro, Restoration of hypoglycemia awareness after islet transplantation. Diabetes Care 31 (2008) 2113-5.

[73] C. Ricordi, B.J. Hering, and A.M. Shapiro, Beta-cell transplantation for diabetes therapy. Lancet 372 (2008) 27-8; author reply 29-30.

[74] T. Tharavanij, A. Betancourt, S. Messinger, P. Cure, C.B. Leitao, D.A. Baidal, T. Froud, C. Ricordi, and R. Alejandro, Improved long-term health-related quality of life after islet transplantation. Transplantation 86 (2008) 1161-7.

[75] D.J. Weber, FDA regulation of allogeneic islets as a biological product. Cell Biochem Biophys 40 (2004) 19-22.

[76] M.J. Barnett, D. McGhee-Wilson, A.M. Shapiro, and J.R. Lakey, Variation in human islet viability based on different membrane integrity stains. Cell Transplant 13 (2004) 481-8.

[77] I.C. Gerling, M. Kotb, D. Fraga, O. Sabek, and A.O. Gaber, No correlation between in vitro and in vivo function of human islets. Transplant Proc 30 (1998) 587-8.

[78] C. Ricordi, J.R. Lakey, and B.J. Hering, Challenges toward standardization of islet isolation technology. Transplant Proc 33 (2001) 1709.

[79] F. Bertuzzi, and C. Ricordi, Prediction of clinical outcome in islet allotransplantation. Diabetes Care 30 (2007) 410-7.

[80] C. Ricordi, Quantitative and qualitative standards for islet isolation assessment in humans and large mammals. Pancreas 6 (1991) 242-4.

[81] C.K. Colton, K.K. Papas, A. Pisania, M.J. Rappel, D.E. Powers, J.J. O'Neil, A. Omer, G.C. Weir, and S. Bonner-Weir, Characterization of islet preparations. in: C. Halberstadt, and D.F. Emerich, (Eds.), Cellular Transplantation: From Laboratory to Clinic, Academic Press, Waltham, MA, 2007, pp. 85-134.

[82] L.A. Fernandez, E.W. Hatch, B. Armann, J.S. Odorico, D.A. Hullett, H.W. Sollinger, and M.S. Hanson, Validation of large particle flow cytometry for the analysis and sorting of intact pancreatic islets. Transplantation 80 (2005) 729-37.

[83] A. Pisania, K.K. Papas, D.E. Powers, M.J. Rappel, A. Omer, S. Bonner-Weir, G.C. Weir, and C.K. Colton, Enumeration of islets by nuclei counting and light microscopic analysis. Lab Invest 90 (2010) 1676-86.

[84] H. Ichii, L. Inverardi, A. Pileggi, R.D. Molano, O. Cabrera, A. Caicedo, S. Messinger, Y. Kuroda, P.O. Berggren, and C. Ricordi, A novel method for the assessment of cellular composition and beta-cell viability in human islet preparations. Am J Transplant 5 (2005) 1635-45.

[85] A. Pisania, G.C. Weir, J.J. O'Neil, A. Omer, V. Tchipashvili, J. Lei, C.K. Colton, and S. Bonner-Weir, Quantitative analysis of cell composition and purity of human pancreatic islet preparations. Lab Invest 90 (2010) 1661-75.

[86] C.N. Street, J.R. Lakey, A.M. Shapiro, S. Imes, R.V. Rajotte, E.A. Ryan, J.G. Lyon, T. Kin, J. Avila, T. Tsujimura, and G.S. Korbutt, Islet graft assessment in the Edmonton Protocol: implications for predicting long-term clinical outcome. Diabetes 53 (2004) 3107-14.

[87] K.E. Dionne, C.K. Colton, and M.L. Yarmush, Effect of hypoxia on insulin secretion by isolated rat and canine islets of Langerhans. Diabetes 42 (1993) 12-21.

[88] N.J. London, S.M. Thirdborough, S.M. Swift, P.R. Bell, and R.F. James, The diabetic "human reconstituted" severe combined immunodeficient (SCID-hu)

mouse: a model for isogeneic, allogeneic, and xenogeneic human islet transplantation. Transplant Proc 23 (1991) 749.

[89] C. Ricordi, D.W. Scharp, and P.E. Lacy, Reversal of diabetes in nude mice after transplantation of fresh and 7-day-cultured (24 degrees C) human pancreatic islets. Transplantation 45 (1988) 994-6.

[90] B. Armann, M.S. Hanson, E. Hatch, A. Steffen, and L.A. Fernandez, Quantification of basal and stimulated ROS levels as predictors of islet potency and function. Am J Transplant 7 (2007) 38-47.

[91] C. Fraker, M.R. Timmins, R.D. Guarino, P.D. Haaland, H. Ichii, D. Molano, A. Pileggi, R. Poggioli, S.C. Presnell, L. Inverardi, M. Zehtab, and C. Ricordi, The use of the BD oxygen biosensor system to assess isolated human islets of langerhans: oxygen consumption as a potential measure of islet potency. Cell Transplant 15 (2006) 745-58.

[92] M. Goto, H. Abe, T. Ito-Sasaki, A. Inagaki, N. Ogawa, K. Fujimori, Y. Kurokawa, T. Matsue, and S. Satomi, A novel predictive method for assessing the quality of isolated pancreatic islets using scanning electrochemical microscopy. Transplant Proc 41 (2009) 311-3.

[93] M. Goto, J. Holgersson, M. Kumagai-Braesch, and O. Korsgren, The ADP/ATP ratio: A novel predictive assay for quality assessment of isolated pancreatic islets. Am J Transplant 6 (2006) 2483-7.

[94] M.S. Hanson, A. Steffen, J.S. Danobeitia, B. Ludwig, and L.A. Fernandez, Flow cytometric quantification of glucose-stimulated beta-cell metabolic flux can reveal impaired islet functional potency. Cell Transplant 17 (2008) 1337-47.

[95] J.H. Kim, S.G. Park, H.N. Lee, Y.Y. Lee, H.S. Park, H.I. Kim, J.E. Yu, S.H. Kim, C.G. Park, J. Ha, S.J. Kim, and K.S. Park, ATP measurement predicts porcine islet transplantation outcome in nude mice. Transplantation 87 (2009) 166-9.

[96] J.S. Mohammed, Y. Wang, T.A. Harvat, J. Oberholzer, and D.T. Eddington, Microfluidic device for multimodal characterization of pancreatic islets. Lab Chip 9 (2009) 97-106.

[97] K.K. Papas, C.K. Colton, R.A. Nelson, P.R. Rozak, E.S. Avgoustiniatos, W.E. Scott, 3rd, G.M. Wildey, A. Pisania, G.C. Weir, and B.J. Hering, Human islet oxygen consumption rate and DNA measurements predict diabetes reversal in nude mice. Am J Transplant 7 (2007) 707-13.

[98] K.K. Papas, A. Pisania, H. Wu, G.C. Weir, and C.K. Colton, A stirred microchamber for oxygen consumption rate measurements with pancreatic islets. Biotechnol Bioeng 98 (2007) 1071-82.

[99] I.R. Sweet, M. Gilbert, S. Scott, I. Todorov, R. Jensen, I. Nair, I. Al-Abdullah, J. Rawson, F. Kandeel, and K. Ferreri, Glucose-stimulated increment in oxygen consumption rate as a standardized test of human islet quality. Am J Transplant 8 (2008) 183-92.

[100] T. Yamamoto, A. Horiguchi, M. Ito, H. Nagata, H. Ichii, C. Ricordi, and S. Miyakawa, Quality control for clinical islet transplantation: organ procurement and preservation, the islet processing facility, isolation, and potency tests. J Hepatobiliary Pancreat Surg 16 (2009) 131-6.

[101] M. Koulmanda, K.K. Papas, A. Qipo, H. Wu, R.N. Smith, G.C. Weir, H. Auchincloss, and C.K. Colton, Islet oxygen consumption rate as a predictor of in vivo efficacy post-transplantation, 7th Congress of the International Xenotransplantation Association, Xenotransplantation, Glasgow, Ireland, 2003, pp. 484.

[102] D.W. Gray, The role of exocrine tissue in pancreatic islet transplantation. Transpl Int 2 (1989) 41-5.

[103] D.W. Gray, and P.J. Morris, Developments in isolated pancreatic islet transplantation. Transplantation 43 (1987) 321-31.

[104] U.J. Hesse, D.E. Sutherland, P.F. Gores, A. Sitges-Serra, and J.S. Najarian, Comparison of splenic and renal subcapsular islet autografting in dogs. Transplantation 41 (1986) 271-4.

[105] R. Caiazzo, V. Gmyr, B. Kremer, T. Hubert, B. Soudan, B. Lukowiak, B. Vandewalle, M.C. Vantyghem, F. Pattou, and J. Kerr-Conte, Quantitative in vivo islet potency assay in normoglycemic nude mice correlates with primary graft function after clinical transplantation. Transplantation 86 (2008) 360-3.

[106] Y. Yonekawa, T. Okitsu, K. Wake, Y. Iwanaga, H. Noguchi, H. Nagata, X. Liu, N. Kobayashi, and S. Matsumoto, A new mouse model for intraportal islet transplantation with limited hepatic lobe as a graft site. Transplantation 82 (2006) 712-5.

[107] F. Thomas, J. Wu, J.L. Contreras, C. Smyth, G. Bilbao, J. He, and J. Thomas, A tripartite anoikis-like mechanism causes early isolated islet apoptosis. Surgery 130 (2001) 333-8.

[108] P. Cattan, T. Berney, S. Schena, R.D. Molano, A. Pileggi, C. Vizzardelli, C. Ricordi, and L. Inverardi, Early assessment of apoptosis in isolated islets of Langerhans. Transplantation 71 (2001) 857-62.

[109] D.G. Pipeleers, M. Pipeleers-Marichal, J.C. Hannaert, M. Berghmans, P.A. In't Veld, J. Rozing, M. Van de Winkel, and W. Gepts, Transplantation of purified islet cells in diabetic rats. I. Standardization of islet cell grafts. Diabetes 40 (1991) 908-19.

[110] D.G. Pipeleers, and M.A. Pipeleers-Marichal, A method for the purification of single A, B and D cells and for the isolation of coupled cells from isolated rat islets. Diabetologia 20 (1981) 654-63.

[111] G.C. Weir, P.A. Halban, P. Meda, C.B. Wollheim, L. Orci, and A.E. Renold, Dispersed adult rat pancreatic islet cells in culture: A, B, and D cell function. Metabolism 33 (1984) 447-53.

[112] K.K. Papas, I. Constantinidis, and A. Sambanis, Cultivation of recombinant, insulin-secreting AtT-20 cells as free and entrapped spheroids. Cytotechnology 13 (1993) 1-12.

[113] A. Pisania, Development of quantitative methods for quality assessment of islets of Langerhans, Department of Chemical Engineering, Massachusetts Institute of Technology, Cambridge, MA, 2007.

[114] B.M. Stubenitsky, M.M. Booster, L. Brasile, E.M. Green, C.E. Haisch, H.K. Singh, R.W. Jacobs, and G. Kootstra, II: Ex vivo viability testing of kidneys after postmortem warm ischemia. ASAIO J 46 (2000) 62-4.

[115] H. Yang, X.M. Jia, J.P. Acker, G. Lung, and L.E. McGann, Routine assessment of viability in split-thickness skin. J Burn Care Rehabil 21 (2000) 99-104.

[116] Y. Zhang, N. Ohkohchi, K. Oikawa, K. Sasaki, and S. Satomi, Assessment of viability of the liver graft in different cardiac arrest models. Transplant Proc 32 (2000) 2345-7.

[117] R. Ricciardi, D.P. Foley, S.H. Quarfordt, F.J. Vittimberga, R.D. Kim, S.E. Donohue, S.M. Wheeler, S. Anwaruddin, M.P. Callery, and W.C. Meyers, Hemodynamic and metabolic variables predict porcine ex vivo liver function. J Surg Res 96 (2001) 114-9.

[118] S. Schwitalla, F. Heres, F.W. Rohl, G. Pfau, and C. Kessling, [Intraoperative oxygen consumption and organ function in liver transplantation]. Anaesthesiol Reanim 26 (2001) 88-94.

[119] J. Martin, C. Yerebakan, H. Goebel, C. Benk, M. Krause, G. Derjung, G. Lutter, M. Siegenthaler, and F. Beyersdorf, Viability of the myocardium after twenty-four-hour heart conservation--a preliminary study. Thorac Cardiovasc Surg 51 (2003) 196-203.

[120] I.R. Sweet, and M. Gilbert, Contribution of calcium influx in mediating glucose-stimulated oxygen consumption in pancreatic islets. Diabetes 55 (2006) 3509-19.

[121] K.K. Papas, C.K. Colton, A. Qipo, H. Wu, R.A. Nelson, B.J. Hering, G.C. Weir, and M. Koulmanda, Prediction of marginal mass required for successful islet transplantation. J Invest Surg 23 (2010) 28-34.

[122] W. Wang, L. Upshaw, D.M. Strong, R.P. Robertson, and J. Reems, Increased oxygen consumption rates in response to high glucose detected by a novel oxygen biosensor system in non-human primate and human islets. J Endocrinol 185 (2005) 445-55.

[123] K.K. Papas, R.C. Long, Jr., A. Sambanis, and I. Constantinidis, Development of a bioartificial pancreas: I. long-term propagation and basal and induced secretion from entrapped betaTC3 cell cultures. Biotechnol Bioeng 66 (1999) 219-30.

[124] K.K. Papas, R.C. Long, Jr., A. Sambanis, and I. Constantinidis, Development of a bioartificial pancreas: II. Effects of oxygen on long-term entrapped betaTC3 cell cultures. Biotechnol Bioeng 66 (1999) 231-7.

[125] N.E. Mukundan, P.C. Flanders, I. Constantinidis, K.K. Papas, and A. Sambanis, Oxygen consumption rates of free and alginate-entrapped beta TC3 mouse insulinoma cells. Biochem Biophys Res Commun 210 (1995) 113-8.

[126] C.A. Low, Transient oxygen consumption rate measurements with the BD Oxygen Biosensor System, Department of Chemical Engineering, Massachusetts Institute of Technology, Cambridge, MA, 2008.

[127] B. Migliavacca, R. Nano, B. Antonioli, S. Marzorati, A.M. Davalli, V. Di Carlo, and F. Bertuzzi, Identification of in vitro parameters predictive of graft function: a study in an animal model of islet transplantation. Transplant Proc 36 (2004) 612-3.

[128] M.R. Rickels, M.H. Schutta, J.F. Markmann, C.F. Barker, A. Naji, and K.L. Teff, {beta}-Cell function following human islet transplantation for type 1 diabetes. Diabetes 54 (2005) 100-6.

[129] O. Korsgren, B. Nilsson, C. Berne, M. Felldin, A. Foss, R. Kallen, T. Lundgren, K. Salmela, A. Tibell, and G. Tufveson, Current status of clinical islet transplantation. Transplantation 79 (2005) 1289-93.

[130] M. Erecinska, J. Bryla, M. Michalik, M.D. Meglasson, and D. Nelson, Energy metabolism in islets of Langerhans. Biochim Biophys Acta 1101 (1992) 273-95.

[131] K.K. Papas, C.K. Colton, J.S. Gounarides, E.S. Roos, M.A. Jarema, M.J. Shapiro, L.L. Cheng, G.W. Cline, G.I. Shulman, H. Wu, S. Bonner-Weir, and G.C. Weir, NMR spectroscopy in beta cell engineering and islet transplantation. Ann N Y Acad Sci 944 (2001) 96-119.

[132] K.K. Papas, R.C. Long, Jr., I. Constantinidis, and A. Sambanis, Role of ATP and Pi in the mechanism of insulin secretion in the mouse insulinoma betaTC3 cell line. Biochem J 326 (Pt 3) (1997) 807-14.

[133] B. Alberts, A. Johnson, J. Lewis, M. Raff, K. Roberts, and P. Walter, Cell Chemistry and Biosynthesis, Molecular biology of the cell, Garland Science, New York, NY, 2002, pp. 47-128.

[134] N.M. Doliba, S.L. Wehrli, A.M. Babsky, and M.D. Osbakken, Encapsulation and perfusion of mitochondria in agarose beads for functional studies with 31P-NMR spectroscopy. Magn Reson Med 39 (1998) 679-84.

[135] H.E. Hohmeier, H. Mulder, G. Chen, R. Henkel-Rieger, M. Prentki, and C.B. Newgard, Isolation of INS-1-derived cell lines with robust ATP-sensitive K+ channel-dependent and -independent glucose-stimulated insulin secretion. Diabetes 49 (2000) 424-30.

[136] G.W. Cline, R.L. Lepine, K.K. Papas, R.G. Kibbey, and G.I. Shulman, 13C NMR isotopomer analysis of anaplerotic pathways in INS-1 cells. J Biol Chem 279 (2004) 44370-5.

[137] R.G. Kibbey, R.L. Pongratz, A.J. Romanelli, C.B. Wollheim, G.W. Cline, and G.I. Shulman, Mitochondrial GTP regulates glucose-stimulated insulin secretion. Cell Metab 5 (2007) 253-64.

[138] D.A. Bradbury, T.D. Simmons, K.J. Slater, and S.P. Crouch, Measurement of the ADP:ATP ratio in human leukaemic cell lines can be used as an indicator of cell viability, necrosis and apoptosis. J Immunol Methods 240 (2000) 79-92.

[139] M.V. Zamaraeva, R.Z. Sabirov, E. Maeno, Y. Ando-Akatsuka, S.V. Bessonova, and Y. Okada, Cells die with increased cytosolic ATP during apoptosis: a bioluminescence study with intracellular luciferase. Cell Death Differ 12 (2005) 1390-7.

[140] P.M. Alves, L.L. Fonseca, C.C. Peixoto, A.C. Almeida, M.J. Carrondo, and H. Santos, NMR studies on energy metabolism of immobilized primary neurons and astrocytes during hypoxia, ischemia and hypoglycemia. NMR Biomed 13 (2000) 438-48.

[141] P.J. Harvey, J.E. Gready, H.M. Hickey, D.G. Le Couteur, and A.J. McLean, 31P and 1H NMR spectroscopic studies of liver extracts of carbon tetrachloride-treated rats. NMR Biomed 12 (1999) 395-401.

[142] T. Ueda, H.S. Ho, S.E. Anderson, and Y. Takeyama, Pancreatitis-induced ascitic fluid and hepatocellular dysfunction in severe acute pancreatitis. J Surg Res 82 (1999) 305-11.

[143] A.M. Shapiro, C. Ricordi, and B. Hering, Edmonton's islet success has indeed been replicated elsewhere. Lancet 362 (2003) 1242.

[144] L. Moberg, H. Johansson, A. Lukinius, C. Berne, A. Foss, R. Kallen, O. Ostraat, K. Salmela, A. Tibell, G. Tufveson, G. Elgue, K. Nilsson Ekdahl, O. Korsgren, and B. Nilsson, Production of tissue factor by pancreatic islet cells as a trigger of detrimental thrombotic reactions in clinical islet transplantation. Lancet 360 (2002) 2039-45.

[145] A.M. Davalli, Y. Ogawa, C. Ricordi, D.W. Scharp, S. Bonner-Weir, and G.C. Weir, A selective decrease in the beta cell mass of human islets transplanted into diabetic nude mice. Transplantation 59 (1995) 817-20.

[146] V.A. Huurman, R. Hilbrands, G.G. Pinkse, P. Gillard, G. Duinkerken, P. van de Linde, P.M. van der Meer-Prins, M.F. Versteeg-van der Voort Maarschalk, K. Verbeeck, B.Z. Alizadeh, C. Mathieu, F.K. Gorus, D.L. Roelen, F.H. Claas, B. Keymeulen, D.G. Pipeleers, and B.O. Roep, Cellular islet autoimmunity associates with clinical outcome of islet cell transplantation. PLoS One 3 (2008) e2435.

[147] N.M. Desai, J.A. Goss, S. Deng, B.A. Wolf, E. Markmann, M. Palanjian, A.P. Shock, S. Feliciano, F.C. Brunicardi, C.F. Barker, A. Naji, and J.F. Markmann, Elevated portal vein drug levels of sirolimus and tacrolimus in islet transplant

recipients: local immunosuppression or islet toxicity? Transplantation 76 (2003) 1623-5.

[148] B.W. Paty, J.S. Harmon, C.L. Marsh, and R.P. Robertson, Inhibitory effects of immunosuppressive drugs on insulin secretion from HIT-T15 cells and Wistar rat islets. Transplantation 73 (2002) 353-7.

[149] M. Laugharne, S. Cross, S. Richards, C. Dawson, L. Ilchyshyn, M. Saleem, P. Mathieson, and R. Smith, Sirolimus toxicity and vascular endothelial growth factor release from islet and renal cell lines. Transplantation 83 (2007) 1635-8.

[150] G.G. Pinkse, W.P. Bouwman, R. Jiawan-Lalai, O.T. Terpstra, J.A. Bruijn, and E. de Heer, Integrin signaling via RGD peptides and anti-beta1 antibodies confers resistance to apoptosis in islets of Langerhans. Diabetes 55 (2006) 312-7.

[151] X. Chen, and D.B. Kaufman, Bioluminescent imaging of transplanted islets. Methods Mol Biol 574 (2009) 75-85.

[152] Z. Medarova, and A. Moore, MRI as a tool to monitor islet transplantation. Nat Rev Endocrinol 5 (2009) 444-52.

[153] G.E. Arteel, R.G. Thurman, J.M. Yates, and J.A. Raleigh, Evidence that hypoxia markers detect oxygen gradients in liver: pimonidazole and retrograde perfusion of rat liver. Br J Cancer 72 (1995) 889-95.

[154] P.O. Carlsson, F. Palm, and G. Mattsson, Low revascularization of experimentally transplanted human pancreatic islets. J Clin Endocrinol Metab 87 (2002) 5418-23.

[155] J. Lau, and P.O. Carlsson, Low revascularization of human islets when experimentally transplanted into the liver. Transplantation 87 (2009) 322-5.

[156] G. Mattsson, L. Jansson, and P.O. Carlsson, Decreased vascular density in mouse pancreatic islets after transplantation. Diabetes 51 (2002) 1362-6.

[157] R. Olsson, J. Olerud, U. Pettersson, and P.O. Carlsson, Increased numbers of low-oxygenated pancreatic islets after intraportal islet transplantation. Diabetes 60 (2011) 2350-3.

[158] N. Sekine, V. Cirulli, R. Regazzi, L.J. Brown, E. Gine, J. Tamarit-Rodriguez, M. Girotti, S. Marie, M.J. MacDonald, C.B. Wollheim, and et al., Low lactate dehydrogenase and high mitochondrial glycerol phosphate dehydrogenase in pancreatic beta-cells. Potential role in nutrient sensing. J Biol Chem 269 (1994) 4895-902.

[159] N. Lifson, K.G. Kramlinger, R.R. Mayrand, and E.J. Lender, Blood flow to the rabbit pancreas with special reference to the islets of Langerhans. Gastroenterology 79 (1980) 466-73.

[160] P.E. Lacy, The pancreatic beta cell. Structure and function. N Engl J Med 276 (1967) 187-95.

[161] Y. Stefan, L. Orci, F. Malaisse-Lagae, A. Perrelet, Y. Patel, and R.H. Unger, Quantitation of endocrine cell content in the pancreas of nondiabetic and diabetic humans. Diabetes 31 (1982) 694-700.

[162] S. Bonner-Weir, Morphological evidence for pancreatic polarity of beta-cell within islets of Langerhans. Diabetes 37 (1988) 616-21.

[163] E.S. Avgoustiniatos, K.E. Dionne, D.F. Wilson, M.L. Yarmush, and C.K. Colton, Measurements of the effective diffusion coefficient in pancreatic islets. Ind Eng Chem Res 46 (2007) 6157-6163.

[164] K.E. Dionne, Effect of hypoxia on insulin secretion and viability of pancreatic tissue., Department of Chemical Engineering, Massachusetts Institute of Technology, Cambridge, MA, 1990.

[165] C.A. Acevedo, C. Weinstein-Oppenheimer, D.I. Brown, H. Huebner, R. Buchholz, and M.E. Young, A mathematical model for the design of fibrin microcapsules with skin cells. Bioprocess Biosyst Eng 32 (2009) 341-51.

[166] E.S. Avgoustiniatos, Oxygen diffusion limitations in pancreatic islet culture and immunoisolation, Department of Chemical Engineering, Massachusetts Institute of Technology, Cambridge, MA, 2002.

[167] K.K. Papas, 2012.

[168] I. Anundi, and H. de Groot, Hypoxic liver cell death: critical Po2 and dependence of viability on glycolysis. Am J Physiol 257 (1989) G58-64.

[169] K.E. Dionne, C.K. Colton, and M.L. Yarmush, Effect of oxygen on isolated pancreatic tissue. ASAIO Trans 35 (1989) 739-41.

[170] K.K. Papas, R.C. Long, Jr., I. Constantinidis, and A. Sambanis, Effects of oxygen on metabolic and secretory activities of beta TC3 cells. Biochim Biophys Acta 1291 (1996) 163-6.

[171] S. Moskalewski, Isolation and Culture of the Islets of Langerhans of the Guinea Pig. Gen Comp Endocrinol 44 (1965) 342-53.

[172] P.E. Lacy, and M. Kostianovsky, Method for the isolation of intact islets of Langerhans from the rat pancreas. Diabetes 16 (1967) 35-9.

[173] D.E. Sutherland, M.W. Steffes, G.E. Bauer, D. McManus, B.D. Noe, and J.S. Najarian, Isolation of human and porcine islets of Langerhans and islet transplantation in pigs. J Surg Res 16 (1974) 102-11.

[174] J.S. Najarian, D.E.R. Sutherland, and M.W. Steffes, Isolation of human islets of Langerhans for transplantation. Transplant Proc 7 (1975) 611-613.

[175] W.F. Ballinger, and P.E. Lacy, Transplantation of intact pancreatic islets in rats. Surgery 72 (1972) 175-86.

[176] C.B. Kemp, M.J. Knight, D.W. Scharp, W.F. Ballinger, and P.E. Lacy, Effect of transplantation site on the results of pancreatic islet isografts in diabetic rats. Diabetologia 9 (1973) 486-91.

[177] C.B. Kemp, D.W. Scharp, M.J. Knight, W.F. Ballinger, and P.E. Lacy, Importance of implantation site of pancreatic islet isografts in treatment of experimental diabetes. Surg Forum 24 (1973) 297-9.

[178] J.S. Najarian, D.E. Sutherland, D. Baumgartner, B. Burke, J.J. Rynasiewicz, A.J. Matas, and F.C. Goetz, Total or near total pancreatectomy and islet autotransplantation for treatment of chronic pancreatitis. Ann Surg 192 (1980) 526-42.

[179] J.S. Najarian, D.E. Sutherland, A.J. Matas, and F.C. Goetz, Human islet autotransplantation following pancreatectomy. Transplant Proc 11 (1979) 336-40.

[180] C. Ricordi, P.E. Lacy, E.H. Finke, B.J. Olack, and D.W. Scharp, Automated method for isolation of human pancreatic islets. Diabetes 37 (1988) 413-20.

[181] C. Ricordi, P.E. Lacy, and D.W. Scharp, Automated islet isolation from human pancreas. Diabetes 38 Suppl 1 (1989) 140-2.

[182] B.J. Hering, R. Kandaswamy, J.V. Harmon, J.D. Ansite, S.M. Clemmings, T. Sakai, S. Paraskevas, P.M. Eckman, J. Sageshima, M. Nakano, T. Sawada, I. Matsumoto, H.J. Zhang, D.E. Sutherland, and J.A. Bluestone, Transplantation of cultured islets from two-layer preserved pancreases in type 1 diabetes with anti-CD3 antibody. Am J Transplant 4 (2004) 390-401.

[183] D.E. Sutherland, A.C. Gruessner, A.M. Carlson, J.J. Blondet, A.N. Balamurugan, K.F. Reigstad, G.J. Beilman, M.D. Bellin, and B.J. Hering, Islet autotransplant outcomes after total pancreatectomy: a contrast to islet allograft outcomes. Transplantation 86 (2008) 1799-802.

[184] M.D. Bellin, D.E. Sutherland, G.J. Beilman, I. Hong-McAtee, A.N. Balamurugan, B.J. Hering, and A. Moran, Similar islet function in islet allotransplant and autotransplant recipients, despite lower islet mass in autotransplants. Transplantation 91 (2011) 367-72.

[185] S. Bonner-Weir, D.F. Trent, and G.C. Weir, Partial pancreatectomy in the rat and subsequent defect in glucose-induced insulin release. J Clin Invest 71 (1983) 1544-53.

[186] J.L. Leahy, H.E. Cooper, D.A. Deal, and G.C. Weir, Chronic hyperglycemia is associated with impaired glucose influence on insulin secretion. A study in normal rats using chronic in vivo glucose infusions. J Clin Invest 77 (1986) 908-15.

[187] K.S. Polonsky, B.D. Given, L.J. Hirsch, H. Tillil, E.T. Shapiro, C. Beebe, B.H. Frank, J.A. Galloway, and E. Van Cauter, Abnormal patterns of insulin secretion in non-insulin-dependent diabetes mellitus. N Engl J Med 318 (1988) 1231-9.

[188] D.R. Laybutt, A.M. Preston, M.C. Akerfeldt, J.G. Kench, A.K. Busch, A.V. Biankin, and T.J. Biden, Endoplasmic reticulum stress contributes to beta cell apoptosis in type 2 diabetes. Diabetologia 50 (2007) 752-63.

[189] A. Lorenzo, B. Razzaboni, G.C. Weir, and B.A. Yankner, Pancreatic islet cell toxicity of amylin associated with type-2 diabetes mellitus. Nature 368 (1994) 756-60.

[190] N. Maclean, and R.F. Ogilvie, Quantitative estimation of the pancreatic islet tissue in diabetic subjects. Diabetes 4 (1955) 367-76.

[191] S. Deng, M. Vatamaniuk, X. Huang, N. Doliba, M.M. Lian, A. Frank, E. Velidedeoglu, N.M. Desai, B. Koeberlein, B. Wolf, C.F. Barker, A. Naji, F.M.

Matschinsky, and J.F. Markmann, Structural and functional abnormalities in the islets isolated from type 2 diabetic subjects. Diabetes 53 (2004) 624-32.

[192] R.N. Smith, S.C. Kent, J. Nagle, M. Selig, A.J. Iafrate, N. Najafian, D.A. Hafler, H. Auchincloss, T. Orban, and E. Cagliero, Pathology of an islet transplant 2 years after transplantation: evidence for a nonimmunological loss. Transplantation 86 (2008) 54-62.

[193] G.T. Westermark, P. Westermark, C. Berne, and O. Korsgren, Widespread amyloid deposition in transplanted human pancreatic islets. N Engl J Med 359 (2008) 977-9.

[194] G.T. Westermark, A.M. Davalli, A. Secchi, F. Folli, T. Kin, C. Toso, A.M. Shapiro, O. Korsgren, G. Tufveson, A. Andersson, and P. Westermark, Further evidence for amyloid deposition in clinical pancreatic islet grafts. Transplantation 93 (2012) 219-23.

[195] L. Jansson, D.L. Eizirik, D.G. Pipeleers, L.A. Borg, C. Hellerstrom, and A. Andersson, Impairment of glucose-induced insulin secretion in human pancreatic islets transplanted to diabetic nude mice. J Clin Invest 96 (1995) 721-6.

[196] L. Makhlouf, V.F. Duvivier-Kali, S. Bonner-Weir, H. Dieperink, G.C. Weir, and M.H. Sayegh, Importance of hyperglycemia on the primary function of allogeneic islet transplants. Transplantation 76 (2003) 657-64.

[197] S. Negi, S.H. Park, A. Jetha, R. Aikin, M. Tremblay, and S. Paraskevas, Evidence of endoplasmic reticulum stress mediating cell death in transplanted human islets. Cell Transplantation 21 (2012) 889-899.

[198] G.C. Weir, S. Bonner-Weir, and J.L. Leahy, Islet mass and function in diabetes and transplantation. Diabetes 39 (1990) 401-5.

[199] M. Korc, et al, Normal function of endocrine pancreas, The Pancreas, Raven Press, New York, 1993, pp. 751-758.

[200] B.W. Volk, Wellmann, K.F., Quantitative studies of the islets of nondiabetic patients, The Diabetic Pancreas, Plenum Medical, New York, 1985, pp. 117-125.

[201] D.E. Sutherland, D.M. Radosevich, M.D. Bellin, B.J. Hering, G.J. Beilman, T.B. Dunn, S. Chinnakotla, S.M. Vickers, B. Bland, A.N. Balamurugan, M.L. Freeman, and T.L. Pruett, Total pancreatectomy and islet autotransplantation for chronic pancreatitis. J Am Coll Surg 214 (2012) 409-24; discussion 424-6.

[202] P.O. Carlsson, F. Palm, A. Andersson, and P. Liss, Markedly decreased oxygen tension in transplanted rat pancreatic islets irrespective of the implantation site. Diabetes 50 (2001) 489-95.

[203] J. Henriksnas, J. Lau, G. Zang, P.O. Berggren, M. Kohler, and P.O. Carlsson, Markedly decreased blood perfusion of pancreatic islets transplanted intraportally into the liver: disruption of islet integrity necessary for islet revascularization. Diabetes 61 (2012) 665-73.

[204] M. Giuliani, W. Moritz, E. Bodmer, D. Dindo, P. Kugelmeier, R. Lehmann, M. Gassmann, P. Groscurth, and M. Weber, Central necrosis in isolated hypoxic human pancreatic islets: evidence for postisolation ischemia. Cell Transplant 14 (2005) 67-76.

[205] A.G. Tsai, P.C. Johnson, and M. Intaglietta, Oxygen gradients in the microcirculation. Physiol Rev 83 (2003) 933-63.

[206] N. Tygstrup, K. Winkler, K. Mellemgaard, and M. Andreassen, Determination of the hepatic arterial blood flow and oxygen supply in man by clamping the hepatic artery during surgery. J Clin Invest 41 (1962) 447-54.

[207] E.S. Avgoustiniatos, and C.K. Colton, Effect of external oxygen mass transfer resistances on viability of immunoisolated tissue. Ann N Y Acad Sci 831 (1997) 145-67.

[208] W. Bennet, B. Sundberg, C.G. Groth, M.D. Brendel, D. Brandhorst, H. Brandhorst, R.G. Bretzel, G. Elgue, R. Larsson, B. Nilsson, and O. Korsgren, Incompatibility between human blood and isolated islets of Langerhans: a finding with implications for clinical intraportal islet transplantation? Diabetes 48 (1999) 1907-14.

[209] M. Goto, H. Johansson, A. Maeda, G. Elgue, O. Korsgren, and B. Nilsson, Low molecular weight dextran sulfate prevents the instant blood-mediated inflammatory reaction induced by adult porcine islets. Transplantation 77 (2004) 741-7.

[210] J.C. Grotting, J. Rosai, A.J. Matas, E.M. Frenzel, W.D. Payne, D.E. Sutherland, and J.S. Najarian, The fate of intraportally transplanted islets in diabetic rats. A morphologic and immunohistochemical study. Am J Pathol 92 (1978) 653-70.

[211] N. Sakata, A. Obenaus, N. Chan, J. Mace, R. Chinnock, and E. Hathout, Factors affecting islet graft embolization in the liver of diabetic mice. Islets 1 (2009) 26-33.

[212] T. Chiba, M.R. Harrison, T. Ohkubo, M.D. Rollins, C.T. Albanese, and R.W. Jennings, Transabdominal oxygenation using perfluorocarbons. J Pediatr Surg 34 (1999) 895-900; discussion 900-1.

[213] P.O. Carlsson, and G. Mattsson, Oxygen tension and blood flow in relation to revascularization in transplanted adult and fetal rat pancreatic islets. Cell Transplant 11 (2002) 813-20.

[214] Y.B. Ahn, G. Xu, L. Marselli, E. Toschi, A. Sharma, S. Bonner-Weir, D.C. Sgroi, and G.C. Weir, Changes in gene expression in beta cells after islet isolation and

transplantation using laser-capture microdissection. Diabetologia 50 (2007) 334-42.

[215] R. Olsson, The microvasculature of endogeneous and transplanted pancreatic islets., Uppsala Universitet, Uppsala, Sweden, 2006, pp. 1-83.

[216] J. Lau, J. Henriksnas, J. Svensson, and P.O. Carlsson, Oxygenation of islets and its role in transplantation. Curr Opin Organ Transplant 14 (2009) 688-93.

[217] I.M. Mahmoud, M.M. Gabr, A.F. Refaie, M.A. el-Baz, M.A. Bakr, and M.A. Ghoneim, Purified murine islet allografts: islet engraftment as influenced by implantation site and glucotoxicity. Transplant Proc 30 (1998) 369-72.

[218] J. Lau, G. Mattsson, C. Carlsson, D. Nyqvist, M. Kohler, P.O. Berggren, L. Jansson, and P.O. Carlsson, Implantation site-dependent dysfunction of transplanted pancreatic islets. Diabetes 56 (2007) 1544-50.

[219] V. Cantaluppi, L. Biancone, G.M. Romanazzi, F. Figliolini, S. Beltramo, M.S. Ninniri, F. Galimi, R. Romagnoli, A. Franchello, M. Salizzoni, P.C. Perin, C. Ricordi, G.P. Segoloni, and G. Camussi, Antiangiogenic and immunomodulatory effects of rapamycin on islet endothelium: relevance for islet transplantation. Am J Transplant 6 (2006) 2601-11.

[220] R.F. Padera, and C.K. Colton, Time course of membrane microarchitecture-driven neovascularization. Biomaterials 17 (1996) 277-84.

[221] G.L. Jones, M.T. Juszczak, S.J. Hughes, P. Kooner, S.H. Powis, and M. Press, Time course and quantification of pancreatic islet revascularization following intraportal transplantation. Cell Transplant 16 (2007) 505-16.

[222] E. Hathout, L. Sowers, R. Wang, A. Tan, J. Mace, R. Peverini, R. Chinnock, and A. Obenaus, In vivo magnetic resonance imaging of vascularization in islet transplantation. Transpl Int 20 (2007) 1059-65.

[223] J.I. Stagner, E. Samols, D.J. Koerker, and C.J. Goodner, Perfusion with anti-insulin gamma globulin indicates a B to A to D cellular perfusion sequence in the pancreas of the rhesus monkey, Macaca mulatta. Pancreas 7 (1992) 26-9.

[224] O. Cabrera, D.M. Berman, N.S. Kenyon, C. Ricordi, P.O. Berggren, and A. Caicedo, The unique cytoarchitecture of human pancreatic islets has implications for islet cell function. Proc Natl Acad Sci U S A 103 (2006) 2334-9.

[225] M.D. Menger, P. Vajkoczy, C. Beger, and K. Messmer, Orientation of microvascular blood flow in pancreatic islet isografts. J Clin Invest 93 (1994) 2280-5.

[226] A. Lukinius, L. Jansson, and O. Korsgren, Ultrastructural evidence for blood microvessels devoid of an endothelial cell lining in transplanted pancreatic islets. Am J Pathol 146 (1995) 429-35.

[227] A.O. Gaber, D.W. Fraga, C.S. Callicutt, I.C. Gerling, O.M. Sabek, and M.Y. Kotb, Improved in vivo pancreatic islet function after prolonged in vitro islet culture. Transplantation 72 (2001) 1730-6.

[228] R. Olsson, and P.O. Carlsson, Better vascular engraftment and function in pancreatic islets transplanted without prior culture. Diabetologia 48 (2005) 469-76.

[229] A.S. Narang, K. Cheng, J. Henry, C. Zhang, O. Sabek, D. Fraga, M. Kotb, A.O. Gaber, and R.I. Mahato, Vascular endothelial growth factor gene delivery for revascularization in transplanted human islets. Pharm Res 21 (2004) 15-25.

[230] P. Vajkoczy, A.M. Olofsson, H.A. Lehr, R. Leiderer, F. Hammersen, K.E. Arfors, and M.D. Menger, Histogenesis and ultrastructure of pancreatic islet graft microvasculature. Evidence for graft revascularization by endothelial cells of host origin. Am J Pathol 146 (1995) 1397-405.

[231] D. Nyqvist, M. Kohler, H. Wahlstedt, and P.O. Berggren, Donor islet endothelial cells participate in formation of functional vessels within pancreatic islet grafts. Diabetes 54 (2005) 2287-93.

[232] G. Miao, R.P. Ostrowski, J. Mace, J. Hough, A. Hopper, R. Peverini, R. Chinnock, J. Zhang, and E. Hathout, Dynamic production of hypoxia-inducible factor-1alpha in early transplanted islets. Am J Transplant 6 (2006) 2636-43.

[233] N. Ferrara, K. Houck, L. Jakeman, and D.W. Leung, Molecular and biological properties of the vascular endothelial growth factor family of proteins. Endocr Rev 13 (1992) 18-32.

[234] N. Ferrara, and S. Bunting, Vascular endothelial growth factor, a specific regulator of angiogenesis. Curr Opin Nephrol Hypertens 5 (1996) 35-44.

[235] B. Vasir, L.P. Aiello, K.H. Yoon, R.R. Quickel, S. Bonner-Weir, and G.C. Weir, Hypoxia induces vascular endothelial growth factor gene and protein expression in cultured rat islet cells. Diabetes 47 (1998) 1894-903.

[236] B. Vasir, P. Reitz, G. Xu, A. Sharma, S. Bonner-Weir, and G.C. Weir, Effects of diabetes and hypoxia on gene markers of angiogenesis (HGF, cMET, uPA and uPAR, TGF-alpha, TGF-beta, bFGF and Vimentin) in cultured and transplanted rat islets. Diabetologia 43 (2000) 763-72.

[237] B. Vasir, J.C. Jonas, G.M. Steil, J. Hollister-Lock, W. Hasenkamp, A. Sharma, S. Bonner-Weir, and G.C. Weir, Gene expression of VEGF and its receptors Flk-1/KDR and Flt-1 in cultured and transplanted rat islets. Transplantation 71 (2001) 924-35.

[238] A. Minchenko, T. Bauer, S. Salceda, and J. Caro, Hypoxic stimulation of vascular endothelial growth factor expression in vitro and in vivo. Lab Invest 71 (1994) 374-9.

[239] D. Shweiki, A. Itin, D. Soffer, and E. Keshet, Vascular endothelial growth factor induced by hypoxia may mediate hypoxia-initiated angiogenesis. Nature 359 (1992) 843-5.

[240] A.P. Levy, N.S. Levy, S. Wegner, and M.A. Goldberg, Transcriptional regulation of the rat vascular endothelial growth factor gene by hypoxia. J Biol Chem 270 (1995) 13333-40.

[241] R.E. Bachelder, A. Crago, J. Chung, M.A. Wendt, L.M. Shaw, G. Robinson, and A.M. Mercurio, Vascular endothelial growth factor is an autocrine survival factor for neuropilin-expressing breast carcinoma cells. Cancer Res 61 (2001) 5736-40.

[242] H.P. Gerber, A.K. Malik, G.P. Solar, D. Sherman, X.H. Liang, G. Meng, K. Hong, J.C. Marsters, and N. Ferrara, VEGF regulates haematopoietic stem cell survival by an internal autocrine loop mechanism. Nature 417 (2002) 954-8.

[243] R.R. Foster, R. Hole, K. Anderson, S.C. Satchell, R.J. Coward, P.W. Mathieson, D.A. Gillatt, M.A. Saleem, D.O. Bates, and S.J. Harper, Functional evidence that vascular endothelial growth factor may act as an autocrine factor on human podocytes. Am J Physiol Renal Physiol 284 (2003) F1263-73.

[244] D.L. Gorden, S.J. Mandriota, R. Montesano, L. Orci, and M.S. Pepper, Vascular endothelial growth factor is increased in devascularized rat islets of Langerhans in vitro. Transplantation 63 (1997) 436-43.

[245] M. Venturini, E. Angeli, P. Maffi, P. Fiorina, F. Bertuzzi, M. Salvioni, F. De Cobelli, C. Socci, L. Aldrighetti, C. Losio, V. Di Carlo, A. Secchi, and A. Del Maschio, Technique, complications, and therapeutic efficacy of percutaneous transplantation of human pancreatic islet cells in type 1 diabetes: the role of US. Radiology 234 (2005) 617-24.

[246] M.G. Evans, G.L. Warnock, and R.V. Rajotte, Comparison of sites for transplantation of canine pancreatic microfragments. Diabetes Res 10 (1989) 35-41.

[247] W. Bennet, B. Sundberg, T. Lundgren, A. Tibell, C.G. Groth, A. Richards, D.J. White, G. Elgue, R. Larsson, B. Nilsson, and O. Korsgren, Damage to porcine islets of Langerhans after exposure to human blood in vitro, or after intraportal transplantation to cynomologus monkeys: protective effects of sCR1 and heparin. Transplantation 69 (2000) 711-9.

[248] M. Goto, C.G. Groth, B. Nilsson, and O. Korsgren, Intraportal pig islet xenotransplantation into athymic mice as an in vivo model for the study of the instant blood-mediated inflammatory reaction. Xenotransplantation 11 (2004) 195-202.

[249] H. Johansson, A. Lukinius, L. Moberg, T. Lundgren, C. Berne, A. Foss, M. Felldin, R. Kallen, K. Salmela, A. Tibell, G. Tufveson, K.N. Ekdahl, G. Elgue, O. Korsgren, and B. Nilsson, Tissue factor produced by the endocrine cells of the islets of Langerhans is associated with a negative outcome of clinical islet transplantation. Diabetes 54 (2005) 1755-62.

[250] M. Goto, J. Tjernberg, D. Dufrane, G. Elgue, D. Brandhorst, K.N. Ekdahl, H. Brandhorst, L. Wennberg, Y. Kurokawa, S. Satomi, J.D. Lambris, P. Gianello, O. Korsgren, and B. Nilsson, Dissecting the instant blood-mediated inflammatory reaction in islet xenotransplantation. Xenotransplantation 15 (2008) 225-34.

[251] L. Moberg, A. Olsson, C. Berne, M. Felldin, A. Foss, R. Kallen, K. Salmela, A. Tibell, G. Tufveson, B. Nilsson, and O. Korsgren, Nicotinamide inhibits tissue factor expression in isolated human pancreatic islets: implications for clinical islet transplantation. Transplantation 76 (2003) 1285-8.

[252] J.I. Weitz, and M.A. Crowther, New anticoagulants: current status and future potential. Am J Cardiovasc Drugs 3 (2003) 201-9.

[253] D.M. Berman, O. Cabrera, N.M. Kenyon, J. Miller, S.H. Tam, V.S. Khandekar, K.M. Picha, A.R. Soderman, R.E. Jordan, P.J. Bugelski, D. Horninger, M. Lark, J.E. Davis, R. Alejandro, P.O. Berggren, M. Zimmerman, J.J. O'Neil, C. Ricordi, and N.S. Kenyon, Interference with tissue factor prolongs intrahepatic islet allograft survival in a nonhuman primate marginal mass model. Transplantation 84 (2007) 308-15.

[254] R.G. Bretzel, M. Brendel, M. Eckhard, D. Brandhorst, C. Jaeger, E. Hatziagelaki, and K. Federlin, Islet transplantation: present clinical situation and future aspects. Exp Clin Endocrinol Diabetes 109 Suppl 2 (2001) S384-99.

[255] T. Mandrup-Poulsen, K. Bendtzen, J.H. Nielsen, G. Bendixen, and J. Nerup, Cytokines cause functional and structural damage to isolated islets of Langerhans. Allergy 40 (1985) 424-9.

[256] A. Rabinovitch, W.L. Suarez-Pinzon, K. Strynadka, J.R. Lakey, and R.V. Rajotte, Human pancreatic islet beta-cell destruction by cytokines involves oxygen free radicals and aldehyde production. J Clin Endocrinol Metab 81 (1996) 3197-202.

[257] A.K. Abbas, and A.H. Lichtman, Immunologic Tolerance, Cellular and Molecular Immunology, Elsevier Saunders, Philadelphia, PA, 2005.

[258] A. Lamblin, A. Tournoys, V. Gmyr, M. Jourdain, J. Lefebvre, J. Kerr-Conte, C. Proye, and F. Pattou, [Coagulation activation with intraportal islets of Langerhans transplantation in swine]. Ann Chir 126 (2001) 743-50.

[259] L. Moberg, O. Korsgren, and B. Nilsson, Neutrophilic granulocytes are the predominant cell type infiltrating pancreatic islets in contact with ABO-compatible blood. Clin Exp Immunol 142 (2005) 125-31.

[260] N.R. Barshes, S. Wyllie, and J.A. Goss, Inflammation-mediated dysfunction and apoptosis in pancreatic islet transplantation: implications for intrahepatic grafts. J Leukoc Biol 77 (2005) 587-97.

[261] W.H. Kim, J.W. Lee, B. Gao, and M.H. Jung, Synergistic activation of JNK/SAPK induced by TNF-alpha and IFN-gamma: apoptosis of pancreatic beta-cells via the p53 and ROS pathway. Cell Signal 17 (2005) 1516-32.

[262] S. Sandler, A. Andersson, and C. Hellerstrom, Inhibitory effects of interleukin 1 on insulin secretion, insulin biosynthesis, and oxidative metabolism of isolated rat pancreatic islets. Endocrinology 121 (1987) 1424-31.

[263] C.A. Delaney, D. Pavlovic, A. Hoorens, D.G. Pipeleers, and D.L. Eizirik, Cytokines induce deoxyribonucleic acid strand breaks and apoptosis in human pancreatic islet cells. Endocrinology 138 (1997) 2610-4.

[264] T. Matsuda, K. Omori, T. Vuong, M. Pascual, L. Valiente, K. Ferreri, I. Todorov, Y. Kuroda, C.V. Smith, F. Kandeel, and Y. Mullen, Inhibition of p38 pathway suppresses human islet production of pro-inflammatory cytokines and improves islet graft function. Am J Transplant 5 (2005) 484-93.

[265] A. Sahu, and M.K. Pangburn, Identification of multiple sites of interaction between heparin and the complement system. Mol Immunol 30 (1993) 679-84.

[266] S.R. Coughlin, Thrombin signalling and protease-activated receptors. Nature 407 (2000) 258-64.

[267] C.T. Esmon, Interactions between the innate immune and blood coagulation systems. Trends Immunol 25 (2004) 536-42.

[268] A. Zarbock, R.K. Polanowska-Grabowska, and K. Ley, Platelet-neutrophil-interactions: linking hemostasis and inflammation. Blood Rev 21 (2007) 99-111.

[269] H. Johansson, M. Goto, D. Dufrane, A. Siegbahn, G. Elgue, P. Gianello, O. Korsgren, and B. Nilsson, Low molecular weight dextran sulfate: a strong candidate drug to block IBMIR in clinical islet transplantation. Am J Transplant 6 (2006) 305-12.

[270] S. Cabric, G. Elgue, B. Nilsson, O. Korsgren, and P. Schmidt, Adenovirus-mediated expression of the anticoagulant hirudin in human islets: a tool to make the islets biocompatible to blood. Cell Transplant 15 (2006) 759-67.

[271] S. Cabric, J. Sanchez, T. Lundgren, A. Foss, M. Felldin, R. Kallen, K. Salmela, A. Tibell, G. Tufveson, R. Larsson, O. Korsgren, and B. Nilsson, Islet surface heparinization prevents the instant blood-mediated inflammatory reaction in islet transplantation. Diabetes 56 (2007) 2008-15.

[272] C.L. Stabler, X.L. Sun, W. Cui, J.T. Wilson, C.A. Haller, and E.L. Chaikof, Surface re-engineering of pancreatic islets with recombinant azido-thrombomodulin. Bioconjug Chem 18 (2007) 1713-5.

[273] A.M. Shapiro, H. Gallant, E. Hao, J. Wong, R. Rajotte, R. Yatscoff, and N. Kneteman, Portal vein immunosuppressant levels and islet graft toxicity. Transplant Proc 30 (1998) 641.

[274] Y. Hirano, T. Mitamura, T. Tamura, K. Ohara, Y. Mine, and H. Noguchi, Mechanism of FK506-induced glucose intolerance in rats. J Toxicol Sci 19 (1994) 61-5.

[275] K. Tamura, T. Fujimura, T. Tsutsumi, K. Nakamura, T. Ogawa, C. Atumaru, Y. Hirano, K. Ohara, K. Ohtsuka, K. Shimomura, and et al., Transcriptional inhibition of insulin by FK506 and possible involvement of FK506 binding protein-12 in pancreatic beta-cell. Transplantation 59 (1995) 1606-13.

[276] A.B. Neto, E. Haapalainen, R. Ferreira, C.F. Feo, E.P. Misiako, G. Vennarecci, A. Porcu, S.A. Dib, S. Goldenberg, P.O. Gomes, and A.T. Nigro, Metabolic and ultrastructural effects of cyclosporin A on pancreatic islets. Transpl Int 12 (1999) 208-12.

[277] Y. Uchizono, M. Iwase, U. Nakamura, N. Sasaki, D. Goto, and M. Iida, Tacrolimus impairment of insulin secretion in isolated rat islets occurs at multiple distal sites in stimulus-secretion coupling. Endocrinology 145 (2004) 2264-72.

[278] E. Bell, X. Cao, J.A. Moibi, S.R. Greene, R. Young, M. Trucco, Z. Gao, F.M. Matschinsky, S. Deng, J.F. Markman, A. Naji, and B.A. Wolf, Rapamycin has a deleterious effect on MIN-6 cells and rat and human islets. Diabetes 52 (2003) 2731-9.

[279] M. Guba, P. von Breitenbuch, M. Steinbauer, G. Koehl, S. Flegel, M. Hornung, C.J. Bruns, C. Zuelke, S. Farkas, M. Anthuber, K.W. Jauch, and E.K. Geissler, Rapamycin inhibits primary and metastatic tumor growth by antiangiogenesis: involvement of vascular endothelial growth factor. Nat Med 8 (2002) 128-35.

[280] J.L. Larsen, R.G. Bennett, T. Burkman, A.L. Ramirez, S. Yamamoto, J. Gulizia, S. Radio, and F.G. Hamel, Tacrolimus and sirolimus cause insulin resistance in normal sprague dawley rats. Transplantation 82 (2006) 466-70.

[281] C. Ricordi, Y.J. Zeng, R. Alejandro, A. Tzakis, R. Venkataramanan, J. Fung, D. Bereiter, D.H. Mintz, and T.E. Starzl, In vivo effect of FK506 on human pancreatic islets. Transplantation 52 (1991) 519-22.

[282] M. Tanemura, A. Saga, K. Kawamoto, T. Machida, T. Deguchi, T. Nishida, Y. Sawa, Y. Doki, M. Mori, and T. Ito, Rapamycin induces autophagy in islets: relevance in islet transplantation. Transplant Proc 41 (2009) 334-8.

[283] S.M. Frisch, and H. Francis, Disruption of epithelial cell-matrix interactions induces apoptosis. J Cell Biol 124 (1994) 619-26.

[284] J. Grossmann, Molecular mechanisms of "detachment-induced apoptosis--Anoikis". Apoptosis 7 (2002) 247-60.

[285] F. Ris, E. Hammar, D. Bosco, C. Pilloud, K. Maedler, M.Y. Donath, J. Oberholzer, E. Zeender, P. Morel, D. Rouiller, and P.A. Halban, Impact of integrin-matrix matching and inhibition of apoptosis on the survival of purified human beta-cells in vitro. Diabetologia 45 (2002) 841-50.

[286] R.N. Wang, and L. Rosenberg, Maintenance of beta-cell function and survival following islet isolation requires re-establishment of the islet-matrix relationship. J Endocrinol 163 (1999) 181-90.

[287] E. Hammar, G. Parnaud, D. Bosco, N. Perriraz, K. Maedler, M. Donath, D.G. Rouiller, and P.A. Halban, Extracellular matrix protects pancreatic beta-cells against apoptosis: role of short- and long-term signaling pathways. Diabetes 53 (2004) 2034-41.

[288] C. Oberg-Welsh, Long-term culture in matrigel enhances the insulin secretion of fetal porcine islet-like cell clusters in vitro. Pancreas 22 (2001) 157-63.

[289] G.M. Beattie, A.M. Montgomery, A.D. Lopez, E. Hao, B. Perez, M.L. Just, J.R. Lakey, M.E. Hart, and A. Hayek, A novel approach to increase human islet cell mass while preserving beta-cell function. Diabetes 51 (2002) 3435-9.

[290] C. Lucas-Clerc, C. Massart, J.P. Campion, B. Launois, and M. Nicol, Long-term culture of human pancreatic islets in an extracellular matrix: morphological and metabolic effects. Mol Cell Endocrinol 94 (1993) 9-20.

[291] D. Bosco, P. Meda, P.A. Halban, and D.G. Rouiller, Importance of cell-matrix interactions in rat islet beta-cell secretion in vitro: role of alpha6beta1 integrin. Diabetes 49 (2000) 233-43.

[292] D. Bosco, C. Gonelle-Gispert, C.B. Wollheim, P.A. Halban, and D.G. Rouiller, Increased intracellular calcium is required for spreading of rat islet beta-cells on extracellular matrix. Diabetes 50 (2001) 1039-46.

[293] T. Kaido, M. Yebra, V. Cirulli, and A.M. Montgomery, Regulation of human beta-cell adhesion, motility, and insulin secretion by collagen IV and its receptor alpha1beta1. J Biol Chem 279 (2004) 53762-9.

[294] N. Kaiser, A.P. Corcos, I. Sarel, and E. Cerasi, Monolayer culture of adult rat pancreatic islets on extracellular matrix: modulation of B-cell function by chronic exposure to high glucose. Endocrinology 129 (1991) 2067-76.

[295] G.M. Beattie, D.A. Lappi, A. Baird, and A. Hayek, Functional impact of attachment and purification in the short term culture of human pancreatic islets. J Clin Endocrinol Metab 73 (1991) 93-8.

[296] M.A. Schwartz, Spreading of human endothelial cells on fibronectin or vitronectin triggers elevation of intracellular free calcium. J Cell Biol 120 (1993) 1003-10.

[297] G.M. Beattie, J.S. Rubin, M.I. Mally, T. Otonkoski, and A. Hayek, Regulation of proliferation and differentiation of human fetal pancreatic islet cells by extracellular matrix, hepatocyte growth factor, and cell-cell contact. Diabetes 45 (1996) 1223-8.

[298] G.M. Beattie, V. Cirulli, A.D. Lopez, and A. Hayek, Ex vivo expansion of human pancreatic endocrine cells. J Clin Endocrinol Metab 82 (1997) 1852-6.

[299] K. Edamura, K. Nasu, Y. Iwami, H. Ogawa, N. Sasaki, and H. Ohgawara, Effect of adhesion or collagen molecules on cell attachment, insulin secretion, and

glucose responsiveness in the cultured adult porcine endocrine pancreas: a preliminary study. Cell Transplant 12 (2003) 439-46.

[300] L.M. Weber, K.N. Hayda, K. Haskins, and K.S. Anseth, The effects of cell-matrix interactions on encapsulated beta-cell function within hydrogels functionalized with matrix-derived adhesive peptides. Biomaterials 28 (2007) 3004-11.

[301] L.M. Weber, and K.S. Anseth, Hydrogel encapsulation environments functionalized with extracellular matrix interactions increase islet insulin secretion. Matrix Biol 27 (2008) 667-73.

[302] J. Virostko, Z. Chen, M. Fowler, G. Poffenberger, A.C. Powers, and E.D. Jansen, Factors influencing quantification of in vivo bioluminescence imaging: application to assessment of pancreatic islet transplants. Mol Imaging 3 (2004) 333-42.

[303] M. Fowler, J. Virostko, Z. Chen, G. Poffenberger, A. Radhika, M. Brissova, M. Shiota, W.E. Nicholson, Y. Shi, B. Hirshberg, D.M. Harlan, E.D. Jansen, and A.C. Powers, Assessment of pancreatic islet mass after islet transplantation using in vivo bioluminescence imaging. Transplantation 79 (2005) 768-76.

[304] X. Chen, X. Zhang, C.S. Larson, M.S. Baker, and D.B. Kaufman, In vivo bioluminescence imaging of transplanted islets and early detection of graft rejection. Transplantation 81 (2006) 1421-7.

[305] C. Toso, J.P. Vallee, P. Morel, F. Ris, S. Demuylder-Mischler, M. Lepetit-Coiffe, N. Marangon, F. Saudek, A.M. James Shapiro, D. Bosco, and T. Berney, Clinical magnetic resonance imaging of pancreatic islet grafts after iron nanoparticle labeling. Am J Transplant 8 (2008) 701-6.

[306] N.V. Evgenov, Z. Medarova, G. Dai, S. Bonner-Weir, and A. Moore, In vivo imaging of islet transplantation. Nat Med 12 (2006) 144-8.

[307] Z. Medarova, P. Vallabhajosyula, A. Tena, N. Evgenov, P. Pantazopoulos, V. Tchipashvili, G. Weir, D. Sachs, and A. Moore, In vivo imaging of autologous islet grafts in the liver and under the kidney capsule in non-human primates. Transplantation 87 (2009) 1659-66.

[308] Y. Lee, M. Ravazzola, B.H. Park, Y.K. Bashmakov, L. Orci, and R.H. Unger, Metabolic mechanisms of failure of intraportally transplanted pancreatic beta-cells in rats: role of lipotoxicity and prevention by leptin. Diabetes 56 (2007) 2295-301.

[309] R. Langer, and J.P. Vacanti, Tissue engineering. Science 260 (1993) 920-6.

[310] J.P. Vacanti, and R. Langer, Tissue engineering: the design and fabrication of living replacement devices for surgical reconstruction and transplantation. Lancet 354 Suppl 1 (1999) SI32-4.

[311] I.F. Tannock, Oxygen diffusion and the distribution of cellular radiosensitivity in tumours. Br J Radiol 45 (1972) 515-24.

[312] A.K. Abbas, and A.H. Lichtman, General Properties of Immune Response, Cellular and Molecular Immunology, Elsevier Saunders, Philadephia, PA, 2005.

[313] V. Kumar, A.K. Abbas, and N. Fausto, Acute and Chronic Inflammation, Robbins and Cotran Pathologic Basis of Disease, Elsevier Saunders, Philadelphia, PA, 2005, pp. 47-86.

[314] E.S. Avgoustiniatos, Oxygen diffusion limitation in pancreatic islet culture and immunoisolation. , Department of Chemical Engineering, Massachusetts Institute of Technology, Cambridge, MA, 2001.

[315] M. Brissova, M.J. Fowler, W.E. Nicholson, A. Chu, B. Hirshberg, D.M. Harlan, and A.C. Powers, Assessment of human pancreatic islet architecture and

composition by laser scanning confocal microscopy. J Histochem Cytochem 53 (2005) 1087-97.

[316] Z.A. Latif, J. Noel, and R. Alejandro, A simple method of staining fresh and cultured islets. Transplantation 45 (1988) 827-30.

[317] V. Kumar, A.K. Abbas, and N. Fausto, Cellular Adaptations, Cell Injury, and Cell Death, Robbins and Cotran Pathologic Basis of Disease Elsevier Saunders, Philadephia, PA, 2005, pp. 3-46.

[318] D.E. Sutherland, 2011.

[319] V.D. Kodibagkar, X. Wang, and R.P. Mason, Physical principles of quantitative nuclear magnetic resonance oximetry. Front Biosci 13 (2008) 1371-84.

[320] P. Parhami, and B.M. Fung, Fluorine-19 relaxation study of perfluoro chemicals as oxygen carriers. J Phys Chem 87 (1983) 1928-1931.

[321] D. Eidelberg, G. Johnson, D. Barnes, P.S. Tofts, D. Delpy, D. Plummer, and W.I. McDonald, 19F NMR imaging of blood oxygenation in the brain. Magn Reson Med 6 (1988) 344-52.

[322] B.A. Berkowitz, C.A. Wilson, D.L. Hatchell, and R.E. London, Quantitative determination of the partial oxygen pressure in the vitrectomized rabbit eye in vivo using 19F NMR. Magn Reson Med 21 (1991) 233-41.

[323] B.A. Berkowitz, J.T. Handa, and C.A. Wilson, Perfluorocarbon temperature measurements using 19F NMR. NMR Biomed 5 (1992) 65-8.

[324] R.P. Mason, H. Shukla, and P.P. Antich, In vivo oxygen tension and temperature: simultaneous determination using 19F NMR spectroscopy of perfluorocarbon. Magn Reson Med 29 (1993) 296-302.

[325] P.S. Hees, and C.H. Sotak, Assessment of changes in murine tumor oxygenation in response to nicotinamide using 19F NMR relaxometry of a perfluorocarbon emulsion. Magn Reson Med 29 (1993) 303-10.

[326] K.A. McGovern, J.S. Schoeniger, J.P. Wehrle, C.E. Ng, and J.D. Glickson, Gel-entrapment of perfluorocarbons: a fluorine-19 NMR spectroscopic method for monitoring oxygen concentration in cell perfusion systems. Magn Reson Med 29 (1993) 196-204.

[327] S.K. Holland, R.P. Kennan, M.M. Schaub, M.J. D'Angelo, and J.C. Gore, Imaging oxygen tension in liver and spleen by 19F NMR. Magn Reson Med 29 (1993) 446-58.

[328] R.P. Mason, Non-invasive physiology: 19F NMR of perfluorocarbons. Artif Cells Blood Substit Immobil Biotechnol 22 (1994) 1141-53.

[329] U. Nöth, S.P. Morrissey, R. Deichmann, H. Adolf, C. Schwarzbauer, J. Lutz, and A. Haase, In vivo measurement of partial oxygen pressure in large vessels and in the reticuloendothelial system using fast 19F-MRI. Magn Reson Med 34 (1995) 738-45.

[330] H.P. Shukla, R.P. Mason, N. Bansal, and P.P. Antich, Regional myocardial oxygen tension: 19F MRI of sequestered perfluorocarbon. Magn Reson Med 35 (1996) 827-33.

[331] J. Lutz, U. Noth, S.P. Morrissey, H. Adolf, R. Deichmann, and A. Haase, Measurement of oxygen tensions in the abdominal cavity and in the skeletal muscle using 19F-MRI of neat PFC droplets. Adv Exp Med Biol 428 (1997) 569-72.

[332] U. Nöth, P. Grohn, A. Jork, U. Zimmermann, A. Haase, and J. Lutz, 19F-MRI in vivo determination of the partial oxygen pressure in perfluorocarbon-loaded

alginate capsules implanted into the peritoneal cavity and different tissues. Magn Reson Med 42 (1999) 1039-47.

[333] S. Hunjan, D. Zhao, A. Constantinescu, E.W. Hahn, P.P. Antich, and R.P. Mason, Tumor oximetry: demonstration of an enhanced dynamic mapping procedure using fluorine-19 echo planar magnetic resonance imaging in the Dunning prostate R3327-AT1 rat tumor. Int J Radiat Oncol Biol Phys 49 (2001) 1097-108.

[334] J.D. Gross, R.C. Long, Jr., I. Constantinidis, and A. Sambanis, Monitoring of dissolved oxygen and cellular bioenergetics within a pancreatic substitute. Biotechnol Bioeng 98 (2007) 261-70.

[335] B.F. Jordan, G.O. Cron, and B. Gallez, Rapid monitoring of oxygenation by 19F magnetic resonance imaging: Simultaneous comparison with fluorescence quenching. Magn Reson Med 61 (2009) 634-8.

[336] F. Goh, and A. Sambanis, In vivo noninvasive monitoring of dissolved oxygen concentration within an implanted tissue-engineered pancreatic construct. Tissue Eng Part C Methods 17 (2011) 887-94.

[337] S. Hunjan, R.P. Mason, A. Constantinescu, P. Peschke, E.W. Hahn, and P.P. Antich, Regional tumor oximetry: 19F NMR spectroscopy of hexafluorobenzene. Int J Radiat Oncol Biol Phys 41 (1998) 161-71.

[338] R.P. Mason, P.P. Antich, E.E. Babcock, A. Constantinescu, P. Peschke, and E.W. Hahn, Non-invasive determination of tumor oxygen tension and local variation with growth. Int J Radiat Oncol Biol Phys 29 (1994) 95-103.

[339] D. Eidelberg, G. Johnson, P.S. Tofts, J. Dobbin, H.A. Crockard, and D. Plummer, 19F imaging of cerebral blood oxygenation in experimental middle cerebral artery occlusion: preliminary results. J Cereb Blood Flow Metab 8 (1988) 276-81.

[340] C.A. Wilson, B.A. Berkowitz, and D.L. Hatchell, Oxygen kinetics in preretinal perfluorotributylamine. Exp Eye Res 55 (1992) 119-26.

[341] C.A. Wilson, B.A. Berkowitz, B.W. McCuen, 2nd, and H.C. Charles, Measurement of preretinal oxygen tension in the vitrectomized human eye using fluorine-19 magnetic resonance spectroscopy. Arch Ophthalmol 110 (1992) 1098-100.

[342] R.P. Mason, S. Hunjan, D. Le, A. Constantinescu, B.R. Barker, P.S. Wong, P. Peschke, E.W. Hahn, and P.P. Antich, Regional tumor oxygen tension: fluorine echo planar imaging of hexafluorobenzene reveals heterogeneity of dynamics. Int J Radiat Oncol Biol Phys 42 (1998) 747-50.

[343] M. Xia, V. Kodibagkar, H. Liu, and R.P. Mason, Tumour oxygen dynamics measured simultaneously by near-infrared spectroscopy and 19F magnetic resonance imaging in rats. Phys Med Biol 51 (2006) 45-60.

[344] D. Zhao, L. Jiang, E.W. Hahn, and R.P. Mason, Comparison of 1H blood oxygen level-dependent (BOLD) and 19F MRI to investigate tumor oxygenation. Magn Reson Med 62 (2009) 357-64.

[345] M. Hillgärtner, H. Zimmermann, S. Mimietz, A. Jork, F. Thürmer, H. Schneider, U. Nöth, C. Hasse, A. Haase, G. Fuhr, M. Rothmund, and U. Zimmermann, Immunoisolation of transplants by entrapment in 19F-labelled alginate gels: production, biocompatibility, stability, and long-term monitoring of functional integrity. Materialwissenschaft und Werkstofftechnik 30 (1999) 783-792.

[346] H.E. Longmaid, 3rd, D.F. Adams, R.D. Neirinckx, C.G. Harrison, P. Brunner, S.E. Seltzer, M.A. Davis, L. Neuringer, and R.P. Geyer, In vivo 19F NMR imaging of liver, tumor, and abscess in rats. Preliminary results. Invest Radiol 20 (1985) 141-5.

[347] A.V. Ratner, R. Hurd, H.H. Muller, B. Bradley-Simpson, W. Pitts, D. Shibata, C. Sotak, and S.W. Young, 19F magnetic resonance imaging of the reticuloendothelial system. Magn Reson Med 5 (1987) 548-54.

[348] D.L. Brown, P.J. Meagher, K.R. Knight, E. Keramidaris, R. Romeo-Meeuw, A.J. Penington, and W.A. Morrison, Survival and function of transplanted islet cells on an in vivo, vascularized tissue engineering platform in the rat: A pilot study. Cell Transplant 15 (2006) 319-24.

[349] K.R. Knight, Y. Uda, M.W. Findlay, D.L. Brown, K.J. Cronin, E. Jamieson, T. Tai, E. Keramidaris, A.J. Penington, J. Rophael, L.C. Harrison, and W.A. Morrison, Vascularized tissue-engineered chambers promote survival and function of transplanted islets and improve glycemic control. FASEB J 20 (2006) 565-7.

[350] A.J. Hussey, M. Winardi, X.L. Han, G.P. Thomas, A.J. Penington, W.A. Morrison, K.R. Knight, and S.J. Feeney, Seeding of pancreatic islets into prevascularized tissue engineering chambers. Tissue Eng Part A 15 (2009) 3823-33.

[351] A.J. Hussey, M. Winardi, J. Wilson, N. Forster, W.A. Morrison, A.J. Penington, K.R. Knight, and S.J. Feeney, Pancreatic islet transplantation using vascularised chambers containing nerve growth factor ameliorates hyperglycaemia in diabetic mice. Cells Tissues Organs 191 (2010) 382-93.

[352] Y.J. Gu, M. Miyamoto, W.X. Cui, B.Y. Xu, Y. Kawakami, T. Yamasaki, H. Setoyama, N. Kinosita, H. Iwata, Y. Ikada, M. Imamura, and K. Inoue, Effect of neovascularization-inducing bioartificial pancreas on survival of syngeneic islet grafts. Transplant Proc 32 (2000) 2494-5.

[353] Y. Kawakami, H. Iwata, Y. Gu, M. Miyamoto, Y. Murakami, T. Yamasaki, W. Cui, Y. Ikada, M. Imamura, and K. Inoue, Modified subcutaneous tissue with

neovascularization is useful as the site for pancreatic islet transplantation. Cell Transplant 9 (2000) 729-32.

[354] Y. Kawakami, H. Iwata, Y.J. Gu, M. Miyamoto, Y. Murakami, A.N. Balamurugan, M. Imamura, and K. Inoue, Successful subcutaneous pancreatic islet transplantation using an angiogenic growth factor-releasing device. Pancreas 23 (2001) 375-81.

[355] T. Linn, D. Erb, D. Schneider, A. Kidszun, A.E. Elcin, R.G. Bretzel, and Y.M. Elcin, Polymers for induction of revascularization in the rat fascial flap: application of vascular endothelial growth factor and pancreatic islet cells. Cell Transplant 12 (2003) 769-78.

[356] Y. Gu, Y. Tabata, Y. Kawakami, A.N. Balamurugan, H. Hori, N. Nagata, A. Satake, W. Cui, M. Qi, Y. Misawa, M. Toma, M. Miyamoto, M. Nozawa, and K. Inoue, Development of a new method to induce angiogenesis at subcutaneous site of streptozotocin-induced diabetic rats for islet transplantation. Cell Transplant 10 (2001) 453-7.

[357] A. Miki, J.D. Rivas-Carrillo, N. Navarro-Alvarez, A. Soto-Gutierrez, Y. Chen, K. Tanaka, M. Narushima, Y. Tabata, T. Okitsu, H. Noguchi, S. Matsumoto, N. Tanaka, and N. Kobayashi, Maintenance of neovascularization at the implantation site of an artificial device by bFGF and endothelial cell transplant. Cell Transplant 15 (2006) 893-901.

[358] P. De Vos, J.L. Hillebrands, B.J. De Haan, J.H. Strubbe, and R. Van Schilfgaarde, Efficacy of a prevascularized expanded polytetrafluoroethylene solid support system as a transplantation site for pancreatic islets. Transplantation 63 (1997) 824-30.

[359] W. Wang, Y. Gu, Y. Tabata, M. Miyamoto, H. Hori, N. Nagata, M. Touma, A.N. Balamurugan, Y. Kawakami, M. Nozawa, and K. Inoue, Reversal of diabetes in

mice by xenotransplantation of a bioartificial pancreas in a prevascularized subcutaneous site. Transplantation 73 (2002) 122-9.

[360] T. Sakurai, A. Satake, N. Nagata, Y. Gu, A. Hiura, K. Doo-Hoon, H. Hori, Y. Tabata, S. Sumi, and K. Inoue, The development of new immunoisolatory devices possessing the ability to induce neovascularization. Cell Transplant 12 (2003) 527-35.

[361] A. Pileggi, R.D. Molano, C. Ricordi, E. Zahr, J. Collins, R. Valdes, and L. Inverardi, Reversal of diabetes by pancreatic islet transplantation into a subcutaneous, neovascularized device. Transplantation 81 (2006) 1318-24.

[362] A.M. Hiscox, A.L. Stone, S. Limesand, J.B. Hoying, and S.K. Williams, An islet-stabilizing implant constructed using a preformed vasculature. Tissue Eng Part A 14 (2008) 433-40.

[363] J.L. Contreras, C.A. Smyth, C. Eckstein, G. Bilbao, J.A. Thompson, C.J. Young, and D.E. Eckhoff, Peripheral mobilization of recipient bone marrow-derived endothelial progenitor cells enhances pancreatic islet revascularization and engraftment after intraportal transplantation. Surgery 134 (2003) 390-8.

[364] H.A. Kim, B.W. Lee, D. Kang, J.H. Kim, S.H. Ihm, and M. Lee, Delivery of hypoxia-inducible VEGF gene to rat islets using polyethylenimine. J Drug Target 17 (2009) 1-9.

[365] J.C. Davila, E.V. Lautsch, and T.E. Palmer, Some physical factors affecting the acceptance of synthetic materials as tissue implants. Ann N Y Acad Sci 146 (1968) 138-47.

[366] B.F. Matlaga, L.P. Yasenchak, and T.N. Salthouse, Tissue response to implanted polymers: the significance of sample shape. J Biomed Mater Res 10 (1976) 391-7.

[367] J.M. Anderson, H. Niven, J. Pelagalli, L.S. Olanoff, and R.D. Jones, The role of the fibrous capsule in the function of implanted drug-polymer sustained release systems. J Biomed Mater Res 15 (1981) 889-902.

[368] P. Beahan, and D. Hull, A study of the interface between a fibrous polyurethane arterial prosthesis and natural tissue. J Biomed Mater Res 16 (1982) 827-38.

[369] S.R. Taylor, and D.F. Gibbons, Effect of surface texture on the soft tissue response to polymer implants. J Biomed Mater Res 17 (1983) 205-27.

[370] W.K. Ward, E.P. Slobodzian, K.L. Tiekotter, and M.D. Wood, The effect of microgeometry, implant thickness and polyurethane chemistry on the foreign body response to subcutaneous implants. Biomaterials 23 (2002) 4185-92.

[371] B.J. Hering, M. Wijkstrom, M.L. Graham, M. Hardstedt, T.C. Aasheim, T. Jie, J.D. Ansite, M. Nakano, J. Cheng, W. Li, K. Moran, U. Christians, C. Finnegan, C.D. Mills, D.E. Sutherland, P. Bansal-Pakala, M.P. Murtaugh, N. Kirchhof, and H.J. Schuurman, Prolonged diabetes reversal after intraportal xenotransplantation of wild-type porcine islets in immunosuppressed nonhuman primates. Nat Med 12 (2006) 301-3.

[372] K. Cardona, G.S. Korbutt, Z. Milas, J. Lyon, J. Cano, W. Jiang, H. Bello-Laborn, B. Hacquoil, E. Strobert, S. Gangappa, C.J. Weber, T.C. Pearson, R.V. Rajotte, and C.P. Larsen, Long-term survival of neonatal porcine islets in nonhuman primates by targeting costimulation pathways. Nat Med 12 (2006) 304-6.

[373] E.S. Avgoustiniatos, and C.K. Colton, Design Considerations in Immunoisolation. in: R.P. Lanza, R. Langer, and W.L. Chick, (Eds.), Principles of Tissue Engineering, R.G. Landes Company, Austin, TX, 1997, pp. 333-346.

[374] C.K. Colton, and E.S. Avgoustiniatos, Bioengineering in development of the hybrid artificial pancreas. J Biomech Eng 113 (1991) 152-70.

[375] H. Wu, E.S. Avgoustiniatos, L. Swette, S. Bonner-Weir, G.C. Weir, and C.K. Colton, In situ electrochemical oxygen generation with an immunoisolation device. Ann N Y Acad Sci 875 (1999) 105-25.

[376] K. Bloch, E. Papismedov, K. Yavriyants, M. Vorobeychik, S. Beer, and P. Vardi, Photosynthetic oxygen generator for bioartificial pancreas. Tissue Eng 12 (2006) 337-44.

[377] E. Pedraza, M.M. Coronel, C.A. Fraker, C. Ricordi, and C.L. Stabler, Preventing hypoxia-induced cell death in beta cells and islets via hydrolytically activated, oxygen-generating biomaterials. Proc Natl Acad Sci U S A 109 (2012) 4245-50.

[378] M.K. Tham, R.D. Walker Jr., and J.H. Modell, Physical properties and gas solubilities in selected fluorinated ethers. J Chem Eng Data 18 (1973) 385-386.

[379] K. Chin, S.F. Khattak, S.R. Bhatia, and S.C. Roberts, Hydrogel-perfluorocarbon composite scaffold promotes oxygen transport to immobilized cells. Biotechnol Prog 24 (2008) 358-66.

[380] A.S. Johnson, R.J. Fisher, G.C. Weir, and C.K. Colton, Oxygen consumption and diffusion in assemblages of respiring spheres: performance enhancement of a bioartificial pancreas. Chem Eng Sci 64 (2009) 4470-4487.

[381] D.G. Pipeleers, P.A. in't Veld, M. Van de Winkel, E. Maes, F.C. Schuit, and W. Gepts, A new in vitro model for the study of pancreatic A and B cells. Endocrinology 117 (1985) 806-16.

[382] A.S. Lewis, and C.K. Colton, Engineering Challenges in Immunobarrier Device Development. in: R.P. Lanza, R. Langer, and J.P. Vacanti, (Eds.), Principles in Tissue Engineering, Elsevier Academic Press, London, United Kingdom, 2007, pp. 405-418.

[383] A.S. Johnson, E. O'Sullivan, L.N. D'Aoust, A. Omer, S. Bonner-Weir, R.J. Fisher, G.C. Weir, and C.K. Colton, Quantitative assessment of islets of Langerhans encapsulated in alginate. Tissue Eng Part C Methods 17 (2011) 435-49.

[384] E.A. Ryan, and A.J. Shapiro, A patient with severe, recurrent hypoglycemia and glycemic lability who underwent islet transplantation. Nat Clin Pract Endocrinol Metab 2 (2006) 349-53; quiz 354.

[385] A. Gangemi, P. Salehi, B. Hatipoglu, J. Martellotto, B. Barbaro, J.B. Kuechle, M. Qi, Y. Wang, P. Pallan, C. Owens, J. Bui, D. West, B. Kaplan, E. Benedetti, and J. Oberholzer, Islet transplantation for brittle type 1 diabetes: the UIC protocol. Am J Transplant 8 (2008) 1250-61.

[386] A. Koh, S. Imes, T. Kin, P. Dinyari, A. Malcolm, C. Toso, A.M. Shapiro, and P. Senior, Supplemental islet infusions restore insulin independence after graft dysfunction in islet transplant recipients. Transplantation 89 (2010) 361-5.

[387] A. Koh, P. Senior, A. Salam, T. Kin, S. Imes, P. Dinyari, A. Malcolm, C. Toso, B. Nilsson, O. Korsgren, and A.M. Shapiro, Insulin-heparin infusions peritransplant substantially improve single-donor clinical islet transplant success. Transplantation 89 (2010) 465-71.

[388] A.M. Posselt, M.D. Bellin, M. Tavakol, G.L. Szot, L.A. Frassetto, U. Masharani, R.K. Kerlan, L. Fong, F.G. Vincenti, B.J. Hering, J.A. Bluestone, and P.G. Stock, Islet transplantation in type 1 diabetics using an immunosuppressive protocol based on the anti-LFA-1 antibody efalizumab. Am J Transplant 10 (2010) 1870-80.

[389] E. Rafael, A. Tibell, M. Ryden, T. Lundgren, L. Savendahl, B. Borgstrom, U. Arnelo, B. Isaksson, B. Nilsson, O. Korsgren, and J. Permert, Intramuscular autotransplantation of pancreatic islets in a 7-year-old child: a 2-year follow-up. Am J Transplant 8 (2008) 458-62.

[390] D.M. Berman, J.J. O'Neil, L.C. Coffey, P.C. Chaffanjon, N.M. Kenyon, P. Ruiz, Jr., A. Pileggi, C. Ricordi, and N.S. Kenyon, Long-term survival of nonhuman primate islets implanted in an omental pouch on a biodegradable scaffold. Am J Transplant 9 (2009) 91-104.

[391] C. Moers, J.M. Smits, M.H. Maathuis, J. Treckmann, F. van Gelder, B.P. Napieralski, M. van Kasterop-Kutz, J.J. van der Heide, J.P. Squifflet, E. van Heurn, G.R. Kirste, A. Rahmel, H.G. Leuvenink, A. Paul, J. Pirenne, and R.J. Ploeg, Machine perfusion or cold storage in deceased-donor kidney transplantation. N Engl J Med 360 (2009) 7-19.

[392] M.J. Taylor, and S.C. Baicu, Current state of hypothermic machine perfusion preservation of organs: The clinical perspective. Cryobiology 60 (2010) S20-35.

[393] Y. Iwanaga, D.E. Sutherland, J.V. Harmon, and K.K. Papas, Pancreas preservation for pancreas and islet transplantation. Curr Opin Organ Transplant 13 (2008) 445-51.

[394] K.K. Papas, B.J. Hering, L. Guenther, M.J. Rappel, C.K. Colton, and E.S. Avgoustiniatos, Pancreas oxygenation is limited during preservation with the two-layer method. Transplant Proc 37 (2005) 3501-4.

[395] A. Agrawal, P.W. So, A. Penman, S. Powis, B. Davidson, M. Press, and B. Fuller, Limited penetration of perfluorocarbon in porcine pancreas preserved by two-layer method with (19)fluorine magnetic resonance spectroscopy and headspace gas chromatography. Cell Transplant 19 (2010) 1021-9.

[396] B. Luer, M. Koetting, P. Efferz, and T. Minor, Role of oxygen during hypothermic machine perfusion preservation of the liver. Transpl Int 23 (2010) 944-50.

[397] G.P. Tolstykh, J.F. Gelineau, L.M. Maier, and L. Bunegin, Novel portable hypothermic pulsatile perfusion preservation technology: Improved viability and function of rodent and canine kidneys. Ann Transplant 15 (2010) 35-43.

[398] R. Magnus, Die Thätigkeit des überlebenden Säugethierherzens bei Durchströmung mit Gasen. Arch Exp Path Pharmakol 47 (1902) 200-208.

[399] J.H. Harrison, J.P. Merrill, and J.E. Murray, Renal homotransplantation in identical twins. Surg Forum 6 (1956) 432-6.

[400] J.P. Merrill, J.E. Murray, J.H. Harrison, and W.R. Guild, Successful homotransplantation of the human kidney between identical twins. J Am Med Assoc 160 (1956) 277-82.

[401] A. Bunzl, A.S. Burgen, B.D. Burns, N. Pedley, and K.G. Terroux, Methods for studying the reflex activity of the frog's spinal cord. Br J Pharmacol Chemother 9 (1954) 229-35.

[402] B.D. Burns, J.G. Robson, and G.K. Smith, The survival of mammalian tissues perfused with intravascular gas mixtures of oxygen and carbon dioxide. Can J Biochem Physiol 36 (1958) 499-504.

[403] D.C. Sabiston, Jr., J.L. Talbert, L.H. Riley, Jr., and A. Blalock, Maintenance of the heart beat by perfusion of the coronary circulation with gaseous oxygen. Ann Surg 150 (1959) 361-70.

[404] R.C. Camishion, A.L. Davies, K. Tokunaga, and R.W. Solit, Retrograde perfusion of the coronary arteries with gaseous oxygen cardiopulmonary bypass. Surgery 59 (1966) 145-54.

[405] J.L. Talbert, L.H. Riley, Jr., D.C. Sabiston, Jr., and A. Blalock, Retrograde perfusion of the coronary sinus with gaseous oxygen. Am Surg 26 (1960) 189-92.

[406] W. Isselhard, M. Berger, H. Denecke, J. Witte, J.H. Fischer, and H. Molzberger, Metabolism of canine kidneys in anaerobic ischemia and in aerobic ischemia by persufflation with gaseous oxygen. Pflugers Arch 337 (1972) 87-106.

[407] W. Isselhard, J. Witte, H. Denecke, M. Berger, J.H. Fischer, and H. Molzberger, Function and metabolism of canine kidneys after aerobic ischemia by retrograde persufflation with gaseous oxygen. Res Exp Med (Berl) 164 (1974) 35-44.

[408] V.L. Gott, J.L. Gonzalez, M.N. Zuhdi, R.L. Varco, and C.W. Lillehei, Retrograde perfusion of the coronary sinus for direct vision aortic surgery. Surg Gynecol Obstet 104 (1957) 319-28.

[409] C. Massimo, L. Boffi, and L. Pozzi, Sinusal standstill with ventricular automatism during retrograde perfusion of the coronary sinus under hypothermia for direct surgical approach to the aortic valves: an experimental study. J Thorac Surg 36 (1958) 227-9.

[410] C.N. Barnard, The operation. A human cardiac transplant: an interim report of a successful operation performed at Groote Schuur Hospital, Cape Town. S Afr Med J 41 (1967) 1271-4.

[411] L.P. Gabel, I. Bihler, and P.E. Dresel, Contractility, metabolism and pharmacological reactions of isolated gas-perfused cat hearts. Circ Res 19 (1966) 891-902.

[412] W. Lochner, G. Arnold, and E.R. Muller-Ruchholtz, Metabolism of the artificially arrested heart and of the gas-perfused heart. Am J Cardiol 22 (1968) 299-311.

[413] H. Denecke, W. Isselhard, W. Stelter, M. Berger, and D. Sachweh, Recovery of the kidney from aerobic and anaerobic ischemia in deep hypothermia, European Society for Experimental Surgery, 6th Congress, Eur Sur Res, 1971, pp. 182.

[414] F. Kuhn-Regnier, J.H. Fischer, and S. Jeschkeit, Coronary oxygen persufflation for long-term myocardial protection. Thorac Cardiovasc Surg 46 Suppl 2 (1998) 308-12.

[415] G.A. Laine, and S.J. Allen, Left ventricular myocardial edema. Lymph flow, interstitial fibrosis, and cardiac function. Circ Res 68 (1991) 1713-21.

[416] F. Kuhn-Regnier, J.H. Fischer, S. Jeschkeit, R. Switkowski, O. Bardakcioglu, R. Sobottke, and E.R. de Vivie, Coronary oxygen persufflation combined with HTK cardioplegia prolongs the preservation time in heart transplantation. Eur J Cardiothorac Surg 17 (2000) 71-6.

[417] G. Yotsumoto, S. Jeschkeit-Schubbert, C. Funcke, F. Kuhn-Regnier, and J.H. Fischer, Total recovery of heart grafts of non-heart-beating donors after 3 hours of hypothermic coronary oxygen persufflation preservation in an orthotopic pig transplantation model. Transplantation 75 (2003) 750-6.

[418] J. Fischer, C. Funcke, S. Jeschkeit-Schubbert, G. Yotsumoto, and F. Kuhn-Regnier, Coronary endothelial function in heart grafts of non-heart-beating donors (NHBD) after 3 h hypothermic COP-preservation and orthotopic transplantation in pigs. Eur Surg Res 33 (2001) 130-131.

[419] J.H. Fischer, C. Funcke, G. Yotsumoto, S. Jeschkeit-Schubbert, and F. Kuhn-Regnier, Maintenance of physiological coronary endothelial function after 3.3 h of hypothermic oxygen persufflation preservation and orthotopic transplantation of non-heart-beating donor hearts. Eur J Cardiothorac Surg 25 (2004) 98-104.

[420] F. Kuhn-Regnier, W. Bloch, I. Tsimpoulis, M. Reismann, O. Dagktekin, S. Jeschkeit-Schubbert, C. Funcke, J.W. Fries, K. Addicks, E.R. de Vivie, and J.H. Fischer, Coronary oxygen persufflation for heart preservation in pigs: analyses of endothelium and myocytes. Transplantation 77 (2004) 28-35.

[421] J.H. Fischer, Methods of Cardiac Oxygen Persufflation. in: K. Uygun, and C.Y. Lee, (Eds.), Organ Preservation and Reengineering, Artech House Publisher, Boston, 2011, pp. 105-126.

[422] J.L. Talbert, L.H. Riley, Jr., D.C. Sabiston, Jr., and A. Blalock, An evaluation of gaseous oxygen perfusion as a method for maintaining renal viability during periods of complete ischemia. Surg Gynecol Obstet 112 (1961) 593-9.

[423] W. Isselhard, H. Denecke, W. Stelter, M. Berger, D. Sachweh, J. Witte, and J.H. Fischer, Function and metabolism of canine kidneys after aerobic ischemia by orthograde persufflation with gaseous oxygen. Res Exp Med (Berl) 159 (1973) 288-97.

[424] W. Isselhard, H. Denecke, J. Witte, M. Berger, and J.H. Fischer, [Renal function after hypothermic kidney ischemia with orthograde and retrograde O 2 - persulflation in situ]. Res Exp Med (Berl) 157 (1972) 231-4.

[425] W. Isselhard, J. Witte, H. Denecke, M. Berger, and J.H. Fischer, [Kidney function following hypothermic aerobic ischemia in situ]. Pflugers Arch 332 (1972) Suppl 332:R26.

[426] D. Sachweh, W. Isselhard, H. Dennecke, W.J. Stelter, M. Berger, H. Lauschke, and W.F. Eigler, Short time kidney preservation by hypothermic oxygen persufflation. Bull Soc Int Chir 31 (1972) 258-63.

[427] J.H. Fischer, A. Czerniak, U. Hauer, and W. Isselhard, A new simple method for optimal storage of ischemically damaged kidneys. Transplantation 25 (1978) 43-9.

[428] W. Isselhard, Efficiency of retrograde oxygen persufflation in prolonged kidney preservation. Eur Surg Res 10 (1978) 19-20.

[429] A. Flatmark, O. Slaattelid, and G. Woxholt, Gaseous persufflation during machine perfusion of human kidneys before transplantation. Eur Surg Res 7 (1975) 83-90.

[430] H. Ross, and M.L. Escott, Gaseous oxygen perfusion of the renal vessels as an adjunct in kidney preservation. Transplantation 28 (1979) 362-4.

[431] H. Ross, and M.L. Escott, Renal preservation with gaseous perfusion. Transplantation 33 (1982) 206-8.

[432] D.E. Pegg, J. Foreman, C.J. Hunt, and M.P. Diaper, The mechanism of action of retrograde oxygen persufflation in renal preservation. Transplantation 48 (1989) 210-7.

[433] K. Rolles, J. Foreman, and D.E. Pegg, Preservation of ischemically injured canine kidneys by retrograde oxygen persufflation. Transplantation 38 (1984) 102-6.

[434] K. Rolles, J. Foreman, and D.E. Pegg, A pilot clinical study of retrograde oxygen persufflation in renal preservation. Transplantation 48 (1989) 339-42.

[435] N.T. Stowe, M.O. Magnusson, K. Jojima, G.M. Chisolm, A.C. Novick, and R.A. Straffon, Combined use of normobaric oxygen perfusion and simple cold storage for extended kidney preservation. Transplant Proc 18 (1986) 553-556.

[436] M. Yin, M.H. Booster, G.J. van der Vusse, J.G. Maessen, W.A. Buurman, and G. Kootstra, Retrograde oxygen persufflation in combination with UW solution enhances adenine nucleotide contents in ischemically damaged rat kidney during cold storage. Transpl Int 9 (1996) 396-402.

[437] J. Treckmann, M. Nagelschmidt, T. Minor, F. Saner, S. Saad, and A. Paul, Function and quality of kidneys after cold storage, machine perfusion, or retrograde oxygen persufflation: results from a porcine autotransplantation model. Cryobiology 59 (2009) 19-23.

[438] J.W. Treckmann, A. Paul, S. Saad, J. Hoffmann, K.H. Waldmann, C.E. Broelsch, and M. Nagelschmidt, Primary organ function of warm ischaemically damaged porcine kidneys after retrograde oxygen persufflation. Nephrol Dial Transplant 21 (2006) 1803-8.

[439] T. Minor, W. Isselhard, Y. Yamamoto, M. Obara, and S. Saad, The effects of allopurinol and SOD on lipid peroxidation and energy metabolism in the liver after ischemia in an aerobic/anaerobic persufflation. Surg Today 23 (1993) 728-32.

[440] J.H. Fischer, Hypothermic liver preservation using different flush solutions and retrograde oxygen persufflation technique. Eur Surg Res 12 (1980) 19-20.

[441] J. Treckmann, T. Minor, S. Saad, A. Ozcelik, M. Malago, C.E. Broelsch, and A. Paul, Retrograde oxygen persufflation preservation of human livers: a pilot study. Liver Transpl 14 (2008) 358-64.

[442] T. Minor, S. Saad, M. Kotting, M. Nagelschmidt, and A. Paul, Endischemic oxygen persufflation to improve viability of marginally preserved donor livers. Transpl Int 11 Suppl 1 (1998) S400-3.

[443] T. Minor, and W. Isselhard, Venous oxygen insufflation to prevent reoxygenation injury after ischemia of a solid organ. Transplantation 58 (1994) 121-3.

[444] T. Minor, and W. Isselhard, Synthesis of high energy phosphates during cold ischemic rat liver preservation with gaseous oxygen insufflation. Transplantation 61 (1996) 20-2.

[445] T. Minor, W. Isselhard, and H. Klauke, Reduction in nonparenchymal cell injury and vascular endothelial dysfunction after cold preservation of the liver by gaseous oxygen. Transpl Int 9 Suppl 1 (1996) S425-8.

[446] T. Minor, H. Klauke, and W. Isselhard, Resuscitation of cadaveric livers from non-heart-beating donors after warm ischemic insult: a novel technique tested in the rat. Experientia 52 (1996) 661-4.

[447] E. Totsuka, U. Fung, K. Hakamada, M. Tanaka, K. Takahashi, M. Nakai, S. Morohashi, A. Nishimura, Y. Ishizawa, H. Ono, Y. Toyoki, S. Narumi, and M. Sasaki, Analysis of clinical variables of donors and recipients with respect to short-term graft outcome in human liver transplantation. Transplant Proc 36 (2004) 2215-8.

[448] T. Piratvisuth, J.M. Tredger, K.A. Hayllar, and R. Williams, Contribution of true cold and rewarming ischemia times to factors determining outcome after orthotopic liver transplantation. Liver Transpl Surg 1 (1995) 296-301.

[449] K.P. Platz, A.R. Mueller, C. Schafer, S. Jahns, O. Guckelberger, and P. Neuhaus, Influence of warm ischemia time on initial graft function in human liver transplantation. Transplant Proc 29 (1997) 3458-9.

[450] T. Minor, H. Klauke, M. Nagelschmidt, and W. Isselhard, Reduction of proteolysis by venous-systemic oxygen persufflation during rat liver preservation and improved functional outcome after transplantation. Transplantation 63 (1997) 365-8.

[451] T. Minor, H. Klauke, B. Vollmar, W. Isselhard, and M.D. Menger, Biophysical aspects of liver aeration by vascular persufflation with gaseous oxygen. Transplantation 63 (1997) 1843-6.

[452] T. Minor, H. Klauke, B. Vollmar, M.D. Menger, and W. Isselhard, Rat liver transplantation after long-term preservation by venous systemic oxygen persufflation. Transplant Proc 29 (1997) 410-1.

[453] T. Minor, S. Saad, M. Kotting, M. Nagelschmidt, and W. Isselhard, Short-term restoration by gaseous oxygen for long-term preservation of predamaged livers from non-heart-beating donors. Transplant Proc 29 (1997) 3474-5.

[454] T. Minor, B. Vollmar, H. Klauke, W. Isselhard, and M.D. Menger, Gaseous oxygenation of the ischemic rat liver. The influence of driving pressure and oxygen concentration on tissue aeration. Adv Exp Med Biol 454 (1998) 91-4.

[455] T. Minor, S. Saad, M. Nagelschmidt, M. Kotting, Z. Fu, A. Paul, and W. Isselhard, Successful transplantation of porcine livers after warm ischemic insult in situ and cold preservation including postconditioning with gaseous oxygen. Transplantation 65 (1998) 1262-4.

[456] S. Saad, T. Minor, M. Kotting, Z.X. Fu, U. Hagn, A. Paul, and M. Nagelschmidt, Extension of ischemic tolerance of porcine livers by cold preservation including postconditioning with gaseous oxygen. Transplantation 71 (2001) 498-502.

[457] T. Minor, J. Stegemann, A. Hirner, and M. Koetting, Impaired autophagic clearance after cold preservation of fatty livers correlates with tissue necrosis upon reperfusion and is reversed by hypothermic reconditioning. Liver Transpl 15 (2009) 798-805.

[458] H. Lauschke, M. Kotting, S. Akbar, and T. Minor, Use of taurine as antioxidant in resuscitating livers from non-heart-beating donors by gaseous oxygen persufflation. J Invest Surg 16 (2003) 7-11.

[459] T. Minor, H. Klauke, and W. Isselhard, Improved preservation of the small bowel by luminal gas oxygenation: energetic status during ischemia and functional integrity upon reperfusion. Transplant Proc 29 (1997) 2994-6.

[460] A. Agrawal, K. Gurusamy, S. Powis, D.W. Gray, B. Fuller, and B.R. Davidson, A meta-analysis of the impact of the two-layer method of preservation on human pancreatic islet transplantation. Cell Transplant 17 (2008) 1315-22.

[461] J. Caballero-Corbalan, T. Eich, T. Lundgren, A. Foss, M. Felldin, R. Kallen, K. Salmela, A. Tibell, G. Tufveson, O. Korsgren, and D. Brandhorst, No beneficial effect of two-layer storage compared with UW-storage on human islet isolation and transplantation. Transplantation 84 (2007) 864-9.

[462] M.J. Taylor, S. Baicu, E. Greene, A. Vazquez, and J. Brassil, Islet isolation from juvenile porcine pancreas after 24-h hypothermic machine perfusion preservation. Cell Transplant 19 (2010) 613-28.

[463] M.J. Taylor, and S.C. Baicu, Hypothermic Perfusion of Pancreas: Emphasis on Preservation prior to Islet Isolation. in: K. Uykun, and C.Y. Lee, (Eds.), Organ Preservation and Reengineering, Artech House Publisher, Boston, 2011, pp. 85-104.

[464] J. Treckmann, C. Moers, J.M. Smits, A. Gallinat, M.H. Maathuis, M. van Kasterop-Kutz, I. Jochmans, J.J. Homan van der Heide, J.P. Squifflet, E. van Heurn, G.R. Kirste, A. Rahmel, H.G. Leuvenink, J. Pirenne, R.J. Ploeg, and A. Paul, Machine perfusion versus cold storage for preservation of kidneys from expanded criteria donors after brain death. Transpl Int 24 (2011) 548-54.

[465] L. Matsuoka, T. Shah, S. Aswad, S. Bunnapradist, Y. Cho, R.G. Mendez, R. Mendez, and R. Selby, Pulsatile perfusion reduces the incidence of delayed graft function in expanded criteria donor kidney transplantation. Am J Transplant 6 (2006) 1473-8.

[466] M.L. Nicholson, S.A. Hosgood, M.S. Metcalfe, J.R. Waller, and N.R. Brook, A comparison of renal preservation by cold storage and machine perfusion using a porcine autotransplant model. Transplantation 78 (2004) 333-7.

[467] R.J. Stratta, P.S. Moore, A.C. Farney, J. Rogers, E.L. Hartmann, A. Reeves-Daniel, M.D. Gautreaux, S.S. Iskandar, and P.L. Adams, Influence of pulsatile perfusion preservation on outcomes in kidney transplantation from expanded criteria donors. J Am Coll Surg 204 (2007) 873-82; discussion 882-4.

[468] J. Wight, J. Chilcott, M. Holmes, and N. Brewer, The clinical and cost-effectiveness of pulsatile machine perfusion versus cold storage of kidneys for transplantation retrieved from heart-beating and non-heart-beating donors. Health Technol Assess 7 (2003) 1-94.

[469] J.V. Guarrera, S.D. Henry, B. Samstein, R. Odeh-Ramadan, M. Kinkhabwala, M.J. Goldstein, L.E. Ratner, J.F. Renz, H.T. Lee, R.S. Brown, Jr., and J.C. Emond, Hypothermic machine preservation in human liver transplantation: the first clinical series. Am J Transplant 10 (2010) 372-81.

[470] P.W. So, and B.J. Fuller, A comparison of the metabolic effects of continuous hypothermic perfusion or oxygenated persufflation during hypothermic storage of rat liver. Cryobiology 43 (2001) 238-47.

[471] J. Stegemann, A. Hirner, U. Rauen, and T. Minor, Gaseous oxygen persufflation or oxygenated machine perfusion with Custodiol-N for long-term preservation of ischemic rat livers? Cryobiology 58 (2009) 45-51.

[472] A.O. Ojo, R.A. Wolfe, P.J. Held, F.K. Port, and R.L. Schmouder, Delayed graft function: risk factors and implications for renal allograft survival. Transplantation 63 (1997) 968-74.

[473] N. Perico, D. Cattaneo, M.H. Sayegh, and G. Remuzzi, Delayed graft function in kidney transplantation. Lancet 364 (2004) 1814-27.

[474] P.O. Carlsson, A. Kiuru, A. Nordin, R. Olsson, J.M. Lin, P. Bergsten, L. Hillered, A. Andersson, and L. Jansson, Microdialysis measurements demonstrate a shift to nonoxidative glucose metabolism in rat pancreatic islets transplanted beneath the renal capsule. Surgery 132 (2002) 487-94.

[475] D.A. Lepore, T.A. Shinkel, N. Fisicaro, T.B. Mysore, L.E. Johnson, A.J. d'Apice, and P.J. Cowan, Enhanced expression of glutathione peroxidase protects islet beta cells from hypoxia-reoxygenation. Xenotransplantation 11 (2004) 53-9.

[476] P. Fiorina, and A. Secchi, Pancreatic islet cell transplant for treatment of diabetes. Endocrinol Metab Clin North Am 36 (2007) 999-1013; ix.

[477] N.A. Turgeon, J.G. Avila, J.A. Cano, J.J. Hutchinson, I.R. Badell, A.J. Page, A.B. Adams, M.H. Sears, P.H. Bowen, A.D. Kirk, T.C. Pearson, and C.P. Larsen, Experience with a novel efalizumab-based immunosuppressive regimen to facilitate single donor islet cell transplantation. Am J Transplant 10 (2010) 2082-91.

[478] D. Yin, J.W. Ding, J. Shen, L. Ma, M. Hara, and A.S. Chong, Liver ischemia contributes to early islet failure following intraportal transplantation: benefits of liver ischemic-preconditioning. Am J Transplant 6 (2006) 60-8.

[479] A.N. Balamurugan, R. Bottino, N. Giannoukakis, and C. Smetanka, Prospective and challenges of islet transplantation for the therapy of autoimmune diabetes. Pancreas 32 (2006) 231-43.

[480] S. Abdelli, J. Ansite, R. Roduit, T. Borsello, I. Matsumoto, T. Sawada, N. Allaman-Pillet, H. Henry, J.S. Beckmann, B.J. Hering, and C. Bonny, Intracellular stress

signaling pathways activated during human islet preparation and following acute cytokine exposure. Diabetes 53 (2004) 2815-23.

[481] M. Heuser, B. Wolf, B. Vollmar, and M.D. Menger, Exocrine contamination of isolated islets of Langerhans deteriorates the process of revascularization after free transplantation. Transplantation 69 (2000) 756-61.

[482] N.J. London, S.M. Swift, and H.A. Clayton, Isolation, culture and functional evaluation of islets of Langerhans. Diabetes Metab 24 (1998) 200-7.

[483] J.E. Davies, S. Winoto-Morbach, K. Ulrichs, R.F. James, and G.S. Robertson, A comparison of the use of two immunomagnetic microspheres for secondary purification of pancreatic islets. Transplantation 62 (1996) 1301-6.

[484] T. Fujioka, P.I. Terasaki, R. Heintz, N. Merideth, R.P. Lanza, T.L. Zheng, and P. Soon-Shiong, Rapid purification of islets using magnetic microspheres coated with anti-acinar cell monoclonal antibodies. Transplantation 49 (1990) 404-7.

[485] G.G. Pinkse, E. Steenvoorde, S. Hogendoorn, M. Noteborn, O.T. Terpstra, J.A. Bruijn, and E. De Heer, Stable transplantation results of magnetically retracted islets: a novel method. Diabetologia 47 (2004) 55-61.

[486] D.J. Kennedy, P. Todd, S. Logan, M. Becker, K.K. Papas, and L.R. Moore, Engineering quadrupole magnetic flow sorting for the isolation of pancreatic islets. Journal of Magnetism and Magnetic Materials 311 (2007) 388-395.

[487] R.M. Shenkman, J.J. Chalmers, B.J. Hering, N. Kirchhof, and K.K. Papas, Quadrupole magnetic sorting of porcine islets of Langerhans. Tissue Eng Part C Methods 15 (2009) 147-56.

[488] S.D. Rowley, M. Loken, J. Radich, L.A. Kunkle, B.J. Mills, T. Gooley, L. Holmberg, P. McSweeney, K. Beach, B. MacLeod, F. Appelbaum, and W.I. Bensinger,

Isolation of CD34+ cells from blood stem cell components using the Baxter Isolex system. Bone Marrow Transplant 21 (1998) 1253-62.

[489] R.L. Pongratz, R.G. Kibbey, C.L. Kirkpatrick, X. Zhao, M. Pontoglio, M. Yaniv, C.B. Wollheim, G.I. Shulman, and G.W. Cline, Mitochondrial dysfunction contributes to impaired insulin secretion in INS-1 cells with dominant-negative mutations of HNF-1alpha and in HNF-1alpha-deficient islets. J Biol Chem 284 (2009) 16808-21.

[490] A.N. Balamurugan, J. He, F. Guo, D.B. Stolz, S. Bertera, X. Geng, X. Ge, M. Trucco, and R. Bottino, Harmful delayed effects of exogenous isolation enzymes on isolated human islets: relevance to clinical transplantation. Am J Transplant 5 (2005) 2671-81.

[491] H.A. Tons, A.G. Baranski, O.T. Terpstra, and E. Bouwman, Isolation of the islets of Langerhans from the human pancreas with magnetic retraction. Transplant Proc 40 (2008) 413-4.

[492] L. Rosenberg, R. Wang, S. Paraskevas, and D. Maysinger, Structural and functional changes resulting from islet isolation lead to islet cell death. Surgery 126 (1999) 393-8.

[493] H. Noguchi, Activation of c-Jun NH2-terminal kinase during islet isolation. Endocr J 54 (2007) 169-76.

[494] H. Noguchi, Y. Nakai, M. Ueda, Y. Masui, S. Futaki, N. Kobayashi, S. Hayashi, and S. Matsumoto, Activation of c-Jun NH2-terminal kinase (JNK) pathway during islet transplantation and prevention of islet graft loss by intraportal injection of JNK inhibitor. Diabetologia 50 (2007) 612-9.

[495] M. Satoh, Y. Yasunami, N. Matsuoka, M. Nakano, T. Itoh, T. Nitta, K. Anzai, J. Ono, M. Taniguchi, and S. Ikeda, Successful islet transplantation to two recipients from

a single donor by targeting proinflammatory cytokines in mice. Transplantation 83 (2007) 1085-92.

[496] P.S. Williams, M. Zborowski, and J.J. Chalmers, Flow rate optimization for the quadrupole magnetic cell sorter. Anal Chem 71 (1999) 3799-807.

[497] T. Anazawa, A.N. Balamurugan, K.K. Papas, E.S. Avgoustiniatos, J. Ferrer, S. Matsumoto, D.E. Sutherland, and B.J. Hering, Improved method of porcine pancreas procurement with arterial flush and ductal injection enhances islet isolation outcome. Transplant Proc 42 (2010) 2032-5.

Appendices

Appendix 2-1: Permission to Reprint (Papas KK *et al*. Curr Opin Org Transplant [2009])

WOLTERS KLUWER HEALTH LICENSE TERMS AND CONDITIONS

Jun 08, 2012

This is a License Agreement between Thomas M Suszynski ("You") and Wolters Kluwer Health ("Wolters Kluwer Health") provided by Copyright Clearance Center ("CCC"). The license consists of your order details, the terms and conditions provided by Wolters Kluwer Health, and the payment terms and conditions.

All payments must be made in full to CCC. For payment instructions, please see information listed at the bottom of this form.

License Number	2924370581699
License date	Jun 08, 2012
Licensed content publisher	Wolters Kluwer Health
Licensed content publication	Current Opinion in Organ Transplantation
Licensed content title	Islet assessment for transplantation
Licensed content author	Klearchos Papas, Thomas Suszynski, and Clark Colton
Licensed content date	Jan 1, 2009
Volume Number	14
Issue Number	6
Type of Use	Dissertation/Thesis
Requestor type	Individual
Order reference number	Papas KK, COOT (2009)
Title of your thesis / dissertation	TISSUE-ENGINEERED ISLET GRAFT DESIGN AND ASSESSMENT
Expected completion date	Sep 2012
Estimated size(pages)	400
Billing Type	Invoice
Billing address	2871 Irving Ave S Apt 1 Minneapolis, MN 55408 United States
Customer reference info	
Total	0.00 USD
Terms and Conditions	

Terms and Conditions

1. A credit line will be prominently placed and include: for books - the author(s), title of book,

editor, copyright holder, year of publication; For journals - the author(s), title of article, title of journal, volume number, issue number and inclusive pages.

2. The requestor warrants that the material shall not be used in any manner which may be considered derogatory to the title, content, or authors of the material, or to Wolters Kluwer.
3. Permission is granted for a one time use only within 12 months from the date of this invoice. Rights herein do not apply to future reproductions, editions, revisions, or other derivative works. Once the 12-month term has expired, permission to renew must be submitted in writing.
4. Permission granted is non-exclusive, and is valid throughout the world in the English language and the languages specified in your original request.
5. Wolters Kluwer cannot supply the requestor with the original artwork or a "clean copy."
6. The requestor agrees to secure written permission from the author (for book material only).
7. Permission is valid if the borrowed material is original to a Wolters Kluwer imprint (Lippincott-Raven Publishers, Williams & Wilkins, Lea & Febiger, Harwal, Igaku-Shoin, Rapid Science, Little Brown & Company, Harper & Row Medical, American Journal of Nursing Co, and Urban & Schwarzenberg - English Language).
8. If you opt not to use the material requested above, please notify Rightslink within 90 days of the original invoice date.
9. Please note that articles in the ahead-of-print stage of publication can be cited and the content may be re-used by including the date of access and the unique DOI number. Any final changes in manuscripts will be made at the time of print publication and will be reflected in the final electronic version of the issue.
   Disclaimer: Articles appearing in the Published Ahead-of-Print section have been peer-reviewed and accepted for publication in the relevant journal and posted online before print publication. Articles appearing as publish ahead-of-print may contain statements, opinions, and information that have errors in facts, figures, or interpretation. Accordingly, Lippincott Williams & Wilkins, the editors and authors and their respective employees are not responsible or liable for the use of any such inaccurate or misleading data, opinion or information contained in the articles in this section.
10. Other Terms and Conditions:

v1.3

If you would like to pay for this license now, please remit this license along with your payment made payable to "COPYRIGHT CLEARANCE CENTER" otherwise you will be invoiced within 48 hours of the license date. Payment should be in the form of a check or money order referencing your account number and this invoice number RLNK500795740. Once you receive your invoice for this order, you may pay your invoice by credit card. Please follow instructions provided at that time.

Make Payment To:
Copyright Clearance Center
Dept 001
P.O. Box 843006
Boston, MA 02284-3006

For suggestions or comments regarding this order, contact RightsLink Customer Support: customercare@copyright.com or +1-877-622-5543 (toll free in the US) or +1-978-646-2777.

Gratis licenses (referencing $0 in the Total field) are free. Please retain this printable

license for your reference. No payment is required.

Appendix 3-1: Permission to Reprint (Suszynski *et al*. Transplant Proc [2008])

ELSEVIER LICENSE
TERMS AND CONDITIONS

Jun 08, 2012

This is a License Agreement between Thomas M Suszynski ("You") and Elsevier ("Elsevier") provided by Copyright Clearance Center ("CCC"). The license consists of your order details, the terms and conditions provided by Elsevier, and the payment terms and conditions.

All payments must be made in full to CCC. For payment instructions, please see information listed at the bottom of this form.

Supplier	Elsevier Limited The Boulevard,Langford Lane Kidlington,Oxford,OX5 1GB,UK
Registered Company Number	1982084
Customer name	Thomas M Suszynski
Customer address	2871 Irving Ave S Minneapolis, MN 55408
License number	2924361380000
License date	Jun 08, 2012
Licensed content publisher	Elsevier
Licensed content publication	Transplantation Proceedings
Licensed content title	The ATP/DNA Ratio Is a Better Indicator of Islet Cell Viability Than the ADP/ATP Ratio
Licensed content author	T.M. Suszynski,G.M. Wildey,E.J. Falde,G.W. Cline,K. Stewart Maynard,N. Ko,J. Sotiris,A. Naji,B.J. Hering,K.K. Papas
Licensed content date	March 2008
Licensed content volume number	40
Licensed content issue number	2
Number of pages	5
Start Page	346
End Page	350
Type of Use	reuse in a thesis/dissertation
Intended publisher of new work	other
Portion	full article
Format	both print and electronic
Are you the author of this Elsevier article?	Yes
Will you be translating?	No

Order reference number	Suszynski T, Trans Proc (2008)
Title of your thesis/dissertation	TISSUE-ENGINEERED ISLET GRAFT DESIGN AND ASSESSMENT
Expected completion date	Sep 2012
Estimated size (number of pages)	400
Elsevier VAT number	GB 494 6272 12
Permissions price	0.00 USD
VAT/Local Sales Tax	0.0 USD / 0.0 GBP
Total	0.00 USD
Terms and Conditions	

INTRODUCTION

1. The publisher for this copyrighted material is Elsevier. By clicking "accept" in connection with completing this licensing transaction, you agree that the following terms and conditions apply to this transaction (along with the Billing and Payment terms and conditions established by Copyright Clearance Center, Inc. ("CCC"), at the time that you opened your Rightslink account and that are available at any time at http://myaccount.copyright.com).

GENERAL TERMS

2. Elsevier hereby grants you permission to reproduce the aforementioned material subject to the terms and conditions indicated.

3. Acknowledgement: If any part of the material to be used (for example, figures) has appeared in our publication with credit or acknowledgement to another source, permission must also be sought from that source. If such permission is not obtained then that material may not be included in your publication/copies. Suitable acknowledgement to the source must be made, either as a footnote or in a reference list at the end of your publication, as follows:

"Reprinted from Publication title, Vol /edition number, Author(s), Title of article / title of chapter, Pages No., Copyright (Year), with permission from Elsevier [OR APPLICABLE SOCIETY COPYRIGHT OWNER]." Also Lancet special credit - "Reprinted from The Lancet, Vol. number, Author(s), Title of article, Pages No., Copyright (Year), with permission from Elsevier."

4. Reproduction of this material is confined to the purpose and/or media for which permission is hereby given.

5. Altering/Modifying Material: Not Permitted. However figures and illustrations may be altered/adapted minimally to serve your work. Any other abbreviations, additions, deletions and/or any other alterations shall be made only with prior written authorization of Elsevier Ltd. (Please contact Elsevier at permissions@elsevier.com)

6. If the permission fee for the requested use of our material is waived in this instance, please be advised that your future requests for Elsevier materials may attract a fee.

7. Reservation of Rights: Publisher reserves all rights not specifically granted in the combination of (i) the license details provided by you and accepted in the course of this licensing transaction, (ii) these terms and conditions and (iii) CCC's Billing and Payment terms and conditions.

8. License Contingent Upon Payment: While you may exercise the rights licensed immediately upon issuance of the license at the end of the licensing process for the transaction, provided that you have disclosed complete and accurate details of your proposed use, no license is finally effective unless and until full payment is received from you (either by publisher or by CCC) as provided in CCC's Billing and Payment terms and conditions. If full payment is not received on a timely basis, then any license preliminarily granted shall be deemed automatically revoked and shall be void as if never granted. Further, in the event that you breach any of these terms and conditions or any of CCC's Billing and Payment terms and conditions, the license is automatically revoked and shall be void as if never granted. Use of materials as described in a revoked license, as well as any use of the materials beyond the scope of an unrevoked license, may constitute copyright infringement and publisher reserves the right to take any and all action to protect its copyright in the materials.

9. Warranties: Publisher makes no representations or warranties with respect to the licensed material.

10. Indemnity: You hereby indemnify and agree to hold harmless publisher and CCC, and their respective officers, directors, employees and agents, from and against any and all claims arising out of your use of the licensed material other than as specifically authorized pursuant to this license.

11. No Transfer of License: This license is personal to you and may not be sublicensed, assigned, or transferred by you to any other person without publisher's written permission.

12. No Amendment Except in Writing: This license may not be amended except in a writing signed by both parties (or, in the case of publisher, by CCC on publisher's behalf).

13. Objection to Contrary Terms: Publisher hereby objects to any terms contained in any purchase order, acknowledgment, check endorsement or other writing prepared by you, which terms are inconsistent with these terms and conditions or CCC's Billing and Payment terms and conditions. These terms and conditions, together with CCC's Billing and Payment terms and conditions (which are incorporated herein), comprise the entire agreement between you and publisher (and CCC) concerning this licensing transaction. In the event of any conflict between your obligations established by these terms and conditions and those established by CCC's Billing and Payment terms and conditions, these terms and conditions shall control.

14. Revocation: Elsevier or Copyright Clearance Center may deny the permissions described in this License at their sole discretion, for any reason or no reason, with a full refund payable to you. Notice of such denial will be made using the contact information provided by you. Failure to receive such notice will not alter or invalidate the denial. In no event will Elsevier or Copyright Clearance Center be responsible or liable for any costs, expenses or damage incurred by you as a result of a denial of your permission request, other than a refund of the amount(s) paid by you to Elsevier and/or Copyright Clearance Center for denied permissions.

LIMITED LICENSE

The following terms and conditions apply only to specific license types:

15. **Translation**: This permission is granted for non-exclusive world **English** rights only unless your license was granted for translation rights. If you licensed translation rights you may only translate this content into the languages you requested. A professional translator must perform all translations and reproduce the content word for word preserving the integrity of the article. If this license is to re-use 1 or 2 figures then permission is granted for non-exclusive world rights in all languages.

16. **Website**: The following terms and conditions apply to electronic reserve and author websites:
Electronic reserve: If licensed material is to be posted to website, the web site is to be password-protected and made available only to bona fide students registered on a relevant course if:
This license was made in connection with a course,
This permission is granted for 1 year only. You may obtain a license for future website posting,
All content posted to the web site must maintain the copyright information line on the bottom of each image,
A hyper-text must be included to the Homepage of the journal from which you are licensing at http://www.sciencedirect.com/science/journal/xxxxx or the Elsevier homepage for books at http://www.elsevier.com , and
Central Storage: This license does not include permission for a scanned version of the material to be stored in a central repository such as that provided by Heron/XanEdu.

17. **Author website** for journals with the following additional clauses:

All content posted to the web site must maintain the copyright information line on the bottom of each image, and the permission granted is limited to the personal version of your paper. You are not allowed to download and post the published electronic version of your article (whether PDF or HTML, proof or final version), nor may you scan the printed edition to create an electronic version.
A hyper-text must be included to the Homepage of the journal from which you are licensing at http://www.sciencedirect.com/science/journal/xxxxx . As part of our normal production process, you will receive an e-mail notice when your article appears on Elsevier's online service ScienceDirect (www.sciencedirect.com). That e-mail will include the article's Digital Object Identifier (DOI). This number provides the electronic link to the published article and should be included in the posting of your personal version. We ask that you wait until you receive this e-mail and have the DOI to do any posting.

Central Storage: This license does not include permission for a scanned version of the material to be stored in a central repository such as that provided by Heron/XanEdu.

18. **Author website** for books with the following additional clauses:
Authors are permitted to place a brief summary of their work online only.
A hyper-text must be included to the Elsevier homepage at http://www.elsevier.com . All content posted to the web site must maintain the copyright information line on the bottom of each image.
You are not allowed to download and post the published electronic version of your chapter, nor may you scan the printed edition to create an electronic version.

Central Storage: This license does not include permission for a scanned version of the material to be stored in a central repository such as that provided by Heron/XanEdu.

19. **Website** (regular and for author): A hyper-text must be included to the Homepage of the journal from which you are licensing at http://www.sciencedirect.com/science/journal/xxxxx. or for books to the Elsevier homepage at http://www.elsevier.com

20. **Thesis/Dissertation**: If your license is for use in a thesis/dissertation your thesis may be submitted to your institution in either print or electronic form. Should your thesis be published commercially, please reapply for permission. These requirements include permission for the Library and Archives of Canada to supply single copies, on demand, of the complete thesis and include permission for UMI to supply single copies, on demand, of the complete thesis. Should your thesis be published commercially, please reapply for permission.

21. **Other Conditions**:

v1.6

If you would like to pay for this license now, please remit this license along with your payment made payable to "COPYRIGHT CLEARANCE CENTER" otherwise you will be invoiced within 48 hours of the license date. Payment should be in the form of a check or money order referencing your account number and this invoice number RLNK500795730. Once you receive your invoice for this order, you may pay your invoice by credit card. Please follow instructions provided at that time.

Make Payment To:
Copyright Clearance Center
Dept 001
P.O. Box 843006
Boston, MA 02284-3006

For suggestions or comments regarding this order, contact RightsLink Customer Support: customercare@copyright.com or +1-877-622-5543 (toll free in the US) or +1-978-646-2777.

Gratis licenses (referencing $0 in the Total field) are free. Please retain this printable license for your reference. No payment is required.

Appendix 3-2: ATP/DNA measurements in porcine islets following chemical treatment (sodium dithionate, sodium azide) and pelleting for ≥20 hours.

Objective: To determine the effect of long-term incubation with sodium dithionate (strong reducing agent) and sodium azide (cytochrome oxidase inhibitor), or pelleting on islet viability – as measured by the ATP/DNA assay (as previously described [55]).

Methods: Porcine islets were isolated as previously described [371]. *Chemical treatment*: About 10 mL of ME199 culture media supplemented with 10% fetal bovine serum and 6000 IEs (porcine islets) were added to each of two T-25 flasks (BD Biosciences, San Jose, CA). Samples (100-µL, n = 3 per flask) were taken prior to addition of any chemical toxin, sonicated and frozen for ATP and DNA quantification [55]. Sodium dithionate (Sigma-Aldrich, St. Louis, MO) was then added to a concentration of 4 mM in one flask, and sodium azide (Sigma-Aldrich, St. Louis, MO) was added to a concentration of 2 mM in the other flask. Both flasks were then cultured for 20 hours at 37°C and 5% CO_2. At the end of the 20-hour culture period, samples (100-µL, n = 3 per flask) were taken, sonicated and frozen. *Pelleting*: About 6000 IEs (porcine islets) were added to a 15-mL conical tube and centrifuged for 2 minutes at 760 rotations per minute (75 x g) to form a pellet. The media was aspirated off, and fresh ME199 culture media supplemented with 10% fetal bovine serum was added to the conical tube. Islets were resuspended and samples (100-µL, n = 3 per flask) were taken, sonicated and frozen for ATP and DNA quantification [55]. After sampling was done, the islets were centrifuged again for 2 minutes at 760 rotations per minute. The conical tube was placed into an incubator (37°C, 5% CO_2) and maintained under those conditions for 23 hours. After the incubation period, samples (100-µL, n = 3 per flask) were taken, sonicated and frozen.

All ATP measurements were performed using CellTiter-Glo luminescent cell viability assay (Promega Corp., Madison, WI) per manufacturer instructions. All DNA measurements were performed using Quant-iT PicoGreen dsDNA assay kit (Invitrogen, Eugene, OR). All ATP/DNA measurements were performed in triplicate (n = 3) and the mean ± SE are presented.

Paired student's t-tests were performed to examine for differences between control (pre-culture) and experimental (post-culture) ATP/DNA measurements following both sodium dithionate and sodium azide treatment.

Results:

There were significant reductions in ATP/DNA of the porcine islet preparation following 20 hours of culture with sodium dithionate ($p = 0.022$) and sodium azide ($p = 0.017$) (**Figure 3-5**). Similarly, there was a significant reduction in ATP/DNA of the porcine islet preparation following 23 hours of incubation as a pellet (**Figure 3-6**). Sodium azide treatment resulted in the largest absolute change in ATP/DNA of any of the treatments, though none of the treatments resulted in ATP/DNA measurements with a value of zero.

Conclusion:

Chemical treatment with sodium dithionate or sodium azide and pelleting significantly reduced ATP/DNA following ≥20 hours of treatment. However, none of the treatments resulted in zero measured ATP and thus may not predictable reduce the viability of an islet preparation for future comparisons between ATP/DNA and ADP/ATP.

Figure Captions (Appendix 3-2)

Figure 3-5: ATP/DNA measurements of porcine islet preparation before and after 20-hour chemical treatment with sodium dithionate (A) or sodium azide (B). There were significant differences in the ATP/DNA between paired control and experimental samples for both sodium dithionate ($p = 0.022$) and sodium azide ($p = 0.017$). *Abbreviations*: ATP, adenosine triphosphate; DNA, deoxyribonucleic acid.

Figure 3-6: ATP/DNA measurements of porcine islet preparation before and after 23-hour incubation as a pellet. There was a significant difference in the ATP/DNA between the control and experimental samples ($p = 0.025$). *Abbreviations*: ATP, adenosine triphosphate; DNA, deoxyribonucleic acid.

Figure 3-5: Chemical treatment

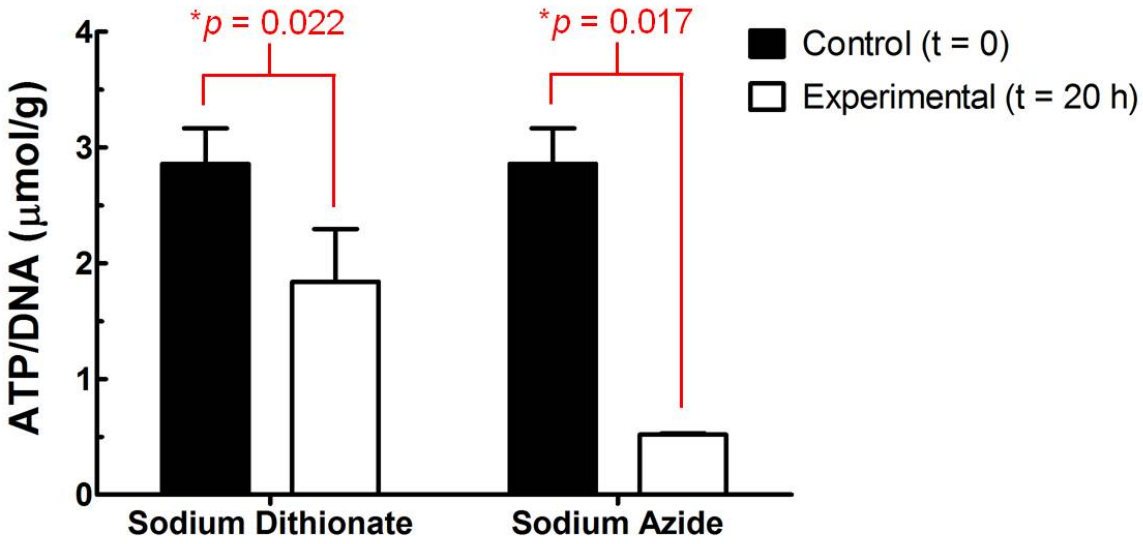

Figure 3-6: Pelleting

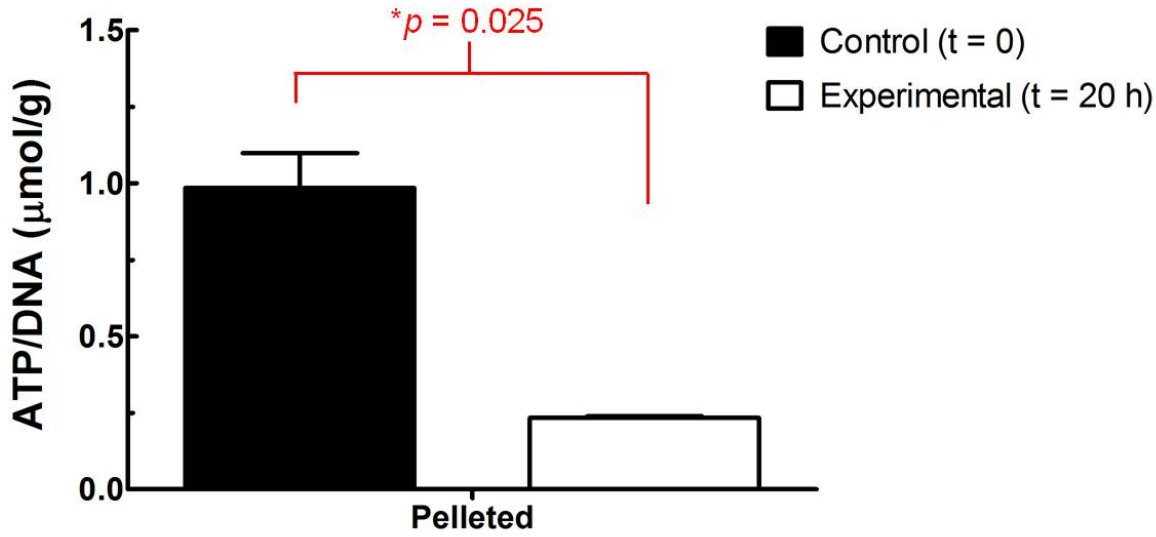

Appendix 3-3: Paired ATP/DNA and ADP/ATP measurements of two different human islet preparations. Both ATP/DNA and ADP/ATP measurements are presented as normalized over the highest value for that preparation..

Figure captions (Appendix 3-3)

Figure 3-7: Normalized ATP/DNA (A) and ADP/ATP (B) measurements for the first human islet preparation. The linear correlation between viability metric and the percent fraction of non-viable (heat-treated) islets was stronger for ATP/DNA (R^2 = 0.94) versus ADP/ATP (R^2 = 0.37). *Abbreviations*: ADP, adenosine diphosphate; ATP, adenosine triphosphate.

Figure 3-8: Normalized ATP/DNA (A) and ADP/ATP (B) measurements for the first human islet preparation. The linear correlation between viability metric and the percent fraction of non-viable (heat-treated) islets was stronger for ATP/DNA (R^2 = 0.89) versus ADP/ATP (R^2 = 0.15). *Abbreviations*: ADP, adenosine diphosphate; ATP, adenosine triphosphate.

Figure 3-7

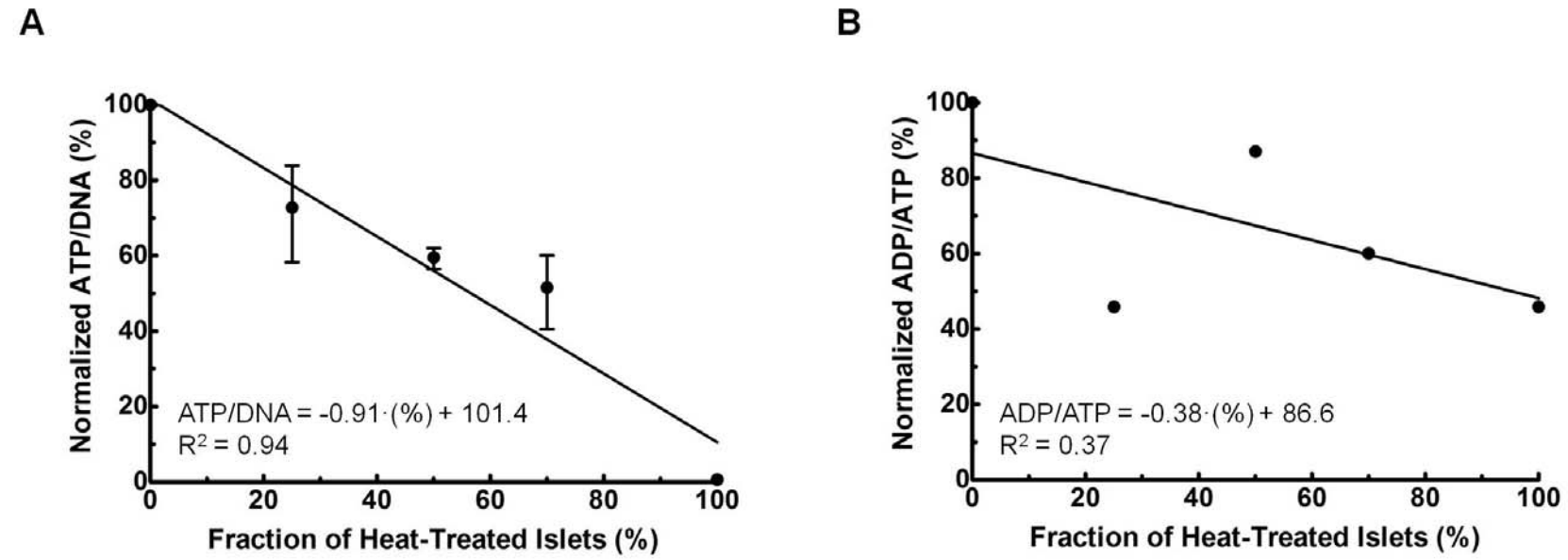
A
Normalized ATP/DNA (%)
100
80
60
40
20
0
0
20
40
60
80
100
Fraction of Heat-Treated Islets (%)
ATP/DNA = -0.91·(%) + 101.4
R2 = 0.94
B
Normalized ADP/ATP (%)
100
80
60
40
20
0
0
20
40
60
80
100
Fraction of Heat-Treated Islets (%)
ADP/ATP = -0.38·(%) + 86.6
R2 = 0.37

Figure 3-8

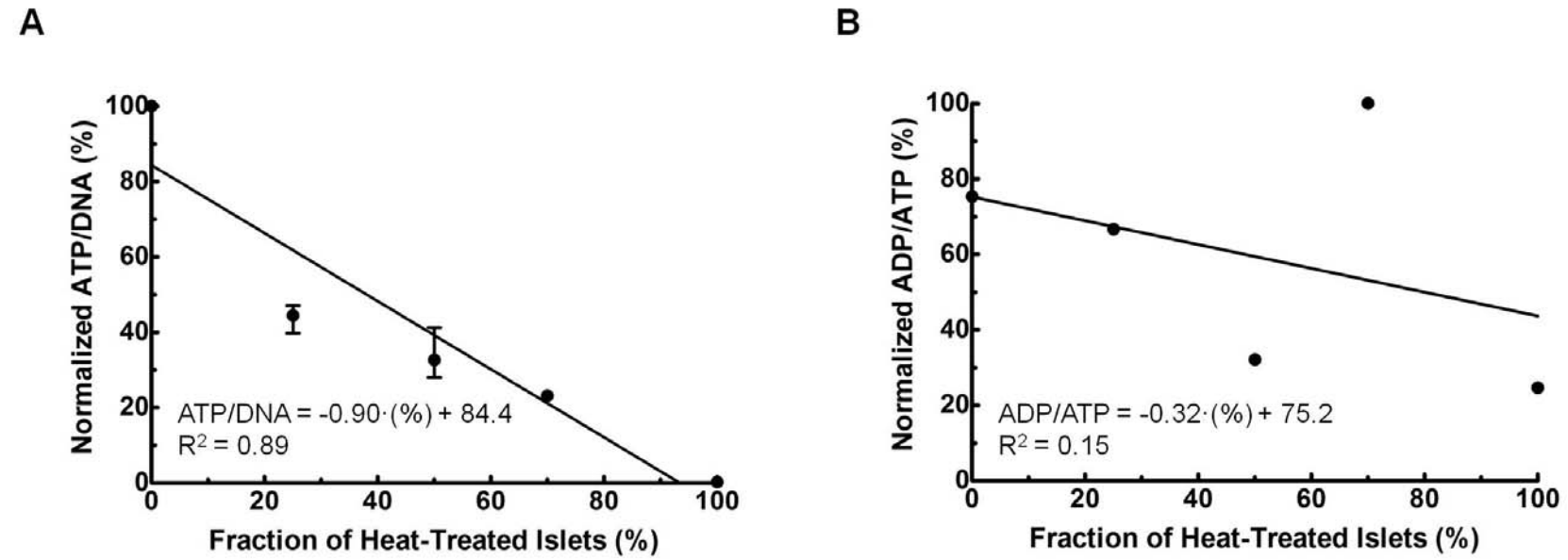
A
Normalized ATP/DNA (%)
100
80
60
40
20
0
0
20
40
60
80
100
Fraction of Heat-Treated Islets (%)
ATP/DNA = -0.90·(%) + 84.4
R2 = 0.89
B
Normalized ADP/ATP (%)
100
80
60
40
20
0
0
20
40
60
80
100
Fraction of Heat-Treated Islets (%)
ADP/ATP = -0.32·(%) + 75.2
R2 = 0.15

Appendix 3-4: Representative ADP/ATP measurements of INS-1 cell preparations. ADP/ATP measurements are presented as normalized over the highest value for that preparation.

Figure Caption (Appendix 3-4)

Figure 3-9: Representative normalized ADP/ATP measurements an INS-1 cell preparation with increasing percent fraction of non-viable (heat-treated) cells. These measurements illustrate the poor correlation between ADP/ATP and percent non-viable fraction, and the frequent negative values obtained using this assay; values obtained from 20-100% percent non-viable fraction were between -0.017 and -0.012. *Abbreviations*: ADP, adenosine diphosphate; ATP, adenosine triphosphate; INS, insulinoma.

Figure 3-9

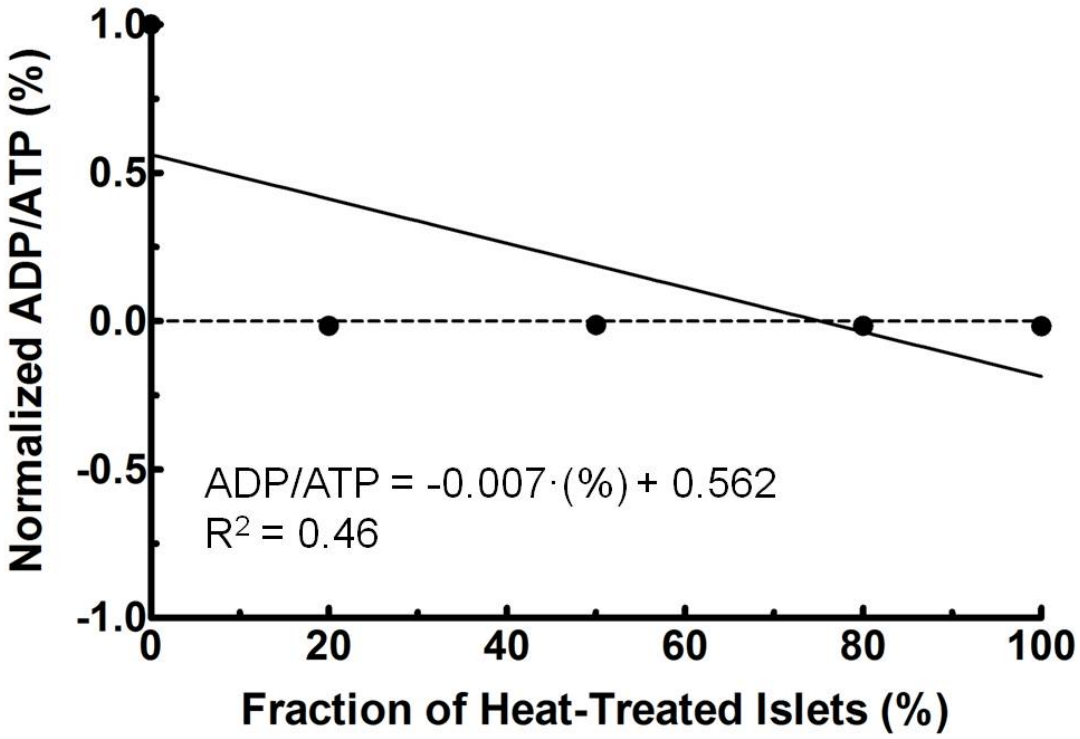
Normalized ADP/ATP (%)
1.0
0.5
0.0
-0.5
-1.0
0
20
40
60
80
100
Fraction of Heat-Treated Islets (%)
ADP/ATP = -0.007·(%) + 0.562
R2 = 0.46

Appendix 6-1: Permission to Reprint (Suszynski *et al*. Transplant Proc [2011])

ELSEVIER LICENSE
TERMS AND CONDITIONS

Jun 08, 2012

This is a License Agreement between Thomas M Suszynski ("You") and Elsevier ("Elsevier") provided by Copyright Clearance Center ("CCC"). The license consists of your order details, the terms and conditions provided by Elsevier, and the payment terms and conditions.

All payments must be made in full to CCC. For payment instructions, please see information listed at the bottom of this form.

Supplier	Elsevier Limited The Boulevard,Langford Lane Kidlington,Oxford,OX5 1GB,UK
Registered Company Number	1982084
Customer name	Thomas M Suszynski
Customer address	2871 Irving Ave S Minneapolis, MN 55408
License number	2924361020879
License date	Jun 08, 2012
Licensed content publisher	Elsevier
Licensed content publication	Transplantation Proceedings
Licensed content title	Assessment of Tissue-Engineered Islet Graft Viability by Fluorine Magnetic Resonance Spectroscopy
Licensed content author	T.M. Suszynski,E.S. Avgoustiniatos,S.A. Stein,E.J. Falde,B.E. Hammer,K.K. Papas
Licensed content date	November 2011
Licensed content volume number	43
Licensed content issue number	9
Number of pages	5
Start Page	3221
End Page	3225
Type of Use	reuse in a thesis/dissertation
Portion	full article
Format	both print and electronic
Are you the author of this Elsevier article?	Yes
Will you be translating?	No
Order reference number	Suszynski T, Trans Proc (2011)

Title of your thesis/dissertation	TISSUE-ENGINEERED ISLET GRAFT DESIGN AND ASSESSMENT
Expected completion date	Sep 2012
Estimated size (number of pages)	400
Elsevier VAT number	GB 494 6272 12
Permissions price	0.00 USD
VAT/Local Sales Tax	0,0 USD / 0,0 GBP
Total	0,00 USD
Terms and Conditions	

INTRODUCTION

1. The publisher for this copyrighted material is Elsevier. By clicking "accept" in connection with completing this licensing transaction, you agree that the following terms and conditions apply to this transaction (along with the Billing and Payment terms and conditions established by Copyright Clearance Center, Inc. ("CCC"), at the time that you opened your Rightslink account and that are available at any time at http://myaccount.copyright.com).

GENERAL TERMS

2. Elsevier hereby grants you permission to reproduce the aforementioned material subject to the terms and conditions indicated.

3. Acknowledgement: If any part of the material to be used (for example, figures) has appeared in our publication with credit or acknowledgement to another source, permission must also be sought from that source. If such permission is not obtained then that material may not be included in your publication/copies. Suitable acknowledgement to the source must be made, either as a footnote or in a reference list at the end of your publication, as follows:

"Reprinted from Publication title, Vol /edition number, Author(s), Title of article / title of chapter, Pages No., Copyright (Year), with permission from Elsevier [OR APPLICABLE SOCIETY COPYRIGHT OWNER]." Also Lancet special credit - "Reprinted from The Lancet, Vol. number, Author(s), Title of article, Pages No., Copyright (Year), with permission from Elsevier."

4. Reproduction of this material is confined to the purpose and/or media for which permission is hereby given.

5. Altering/Modifying Material: Not Permitted. However figures and illustrations may be altered/adapted minimally to serve your work. Any other abbreviations, additions, deletions and/or any other alterations shall be made only with prior written authorization of Elsevier Ltd. (Please contact Elsevier at permissions@elsevier.com)

6. If the permission fee for the requested use of our material is waived in this instance, please be advised that your future requests for Elsevier materials may attract a fee.

7. Reservation of Rights: Publisher reserves all rights not specifically granted in the combination of (i) the license details provided by you and accepted in the course of this licensing transaction, (ii)

these terms and conditions and (iii) CCC's Billing and Payment terms and conditions.

8. License Contingent Upon Payment: While you may exercise the rights licensed immediately upon issuance of the license at the end of the licensing process for the transaction, provided that you have disclosed complete and accurate details of your proposed use, no license is finally effective unless and until full payment is received from you (either by publisher or by CCC) as provided in CCC's Billing and Payment terms and conditions. If full payment is not received on a timely basis, then any license preliminarily granted shall be deemed automatically revoked and shall be void as if never granted. Further, in the event that you breach any of these terms and conditions or any of CCC's Billing and Payment terms and conditions, the license is automatically revoked and shall be void as if never granted. Use of materials as described in a revoked license, as well as any use of the materials beyond the scope of an unrevoked license, may constitute copyright infringement and publisher reserves the right to take any and all action to protect its copyright in the materials.

9. Warranties: Publisher makes no representations or warranties with respect to the licensed material.

10. Indemnity: You hereby indemnify and agree to hold harmless publisher and CCC, and their respective officers, directors, employees and agents, from and against any and all claims arising out of your use of the licensed material other than as specifically authorized pursuant to this license.

11. No Transfer of License: This license is personal to you and may not be sublicensed, assigned, or transferred by you to any other person without publisher's written permission.

12. No Amendment Except in Writing: This license may not be amended except in a writing signed by both parties (or, in the case of publisher, by CCC on publisher's behalf).

13. Objection to Contrary Terms: Publisher hereby objects to any terms contained in any purchase order, acknowledgment, check endorsement or other writing prepared by you, which terms are inconsistent with these terms and conditions or CCC's Billing and Payment terms and conditions. These terms and conditions, together with CCC's Billing and Payment terms and conditions (which are incorporated herein), comprise the entire agreement between you and publisher (and CCC) concerning this licensing transaction. In the event of any conflict between your obligations established by these terms and conditions and those established by CCC's Billing and Payment terms and conditions, these terms and conditions shall control.

14. Revocation: Elsevier or Copyright Clearance Center may deny the permissions described in this License at their sole discretion, for any reason or no reason, with a full refund payable to you. Notice of such denial will be made using the contact information provided by you. Failure to receive such notice will not alter or invalidate the denial. In no event will Elsevier or Copyright Clearance Center be responsible or liable for any costs, expenses or damage incurred by you as a result of a denial of your permission request, other than a refund of the amount(s) paid by you to Elsevier and/or Copyright Clearance Center for denied permissions.

LIMITED LICENSE

The following terms and conditions apply only to specific license types:

15. **Translation**: This permission is granted for non-exclusive world **English** rights only unless your license was granted for translation rights. If you licensed translation rights you may only translate this content into the languages you requested. A professional translator must perform all translations and reproduce the content word for word preserving the integrity of the article. If this license is to re-use 1 or 2 figures then permission is granted for non-exclusive world rights in all languages.

16. **Website**: The following terms and conditions apply to electronic reserve and author websites:
Electronic reserve: If licensed material is to be posted to website, the web site is to be password-protected and made available only to bona fide students registered on a relevant course if:
This license was made in connection with a course,
This permission is granted for 1 year only. You may obtain a license for future website posting,
All content posted to the web site must maintain the copyright information line on the bottom of each image,
A hyper-text must be included to the Homepage of the journal from which you are licensing at http://www.sciencedirect.com/science/journal/xxxxx or the Elsevier homepage for books at http://www.elsevier.com , and
Central Storage: This license does not include permission for a scanned version of the material to be stored in a central repository such as that provided by Heron/XanEdu.

17. **Author website** for journals with the following additional clauses:

All content posted to the web site must maintain the copyright information line on the bottom of each image, and the permission granted is limited to the personal version of your paper. You are not allowed to download and post the published electronic version of your article (whether PDF or HTML, proof or final version), nor may you scan the printed edition to create an electronic version.
A hyper-text must be included to the Homepage of the journal from which you are licensing at http://www.sciencedirect.com/science/journal/xxxxx . As part of our normal production process, you will receive an e-mail notice when your article appears on Elsevier's online service ScienceDirect (www.sciencedirect.com). That e-mail will include the article's Digital Object Identifier (DOI). This number provides the electronic link to the published article and should be included in the posting of your personal version. We ask that you wait until you receive this e-mail and have the DOI to do any posting.

Central Storage: This license does not include permission for a scanned version of the material to be stored in a central repository such as that provided by Heron/XanEdu.

18. **Author website** for books with the following additional clauses:
Authors are permitted to place a brief summary of their work online only.
A hyper-text must be included to the Elsevier homepage at http://www.elsevier.com . All content posted to the web site must maintain the copyright information line on the bottom of each image.
You are not allowed to download and post the published electronic version of your chapter, nor may you scan the printed edition to create an electronic version.

Central Storage: This license does not include permission for a scanned version of the material to be stored in a central repository such as that provided by Heron/XanEdu.

19. **Website** (regular and for author): A hyper-text must be included to the Homepage of the journal from which you are licensing at http://www.sciencedirect.com/science/journal/xxxxx. or for books to the Elsevier homepage at http://www.elsevier.com

20. **Thesis/Dissertation**: If your license is for use in a thesis/dissertation your thesis may be submitted to your institution in either print or electronic form. Should your thesis be published commercially, please reapply for permission. These requirements include permission for the Library and Archives of Canada to supply single copies, on demand, of the complete thesis and include permission for UMI to supply single copies, on demand, of the complete thesis. Should your thesis be published commercially, please reapply for permission.

21. **Other Conditions**:

v1.6

If you would like to pay for this license now, please remit this license along with your payment made payable to "COPYRIGHT CLEARANCE CENTER" otherwise you will be invoiced within 48 hours of the license date. Payment should be in the form of a check or money order referencing your account number and this invoice number RLNK500795725. Once you receive your invoice for this order, you may pay your invoice by credit card. Please follow instructions provided at that time.

Make Payment To:
Copyright Clearance Center
Dept 001
P.O. Box 843006
Boston, MA 02284-3006

For suggestions or comments regarding this order, contact RightsLink Customer Support: customercare@copyright.com or +1-877-622-5543 (toll free in the US) or +1-978-646-2777.

Gratis licenses (referencing $0 in the Total field) are free. Please retain this printable license for your reference. No payment is required.

Appendix 6-2: Summary of *T*1 curve fitting equations and representative fitting.

Raw ^{19}F-MRS data following standard inversion recovery analysis was fitted to a non-linear exponential function to obtain the characteristic spin-lattice relaxation time (*T*1) value for a sample.

*T*1 defines the average time it takes for a nucleus to return to thermal equilibrium following perturbation into the transverse plane, such that in a static magnetic field along the longitudinal axis (z-component of the magnetization) obeys the following **Equation 6-29** (Bloch equation):

(6-29) $$\frac{dM_z}{dt} = -\frac{(M_z - M_o)}{T1}$$

Since the radiofrequency pulse used for inversion recovery is short relative to the relaxation time, the Bloch equation describes the times in between pulses and can be solved by integrating from *t* = 0 to *t* to give (**Equation 6-30**):

(6-30) $$M_z(t) = M_o + (M_z(t) - M_0) \cdot e^{-\tau/T1}$$

Following the 90° pulse in the inversion recovery sequence, *Equation 6-30* can be further simplified since $M_z(0) = 0$ (**Equation 6-31**):

(6-31) $$M_z(t) = M_o \cdot \left(1 - 2e^{-\tau/T1}\right)$$

A short computational routine was generated using the *cftool* in Matlab R2008a v 7.6.0 (Mathworks, Natick, MA) to fit experimental data to **Equation 6-32**, where A, C and *T*1 are fitting constants.

(6-32) $$M_z = A \cdot \left(1 - 2e^{-\tau/T1}\right) + C$$

Figure 6-18 illustrates a representative graph resulting from the curve fitting analysis and a sample output showing the *T*1 value generated by the model. **Figure 6-19** illustrates a representative set of raw inversion recovery data collected during analysis of samples presented in Suszynski *et al*. [56].

Figure Captions (Appendix 6-2)

Figure 6-18: Representative graph resulting from curve fitting analysis of raw inversion recovery data (left) and a sample output showing the *T*1 value generated by the model (right). Abbreviation: *T*1, spin-lattice relaxation time.

Figure 6-19: representative set of raw inversion recovery data collected during analysis of samples presented in Suszynski *et al*. [56]. Note the lengthening relaxation time with increasing numbers of islet equivalents seeded into tissue-engineered grafts.

Figure 6-18: Representative curve fitting and model output

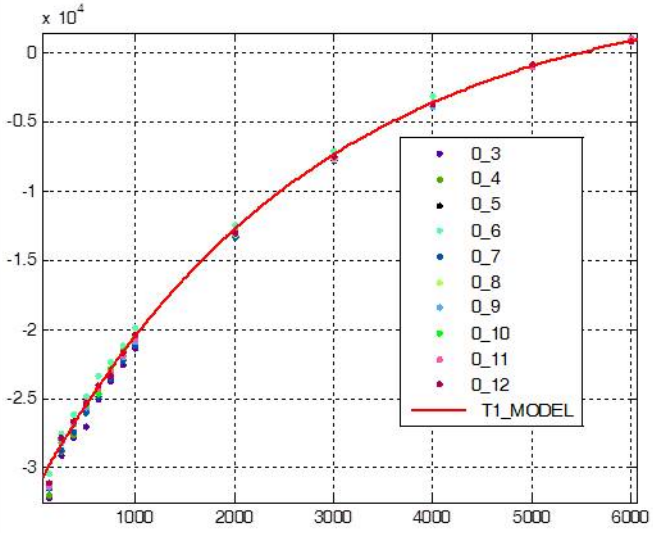

General model:
f(Tau) = *A**(1-2*exp(-Tau/*T*1)) + *C*
Coefficients (with 95% confidence bounds):
A = 3.813e+004 (3.686e+004, 3.94e+004)
C = -917 (-1496, -338.4)
*T*1 = 2710 (2443, 2977)

Goodness of fit:
SSE: 1.34e+006
R-square: 0.9992
Adjusted R-square: 0.999

Figure 6-19: Representative set of raw inversion recovery data from Suszynski *et al*.

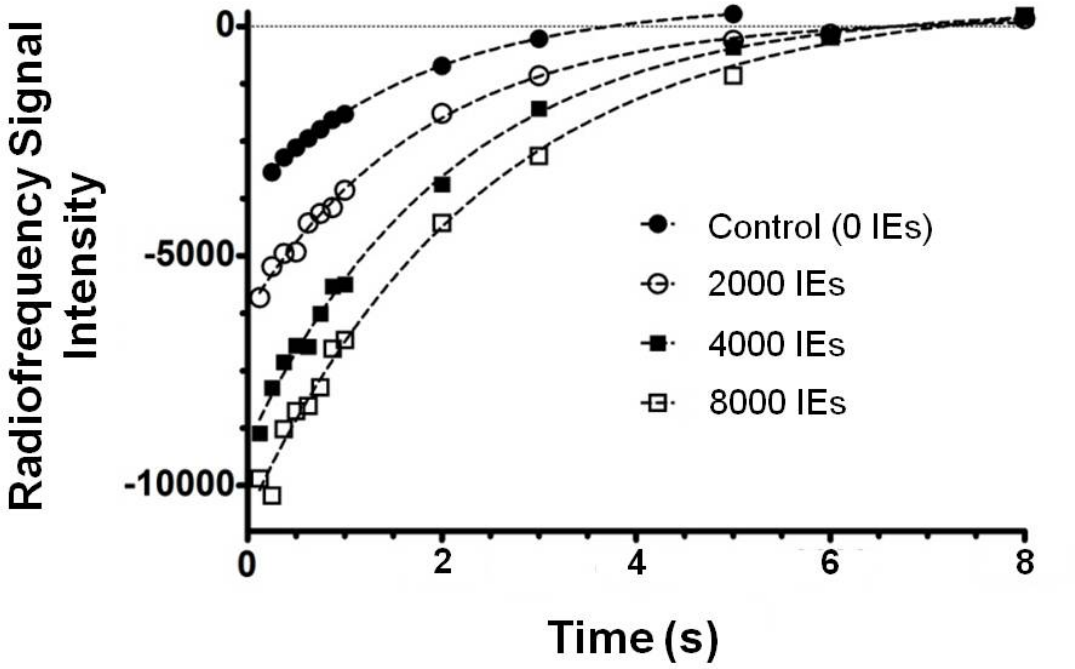

Appendix 7-1: Permission to Reprint (Suszynski *et al*. Cryobiology [2012])

ELSEVIER LICENSE
TERMS AND CONDITIONS

Jun 08, 2012

This is a License Agreement between Thomas M Suszynski ("You") and Elsevier ("Elsevier") provided by Copyright Clearance Center ("CCC"). The license consists of your order details, the terms and conditions provided by Elsevier, and the payment terms and conditions.

All payments must be made in full to CCC. For payment instructions, please see information listed at the bottom of this form.

Supplier	Elsevier Limited The Boulevard,Langford Lane Kidlington,Oxford,OX5 1GB,UK
Registered Company Number	1982084
Customer name	Thomas M Suszynski
Customer address	2871 Irving Ave S Minneapolis, MN 55408
License number	2924380328935
License date	Jun 08, 2012
Licensed content publisher	Elsevier
Licensed content publication	Cryobiology
Licensed content title	Persufflation (or gaseous oxygen perfusion) as a method of organ preservation
Licensed content author	Thomas M. Suszynski,Michael D. Rizzari,William E. Scott,Linda A. Tempelman,Michael J. Taylor,Klearchos K. Papas
Licensed content date	June 2012
Licensed content volume number	64
Licensed content issue number	3
Number of pages	19
Start Page	125
End Page	143
Type of Use	reuse in a thesis/dissertation
Intended publisher of new work	other
Portion	full article
Format	both print and electronic
Are you the author of this Elsevier article?	Yes
Will you be translating?	No

Order reference number	Suszynski T, Cryobiology (2012)
Title of your thesis/dissertation	TISSUE-ENGINEERED ISLET GRAFT DESIGN AND ASSESSMENT
Expected completion date	Sep 2012
Estimated size (number of pages)	400
Elsevier VAT number	GB 494 6272 12
Permissions price	0.00 USD
VAT/Local Sales Tax	0.0 USD / 0.0 GBP
Total	0.00 USD
Terms and Conditions	

INTRODUCTION

1. The publisher for this copyrighted material is Elsevier. By clicking "accept" in connection with completing this licensing transaction, you agree that the following terms and conditions apply to this transaction (along with the Billing and Payment terms and conditions established by Copyright Clearance Center, Inc. ("CCC"), at the time that you opened your Rightslink account and that are available at any time at http://myaccount.copyright.com).

GENERAL TERMS

2. Elsevier hereby grants you permission to reproduce the aforementioned material subject to the terms and conditions indicated.

3. Acknowledgement: If any part of the material to be used (for example, figures) has appeared in our publication with credit or acknowledgement to another source, permission must also be sought from that source. If such permission is not obtained then that material may not be included in your publication/copies. Suitable acknowledgement to the source must be made, either as a footnote or in a reference list at the end of your publication, as follows:

"Reprinted from Publication title, Vol /edition number, Author(s), Title of article / title of chapter, Pages No., Copyright (Year), with permission from Elsevier [OR APPLICABLE SOCIETY COPYRIGHT OWNER]." Also Lancet special credit - "Reprinted from The Lancet, Vol. number, Author(s), Title of article, Pages No., Copyright (Year), with permission from Elsevier."

4. Reproduction of this material is confined to the purpose and/or media for which permission is hereby given.

5. Altering/Modifying Material: Not Permitted. However figures and illustrations may be altered/adapted minimally to serve your work. Any other abbreviations, additions, deletions and/or any other alterations shall be made only with prior written authorization of Elsevier Ltd. (Please contact Elsevier at permissions@elsevier.com)

6. If the permission fee for the requested use of our material is waived in this instance, please be advised that your future requests for Elsevier materials may attract a fee.

7. Reservation of Rights: Publisher reserves all rights not specifically granted in the combination of (i) the license details provided by you and accepted in the course of this licensing transaction, (ii) these terms and conditions and (iii) CCC's Billing and Payment terms and conditions.

8. License Contingent Upon Payment: While you may exercise the rights licensed immediately upon issuance of the license at the end of the licensing process for the transaction, provided that you have disclosed complete and accurate details of your proposed use, no license is finally effective unless and until full payment is received from you (either by publisher or by CCC) as provided in CCC's Billing and Payment terms and conditions. If full payment is not received on a timely basis, then any license preliminarily granted shall be deemed automatically revoked and shall be void as if never granted. Further, in the event that you breach any of these terms and conditions or any of CCC's Billing and Payment terms and conditions, the license is automatically revoked and shall be void as if never granted. Use of materials as described in a revoked license, as well as any use of the materials beyond the scope of an unrevoked license, may constitute copyright infringement and publisher reserves the right to take any and all action to protect its copyright in the materials.

9. Warranties: Publisher makes no representations or warranties with respect to the licensed material.

10. Indemnity: You hereby indemnify and agree to hold harmless publisher and CCC, and their respective officers, directors, employees and agents, from and against any and all claims arising out of your use of the licensed material other than as specifically authorized pursuant to this license.

11. No Transfer of License: This license is personal to you and may not be sublicensed, assigned, or transferred by you to any other person without publisher's written permission.

12. No Amendment Except in Writing: This license may not be amended except in a writing signed by both parties (or, in the case of publisher, by CCC on publisher's behalf).

13. Objection to Contrary Terms: Publisher hereby objects to any terms contained in any purchase order, acknowledgment, check endorsement or other writing prepared by you, which terms are inconsistent with these terms and conditions or CCC's Billing and Payment terms and conditions. These terms and conditions, together with CCC's Billing and Payment terms and conditions (which are incorporated herein), comprise the entire agreement between you and publisher (and CCC) concerning this licensing transaction. In the event of any conflict between your obligations established by these terms and conditions and those established by CCC's Billing and Payment terms and conditions, these terms and conditions shall control.

14. Revocation: Elsevier or Copyright Clearance Center may deny the permissions described in this License at their sole discretion, for any reason or no reason, with a full refund payable to you. Notice of such denial will be made using the contact information provided by you. Failure to receive such notice will not alter or invalidate the denial. In no event will Elsevier or Copyright Clearance Center be responsible or liable for any costs, expenses or damage incurred by you as a result of a denial of your permission request, other than a refund of the amount(s) paid by you to Elsevier and/or Copyright Clearance Center for denied permissions.

LIMITED LICENSE

The following terms and conditions apply only to specific license types:

15. **Translation**: This permission is granted for non-exclusive world **English** rights only unless your license was granted for translation rights. If you licensed translation rights you may only translate this content into the languages you requested. A professional translator must perform all translations and reproduce the content word for word preserving the integrity of the article. If this license is to re-use 1 or 2 figures then permission is granted for non-exclusive world rights in all languages.

16. **Website**: The following terms and conditions apply to electronic reserve and author websites:
Electronic reserve: If licensed material is to be posted to website, the web site is to be password-protected and made available only to bona fide students registered on a relevant course if:
This license was made in connection with a course,
This permission is granted for 1 year only. You may obtain a license for future website posting,
All content posted to the web site must maintain the copyright information line on the bottom of each image,
A hyper-text must be included to the Homepage of the journal from which you are licensing at http://www.sciencedirect.com/science/journal/xxxxx or the Elsevier homepage for books at http://www.elsevier.com , and
Central Storage: This license does not include permission for a scanned version of the material to be stored in a central repository such as that provided by Heron/XanEdu.

17. **Author website** for journals with the following additional clauses:

All content posted to the web site must maintain the copyright information line on the bottom of each image, and the permission granted is limited to the personal version of your paper. You are not allowed to download and post the published electronic version of your article (whether PDF or HTML, proof or final version), nor may you scan the printed edition to create an electronic version.
A hyper-text must be included to the Homepage of the journal from which you are licensing at http://www.sciencedirect.com/science/journal/xxxxx . As part of our normal production process, you will receive an e-mail notice when your article appears on Elsevier's online service ScienceDirect (www.sciencedirect.com). That e-mail will include the article's Digital Object Identifier (DOI). This number provides the electronic link to the published article and should be included in the posting of your personal version. We ask that you wait until you receive this e-mail and have the DOI to do any posting.

Central Storage: This license does not include permission for a scanned version of the material to be stored in a central repository such as that provided by Heron/XanEdu.

18. **Author website** for books with the following additional clauses:
Authors are permitted to place a brief summary of their work online only.
A hyper-text must be included to the Elsevier homepage at http://www.elsevier.com . All content posted to the web site must maintain the copyright information line on the bottom of each image.
You are not allowed to download and post the published electronic version of your chapter, nor may you scan the printed edition to create an electronic version.

Central Storage: This license does not include permission for a scanned version of the material to be stored in a central repository such as that provided by Heron/XanEdu.

19. **Website** (regular and for author): A hyper-text must be included to the Homepage of the journal from which you are licensing at http://www.sciencedirect.com/science/journal/xxxxx. or for books to the Elsevier homepage at http://www.elsevier.com

20. **Thesis/Dissertation**: If your license is for use in a thesis/dissertation your thesis may be submitted to your institution in either print or electronic form. Should your thesis be published commercially, please reapply for permission. These requirements include permission for the Library and Archives of Canada to supply single copies, on demand, of the complete thesis and include permission for UMI to supply single copies, on demand, of the complete thesis. Should your thesis be published commercially, please reapply for permission.

21. **Other Conditions**:

v1.6

If you would like to pay for this license now, please remit this license along with your payment made payable to "COPYRIGHT CLEARANCE CENTER" otherwise you will be invoiced within 48 hours of the license date. Payment should be in the form of a check or money order referencing your account number and this invoice number RLNK500795755. Once you receive your invoice for this order, you may pay your invoice by credit card. Please follow instructions provided at that time.

Make Payment To:
Copyright Clearance Center
Dept 001
P.O. Box 843006
Boston, MA 02284-3006

For suggestions or comments regarding this order, contact RightsLink Customer Support: customercare@copyright.com or +1-877-622-5543 (toll free in the US) or +1-978-646-2777.

Gratis licenses (referencing $0 in the Total field) are free. Please retain this printable license for your reference. No payment is required.

Appendix 7-2: Permission to Reprint (Suszynski *et al*. Xenotransplant [2011])

JOHN WILEY AND SONS LICENSE TERMS AND CONDITIONS

Jun 08, 2012

This is a License Agreement between Thomas M Suszynski ("You") and John Wiley and Sons ("John Wiley and Sons") provided by Copyright Clearance Center ("CCC"). The license consists of your order details, the terms and conditions provided by John Wiley and Sons, and the payment terms and conditions.

All payments must be made in full to CCC. For payment instructions, please see information listed at the bottom of this form.

License Number	2924370330377
License date	Jun 08, 2012
Licensed content publisher	John Wiley and Sons
Licensed content publication	Xenotransplantation
Licensed content title	Paramagnetic microparticles do not elicit islet cytotoxicity with co-culture or host immune reactivity after implantation
Licensed content author	Thomas M. Suszynski,Michael D. Rizzari,Louis S. Kidder,Kate Mueller,Christopher S. Chapman,Jennifer P. Kitzmann,Rebecca L. Pongratz,Gary W. Cline,Paul W. Todd,David J. Kennedy,Timothy D. O'Brien,Efstathios S. Avgoustiniatos,Henk-Jan Schuurman,Klearchos K. Papas
Licensed content date	Aug 18, 2011
Start page	239
End page	244
Type of use	Dissertation/Thesis
Requestor type	Author of this Wiley article
Format	Print and electronic
Portion	Full article
Will you be translating?	No
Order reference number	Suszynski TM, Xenotransplant (2011)
Total	0.00 USD
Terms and Conditions	

TERMS AND CONDITIONS

This copyrighted material is owned by or exclusively licensed to John Wiley & Sons, Inc. or one of its group companies (each a "Wiley Company") or a society for whom a Wiley Company has exclusive publishing rights in relation to a particular journal (collectively WILEY"). By clicking "accept" in connection with completing this licensing transaction, you agree that the following terms and conditions apply to this transaction (along with the billing and payment terms and conditions established by the Copyright Clearance Center Inc., ("CCC's Billing and Payment terms and conditions"), at the time that you opened your Rightslink account (these are available at any time at http://myaccount.copyright.com)

Terms and Conditions

1. The materials you have requested permission to reproduce (the "Materials") are protected by copyright.

2. You are hereby granted a personal, non-exclusive, non-sublicensable, non-transferable, worldwide, limited license to reproduce the Materials for the purpose specified in the licensing process. This license is for a one-time use only with a maximum distribution equal to the number that you identified in the licensing process. Any form of republication granted by this licence must be completed within two years of the date of the grant of this licence (although copies prepared before may be distributed thereafter). The Materials shall not be used in any other manner or for any other purpose. Permission is granted subject to an appropriate acknowledgement given to the author, title of the material/book/journal and the publisher. You shall also duplicate the copyright notice that appears in the Wiley publication in your use of the Material. Permission is also granted on the understanding that nowhere in the text is a previously published source acknowledged for all or part of this Material. Any third party material is expressly excluded from this permission.

3. With respect to the Materials, all rights are reserved. Except as expressly granted by the terms of the license, no part of the Materials may be copied, modified, adapted (except for minor reformatting required by the new Publication), translated, reproduced, transferred or distributed, in any form or by any means, and no derivative works may be made based on the Materials without the prior permission of the respective copyright owner. You may not alter, remove or suppress in any manner any copyright, trademark or other notices displayed by the Materials. You may not license, rent, sell, loan, lease, pledge, offer as security, transfer or assign the Materials, or any of the rights granted to you hereunder to any other person.

4. The Materials and all of the intellectual property rights therein shall at all times remain the exclusive property of John Wiley & Sons Inc or one of its related companies (WILEY) or their respective licensors, and your interest therein is only that of having possession of and the right to reproduce the Materials pursuant to Section 2 herein during the continuance of this Agreement. You agree that you own no right, title or interest in or to the Materials or any of the intellectual property rights therein. You shall have no rights hereunder other than the license as provided for above in Section 2. No right, license or interest to any trademark, trade name, service mark or other branding ("Marks") of WILEY or its licensors is granted hereunder, and you agree that you shall not assert any such right, license or interest with respect thereto.

5. NEITHER WILEY NOR ITS LICENSORS MAKES ANY WARRANTY OR REPRESENTATION OF ANY KIND TO YOU OR ANY THIRD PARTY, EXPRESS, IMPLIED OR STATUTORY, WITH RESPECT TO THE MATERIALS OR THE ACCURACY OF ANY INFORMATION CONTAINED IN THE MATERIALS, INCLUDING, WITHOUT LIMITATION, ANY IMPLIED WARRANTY OF MERCHANTABILITY, ACCURACY, SATISFACTORY QUALITY, FITNESS FOR A PARTICULAR PURPOSE, USABILITY, INTEGRATION OR NON-INFRINGEMENT AND ALL SUCH WARRANTIES ARE HEREBY EXCLUDED BY WILEY AND ITS LICENSORS AND WAIVED BY YOU.

6. WILEY shall have the right to terminate this Agreement immediately upon breach of this Agreement by you.

7. You shall indemnify, defend and hold harmless WILEY, its Licensors and their respective directors, officers, agents and employees, from and against any actual or threatened claims, demands, causes of action or proceedings arising from any breach of this Agreement by you.

8. IN NO EVENT SHALL WILEY OR ITS LICENSORS BE LIABLE TO YOU OR ANY OTHER PARTY OR ANY OTHER PERSON OR ENTITY FOR ANY SPECIAL, CONSEQUENTIAL, INCIDENTAL, INDIRECT, EXEMPLARY OR PUNITIVE DAMAGES, HOWEVER CAUSED, ARISING OUT OF OR IN CONNECTION WITH THE DOWNLOADING, PROVISIONING, VIEWING OR USE OF THE MATERIALS REGARDLESS OF THE FORM OF ACTION, WHETHER FOR BREACH OF CONTRACT, BREACH OF WARRANTY, TORT, NEGLIGENCE, INFRINGEMENT OR OTHERWISE (INCLUDING, WITHOUT LIMITATION, DAMAGES BASED ON LOSS OF PROFITS, DATA, FILES, USE, BUSINESS OPPORTUNITY OR CLAIMS OF THIRD PARTIES), AND WHETHER OR NOT THE PARTY HAS BEEN ADVISED OF THE POSSIBILITY OF SUCH DAMAGES. THIS LIMITATION SHALL APPLY NOTWITHSTANDING ANY FAILURE OF ESSENTIAL PURPOSE OF ANY LIMITED REMEDY PROVIDED HEREIN.

9. Should any provision of this Agreement be held by a court of competent jurisdiction to be illegal, invalid, or unenforceable, that provision shall be deemed amended to achieve as nearly

as possible the same economic effect as the original provision, and the legality, validity and enforceability of the remaining provisions of this Agreement shall not be affected or impaired thereby.

10. The failure of either party to enforce any term or condition of this Agreement shall not constitute a waiver of either party's right to enforce each and every term and condition of this Agreement. No breach under this agreement shall be deemed waived or excused by either party unless such waiver or consent is in writing signed by the party granting such waiver or consent. The waiver by or consent of a party to a breach of any provision of this Agreement shall not operate or be construed as a waiver of or consent to any other or subsequent breach by such other party.

11. This Agreement may not be assigned (including by operation of law or otherwise) by you without WILEY's prior written consent.

12. Any fee required for this permission shall be non-refundable after thirty (30) days from receipt.

13. These terms and conditions together with CCC's Billing and Payment terms and conditions (which are incorporated herein) form the entire agreement between you and WILEY concerning this licensing transaction and (in the absence of fraud) supersedes all prior agreements and representations of the parties, oral or written. This Agreement may not be amended except in writing signed by both parties. This Agreement shall be binding upon and inure to the benefit of the parties' successors, legal representatives, and authorized assigns.

14. In the event of any conflict between your obligations established by these terms and conditions and those established by CCC's Billing and Payment terms and conditions, these terms and conditions shall prevail.

15. WILEY expressly reserves all rights not specifically granted in the combination of (i) the license details provided by you and accepted in the course of this licensing transaction, (ii) these terms and conditions and (iii) CCC's Billing and Payment terms and conditions.

16. This Agreement will be void if the Type of Use, Format, Circulation, or Requestor Type was misrepresented during the licensing process.

17. This Agreement shall be governed by and construed in accordance with the laws of the State of New York, USA, without regards to such state's conflict of law rules. Any legal action, suit or proceeding arising out of or relating to these Terms and Conditions or the breach thereof shall be instituted in a court of competent jurisdiction in New York County in the State of New York in the United States of America and each party hereby consents and submits to the personal jurisdiction of such court, waives any objection to venue in such court and consents to service of process by registered or certified mail, return receipt requested, at the last known address of such party.

Wiley Open Access Terms and Conditions

All research articles published in Wiley Open Access journals are fully open access: immediately freely available to read, download and share. Articles are published under the terms of the Creative Commons Attribution Non Commercial License, which permits use, distribution and reproduction in any medium, provided the original work is properly cited and is not used for commercial purposes. The license is subject to the Wiley Open Access terms and conditions:
Wiley Open Access articles are protected by copyright and are posted to repositories and websites in accordance with the terms of the Creative Commons Attribution Non Commercial License. At the time of deposit, Wiley Open Access articles include all changes made during peer review, copyediting, and publishing. Repositories and websites that host the article are responsible for incorporating any publisher-supplied amendments or retractions issued subsequently.
Wiley Open Access articles are also available without charge on Wiley's publishing platform, **Wiley Online Library** or any successor sites.

Use by non-commercial users

For non-commercial and non-promotional purposes individual users may access, download,

copy, display and redistribute to colleagues Wiley Open Access articles, as well as adapt, translate, text- and data-mine the content subject to the following conditions:

- The authors' moral rights are not compromised. These rights include the right of "paternity" (also known as "attribution" - the right for the author to be identified as such) and "integrity" (the right for the author not to have the work altered in such a way that the author's reputation or integrity may be impugned).
- Where content in the article is identified as belonging to a third party, it is the obligation of the user to ensure that any reuse complies with the copyright policies of the owner of that content.
- If article content is copied, downloaded or otherwise reused for non-commercial research and education purposes, a link to the appropriate bibliographic citation (authors, journal, article title, volume, issue, page numbers, DOI and the link to the definitive published version on Wiley Online Library) should be maintained. Copyright notices and disclaimers must not be deleted.
- Any translations, for which a prior translation agreement with Wiley has not been agreed, must prominently display the statement: "This is an unofficial translation of an article that appeared in a Wiley publication. The publisher has not endorsed this translation."

Use by commercial "for-profit" organisations

Use of Wiley Open Access articles for commercial, promotional, or marketing purposes requires further explicit permission from Wiley and will be subject to a fee. Commercial purposes include:

- Copying or downloading of articles, or linking to such articles for further redistribution, sale or licensing;
- Copying, downloading or posting by a site or service that incorporates advertising with such content;
- The inclusion or incorporation of article content in other works or services (other than normal quotations with an appropriate citation) that is then available for sale or licensing, for a fee (for example, a compilation produced for marketing purposes, inclusion in a sales pack)
- Use of article content (other than normal quotations with appropriate citation) by for-profit organisations for promotional purposes
- Linking to article content in e-mails redistributed for promotional, marketing or educational purposes;
- Use for the purposes of monetary reward by means of sale, resale, licence, loan, transfer or other form of commercial exploitation such as marketing products
- Print reprints of Wiley Open Access articles can be purchased from: corporatesales@wiley.com

Other Terms and Conditions:

BY CLICKING ON THE "I AGREE..." BOX, YOU ACKNOWLEDGE THAT YOU HAVE READ AND FULLY UNDERSTAND EACH OF THE SECTIONS OF AND PROVISIONS SET FORTH IN THIS AGREEMENT AND THAT YOU ARE IN AGREEMENT WITH AND ARE WILLING TO ACCEPT ALL OF YOUR OBLIGATIONS AS SET FORTH IN THIS AGREEMENT.

v1.7

If you would like to pay for this license now, please remit this license along with your payment made payable to "COPYRIGHT CLEARANCE CENTER" otherwise you will be invoiced within 48 hours of the license date. Payment should be in the form of a check or money order referencing your account number and this invoice number RLNK500795737. Once you receive your invoice for this order, you may pay your invoice by credit card. Please follow instructions provided at that time.

Make Payment To:
Copyright Clearance Center
Dept 001
P.O. Box 843006
Boston, MA 02284-3006

For suggestions or comments regarding this order, contact RightsLink Customer Support: customercare@copyright.com or +1-877-622-5543 (toll free in the US) or +1-978-646-2777.

Gratis licenses (referencing $0 in the Total field) are free. Please retain this printable license for your reference. No payment is required.

Appendix 7-3: Permission to Reprint (Rizzari MD *et al*. Transplant Proc [2010])

ELSEVIER LICENSE
TERMS AND CONDITIONS

Jun 08, 2012

This is a License Agreement between Thomas M Suszynski ("You") and Elsevier ("Elsevier") provided by Copyright Clearance Center ("CCC"). The license consists of your order details, the terms and conditions provided by Elsevier, and the payment terms and conditions.

All payments must be made in full to CCC. For payment instructions, please see information listed at the bottom of this form.

Supplier	Elsevier Limited The Boulevard,Langford Lane Kidlington,Oxford,OX5 1GB,UK
Registered Company Number	1982084
Customer name	Thomas M Suszynski
Customer address	2871 Irving Ave S Minneapolis, MN 55408
License number	2924370837818
License date	Jun 08, 2012
Licensed content publisher	Elsevier
Licensed content publication	Transplantation Proceedings
Licensed content title	Surgical Protocol Involving the Infusion of Paramagnetic Microparticles for Preferential Incorporation Within Porcine Islets
Licensed content author	M.D. Rizzari,T.M. Suszynski,L.S. Kidder,S.A. Stein,T.D. O'Brien,V.S.K. Sajja,W.E. Scott,V.A. Kirchner,B.P. Weegman,E.S. Avgoustiniatos,P.W. Todd,D.J. Kennedy,B.E. Hammer,D.E.R. Sutherland,B.J. Hering,K.K. Papas
Licensed content date	December 2010
Licensed content volume number	42
Licensed content issue number	10
Number of pages	4
Start Page	4209
End Page	4212
Type of Use	reuse in a thesis/dissertation
Intended publisher of new work	other
Portion	full article
Format	both print and electronic
Are you the author of this	Yes

Elsevier article?	
Will you be translating?	No
Order reference number	Rizzari MD, Trans Proc (2010)
Title of your thesis/dissertation	TISSUE-ENGINEERED ISLET GRAFT DESIGN AND ASSESSMENT
Expected completion date	Sep 2012
Estimated size (number of pages)	400
Elsevier VAT number	GB 494 6272 12
Permissions price	0.00 USD
VAT/Local Sales Tax	0.0 USD / 0.0 GBP
Total	0.00 USD
Terms and Conditions	

INTRODUCTION

1. The publisher for this copyrighted material is Elsevier. By clicking "accept" in connection with completing this licensing transaction, you agree that the following terms and conditions apply to this transaction (along with the Billing and Payment terms and conditions established by Copyright Clearance Center, Inc. ("CCC"), at the time that you opened your Rightslink account and that are available at any time at http://myaccount.copyright.com).

GENERAL TERMS

2. Elsevier hereby grants you permission to reproduce the aforementioned material subject to the terms and conditions indicated.

3. Acknowledgement: If any part of the material to be used (for example, figures) has appeared in our publication with credit or acknowledgement to another source, permission must also be sought from that source. If such permission is not obtained then that material may not be included in your publication/copies. Suitable acknowledgement to the source must be made, either as a footnote or in a reference list at the end of your publication, as follows:

"Reprinted from Publication title, Vol /edition number, Author(s), Title of article / title of chapter, Pages No., Copyright (Year), with permission from Elsevier [OR APPLICABLE SOCIETY COPYRIGHT OWNER]." Also Lancet special credit - "Reprinted from The Lancet, Vol. number, Author(s), Title of article, Pages No., Copyright (Year), with permission from Elsevier."

4. Reproduction of this material is confined to the purpose and/or media for which permission is hereby given.

5. Altering/Modifying Material: Not Permitted. However figures and illustrations may be altered/adapted minimally to serve your work. Any other abbreviations, additions, deletions and/or any other alterations shall be made only with prior written authorization of Elsevier Ltd. (Please contact Elsevier at permissions@elsevier.com)

6. If the permission fee for the requested use of our material is waived in this instance, please be

advised that your future requests for Elsevier materials may attract a fee.

7. Reservation of Rights: Publisher reserves all rights not specifically granted in the combination of (i) the license details provided by you and accepted in the course of this licensing transaction, (ii) these terms and conditions and (iii) CCC's Billing and Payment terms and conditions.

8. License Contingent Upon Payment: While you may exercise the rights licensed immediately upon issuance of the license at the end of the licensing process for the transaction, provided that you have disclosed complete and accurate details of your proposed use, no license is finally effective unless and until full payment is received from you (either by publisher or by CCC) as provided in CCC's Billing and Payment terms and conditions. If full payment is not received on a timely basis, then any license preliminarily granted shall be deemed automatically revoked and shall be void as if never granted. Further, in the event that you breach any of these terms and conditions or any of CCC's Billing and Payment terms and conditions, the license is automatically revoked and shall be void as if never granted. Use of materials as described in a revoked license, as well as any use of the materials beyond the scope of an unrevoked license, may constitute copyright infringement and publisher reserves the right to take any and all action to protect its copyright in the materials.

9. Warranties: Publisher makes no representations or warranties with respect to the licensed material.

10. Indemnity: You hereby indemnify and agree to hold harmless publisher and CCC, and their respective officers, directors, employees and agents, from and against any and all claims arising out of your use of the licensed material other than as specifically authorized pursuant to this license.

11. No Transfer of License: This license is personal to you and may not be sublicensed, assigned, or transferred by you to any other person without publisher's written permission.

12. No Amendment Except in Writing: This license may not be amended except in a writing signed by both parties (or, in the case of publisher, by CCC on publisher's behalf).

13. Objection to Contrary Terms: Publisher hereby objects to any terms contained in any purchase order, acknowledgment, check endorsement or other writing prepared by you, which terms are inconsistent with these terms and conditions or CCC's Billing and Payment terms and conditions. These terms and conditions, together with CCC's Billing and Payment terms and conditions (which are incorporated herein), comprise the entire agreement between you and publisher (and CCC) concerning this licensing transaction. In the event of any conflict between your obligations established by these terms and conditions and those established by CCC's Billing and Payment terms and conditions, these terms and conditions shall control.

14. Revocation: Elsevier or Copyright Clearance Center may deny the permissions described in this License at their sole discretion, for any reason or no reason, with a full refund payable to you. Notice of such denial will be made using the contact information provided by you. Failure to receive such notice will not alter or invalidate the denial. In no event will Elsevier or Copyright Clearance Center be responsible or liable for any costs, expenses or damage incurred by you as a result of a denial of your permission request, other than a refund of the amount(s) paid by you to Elsevier and/or Copyright Clearance Center for denied permissions.

LIMITED LICENSE

The following terms and conditions apply only to specific license types:

15. **Translation**: This permission is granted for non-exclusive world **English** rights only unless your license was granted for translation rights. If you licensed translation rights you may only translate this content into the languages you requested. A professional translator must perform all translations and reproduce the content word for word preserving the integrity of the article. If this license is to re-use 1 or 2 figures then permission is granted for non-exclusive world rights in all languages.

16. **Website**: The following terms and conditions apply to electronic reserve and author websites:
Electronic reserve: If licensed material is to be posted to website, the web site is to be password-protected and made available only to bona fide students registered on a relevant course if:
This license was made in connection with a course,
This permission is granted for 1 year only. You may obtain a license for future website posting,
All content posted to the web site must maintain the copyright information line on the bottom of each image,
A hyper-text must be included to the Homepage of the journal from which you are licensing at http://www.sciencedirect.com/science/journal/xxxxx or the Elsevier homepage for books at http://www.elsevier.com , and
Central Storage: This license does not include permission for a scanned version of the material to be stored in a central repository such as that provided by Heron/XanEdu.

17. **Author website** for journals with the following additional clauses:

All content posted to the web site must maintain the copyright information line on the bottom of each image, and the permission granted is limited to the personal version of your paper. You are not allowed to download and post the published electronic version of your article (whether PDF or HTML, proof or final version), nor may you scan the printed edition to create an electronic version.
A hyper-text must be included to the Homepage of the journal from which you are licensing at http://www.sciencedirect.com/science/journal/xxxxx . As part of our normal production process, you will receive an e-mail notice when your article appears on Elsevier's online service ScienceDirect (www.sciencedirect.com). That e-mail will include the article's Digital Object Identifier (DOI). This number provides the electronic link to the published article and should be included in the posting of your personal version. We ask that you wait until you receive this e-mail and have the DOI to do any posting.

Central Storage: This license does not include permission for a scanned version of the material to be stored in a central repository such as that provided by Heron/XanEdu.

18. **Author website** for books with the following additional clauses:
Authors are permitted to place a brief summary of their work online only.
A hyper-text must be included to the Elsevier homepage at http://www.elsevier.com . All content posted to the web site must maintain the copyright information line on the bottom of each image.
You are not allowed to download and post the published electronic version of your chapter, nor

may you scan the printed edition to create an electronic version.

Central Storage: This license does not include permission for a scanned version of the material to be stored in a central repository such as that provided by Heron/XanEdu.

19. **Website** (regular and for author): A hyper-text must be included to the Homepage of the journal from which you are licensing at http://www.sciencedirect.com/science/journal/xxxxx. or for books to the Elsevier homepage at http://www.elsevier.com

20. **Thesis/Dissertation**: If your license is for use in a thesis/dissertation your thesis may be submitted to your institution in either print or electronic form. Should your thesis be published commercially, please reapply for permission. These requirements include permission for the Library and Archives of Canada to supply single copies, on demand, of the complete thesis and include permission for UMI to supply single copies, on demand, of the complete thesis. Should your thesis be published commercially, please reapply for permission.

21. **Other Conditions**:

v1.6

If you would like to pay for this license now, please remit this license along with your payment made payable to "COPYRIGHT CLEARANCE CENTER" otherwise you will be invoiced within 48 hours of the license date. Payment should be in the form of a check or money order referencing your account number and this invoice number RLNK500795743. Once you receive your invoice for this order, you may pay your invoice by credit card. Please follow instructions provided at that time.

Make Payment To:
Copyright Clearance Center
Dept 001
P.O. Box 843006
Boston, MA 02284-3006

For suggestions or comments regarding this order, contact RightsLink Customer Support: customercare@copyright.com or +1-877-622-5543 (toll free in the US) or +1-978-646-2777.

Gratis licenses (referencing $0 in the Total field) are free. Please retain this printable license for your reference. No payment is required.